Development of a 3D *ex vivo* Culture System to Study Osteocyte Mechanobiology

by

Rachel Lilia Wilmoth

B.S., Santa Clara University, 2010

M.S., University of Colorado Boulder, 2017

A thesis submitted to the
Faculty of the Graduate School of the
University of Colorado in partial fulfillment
of the requirements for the degree of
Doctor of Philosophy
Department of Mechanical Engineering
2021

Committee Members

Dr. Stephanie Bryant

Dr. Sarah Calve

Dr. Virginia Ferguson

Dr. Maureen Lynch

Dr. Corey Neu

Wilmoth, Rachel Lilia (Ph.D., Mechanical Engineering)

Development of a 3D *ex vivo* Culture System to Study Osteocyte Mechanobiology

Thesis directed by Virginia L. Ferguson, Ph.D. and Stephanie J. Bryant, Ph.D.

Osteocytes are the most common type of cell in bone, and they reside within the mineralized bone matrix in a three-dimensional (3D) interconnected network of dendritic cells. Osteocytes are mechanosensitive cells that maintain bone homeostasis by directing bone formation or resorption in response to changes in mechanical loading. In the subchondral bone plate, the osteocytes contribute to degeneration during diseases such as osteoarthritis that is accompanied by bone and cartilage deterioration. Yet, it is difficult to study osteocyte mechanobiology *in vivo,* and existing 2D and 3D *in vitro* culture methods are insufficient.

The goal of this dissertation was to develop a 3D *ex vivo* culture system to study osteocyte mechanobiology, specifically within the subchondral bone plate. A 3D *ex vivo* culture system to study osteocyte mechanobiology needs both biological relevance (*i.e.*, mature osteocytes, bone matrix deposition, and 3D interconnected dendritic network) and mechanical relevance (bone-level strains and interstitial fluid flow). This work used the tunable poly(ethylene glycol) (PEG) hydrogel system to develop a 3D culture system. This work developed a degradable PEG hydrogel that enhanced osteocyte differentiation and bone matrix deposition in 3D. Using this degradable PEG hydrogel system, we investigated how osteocyte dendritic network formation is influenced by physical and biochemical factors. The dimensionality (2D culture vs. 3D hydrogel) greatly influenced differentiation and significantly altered the osteocyte response to Prostaglandin E2, a molecule that is rapidly produced by osteocytes in response to mechanical loading Finally, the degradable PEG hydrogel was incorporated into a bilayer composite hydrogel system that was

designed to control the bone-level strains and induce interstitial fluid flow, mimicking the loading environment in subchondral bone. This dissertation thus contributes an improved understanding of the physical and biochemical cues that support osteocyte differentiation and dendrite formation in 3D. Further, this system supports the study of osteocyte mechanobiology in a physiologically relevant *ex vivo* model that captures both biological and mechanical relevance to the subchondral bone plate.

Acknowledgements

Graduate school has truly been a journey, and I am so thankful for all the people who have supported, challenged, and inspired me throughout this journey. First, thank you to my research advisors, Virginia Ferguson and Stephanie Bryant. Ginger, your support and kindness are part of the reason why I chose to come to CU Boulder, and why I chose to stay even with some doubts after my first year. Thank you for always taking my goals and interests into consideration and encouraging me to take on this increasingly biological research project. You have always made it clear that not only do you want to support my research, but you want to support me as a person. You take the time to ask me about what I did over the weekend, or if I was able to go ski the last 24" storm. You have challenged me to be a better writer, researcher, and teacher. Thank you for being such an integral part of my Ph.D. journey. Stephanie, thank you for bringing me into your group, being a patient teacher when I didn't understand some chemical engineering concepts, and always challenging me to be a diligent researcher. Your attention to detail and inquisitive questions have inspired me to delve deeper into the "whys" of my research. You have always made it clear that you deeply care about my wellbeing and you make the time to help me even when I am in a time-crunch. You have also challenged me to be a better writer, researcher, and teacher. Thank you for helping me get through this journey!

Next, thank you to all my lab-mates. Both the Ferguson and Bryant groups are filled with people who have built supportive and inclusive environments. Not only do I feel supported in my research (like asking how to do literally everything), but I feel supported as a person. Both groups jumped to offer "one more practice defense," after already sitting through a nearly 2-hour first practice, which just shows how much you all care about me. Aaron – thank you for teaching me so many of the techniques that I used in this dissertation and thank you for making me feel welcome

when I started working in the Bryant group. Sadhana – thank you for spending countless hours making hydrogels with me and for training me on PCR. Mollie and Sarah – thank you both for your companionship, willingness to listen to me vent, willingness to help me brainstorm any research ideas, and for always making me laugh when I need it the most in lab. Jenn – thank you for always being willing to give me advice on my statistics, or figure, or really anything. You and I joined the lab around the same time and I have always been inspired by your work ethic and enthusiasm for teaching others. From more hours in the mouse room than either of us wanted, to more mouse dissections than I wanted (I think you wanted them all), to defending in the same year, thank you for your companionship. Kristine – thank you for your companionship, leadership, and always answering my statistics questions (even if it was the same question over and over). You are such an inspiring leader, teacher, and researcher, and I am so glad that I got to learn from you. Adrienne and Ellyse – even though you weren't in my lab, both of you have been integral to parts of my PhD journey in helping me understand new techniques, commiserating about similar research issues, or explaining how to do a simple molar calculation (@Ellyse). In the end, I'd like all my past and present lab mates to know that your companionship and support have helped me finish this journey!

Next, thank you to my teammates and coaches on Quandary/Kali. Playing ultimate frisbee with you all is a huge part of the reason why I enjoyed my third and fourth years of grad school. Thank you for always helping me laugh after a long, frustrating day in the lab, even if it was 20 degrees outside at our 8 pm practice. Thank you for showing me that hard work and unconditional trust pay off, and that working towards and achieving a common goal is such a satisfying feeling. Above all, thank you for providing so much laughter to my life through so much weirdness.

Finally, thank you to the friends and family who have truly helped me finish this journey. Jeanne, I cannot imagine grad school without you. Ever since our 6AM DMV appointment, we have been together on this journey. From the countless hours of problem sets and studying in our first two years, to recharging in the Colorado outdoors together, your friendship means the world to me. Thank you for always listening to me, reassuring me, and throughout this entire journey, just helping me know that I wasn't alone in my doubts and frustrations. To all my Moorhead roommates, thank you for always being down for impromptu Catan or Fat Tuesdays to lighten the heaviness of grad school. David and Annika – thank you both for always making me laugh, providing a listening ear, and going on adventures with me. I can't imagine Colorado without both of you. Natalie – you have always understood me and known how to comfort me when I am down. I am so glad that we were able to live in the same state for most of my Ph.D. and share adventures, lunches, and even just phone calls. Your dedication and hard work have always been an inspiration for me. To my family, you have always encouraged me to challenge myself and value education, and without that I doubt I would have even started this Ph.D. journey. Thank you for always rooting for me along the way and giving me the confidence-boosts when I need them the most. Jessie – your friendship has consoled and supported me and our adventures have recharged me. And of course, thank you to my best friend and fiancé, Darrin. Sometimes, I know that you believed in me more than I believed in myself and knowing that was enough to keep me going. Thank you for your steadfast confidence in me. In the stressful times, thank you for cooking for me, making me laugh, and always being down for a de-stress trail run. Thank you for your patience with me, for always reminding me how much there is to be grateful for, and for encouraging me to find passion in my work. Every adventure and every day are just more fun with you. Your friendship and love have made this accomplishment possible.

Funding sources that made this research possible: NIH 1R21AR069791-01A1, NIH 1R01AR069060-01A1, NIH National Institute of Aging Integrative Physiology of Aging Training Grant under Award T32AG000279-16A1, CU Boulder Department of Mechanical Engineering.

Table of Contents

List of Figures

List of Tables

1. Introduction

1.1 Bone

1.1.1 Bone Composition

Bone is a hierarchical tissue and macroscopically is classified as either cortical or trabecular bone (Figure 1.1). Cortical bone makes up the majority of the bone mass (roughly 80%), exhibits low porosity, and serves to mechanically support and protect the body.[1] On the other hand, trabecular bone comprises the remainder of the bone mass and is characterized by lower compressive strength, high porosity, and low bone density (only 25-30% of the tissue volume is composed of bone).[2] Trabecular bone is organized in an interconnected network of plate- and rod-like structural elements that gives it a sponge-like appearance and also increases its surface area in contact with marrow.

Microscopically, both cortical and trabecular bone are organized into units called osteons. Each osteon is made up of concentric layers (or lamellae) of tissue, giving osteons the appearance of tree trunks, which are centered around a Haversian canal in cortical bone. Within each lamella, small cavities called lacunae encase the cell body of osteocytes, which are connected to neighboring osteocytes via canalicular channels. Osteocytes are surrounded by bone matrix, which is comprised of both organic and inorganic materials. 90% of the organic matrix is collagen type I, which is organized into fibers that are approximately 150 nm in diameter and 10 μm in length. At the nanometer length scale, collagen fibers are comprised of collagen fibrils, and each fibril contains five collagen molecules that are staggered and separated by 67 nm holes that are filled with mineral deposition. Bone mineral makes up roughly 65% of bone's wet weight and is composed primarily of calcium hydroxyapatite ($Ca_{10}[PO_4]_6[OH]_2$).[3] In contrast to the naturally

occurring geologic hydroxyapatite, bone's hydroxyapatite crystals are relatively small and contain many lattice-substituted impurities. The organic matrix (primarily collagen) contributes to bone's flexibility, while the inorganic mineral network provides stiffness to the bone.

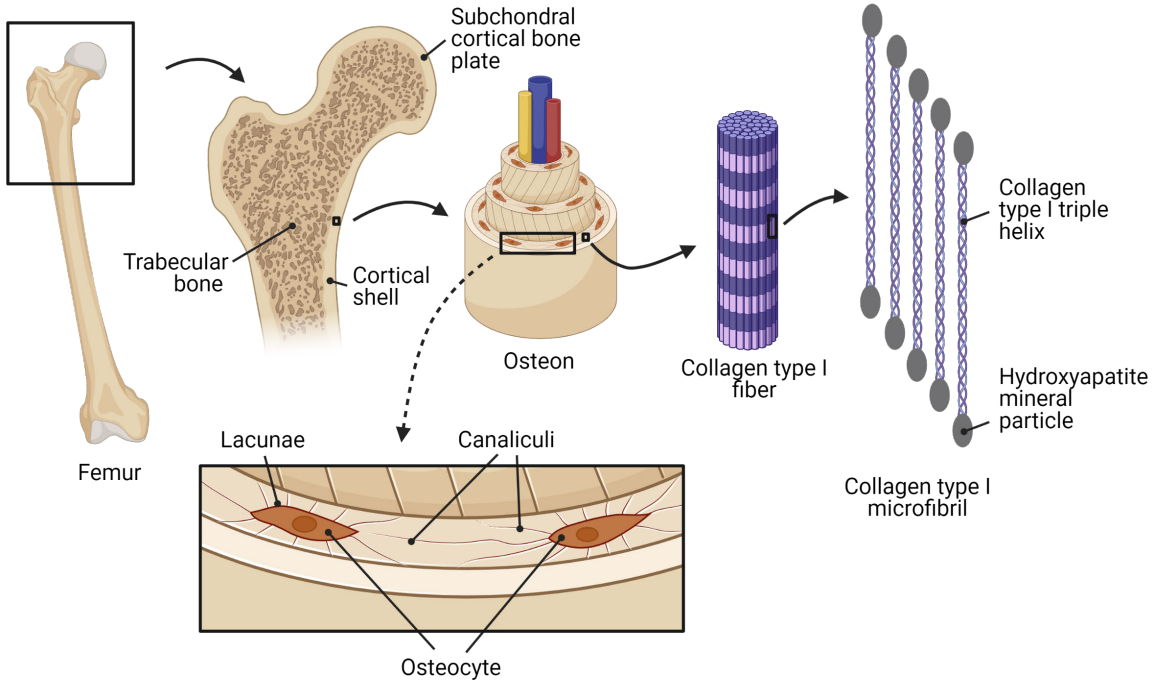

Figure 1.1: Hierarchical composition of bone. *Figure created with BioRender.com*

The 10% of the organic matrix that is not collagen type I consists of various other types of collagen (types III, V, and X), non-collagenous proteins (*e.g.* osteocalcin, fibronectin, osteopontin, osteonectin, dentin matrix protein 1 [DMP1], matrix extracellular phosphoglycoprotein [MEPE], alkaline phosphatase [ALP], sclerostin, receptor activator of nuclear factor kappa-β ligand [RANKL], osteoprotegerin [OPG]), and proteoglycans (*e.g.* decorin, biglycan, hyaluronan, perlecan). These proteins and proteoglycans are key regulators of bone matrix development and homeostasis.

Embedded within and surrounding the bone matrix are three bone cell types with distinct functions: osteoblasts, osteoclasts, and osteocytes (Figure 1.2). Osteoblasts and osteoclasts reside on the bone surface and are responsible for bone formation and resorption, respectively. On the other hand, osteocytes are embedded within the bone matrix, and although they remodel the matrix immediately surrounding them on a small scale,[4–6] their primary function is to coordinate the activity of osteoblasts and osteoclasts in response to mechanical and hormonal cues. These three cell populations communicate via paracrine signaling through the lacunocanalicular network and via gap junctions at the bone surface. Osteocytes close to the bone surface form gap junctions with osteoblasts and osteoclasts on the surface via canaliculi.

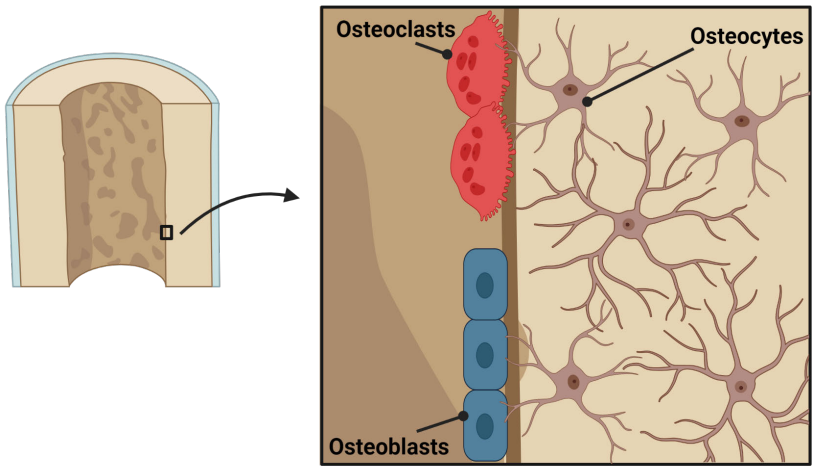

Figure 1.2: Three bone cell types: osteocytes, osteoclasts, and osteoblasts. Each cell type has a distinct function in bone development and homoeostasis. *Figure created with BioRender.com*

1.1.2 Subchondral Bone Plate

In any articulating joint, a unique set of tissues make up the osteochondral unit at the articulating surface: articular cartilage overlying a subchondral bone plate, with an interfacial thin calcified cartilage layer (Figure 1.3). These tissues differ in their mechanical properties and in their

composition of extracellular matrix (ECM).[7,8] Although they are distinct, each tissue layer is physically connected and communicates with each other via transfer of mechanical loads and biochemical signaling.[9,10] Thus, it is critical to understand the mechanobiology of the osteocytes within the subchondral bone plate because they likely contribute to bone and cartilage degeneration during diseases such as osteoarthritis (OA). During the progression of OA, bone and cartilage both undergo physical changes; for example, cartilage permeability increases,[11] which in turn increases the fluid flow in bone and cartilage.[12,13] Osteocytes detect the increased fluid flow in subchondral bone, leading them to secrete signaling molecules that affect chondrocyte, osteoblast, and osteoclast activities that contribute to further osteochondral degeneration.[7,9,10,14–16]

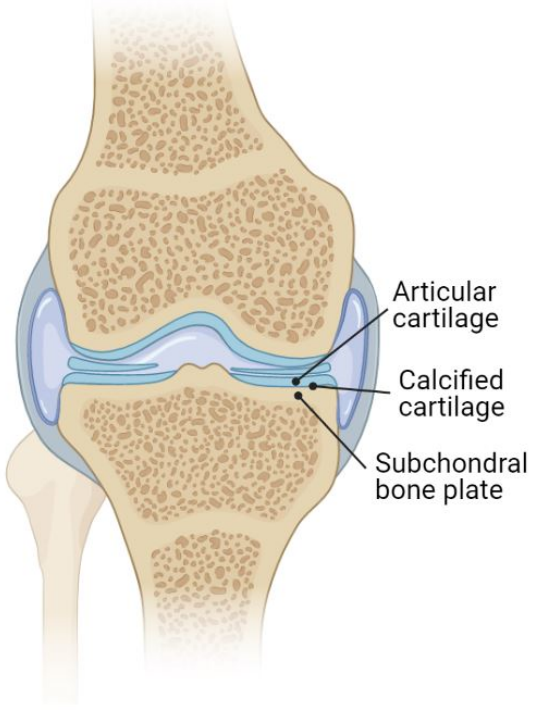

Figure 1.3: The osteochondral unit is comprised of articular cartilage overlying a subchondral bone plate with a thin interfacial calcified cartilage layer in between. *Figure created with BioRender.com*

1.1.3 Bone Development

Collagen type I is assembled via cellular and extracellular processes. Each molecule is made up of approximately 3000 amino acids and is approximately 300 nm in length.[2] Its triple helix organization is comprised of three chains of repeating units of Gly-X-Y, with proline and hydroxyproline being the most common residues for X and Y, respectively.[17] Hydroxyproline is abundant in collagen and is critical to maintain the stability of the triple helix through hydrogen bonding between its hydroxyl group and water molecules. Collagen is first assembled as a procollagen molecule within the cell, which consists of the triple helix with terminal N- and C-propeptides. After exocytosis, the propeptide regions are enzymatically cleaved, which leaves nonhelical end domains and a mature collagen molecule.

Bone mineral deposition is also regulated by both cellular and extracellular factors. First, a collagen matrix is required, as hydroxyapatite in bone is oriented on this matrix. This is supported by the finding that bones of patients with osteogenesis imperfecta, a disease associated with defects in collagen structure,[18,19] have smaller hydroxyapatite crystals than normal.[20,21] Mineral is initially deposited as amorphous calcium phosphate[22,23] via osteoblast exocytosis of vesicles containing mineral aggregates.[24–27] The initial nucleation of mineralization then occurs at binding sites on the collagen matrix in the gaps between collagen molecules and at the ends of collagen fibrils.[28–31] The hydroxyapatite crystals that form in this nucleation phase are poorly organized and contain little carbonate. Following nucleation, the crystals grow: a phase called primary mineralization. In this phase, the crystals become more plate-like and align themselves with the collagen fibrils and the longitudinal axis of the bone. During primary mineralization, 65-70% of the total crystals are rapidly deposited within the collagen matrix in roughly 3 weeks.[2] The secondary mineralization

phase then occurs over months to years, where some new crystals are formed and existing crystals become larger and more crystalline.

1.1.4 Bone Cell Development

Osteoblasts arise from mesenchymal stem cells that differentiate into osteoblasts when exposed to specific transcription factors, specifically those activated by bone morphogenic proteins (BMPs) and Wnts.[32] Mature osteoblasts are cuboidal cells that secrete high levels of protein, specifically alkaline phosphatase (ALP), bone sialoprotein (BSP), osteocalcin, osteopontin, osteonectin, and type I collagen, among others. They also secrete high levels of mineral in the form of amorphous calcium phosphate. Extensive heterogeneity in osteoblast gene and protein expression has been reported, even among neighboring cells that appear histologically similar.[33]

Osteoclasts arise from the hematopoietic monocyte-macrophage lineage in the bone marrow. Two factors that are necessary for osteoclastogenesis are macrophage colony-stimulating factors (M-CSFs) and receptor activator of nuclear factor kappa-B ligand (RANKL). Other growth factors, cytokines, and matrix metalloproteinases (MMPs) that are secreted by osteoblasts and osteocytes regulate osteoclastogenesis as well.

After becoming partly surrounded by osteoid, or newly formed bone, an osteoblast undergoes functional and morphological changes that mark the beginning of its differentiation into an osteocyte. Depending on the species and age of the animal, it has been estimated that ~10-30% of osteoblasts transform into osteocytes.[33] The fundamental mode of osteoblast entrapment in osteoid remains a mystery, but it is likely a combination of the several theories, with two being the most prominent: (1) osteoblasts entrap themselves in their deposited matrix and (2) some osteoblasts slow or stop their rate of matrix deposition and thus become entrapped by other

osteoblasts' deposition.[33] After entrapment in osteoid or once differentiation has been initiated, the cells are often referred to as any of the following: "osteoid-osteoblasts," "pre-osteocytes," "osteocytic osteoblasts," "early osteocytes," or "young osteocytes" to distinguish intermediate transitional stages.

Many of the cellular and molecular mechanisms that initiate and regulate osteocyte differentiation are not fully understood, largely because of the difficulty in studying cells entombed in mineralized tissue and the variable expression at different stages and among cell types. One theory posits that as the newly-formed bone layer grows, the osteoblasts on the surface become farther from the embedded osteocytes with which they are in contact with, and eventually the embedded osteocytes secrete a molecular signal that is transported to the surface to induce osteoblast-to-osteocyte differentiation.[34] Various other theories suggest that the differentiation is driven by Transforming Growth Factor β-related signaling mechanisms or by transcription factors, such as *Runx2* which activates osteoblast/osteocyte markers.[33]

The osteoblast-to-osteocyte transition process has been increasingly studied in recent decades and has some well-documented markers (Figure 1.4).[33,35–37] Three morphological changes that are agreed upon are: (1) a decrease in cell body size, (2) increase in cell processes, and (3) changes to intracellular organelles.[33] Differentiating osteocytes also down-regulate, or end, production of many extracellular proteins, such as osteocalcin, collagen type I, and Alkaline Phosphatase (ALP), among others.[33] There are several markers that indicate differentiation (gene name in parentheses): E11/gp38 (*Pdpn*) is one of the earliest markers, followed by Matrix extracellular phosphoglycoprotein (*Mepe*), Phosphate Regulating Endopeptidase Homolog X-Linked (*Phex*), Dentin matrix acidic phosphoprotein 1 (*Dmp1*), Sclerostin (*Sost*) and Fibroblast growth factor 23 (*Fgf23*). Sclerostin and FGF23 indicate mature osteocyte differentiation.[38]

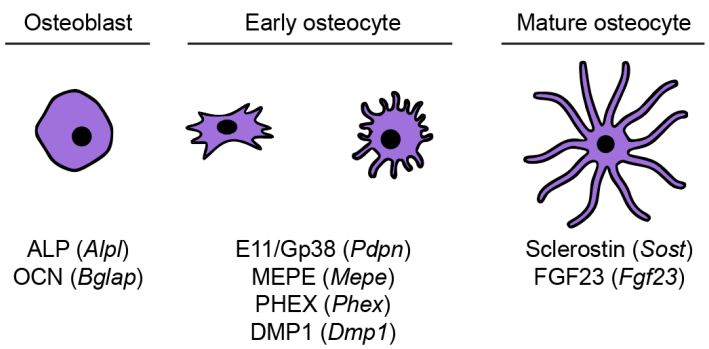

Figure 1.4: Markers of osteoblast-to-osteocyte differentiation: changes in morphology and protein expression. Gene names are given in parentheses. *Figure created with BioRender.com*

1.2 Osteocytes

1.2.1 Lacunocanalicular Network Structure and Composition

In vivo, osteocytes are connected to each other via a lacunocanalicular network (LCN, Figure 1.1 and Figure 1.5). Cell bodies are encased within lacunae—small, rounded cavities in the bone matrix—with approximately 0.5-1 μm pericellular space between the cell membrane and lacunar wall.[39] Each cell body develops approximately 50-60 dendrites, which extend outward to form connexin 43 gap junctions[40] with neighboring cell dendrites.[15] The dendrites, which have an average length of 30 μm[41] and diameter of 100-150 nm,[39] extend through small channels called canaliculi. The canaliculi have a diameter of approximately 200-250 nm, leaving 50-150 nm annular space between the dendrite and channel wall.[39] The LCN extends throughout bone and to the bone surface, where the dendrites form gap junctions with osteoblasts and osteoclasts. The interconnected LCN in bone is comparable to the neural network in both size (total length of processes) and number of connections.[42]

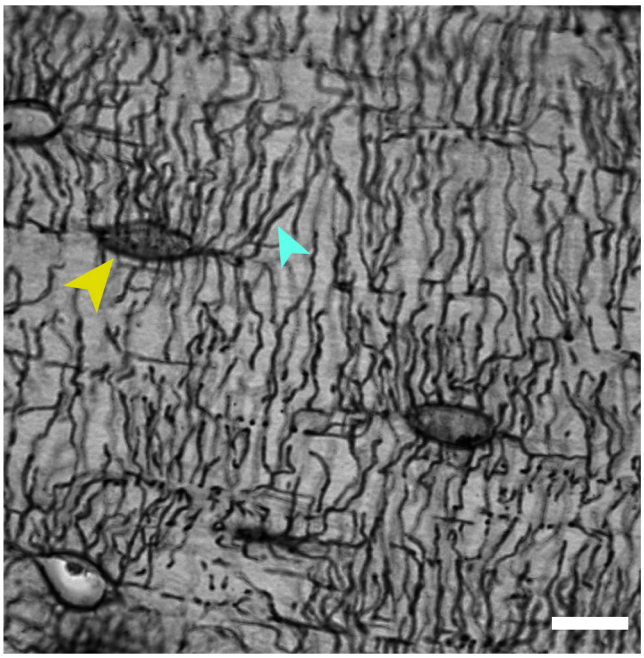

Figure 1.5: Lacunocanalicular Network (LCN): osteocyte cell bodies encased in rounded lacunae (yellow arrow) are connected to each other via dendrites which extend throughout canaliculi (blue arrow). Image was taken of mouse cortical bone after silver nitrate staining. Scale bar is 10 μm.

A thin layer of collagen type I lines the walls of the LCN, but the remaining pericellular space between the cell cytoskeleton and the walls is not empty. Rather, the pericellular space in the LCN is composed of extracellular proteins and proteoglycans, and is sometimes called the glycocalyx (Figure 1.6).[43,44] The two main functions of the pericellular matrix are to (1) tether the osteocyte cell body and dendrites to the lacunar/canaliculi walls and (2) provide the osteocyte for a way to sense mechanical loads (*e.g.* fluid flow or direct matrix strain).[43,45] Extracellular proteins in the pericellular matrix include collagen, fibronectin, and vitronectin, and osteocyte cell bodies and dendrites attach to these proteins via cell surface receptors such as CD44 and integrins. Along the dendrites, "collagen hillocks" have been observed with ~130 nm spacing.[46] These collagen protrusions extend outwards from the canalicular wall and attach to the dendrites via integrins that are connected to the actin cytoskeleton through focal adhesions.[47] The main proteoglycan of the

pericellular matrix is perlecan,[45,48] which also plays a key role in LCN formation, as mice without perlecan develop a LCN with reduced size and number of canaliculi.[49]

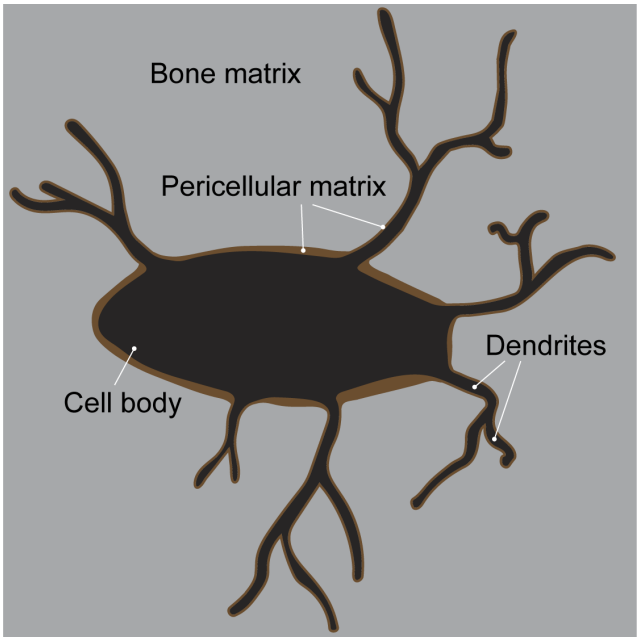

Figure 1.6: Osteocyte cell body and dendrites are surrounded by a pericellular matrix composed of extracellular proteins and proteoglycans.

Interestingly, the integrin-based focal adhesions that tether osteocytes to the pericellular matrix differ between the cell body and dendrites. In both locations, integrins span from the cytoplasm to the pericellular matrix, with the α subunit attaching to the pericellular matrix ligands and the β subunit contributing to intracellular signaling mechanisms. On the dendrites, integrin β3 (with αv subunit) is found, whereas on the cell body, only β1 is found (with varying α subunits including 1, 2, 3, 5, and 5).[43,46] Further, on the cell body, β1 forms traditional large focal adhesions with vinculin and paxillin, but on the dendrites, β3 forms atypical, smaller focal adhesions with specialized channel proteins such as pannexin-1, P2X7R, and CaV3.2-1.[43,50] It is thought that the

dendritic focal adhesions are atypical to fit into smaller pericellular locations along the canaliculi and into smaller cytoplasmic locations within the dendrites.

The LCN enables gap junctional and paracrine signaling throughout the dense bone tissue. Gap junctions permit direct exchange of secondary messenger molecules <1.2 kDa in size (*e.g.*, cAMP, Ca^{2+}, ATP, prostaglandins) between cells.[51] Osteocytes share these secondary messengers in part to amplify a local response (such as to fluid flow).[52] Larger solutes up to ~70 kDa (*e.g.*, sclerostin, RANKL, and PTH) can be transported throughout the LCN via fluid movement.[53]

1.2.2 Sensing and Responding to Mechanical Loads

Osteocytes have become known as the "mechanostat" for bone; they sense and respond to mechanical cues with a cellular response. Osteocytes respond to multiple types of loading such as direct matrix strains, hydraulic pressure, and interstitial fluid flow.[15] *In vivo,* strain-amplification at lacunae occurs due to the softer pericellular matrix that surrounds osteocytes, where strain increases by 1.4 to 2.7-fold.[54] However, the strain amplification that occurs due to fluid flow throughout the LCN is estimated to amplify the tissue-level strains on the cell's cytoskeleton by 10 to 100-fold.[14] The higher strain amplification due to fluid flow in addition to the *in vitro* experiments that show osteocytes to be more sensitive to fluid flow than strains[14,55] supports the consensus that fluid flow through the LCN dominates the mechanical stimuli sensed by osteocytes.

Osteocyte mechanosensation of the LCN fluid flow occurs through several different cellular mechanisms. The first response to mechanical loading is an increase in cytoplasmic Ca^{2+}, which is triggered by the opening of mechanically sensitive ion channels.[56] Primary cilia also orient themselves in the direction of fluid flow, and removal of cilia changes the osteocyte response to fluid flow.[57] As fluid moves throughout the LCN, the perlecan that tethers the cytoplasm is subjected to a drag force, which the cell membrane senses, and which is evidenced by the

diminished response to mechanical loading in perlecan-deficient mice.[49] Finally, osteocytes depend on both β1 and β3 integrins to sense and respond to mechanical loads.[58–60]

Dendrites are responsible for most of the mechanosensation due to LCN fluid flow. This is partly due to the increased fluid flow in the canaliculi as compared to the lacunae, due to the smaller pericellular space.[14] Additionally, cellular experiments have shown that dendrites produce a cellular response at much lower loads than the softer cell body does.[61–63]

At a macroscale, increased mechanical loading increases bone formation while decreased mechanical loading increases bone remodeling, which was first theorized by Wolff's Law in 1834.[64] Osteocytes, being incredibly mechanosensitive, orchestrate these changes by secreting signaling proteins that directly regulate osteoblast bone formation and osteoclast bone resorption (Table 1.1). The mechanisms by which osteocytes alter their production of these (and other) signaling molecules are not fully understood. One secondary messenger that osteocytes produce in response to mechanical loading[65,66] and that also induces downstream protein expression changes in osteocytes is Prostaglandin E2 (PGE_2).[67–69] PGE_2 is rapidly secreted by osteocytes via connexin 43 hemichannels[70] in response to mechanical loading on the order of minutes.[65,66,71,72] Then, by autocrine signaling, PGE_2 binds to cell surface receptors on osteocytes to initialize intracellular signaling cascades that alter expression of some of the proteins outlined in Table 1.1, (*e.g.*, increased PGE_2 decreases sclerostin, an anabolic effect[73]).

Table 1.1: Key proteins secreted by osteocytes to regulate anabolic and catabolic activity.

Gene Name	Protein Name	Category	Function
Il6	IL-6	Catabolic signaling	↑ leads to bone resorption [74–77]
Tnfrsf11b	Osteoprotegerin (OPG)	Catabolic signaling	↓ leads to bone resorption [78]
Tnfsf11	Receptor activator of nuclear factor kappa B ligand (RANKL)	Catabolic signaling	↑ leads to bone resorption [78–82]
Bglap	Osteocalcin (OCN)	Anabolic signaling	↓ leads to bone formation [83,84]
Sost	Sclerostin	Anabolic signaling	↓ leads to bone formation [85] ↑ leads to bone resorption [86]

1.2.3 Prostaglandin E2 Signaling

PGE_2 is one of the earliest responses secreted by osteocytes in response to mechanical loading and has an overall anabolic effect on bone.[87–89] Yet, the mechanisms by which PGE_2 affects osteocyte production of key anabolic or catabolic signaling proteins is not fully understood. Figure 1.7 is a compilation of several recent studies that have elucidated some of the intracellular signaling pathways (but show some inconsistencies) in primarily bone cells when stimulated with PGE_2 binding to one of the two EP receptors responsible for most anabolic signaling effects, EP2 or EP4.[90–92]

Briefly, PGE_2 binds to any of the four EP receptor subtypes (EP1, EP2, EP3, EP4). EP2 and EP4 activation increases intracellular 3,5'-cyclic adenosine monophosphate (cAMP) levels while EP1 and EP3 activation has other effects (EP3 decreases cAMP and EP1 increases Ca^{2+}).[68] Increased intracellular cAMP activates the protein kinase A (PKA) pathway,[52,69] which leads to

phosphorylation of glycogen synthase kinase-3β (GSK-3β).[93] Phosphorylation of GSK-3β inhibits β-catenin degradation in the cytosol.[94] Accumulation of β-catenin in the cytosol leads to nuclear translocation of β-catenin and transcriptional activation of T-cell factor (TCF)-regulated gene expression,[95] including the gene *Ptgs2*, which encodes the protein cyclooxygenase-2.[93] One key difference between EP2 and EP4 is that EP2 likely dominates the cAMP/PKA-mediated phosphorylation of GSK-3β, whereas only EP4 couples to phosphatidylinositol 3-kinase (PI3K)-mediated GSK-3β phosphorylation.[68,93] This may be related to the difference in cAMP stimulation: at comparable protein levels and equal PGE_2 stimulation, EP2 stimulated cAMP formation ~71-fold as compared to ~10-fold from EP4.[96] It is also possible that this difference is also explained by the PGE_2 desensitization that EP4 undergoes but EP2 does not.[97] PI3K activation (from EP4) has also been shown to phosphorylate the extracellular signal-regulates kinases (ERKs), which induces expression of early growth response factor-1 (EGR-1) that was not observed with EP2 stimulation.[96] A number of genes including *Ptges* (encoding PGE_2 synthase, or mPGES1) are known to be regulated by EGR-1,[96] and PGE_2 has been shown to increase *Ptges*.[98]

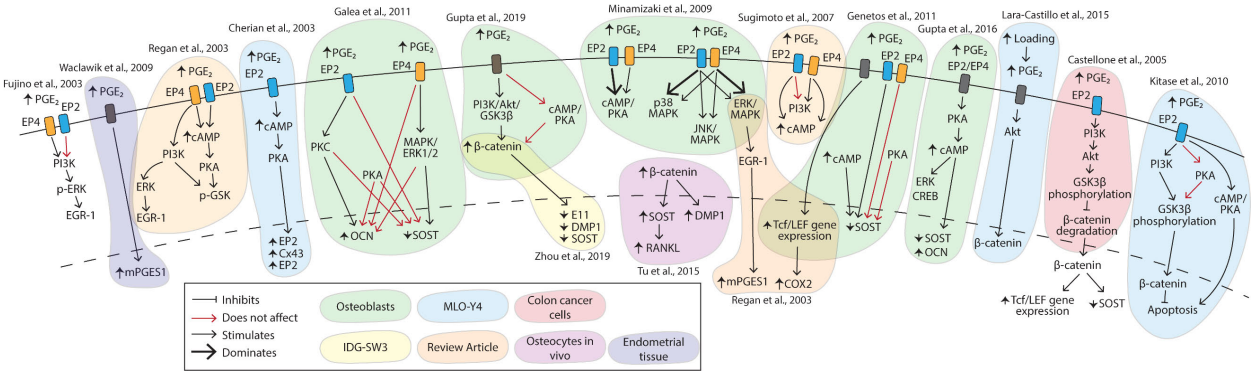

Figure 1.7: PGE_2-induced signaling pathways as activated by the cell surface receptors EP2 and EP4. The findings from each study are color-coded by the cell type. The red arrows were specifically shown in the experiment to not affect the downstream signaling, which is different than either inhibition or stimulation.

1.3 *In vitro* Study of Osteocytes

It has been difficult to study osteocyte mechanobiology and signaling *in vivo* for several reasons. First, it is difficult to isolate and control the effects of different mechanical stimuli (*e.g.* fluid flow vs. strain) on osteocytes embedded within the LCN. Second, any techniques to study signaling that require high resolution imaging have been difficult until recent advances were developed in confocal microscopy[42] due to the location of osteocytes within the heavily mineralized bone tissue. Third, a transgenic mouse model that targets only mature osteocytes has not been developed until very recently (2019) and there are undesirable side effects with this model that limit its utility.[99] A transgenic model that targets only mature osteocytes would enable *in vivo* experimental knockouts, but without this model it is difficult to isolate the effects of any treatment on osteocytes alone. This is particularly challenging because osteoblasts are from the same lineage as osteocytes and therefore express many of the same genes and proteins as osteocytes. Therefore, the bulk of osteocyte mechanobiology and cell signaling experiments to date have used *in vitro* cultures.

1.3.1 Cell Lines

Although protocols exist for isolating primary osteocytes (*e.g.*, from mature mice[100]), the protocols are time-intensive and require many animals to obtain the necessary cell numbers for most *in vitro* experiments. Primary osteocytes are post-mitotic and therefore rarely proliferate, and even de-differentiate in 2D cultures.[101] When cultured in 2D, isolated primary osteocytes show increased expression of osteoblast markers as compared to when cultured in 3D, indicating that osteocytes can de-differentiate back into osteoblasts depending on the extracellular matrix cues.[102] These challenges led to the development of several osteocyte-like cell lines that most *in vitro*

osteocyte research currently uses. These cell lines have enabled the field of osteocyte biology to exponentially expand in the past 20 years.[103]

The first osteocyte cell line that was developed is also the most frequently used cell line: MLO-Y4. These murine cells resemble early osteocytes and were derived from long bones from a transgenic mouse with the immortalizing T-antigen expression under control of the osteocalcin (OCN) promoter.[104] MLO-Y4 cells proliferate rapidly and express high levels of OCN, connexin 43, E11, CD44, DMP1, MEPE, and PHEX. These cells are highly dendritic and responsive to mechanical loading and thus have been used to extensively study osteocyte mechanobiology (approximately 300 publications to date using these cells[103,105]). However, MLO-Y4 cells show limited capacity to express the mature osteocyte markers of FGF23 and sclerostin.

The HOB-01-C1 was the first human cell line developed to resemble early osteocytes. These cells extend cellular dendrites and express low levels of ALP with high levels of CD44 and OCN.[106] However, this cell line has not been used to the same extent as the mouse-derived cell lines, likely due to the expedited progress of mouse genetics.

The MLO-A5 murine cell line resembles osteoid-osteocytes, with the ability to mineralize without β-glycerolphosphate in ~7 days in sheets that resemble primary mineralization.[107] MLO-A5 cells were established from the same animals as the MLO-Y4 cells.[107] In culture, these cells express high levels of late osteoblast markers, including ALP, collagen type I, bone sialoprotein (BSP), parathyroid hormone (PTH), type 1 receptor, and OCN.[107] In later culture times, these cells develop dendrites and can express osteocyte markers such as E11.[108]

The IDG-SW3 cells were derived from double transgenic mice: mice with a temperature sensitive SV40 T-antigen were crossed with mice where the *Dmp1* promoter drives Green

Fluorescent Protein (GFP).[109] The temperature sensitive SV40 T-antigen enables these cells to rapidly proliferate in their immortalized state at 33˚C, but when cultured at 37˚C, they end expression of the T-antigen, no longer proliferate, and begin to differentiate. These cells display an initial osteoblast-like phenotype, but after extended culture in osteogenic media they express mature osteocyte markers such as *Sost* and *Fgf23*,[109] making them an ideal cell line to study the osteoblast-to-osteocyte transition.

The OCY454 cell line was derived from the same double transgenic mouse line as the IDG-SW3 cells, but these cells produce sclerostin (and *Sost*) after 10-14 days,[110] a much shorter culture period than the IDG-SW3 cells require. OCY454 cells are a more recently developed cell line than the IDG-SW3 cells, and thus have not been studied as extensively, although they have been shown to respond to parathyroid hormone[110] and mechanical stimulation.[111]

The most recently developed osteocyte cell line is the OmGFP66, first published on in 2019.[112] This cell line was derived from mice with a membrane-targeted GFP driven by the *Dmp1* promoter. This cell line is a promising new addition to the osteocyte cell lines because these cells express osteocyte markers (E11, DMP1, sclerostin) after 7-14 days and form lacunocanalicular-like structures in 2D culture.[112]

1.3.2 Mechanobiology

Most osteocyte studies of mechanobiology *in vitro* to date use 2D cultures. These studies primarily induce mechanical loading by culturing cells on a 2D substrate and either stretching that substrate to induce a direct matrix strain or flowing fluid over the cell monolayer to subject to fluid shear stress. The results from these studies have been fundamental in understanding the mechanobiology and mechanotransduction of osteocytes. For example, osteoblasts (T23) and osteocytes (MLO-Y4) subjected to fluid flow both secrete PGE2 via β-catenin activation, but the

sensitivity and kinetics greatly differ between the cell populations.[65] Yet, 2D cultures of osteocytes are limited because of the osteocyte dedifferentiation that occurs and for the lack of 3D environmental cues that are necessary to resemble *in vivo* conditions.[113]

A few recent novel studies have developed 3D *in vitro* culture systems to study osteocyte mechanobiology.[110,114–118] For example, one study developed a 3D osteocyte-osteoblast co-culture system combined with cyclic strains ranging from 0.4-0.5% to study strain-induced osteocyte regulation of osteoblast bone formation.[114] Another study cultured osteocytes in a 3D collagen gel to mimic aspects of the loading environment around a dental implant.[116] Other studies developed 3D culture systems that replicate aspects of *in vivo* osteocyte cell density, function, and phenotype and that incorporate loading via fluid perfusion.[110,115,117] Yet another study developed an osteocyte 3D culture system to study the effects of damaging levels of loading on osteocyte signaling to bone marrow cells. However, these studies that combine 3D osteocyte culture systems with mechanical stimulation are limited in their ability to culture osteocytes with a mature phenotype while also recapitulating physiological bone-levels of strain (*i.e.*, between 0.001% and 0.3%),[53,119] in combination with fluid flow.

1.4 Bone Tissue Engineering Scaffolds

The *in vitro* model that best mimics the physiology of *in vivo* conditions is a bone explant. Yet, osteocytes in bone explants decrease their production of sclerostin and FGF23[120] and decrease in viability over time.[121,122] Additionally, studying osteocyte mechanobiology in bone explants retains the same challenge as *in vivo*: it is difficult to isolate and control the effects of different mechanical stimuli. Therefore, 3D osteocyte cultures have been developed using bone tissue engineering scaffolds.

Tissue engineering scaffolds generally fall into two categories: natural or synthetic. Natural scaffolds are derived from proteins or proteoglycans, such as collagen, silk, gelatin, agarose, alginate, and hyaluronic acid. Natural polymers contain naturally occurring cell attachment sites, are degradable by cells, and emulate the pericellular or extracellular matrix of tissue. For bone tissue engineering, collagen I scaffolds have been widely used for 3D culture systems for their biocompatibility, availability, ease of use, and ability to support osteocyte differentiation and dendritic formations.[123] Yet, natural polymers, including collagen scaffolds, are limited by their batch variability, tunability, and mechanical properties. For example, the elastic modulus of collagen gels is often in the single kPa range, yet osteogenic differentiation is enhanced in scaffolds with an elastic modulus in the 10-20 kPa range.[124,125]

Synthetic polymers offer much more tunability than natural polymers, and include poly(N-isopropylacrylamide), polycaprolactone, poly-L-lactic acid, and poly(ethylene glycol) (PEG). Although synthetic polymers do not have a natural affinity for cells, they can be easily modified by tethering in cell attachment motifs, growth factors, and even natural polymers such as chondroitin sulfate[126] or collagen.[127] Synthetic polymers can be crosslinked via a variety of physical, chemical, or ionic mechanisms.

Mineral particles have also been incorporated into synthetic and natural scaffolds to mimic the nonorganic component of bone. Hydroxyapatite (HA), tricalcium phosphate, and biphasic calcium phosphate particles have all shown promising osteogenic results when incorporated into other scaffolds.[115,117,128,129] It is thought that incorporation of mineral particles provides osteocytes with mineral nucleation sites, which emulates osteoid development in osteoblast- and osteocyte-mediated bone formation.

1.4.1 Poly(ethylene glycol) Hydrogels

One of the more common synthetic scaffolds used in a variety of tissue engineering applications are PEG hydrogels. Hydrogels are a subset of crosslinked scaffolds that are hydrophilic and retain a high-water content. The high-water content mimics native tissues and allows for transport. PEG is cytocompatible, hydrophilic, and incredibly tunable, making it ideal for tissue engineering.[130] In order to form a crosslinked network, the PEG is functionalized with a chemically reactive group, such as a norbornene in the case of PEG thiol-norbornene photoclick chemistry hydrogels. With this chemistry, any biological moiety (such as RGD, growth factors, or collagen I) can be covalently tethered (and thus immobilized) to the PEG monomer by functionalizing the moiety with a cysteine or thiol.[131] The hydrogel can form a crosslinked network by also incorporating a crosslinker (*e.g.* PEG-dithiol) and initiating the free-radical polymerization. This method of polymerization in this dissertation uses a photoinitiator that is cleaved by UV light to produce radicals that propagate through the reactive groups via step-growth polymerization.

Given the tight polymer mesh of PEG hydrogels, cell-mediated degradation is necessary to allow for cell-mediated extracellular matrix (ECM) deposition.[132] Incorporation of MMP-sensitive crosslinks into a hydrogel enhanced osteogenesis,[37,38] supported ECM deposition,[133,134] and was biocompatible in a subcutaneous implant.[134] To replace the hydrogel with neotissue and develop an LCN, reverse gelation must occur at the same time as macroscopic tissue growth, a delicate balance to reach.[135]

1.5 Motivation and Specific Aims

Osteocytes amount to greater than 95% of the total bone cells in the body and reside within the mineralized bone matrix in an interconnected lacunocanalicular network. The primary function of osteocytes is to coordinate the activity of bone forming osteoblasts and bone resorbing osteoclasts in response to mechanical and hormonal cues.[38,136] The sensitivity to mechanical loads and the corresponding cellular response is often referred to as mechanobiology. Due to their key regulatory and mechanobiology capabilities, osteocytes are integral to maintaining healthy bone homeostasis, and deregulating bone homeostasis in disease states.[137]

Osteoarthritis (OA) causes disability and pain for over 30 million adults in the U.S.[138] The cause of this pain is the degeneration of the osteochondral unit, which is comprised of articulating cartilage, calcified cartilage, and subchondral bone. During the progression of OA, bone and cartilage both undergo property changes; for example, cartilage permeability increases,[11] which in turn increases the fluid flow in bone.[12,13] Osteocytes embedded in this bone detect the increased fluid flow and then secrete signaling molecules that affect osteoblast bone formation and osteoclast bone resorption that further contribute to osteochondral degeneration.[7,9,10,14–16] A hallmark of late-stage OA is a thickening of the subchondral bone plate, which is likely mediated by the osteocyte-initiated anabolic signaling in response to increased fluid flows. Thus, osteocyte signaling in response to increased fluid flow is crucial to better understanding the contribution of bone and cartilage degeneration to the progression of diseases such as OA.

Insufficient tools exist to study osteocyte mechanobiology within the subchondral bone plate. Studying osteocyte mechanobiology mechanisms *in vivo* is challenging due to the difficulty in isolating and controlling the effects of different mechanical stimuli (*e.g.* fluid flow vs. strain) on osteocytes embedded within the lacunocanalicular network. To date, most osteocyte

mechanobiology studies use *in vitro*, two-dimensional (2D) cultures of osteocytes, which have been fundamental in increasing our understanding of osteocyte mechanobiology. Yet, 2D cultures lack the ability to support a mature osteocyte phenotype in primary osteocytes and osteocyte cells lines.[113] Additionally, they lack a three-dimensional (3D) extracellular matrix (ECM) that more accurately resembles *in vivo* conditions. Some recently developed 3D osteocyte culture models exist but lack the combination of a mature osteocyte phenotype with physiologically relevant matrix strains and fluid perfusion relevant to the subchondral bone plate.

Therefore, the overarching goal of this work is to develop a 3D *ex vivo* culture system to study osteocyte mechanobiology, specifically within the subchondral bone plate. **The first aim of this work is to develop a 3D degradable hydrogel system that promotes osteocyte differentiation and bone extracellular matrix deposition.** Poly(ethylene glycol) (PEG) hydrogels are cytocompatible, hydrophilic, and incredibly tunable, making them ideal for tissue engineering scaffolds.[130] Yet, the tight polymer mesh of PEG hydrogels requires cell-mediated degradation to allow for ECM deposition and extension of cellular dendrites.[132] IDG-SW3 cells can produce a mineralized collagen matrix and transition from osteoblasts to mature osteocytes, but there are no known tunable hydrogel systems that support IDG-SW3 differentiation. The three sub-aims are as follows: (1) Identify a matrix metalloproteinase (MMP)-sensitive hydrogel which would support IDG-SW3 cell-mediated degradation. (2) Assess IDG-SW3 differentiation within the MMP-sensitive degradable hydrogel and compare to a non-degradable hydrogel and 2D culture on tissue culture polystyrene. (3) Examine the effect of cell encapsulation density on cellular morphology and bone ECM deposition. In particular, cell density was identified as a key regulator of osteoblast-to-osteocyte differentiation[139–141] and will influence cell-cell contacts as well as the amount of total ECM deposited.

The second aim of this work is to investigate physical and biochemical factors that influence dendrite formation in a 3D hydrogel. *In vivo,* osteocytes reside within a highly interconnected 3D environment known as the lacunocanalicular network (LCN), characterized by ~30 dendrites extending outwards from each cell body to form gap junctions with neighboring cells. Osteocytes use the LCN to communicate via autocrine and paracrine signaling, but also via direct gap junctions between cells. In Aim 1, dendrite extension was not observed to a great extent. In this second aim, OCY454 cells, which are known to produce mature osteocyte markers (*e.g.* sclerostin) after a much shorter culture period than IDG-SW3 cells, were cultured in a variety of PEG hydrogels. Physical factors, such as crosslinking density, modulus, and degradability were varied, as these factors can influence differentiation and cell spreading.[124,142] Additionally, a variety of biochemical factors were included, such as transforming growth factor-β3, collagen I, RGD, and hydroxyapatite, which are known to influence dendrite extension and osteocyte differentiation.[123,143,144] With the varying physical and biochemical factors, osteocyte differentiation gene expression and dendrite formation (via confocal microscopy) were assessed.

The third aim of this work is to elucidate the effect of culture environment on the gene expression response to Prostaglandin E2. PGE_2 is synthesized and released by osteocytes as an early response to mechanical loading,[95] but its autocrine signaling effect on osteocytes is not well understood. It is challenging to isolate the effects of PGE_2 on osteocytes *in vivo* because this molecule affects both osteoblast and osteoclast activity. Thus, osteocyte PGE_2 signaling has largely been studied *in vitro* in 2D cultures of either osteoblasts[55,65,67,73–75,89,145–148] or MLO-Y4 osteocyte-like cells.[65,66,147,149–151] Yet, these studies use cells that do not produce mature osteocyte markers (*e.g. Sost*, which encodes sclerostin) and it is known that the stage of differentiation affects cell behavior in osteoblasts and osteocytes.[65,71] Thus, we aimed to investigate if the dimensionality

(i.e., 2D vs. 3D), which greatly impacts osteocyte differentiation,[115,128,152] also impacts the osteocyte response to PGE_2. The gene expression for a variety of PGE_2-signaling, anabolic-signaling, or catabolic-signaling markers were measured after PGE_2 treatment in IDG-SW3 osteocytes cultured in 2D and 3D.

The fourth aim of this work is to develop an osteocyte 3D ex vivo model that recapitulates key aspects of osteochondral loading in osteoarthritis. Existing 3D osteocyte culture systems that succeed in mimicking aspects of *in vivo* osteocyte phenotype and incorporate mechanical stimulation are limited. No 3D models exist that adequately recapitulate physiological bone-levels of strain combined with fluid flow within the subchondral bone, while also supporting a mature osteocyte phenotype. While numerous studies use bilayer scaffolds for osteochondral defect repair models (e.g.,[153–161]), few studies examine osteocytes in these scaffolds. This aim develops a 3D hydrogel bilayer composite that supports osteocyte differentiation and bone matrix deposition in a bone-like layer. When loaded in compression, the composite design recapitulates key aspects of the osteochondral unit's complex loading environment. Specifically, the design achieves near-physiological levels of strain in combination with fluid flow.

1.6 References

1. Fuchs, R. K., Thompson, W. R. & Warden, S. J. Bone biology. in *Bone Repair Biomaterials* 15–52 (Elsevier, 2019). doi:10.1016/B978-0-08-102451-5.00002-0.

2. Burr, D. B. & Akkus, O. Bone Morphology and Organization. in *Basic and Applied Bone Biology* 3–25 (Elsevier, 2014). doi:10.1016/B978-0-12-416015-6.00001-0.

3. Boskey, A. L. & Robey, P. G. The Regulatory Role of Matrix Proteins in Mineralization of Bone. in *Osteoporosis* 235–255 (Elsevier, 2013). doi:10.1016/B978-0-12-415853-5.00011-X.

4. Qing, H. & Bonewald, L. F. Osteocyte remodeling of the perilacunar and pericanalicular matrix. *International journal of oral science* **1**, 59 (2009).

5. Yee, C. S., Schurman, C. A., White, C. R. & Alliston, T. Investigating Osteocytic Perilacunar/Canalicular Remodeling. *Curr Osteoporos Rep* **17**, 157–168 (2019).

6. Qing, H. *et al.* Demonstration of osteocytic perilacunar/canalicular remodeling in mice during lactation. *J Bone Miner Res* **27**, 1018–1029 (2012).

7. Burr, D. B. The importance of subchondral bone in osteoarthrosis: *Current Opinion in Rheumatology* **10**, 256–262 (1998).

8. Goldring, S. R. & Goldring, M. B. Changes in the osteochondral unit during osteoarthritis: structure, function and cartilage–bone crosstalk. *Nature Reviews Rheumatology* (2016) doi:10.1038/nrrheum.2016.148.

9. Findlay, D. M. & Kuliwaba, J. S. Bone–cartilage crosstalk: a conversation for understanding osteoarthritis. *Bone Research* **4**, 16028 (2016).

10. Funck-Brentano, T. & Cohen-Solal, M. Crosstalk between cartilage and bone: When bone cytokines matter. *Cytokine & Growth Factor Reviews* **22**, 91–97 (2011).

11. Hwang, J. *et al.* Increased hydraulic conductance of human articular cartilage and subchondral bone plate with progression of osteoarthritis. *Arthritis & Rheumatism* **58**, 3831–3842 (2008).

12. Stender, M. E., Regueiro, R. A. & Ferguson, V. L. A poroelastic finite element model of the bone–cartilage unit to determine the effects of changes in permeability with osteoarthritis. *Computer Methods in Biomechanics and Biomedical Engineering* 1–13 (2016) doi:10.1080/10255842.2016.1233326.

13. Stender, M. E., Carpenter, R. D., Regueiro, R. A. & Ferguson, V. L. An evolutionary model of osteoarthritis including articular cartilage damage, and bone remodeling in a computational study. *Journal of Biomechanics* (2016) doi:10.1016/j.jbiomech.2016.09.024.

14. Fritton, S. P. & Weinbaum, S. Fluid and Solute Transport in Bone: Flow-Induced Mechanotransduction. *Annual Review of Fluid Mechanics* **41**, 347–374 (2009).

15. Hemmatian, H., Bakker, A. D., Klein-Nulend, J. & van Lenthe, G. H. Aging, Osteocytes, and Mechanotransduction. *Curr Osteoporos Rep* **15**, 401–411 (2017).

16. Mazur, C. M. *et al.* Osteocyte dysfunction promotes osteoarthritis through MMP13-dependent suppression of subchondral bone homeostasis. *Bone Res* **7**, 34 (2019).

17. Beck, K. & Brodsky, B. Supercoiled Protein Motifs: The Collagen Triple-Helix and the alpha-Helical Coiled Coil. 13.

18. Marini, J. C. *et al.* Consortium for osteogenesis imperfecta mutations in the helical domain of type I collagen: regions rich in lethal mutations align with collagen binding sites for integrins and proteoglycans. *Human Mutation* **28**, 209–221 (2007).

19. Blank, R. D. & Boskey, A. L. Genetic Collagen Diseases: Influence of Collagen Mutationson Structure and Mechanical Behavior. in *Collagen: Structure and Mechanics* (ed. Fratzl, P.) 447–474 (Springer US, 2008). doi:10.1007/978-0-387-73906-9_16.

20. Traub, W., Arad, T., Vetter, U. & Weiner, S. Ultrastructural studies of bones from patients with osteogenesis imperfecta. *Matrix Biology* **14**, 337–345 (1994).

21. Vetter, U., Eanes, E. D., Kopp, J. B., Termine, J. D. & Robey, P. G. Changes in apatite crystal size in bones of patients with osteogenesis imperfecta. *Calcif Tissue Int* **49**, 248–250 (1991).

22. Boskey, A. L. Amorphous Calcium Phosphate: The Contention of Bone. *J Dent Res* **76**, 1433–1436 (1997).

23. Combes, C. & Rey, C. Amorphous calcium phosphates: Synthesis, properties and uses in biomaterials. *Acta Biomaterialia* **6**, 3362–3378 (2010).

24. Dey, A. *et al.* The role of prenucleation clusters in surface-induced calcium phosphate crystallization. *Nature Materials* **9**, 1010–1014 (2010).

25. Mahamid, J. *et al.* Mapping amorphous calcium phosphate transformation into crystalline mineral from the cell to the bone in zebrafish fin rays. *Proceedings of the National Academy of Sciences* **107**, 6316–6321 (2010).

26. Nollet, M. *et al.* Autophagy in osteoblasts is involved in mineralization and bone homeostasis. *Autophagy* **10**, 1965–1977 (2014).

27. Anderson, H. C. Matrix vesicles and calcification. *Curr Rheumatol Rep* **5**, 222–226 (2003).

28. Zhang, W., Huang, Z.-L., Liao, S.-S. & Cui, F.-Z. Nucleation sites of calcium phosphate crystals during collagen mineralization. *Journal of the American Ceramic Society* **86**, 1052–1054 (2003).

29. Magne, D., Weiss, P., Bouler, J.-M., Laboux, O. & Daculsi, G. Study of the Maturation of the Organic (Type I Collagen) and Mineral (Nonstoichiometric Apatite) Constituents of a Calcified Tissue (Dentin) as a Function of Location: A Fourier Transform Infrared Microspectroscopic Investigation. *Journal of Bone and Mineral Research* **16**, 750–757 (2001).

30. Jiao, K. *et al.* Complementarity and Uncertainty in Intrafibrillar Mineralization of Collagen. *Advanced Functional Materials* **26**, 6858–6875 (2016).

31. Niu, L.-N. *et al.* Collagen intrafibrillar mineralization as a result of the balance between osmotic equilibrium and electroneutrality. *Nat Mater* **16**, 370–378 (2017).

32. Bellido, T., Plotkin, L. I. & Bruzzaniti, A. Bone Cells. in *Basic and Applied Bone Biology* 27–45 (Elsevier, 2014). doi:10.1016/B978-0-12-416015-6.00002-2.

33. Franz-Odendaal, T. A., Hall, B. K. & Witten, P. E. Buried alive: How osteoblasts become osteocytes. *Developmental Dynamics* **235**, 176–190 (2006).

34. Palumbo, C., Palazzini, S., Zaffe, D. & Marotti, G. Osteocyte Differentiation in the Tibia of Newborn Rabbit: An Ultrastructural Study of the Formation of Cytoplasmic Processes. *Acta Anatomica* **137**, 350–358 (1990).

35. Dallas, S. L. & Bonewald, L. F. Dynamics of the transition from osteoblast to osteocyte. *Ann. N. Y. Acad. Sci.* **1192**, 437–443 (2010).

36. Noble, B. S. The osteocyte lineage. *Archives of Biochemistry and Biophysics* **473**, 106–111 (2008).

37. Bonewald, L. F. Osteocyte Biology. in *Osteoporosis* 209–234 (Elsevier, 2013). doi:10.1016/B978-0-12-415853-5.00010-8.

38. Bonewald, L. F. The amazing osteocyte. *Journal of Bone and Mineral Research* **26**, 229–238 (2011).

39. You, L.-D., Weinbaum, S., Cowin, S. C. & Schaffler, M. B. Ultrastructure of the osteocyte process and its pericellular matrix. *Anat. Rec.* **278A**, 505–513 (2004).

40. Ribeiro-Rodrigues, T. M., Martins-Marques, T., Morel, S., Kwak, B. R. & Girão, H. Role of connexin 43 in different forms of intercellular communication – gap junctions, extracellular vesicles and tunnelling nanotubes. *J Cell Sci* **130**, 3619–3630 (2017).

41. Price, C., Zhou, X., Li, W. & Wang, L. Real-Time Measurement of Solute Transport Within the Lacunar-Canalicular System of Mechanically Loaded Bone: Direct Evidence for Load-Induced Fluid Flow. *J Bone Miner Res* **26**, 277–285 (2011).

42. Dallas, S. L. & Moore, D. S. Using confocal imaging approaches to understand the structure and function of osteocytes and the lacunocanalicular network. *Bone* **138**, 115463 (2020).

43. Qin, L., Liu, W., Cao, H. & Xiao, G. Molecular mechanosensors in osteocytes. *Bone Res* **8**, 23 (2020).

44. Burra, S., Nicolella, D. P. & Jiang, J. X. Dark horse in osteocyte biology. *Commun Integr Biol* **4**, 48–50 (2011).

45. Wang, B. *et al.* Perlecan-Containing Pericellular Matrix Regulates Solute Transport and Mechanosensing Within the Osteocyte Lacunar-Canalicular System. *Journal of Bone and Mineral Research* **29**, 878–891 (2014).

46. McNamara, L. M., Majeska, R. J., Weinbaum, S., Friedrich, V. & Schaffler, M. B. Attachment of Osteocyte Cell Processes to the Bone Matrix. *The Anatomical Record* **292**, 355–363 (2009).

47. Geoghegan, I. P., Hoey, D. A. & McNamara, L. M. Integrins in Osteocyte Biology and Mechanotransduction. *Curr Osteoporos Rep* **17**, 195–206 (2019).

48. Wijeratne, S. S. *et al.* Single molecule force measurements of perlecan/HSPG2: A key component of the osteocyte pericellular matrix. *Matrix Biology* **50**, 27–38 (2016).

49. Thompson, W. R. *et al.* Perlecan/Hspg2 deficiency alters the pericellular space of the lacunocanalicular system surrounding osteocytic processes in cortical bone. *J Bone Miner Res* **26**, 618–629 (2011).

50. Cabahug-Zuckerman, P. *et al.* Potential role for a specialized β3 integrin-based structure on osteocyte processes in bone mechanosensation. *J Orthop Res* **36**, 642–652 (2018).

51. Buo, A. M. & Stains, J. P. Gap junctional regulation of signal transduction in bone cells. *FEBS Letters* **588**, 1315–1321 (2014).

52. Gupta, A. *et al.* Communication of cAMP by connexin43 gap junctions regulates osteoblast signaling and gene expression. *Cellular Signalling* **28**, 1048–1057 (2016).

53. Schaffler, M. B., Cheung, W.-Y., Majeska, R. & Kennedy, O. Osteocytes: Master Orchestrators of Bone. *Calcified Tissue International* **94**, 5–24 (2014).

54. Rath Bonivtch, A., Bonewald, L. F. & Nicolella, D. P. Tissue strain amplification at the osteocyte lacuna: A microstructural finite element analysis. *Journal of Biomechanics* **40**, 2199–2206 (2007).

55. Smalt, R., Mitchell, F. T., Howard, R. L. & Chambers, T. J. Induction of NO and prostaglandin E2 in osteoblasts by wall-shear stress but not mechanical strain. *American Journal of Physiology-Endocrinology And Metabolism* **273**, E751–E758 (1997).

56. Yu, K. *et al.* Mechanical loading disrupts osteocyte plasma membranes which initiates mechanosensation events in bone. *J Orthop Res* **36**, 653–662 (2018).

57. Malone, A. M. D. *et al.* Primary cilia mediate mechanosensing in bone cells by a calcium-independent mechanism. *Proc Natl Acad Sci U S A* **104**, 13325–13330 (2007).

58. Litzenberger, J. B., Tang, W. J., Castillo, A. B. & Jacobs, C. R. Deletion of β1 Integrins from Cortical Osteocytes Reduces Load-Induced Bone Formation. *Cel. Mol. Bioeng.* **2**, 416–424 (2009).

59. Haugh, M. G., Vaughan, T. J. & McNamara, L. M. The role of integrin α(V)β(3) in osteocyte mechanotransduction. *J Mech Behav Biomed Mater* **42**, 67–75 (2015).

60. Thi, M. M., Suadicani, S. O., Schaffler, M. B., Weinbaum, S. & Spray, D. C. Mechanosensory responses of osteocytes to physiological forces occur along processes and not cell body and require αVβ3 integrin. *PNAS* **110**, 21012–21017 (2013).

61. Wu, D., Ganatos, P., Spray, D. C. & Weinbaum, S. On the electrophysiological response of bone cells using a Stokesian fluid stimulus probe for delivery of quantifiable localized picoNewton level forces. *J Biomech* **44**, 1702–1708 (2011).

62. Wu, D., Schaffler, M. B., Weinbaum, S. & Spray, D. C. Matrix-dependent adhesion mediates network responses to physiological stimulation of the osteocyte cell process. *PNAS* **110**, 12096–12101 (2013).

63. Burra, S. *et al.* Dendritic processes of osteocytes are mechanotransducers that induce the opening of hemichannels. *PNAS* **107**, 13648–13653 (2010).

64. Robling, A. G., Fuchs, R. K. & Burr, D. B. Mechanical Adaptation. in *Basic and Applied Bone Biology* 175–204 (Elsevier, 2014). doi:10.1016/B978-0-12-416015-6.00009-5.

65. Kamel, M. A., Picconi, J. L., Lara-Castillo, N. & Johnson, M. L. Activation of B-catenin signaling in MLO-Y4 osteocytic cells versus 2T3 osteoblastic cells by fluid flow shear stress and PGE2: Implications for the study of mechanosensation in bone. *Bone* **47**, 872–881 (2010).

66. Cheng, B. *et al.* PGE2 is essential for gap junction-mediated intercellular communication between osteocyte-like MLO-Y4 cells in response to mechanical strain. *Endocrinology* **142**, 3464–3473 (2001).

67. Galea, G. L. *et al.* Sost down-regulation by mechanical strain in human osteoblastic cells involves PGE2 signaling via EP4. *FEBS Letters* **585**, 2450–2454 (2011).

68. Sugimoto, Y. & Narumiya, S. Prostaglandin E Receptors. *Journal of Biological Chemistry* **282**, 11613–11617 (2007).

69. Cherian, P. P. *et al.* Effects of Mechanical Strain on the Function of Gap Junctions in Osteocytes Are Mediated through the Prostaglandin EP2 Receptor. *Journal of Biological Chemistry* **278**, 43146–43156 (2003).

70. Cherian, P. P. *et al.* Mechanical Strain Opens Connexin 43 Hemichannels in Osteocytes: A Novel Mechanism for the Release of Prostaglandin. *MBoC* **16**, 3100–3106 (2005).

71. Westbroek, I. *et al.* Differential Stimulation of Prostaglandin G/H Synthase-2 in Osteocytes and Other Osteogenic Cells by Pulsating Fluid Flow. *Biochemical and Biophysical Research Communications* **268**, 414–419 (2000).

72. Klein-Nulend, J. *et al.* Sensitivity of osteocytes to biomechanical stress in vitro. *The FASEB Journal* **9**, 441–445 (1995).

73. Genetos, D. C., Yellowley, C. E. & Loots, G. G. Prostaglandin E2 Signals Through PTGER2 to Regulate Sclerostin Expression. *PLoS ONE* **6**, e17772 (2011).

74. Liu, X.-H., Kirschenbaum, A., Yao, S. & Levine, A. C. Interactive Effect of Interleukin-6 and Prostaglandin E2 on Osteoclastogenesis via the OPG/RANKL/RANK System. *Annals of the New York Academy of Sciences* **1068**, 225–233 (2006).

75. Kumei, Y. *et al. Microgravity induces prostaglandin E2 and interleukin-6 production in normal rat osteoblasts: role in bone demineralization*. (Elsevier, 1996).

76. Wu, Q., Zhou, X., Huang, D., Ji, Y. & Kang, F. IL-6 Enhances Osteocyte-Mediated Osteoclastogenesis by Promoting JAK2 and RANKL Activity ***In Vitro***. *Cellular Physiology and Biochemistry* **41**, 1360–1369 (2017).

77. Zhou, M., Li, S. & Pathak, J. L. Pro-inflammatory Cytokines and Osteocytes. *Curr Osteoporos Rep* **17**, 97–104 (2019).

78. Cao, J., Venton, L., Sakata, T. & Halloran, B. P. Expression of RANKL and OPG correlates with age-related bone loss in male C57BL/6 mice. *J. Bone Miner. Res.* **18**, 270–277 (2003).

79. Cabahug-Zuckerman, P. *et al.* Osteocyte Apoptosis Caused by Hindlimb Unloading is Required to Trigger Osteocyte RANKL Production and Subsequent Resorption of Cortical and Trabecular Bone in Mice Femurs. *Journal of Bone and Mineral Research* **31**, 1356–1365 (2016).

80. Nakashima, T. *et al.* Evidence for osteocyte regulation of bone homeostasis through RANKL expression. *Nature Medicine* **17**, 1231–1234 (2011).

81. Xiong, J. *et al.* Osteocytes, not Osteoblasts or Lining Cells, are the Main Source of the RANKL Required for Osteoclast Formation in Remodeling Bone. *PLoS One* **10**, (2015).

82. Xiong, J. & O'Brien, C. A. Osteocyte RANKL: New insights into the control of bone remodeling. *J Bone Miner Res* **27**, 499–505 (2012).

83. Ducy, P., Desbois, C., Boyce, B. & Pinero, G. Increased bone formation in osteocalcin-deficient mice. *Nature (London)* **382**, 448–452 (1996).

84. Zoch, M. L., Clemens, T. L. & Riddle, R. C. New insights into the biology of osteocalcin. *Bone* **82**, 42–49 (2016).

85. Winkler, D. G. *et al.* Osteocyte control of bone formation via sclerostin,a novel BMP antagonist. *EMBO J* **22**, 6267–6276 (2003).

86. Wijenayaka, A. R. *et al.* Sclerostin Stimulates Osteocyte Support of Osteoclast Activity by a RANKL-Dependent Pathway. *PLoS One* **6**, (2011).

87. Jee, W. S. S. & Ma, Y. F. The in vivo anabolic actions of prostaglandins in bone. *Bone* **21**, 297–304 (1997).

88. Ke, H. Z. *et al.* Prostaglandin E2 increases bone strength in intact rats and in ovariectomized rats with established osteopenia. *Bone* **23**, 249–255 (1998).

89. Suzuki, H. *et al.* The role of autonomously secreted PGE2 and its autocrine/paracrine effect on bone matrix mineralization at the different stages of differentiating MC3T3-E1 cells. *Biochemical and Biophysical Research Communications* **524**, 929–935 (2020).

90. Yoshida, K. *et al.* Stimulation of bone formation and prevention of bone loss by prostaglandin E EP4 receptor activation. *Proc Natl Acad Sci U S A* **99**, 4580–4585 (2002).

91. Paralkar, V. M. *et al.* An EP2 receptor-selective prostaglandin E2 agonist induces bone healing. *Proceedings of the National Academy of Sciences* **100**, 6736–6740 (2003).

92. Li, M. *et al.* A Novel, Non-Prostanoid EP2 Receptor-Selective Prostaglandin E2 Agonist Stimulates Local Bone Formation and Enhances Fracture Healing. *Journal of Bone and Mineral Research* **18**, 2033–2042 (2003).

93. Regan, J. W. EP2 and EP4 prostanoid receptor signaling. *Life Sciences* **74**, 143–153 (2003).

94. Castellone, M. D., Teramoto, H., Williams, B. O., Druey, K. M. & Gutkind, J. S. Prostaglandin E2 Promotes Colon Cancer Cell Growth Through a Gs-Axin-b-Catenin Signaling Axis. **310**, 8 (2005).

95. Kitase, Y. *et al.* Mechanical induction of PGE2 in osteocytes blocks glucocorticoid-induced apoptosis through both the β-catenin and PKA pathways. *Journal of Bone and Mineral Research* **25**, 2657–2668 (2010).

96. Fujino, H., Xu, W. & Regan, J. W. Prostaglandin E2 Induced Functional Expression of Early Growth Response Factor-1 by EP4, but Not EP2, Prostanoid Receptors via the Phosphatidylinositol 3-Kinase and Extracellular Signal-regulated Kinases. *Journal of Biological Chemistry* **278**, 12151–12156 (2003).

97. Nishigaki, N., Negishi, M. & Ichikawa, A. Two Gs-coupled prostaglandin E receptor subtypes, EP2 and EP4, differ in desensitization and sensitivity to the metabolic inactivation of the agonist. *Mol Pharmacol* **50**, 1031–1037 (1996).

98. Waclawik, A., Jabbour, H. N., Blitek, A. & Ziecik, A. J. Estradiol-17β, Prostaglandin E2 (PGE2), and the PGE2 Receptor Are Involved in PGE2 Positive Feedback Loop in the Porcine Endometrium. *Endocrinology* **150**, 3823–3832 (2009).

99. Maurel, D. B. *et al.* Characterization of a novel murine Sost ER T2 Cre model targeting osteocytes. *Bone Research* **7**, 1–13 (2019).

100. Rath Stern, A. *et al.* Isolation and culture of primary osteocytes from the long bones of skeletally mature and aged mice. *BioTechniques* **52**, (2012).

101. Torreggiani, E. *et al.* Preosteocytes/Osteocytes Have the Potential to Dedifferentiate Becoming a Source of Osteoblasts. *PLoS One* **8**, (2013).

102. Sawa, N., Fujimoto, H., Sawa, Y., Yamashita, J. & Link to external site, this link will open in a new window. Alternating Differentiation and Dedifferentiation between Mature Osteoblasts and Osteocytes. *Scientific Reports (Nature Publisher Group); London* **9**, 1–9 (2019).

103. Divieti Pajevic, P. New and Old Osteocytic Cell Lines and 3D Models. *Curr Osteoporos Rep* (2020) doi:10.1007/s11914-020-00613-3.

104. Kato, Y., Windle, J. J., Koop, B. A., Mundy, G. R. & Bonewald, L. F. Establishment of an Osteocyte-like Cell Line, MLO-Y4. *Journal of Bone and Mineral Research* **12**, 2014–2023 (1997).

105. Robling, A. G. & Bonewald, L. F. The Osteocyte: New Insights. *Annual Review of Physiology* **82**, 485–506 (2020).

106. Bodine, P. V., Vernon, S. K. & Komm, B. S. Establishment and hormonal regulation of a conditionally transformed preosteocytic cell line from adult human bone. *Endocrinology* **137**, 4592–4604 (1996).

107. Kato, Y. *et al.* Establishment of an osteoid preosteocyte-like cell MLO-A5 that spontaneously mineralizes in culture. *Journal of Bone and Mineral Research* **16**, 1622–1633 (2001).

108. Barragan-Adjemian, C. *et al.* Mechanism by which MLO-A5 Late Osteoblasts/Early Osteocytes Mineralize in Culture: Similarities with Mineralization of Lamellar Bone. *Calcif Tissue Int* **79**, 340–353 (2006).

109. Woo, S. M., Rosser, J., Dusevich, V., Kalajzic, I. & Bonewald, L. F. Cell line IDG-SW3 replicates osteoblast-to-late-osteocyte differentiation in vitro and accelerates bone formation in vivo. *J Bone Miner Res* **26**, 2634–2646 (2011).

110. Spatz, J. M. *et al.* The Wnt Inhibitor Sclerostin Is Up-regulated by Mechanical Unloading in Osteocytes in Vitro. *Journal of Biological Chemistry* **290**, 16744–16758 (2015).

111. Xu, L. H., Shao, H., Ma, Y.-H. V. & You, L. OCY454 Osteocytes as an in Vitro Cell Model for Bone Remodeling Under Mechanical Loading. *Journal of Orthopaedic Research* **0**,.

112. Wang, K. *et al.* A Novel Osteogenic Cell Line That Differentiates Into GFP-Tagged Osteocytes and Forms Mineral With a Bone-Like Lacunocanalicular Structure. *Journal of Bone and Mineral Research* **34**, 979–995 (2019).

113. Zhang, C., Bakker, A. D., Klein-Nulend, J. & Bravenboer, N. Studies on Osteocytes in Their 3D Native Matrix Versus 2D In Vitro Models. *Current Osteoporosis Reports* **17**, 207–216 (2019).

114. Vazquez, M. *et al.* A New Method to Investigate How Mechanical Loading of Osteocytes Controls Osteoblasts. *Front Endocrinol (Lausanne)* **5**, (2014).

115. Sun, Q. *et al.* Ex vivo replication of phenotypic functions of osteocytes through biomimetic 3D bone tissue construction. *Bone* **106**, 148–155 (2018).

116. Takemura, Y. *et al.* Mechanical loading induced osteocyte apoptosis and connexin 43 expression in three-dimensional cell culture and dental implant model. *Journal of Biomedical Materials Research Part A* **107**, 815–827 (2019).

117. Choudhary, S. *et al.* Hypoxic Three-Dimensional Cellular Network Construction Replicates Ex Vivo the Phenotype of Primary Human Osteocytes. *Tissue Engineering Part A* **24**, 458–468 (2018).

118. Kurata, K., Heino, T. J., Higaki, H. & Väänänen, H. K. Bone Marrow Cell Differentiation Induced by Mechanically Damaged Osteocytes in 3D Gel-Embedded Culture. *Journal of Bone and Mineral Research* **21**, 616–625 (2006).

119. Fritton, S. P., McLeod, K. J. & Rubin, C. T. Quantifying the strain history of bone: spatial uniformity and self-similarity of low-magnitude strains. *Journal of biomechanics* **33**, 317–325 (2000).

120. Brolese, E., Buser, D., Kuchler, U., Schaller, B. & Gruber, R. Human bone chips release of sclerostin and FGF-23 into the culture medium: an in vitro pilot study. *Clinical Oral Implants Research* **26**, 1211–1214 (2015).

121. Chan, M. E. *et al.* A Trabecular Bone Explant Model of Osteocyte–Osteoblast Co-Culture for Bone Mechanobiology. *Cel. Mol. Bioeng.* **2**, 405–415 (2009).

122. Takai, E., Mauck, R. L., Hung, C. T. & Guo, X. E. Osteocyte Viability and Regulation of Osteoblast Function in a 3D Trabecular Bone Explant Under Dynamic Hydrostatic Pressure. *Journal of Bone and Mineral Research* **19**, 1403–1410 (2004).

123. Bernhardt, A., Weiser, E., Wolf, S., Vater, C. & Gelinsky, M. Primary Human Osteocyte Networks in Pure and Modified Collagen Gels. *Tissue Engineering Part A* **25**, 1347–1355 (2019).

124. Mullen, C. A., Vaughan, T. J., Billiar, K. L. & McNamara, L. M. The Effect of Substrate Stiffness, Thickness, and Cross-Linking Density on Osteogenic Cell Behavior. *Biophysical Journal* **108**, 1604–1612 (2015).

125. Huebsch, N. *et al.* Harnessing traction-mediated manipulation of the cell/matrix interface to control stem-cell fate. *Nature Materials* **9**, 518–526 (2010).

126. Aisenbrey, E. A. & Bryant, S. J. The role of chondroitin sulfate in regulating hypertrophy during MSC chondrogenesis in a cartilage mimetic hydrogel under dynamic loading. *Biomaterials* **190–191**, 51–62 (2019).

127. Holmes, R. *et al.* Thiol-Ene Photo-Click Collagen-PEG Hydrogels: Impact of Water-Soluble Photoinitiators on Cell Viability, Gelation Kinetics and Rheological Properties. *Polymers* **9**, 226 (2017).

128. Boukhechba, F. *et al.* Human Primary Osteocyte Differentiation in a 3D Culture System. *Journal of Bone and Mineral Research* **24**, 1927–1935 (2009).

129. Carles-Carner, M., Saleh, L. S. & Bryant, S. J. The effects of hydroxyapatite nanoparticles embedded in a MMP-sensitive photoclickable PEG hydrogel on encapsulated MC3T3-E1 pre-osteoblasts. *Biomed. Mater.* **13**, 045009 (2018).

130. Fairbanks, B. D. *et al.* A Versatile Synthetic Extracellular Matrix Mimic via Thiol-Norbornene Photopolymerization. *Advanced Materials* **21**, 5005–5010 (2009).

131. Hoyle, C. E. & Bowman, C. N. Thiol-Ene Click Chemistry. *Angewandte Chemie International Edition* **49**, 1540–1573 (2010).

132. McKinnon, D. D., Kloxin, A. M. & Anseth, K. S. Synthetic hydrogel platform for three-dimensional culture of embryonic stem cell-derived motor neurons. *Biomaterials Science* **1**, 460 (2013).

133. Sridhar, B. V. *et al.* Development of a Cellularly Degradable PEG Hydrogel to Promote Articular Cartilage Extracellular Matrix Deposition. *Advanced Healthcare Materials* **4**, 702–713 (2015).

134. Amer, L. D. & Bryant, S. J. The In Vitro and In Vivo Response to MMP-Sensitive Poly(Ethylene Glycol) Hydrogels. *Annals of Biomedical Engineering* **44**, 1959–1969 (2016).

135. Schneider, M. C. *et al.* Local Heterogeneities Improve Matrix Connectivity in Degradable and Photoclickable Poly(ethylene glycol) Hydrogels for Applications in Tissue Engineering. *ACS Biomater. Sci. Eng.* **3**, 2480–2492 (2017).

136. Klein-Nulend, J., Bakker, A. D., Bacabac, R. G., Vatsa, A. & Weinbaum, S. Mechanosensation and transduction in osteocytes. *Bone* **54**, 182–190 (2013).

137. Spyropoulou, A., Karamesinis, K. & Basdra, E. K. Mechanotransduction pathways in bone pathobiology. *Biochimica et Biophysica Acta (BBA) - Molecular Basis of Disease* **1852**, 1700–1708 (2015).

138. Cisternas, M. G. *et al.* Alternative Methods for Defining Osteoarthritis and the Impact on Estimating Prevalence in a US Population-Based Survey. *Arthritis Care & Research* **68**, 574–580 (2016).

139. Mc Garrigle, M. J., Mullen, C. A., Haugh, M. G., Voisin, M. C. & McNamara, L. M. Osteocyte differentiation and the formation of an interconnected cellular network in vitro. *European Cells & Materials* **31**, 323–340 (2016).

140. Mullen, C. A., Haugh, M. G., Schaffler, M. B., Majeska, R. J. & McNamara, L. M. Osteocyte differentiation is regulated by extracellular matrix stiffness and intercellular separation. *Journal of the Mechanical Behavior of Biomedical Materials* **28**, 183–194 (2013).

141. Kim, K., Dean, D., Mikos, A. G. & Fisher, J. P. Effect of Initial Cell Seeding Density on Early Osteogenic Signal Expression of Rat Bone Marrow Stromal Cells Cultured on Cross-Linked Poly(propylene fumarate) Disks. *Biomacromolecules* **10**, 1810–1817 (2009).

142. Aziz, A. H. & Bryant, S. J. A comparison of human mesenchymal stem cell osteogenesis in poly(ethylene glycol) hydrogels as a function of MMP-sensitive crosslinker and crosslink density in chemically defined medium. *Biotechnology and Bioengineering* **116**, 1523–1536 (2019).

143. Kaur, K., Das, S. & Ghosh, S. Regulation of Human Osteoblast-to-Osteocyte Differentiation by Direct-Write 3D Microperiodic Hydroxyapatite Scaffolds. *ACS Omega* **4**, 1504–1515 (2019).

144. Liu, W. *et al.* TGF-β1 facilitates cell–cell communication in osteocytes via connexin43- and pannexin1-dependent gap junctions. *Cell Death Discov.* **5**, 141 (2019).

145. Lee, C. M., Genetos, D. C., You, Z. & Yellowley, C. E. Hypoxia regulates PGE2 release and EP1 receptor expression in osteoblastic cells. *Journal of Cellular Physiology* **212**, 182–188 (2007).

146. Liu, X.-H. *et al.* Prostaglandin E2 modulates components of the Wnt signaling system in bone and prostate cancer cells. *Biochemical and Biophysical Research Communications* **394**, 715–720 (2010).

147. McGarry, J. G., Klein-Nulend, J. & Prendergast, P. J. The effect of cytoskeletal disruption on pulsatile fluid flow-induced nitric oxide and prostaglandin E2 release in osteocytes and osteoblasts. *Biochemical and Biophysical Research Communications* **330**, 341–348 (2005).

148. Bakker, A. D., Soejima, K., Klein-Nulend, J. & Burger, E. H. The production of nitric oxide and prostaglandin E2 by primary bone cells is shear stress dependent. *Journal of Biomechanics* **34**, 671–677 (2001).

149. Cherian, P. P. *et al.* Mechanical strain opens connexin 43 hemichannels in osteocytes: a novel mechanism for the release of prostaglandin. *Molecular biology of the cell* **16**, 3100–3106 (2005).

150. Kitase, Y. *et al.* Mechanical induction of PGE2 in osteocytes blocks glucocorticoid-induced apoptosis through both the β-catenin and PKA pathways. *Journal of Bone and Mineral Research* **25**, 2657–2668 (2010).

151. Zhang, J.-N. *et al.* The role of the sphingosine-1-phosphate signaling pathway in osteocyte mechanotransduction. *Bone* **79**, 71–78 (2015).

152. Aziz, A. H., Wilmoth, R. L., Ferguson, V. L. & Bryant, S. J. IDG-SW3 Osteocyte Differentiation and Bone Extracellular Matrix Deposition Are Enhanced in a 3D Matrix Metalloproteinase-Sensitive Hydrogel. *ACS Appl. Bio Mater.* **3**, 1666–1680 (2020).

153. Aziz, A. H., Eckstein, K., Ferguson, V. L. & Bryant, S. J. The effects of dynamic compressive loading on human mesenchymal stem cell osteogenesis in the stiff layer of a bilayer hydrogel. *Journal of Tissue Engineering and Regenerative Medicine* **13**, 946–959 (2019).

154. Galperin, A. *et al.* Integrated Bi-Layered Scaffold for Osteochondral Tissue Engineering. *Advanced Healthcare Materials* **2**, 872–883 (2013).

155. Gan, D. *et al.* Mussel-Inspired Tough Hydrogel with In Situ Nanohydroxyapatite Mineralization for Osteochondral Defect Repair. *Advanced Healthcare Materials* **8**, 1901103 (2019).

156. Kim, B. J. *et al.* Restoration of articular osteochondral defects in rat by a bi-layered hyaluronic acid hydrogel plug with TUDCA-PLGA microsphere. *Journal of Industrial and Engineering Chemistry* **61**, 295–303 (2018).

157. Lin, D. *et al.* A viscoelastic PEGylated poly(glycerol sebacate)-based bilayer scaffold for cartilage regeneration in full-thickness osteochondral defect. *Biomaterials* **253**, 120095 (2020).

158. Liu, K., Liu, Y., Duan, Z., Ma, X. & Fan, D. A biomimetic bi-layered tissue engineering scaffolds for osteochondral defects repair. *Sci. China Technol. Sci.* (2020) doi:10.1007/s11431-020-1597-4.

159. Liu, X. *et al.* A Biomimetic Biphasic Osteochondral Scaffold with Layer-Specific Release of Stem Cell Differentiation Inducers for the Reconstruction of Osteochondral Defects. *Advanced Healthcare Materials* **n/a**, 2000076.

160. Steinmetz, N. J., Aisenbrey, E. A., Westbrook, K. K., Qi, H. J. & Bryant, S. J. Mechanical loading regulates human MSC differentiation in a multi-layer hydrogel for osteochondral tissue engineering. *Acta Biomaterialia* **21**, 142–153 (2015).

161. Zhu, X. *et al.* Biomimetic Bacterial Cellulose-Enhanced Double-Network Hydrogel with Excellent Mechanical Properties Applied for the Osteochondral Defect Repair. *ACS Biomater. Sci. Eng.* **4**, 3534–3544 (2018).

2. Osteocyte Differentiation and Bone Extracellular Matrix Deposition Are Enhanced in a 3D Matrix Metalloproteinase-Sensitive Hydrogel.

This chapter is published in full as: Aziz, A. H.[§], Wilmoth, R. L.[§], Ferguson, V. L. & Bryant, S. J. IDG-SW3 Osteocyte Differentiation and Bone Extracellular Matrix Deposition Are Enhanced in a 3D Matrix Metalloproteinase-Sensitive Hydrogel. *ACS Appl. Bio Mater.* **3**, 1666–1680 (2020).

[§]Equal contributing authors

2.1 Abstract

Osteocytes reside within a heavily mineralized matrix making them difficult to study *in vivo* and to extract for studies *in vitro.* IDG-SW3 cells are capable of producing mineralized collagen matrix and transitioning from osteoblasts to mature osteocytes, thus offering an alternative to study osteoblast to late osteocyte differentiation *in vitro*. The goal for this work was to develop a 3D degradable hydrogel to support IDG-SW3 differentiation and deposition of bone ECM. In 2D, the genes *Mmp2* and *Mmp13* increased during IDG-SW3 differentiation and were used as targets to create a MMP-sensitive poly(ethylene glycol) hydrogel containing the peptide crosslink GCGPLG-LWARCG and RGD to promote cell attachment. IDG-SW3 differentiation in the MMP-sensitive hydrogels improved over non-degradable hydrogels and standard 2D culture. Alkaline phosphatase activity at day 14 was higher, *Dmp1* and *Phex* were 8.1-fold and 3.8-fold higher, respectively, and DMP1 protein expression was more pronounced in the MMP-sensitive hydrogels compared to non-degradable hydrogels. Cell-encapsulation density (cells/ml precursor) influenced formation of dendrite-like cellular process and mineral and collagen deposition with $80x10^6$ performing better than $2x10^6$ or $20x10^6$, while connexin 43 was not affected by cell density. The cell density effects were more pronounced in the MMP-sensitive hydrogels over non-degradable hydrogels. This study identified that high cell encapsulation density and a hydrogel susceptible to

cell-mediated degradation enhanced mineralized collagen matrix and osteocyte differentiation. Overall, a promising hydrogel is presented that supports IDG-SW3 cell maturation from osteoblasts to osteocytes in 3D.

2.2 Introduction

In bone, osteocytes are the most abundant cells and are vital in regulating homeostasis and healing.[1,2] Osteocytes sense mechanical cues that transfer through the bone lacuno-canalicular network (LCN) during load-bearing activities, and in turn serve as orchestrators of bone remodeling by regulating bone formation and resorption in osteoblasts and osteoclasts.[3–5] Osteocytes arise from osteoblasts; when osteoblasts become encased in newly formed osteoid, the entrapped cells form dendrites that extend towards the mineralizing front or vascular space.[6] The osteocyte dendritic processes facilitate cellular communication throughout bony tissue by creating a highly interconnected, three-dimensional (3D) cellular network.[6–8] While our understanding of osteocyte biology and function is improving, our understanding is far from complete. Novel *in vivo* studies have shed some light on osteocyte mechanisms (e.g.,[9–13]), but such studies are difficult and costly. *In vitro* models that support the mature osteocyte phenotype and mimic *in vivo* conditions are thus needed to study osteocyte function in a controlled environment.[14]

The location of osteocytes within the mineralized matrix of bone makes primary osteocyte isolation and culture particularly challenging.[15] As an alternative, osteocyte-related cell lines enable *in vitro* study of osteocytes, such as studying the mechanisms by which osteocytes mineralize bone [16] or respond to fluid shear stress.[17] MLO-Y4 cells exhibit osteocyte properties including a dendritic morphology concomitant with high expression of osteocalcin, low expression of the osteoblast marker, alkaline phosphatase, but limited ability to mineralize.[18] MLO-A5 cells exhibit a post-osteoblast phenotype with high alkaline phosphatase and rapid mineralization.

However, both these osteocyte-related cell lines lack markers of mature osteocytes, such as *Dmp1* (encoding for dentine matrix protein 1) and *Phex* (encoding for phosphate-regulating neutral endopeptidase, X-linked).[19]

More recently, the murine IDG-SW3 cell line was developed to study the transition from osteoblasts to osteocytes.[20] IDG-SW3 cells cultured on collagen-coated plates showed up-regulation of mature osteocyte markers, including *Dmp1* and *Phex*, and produced a mineralized matrix.[20] Recent 2D studies have investigated IDG-SW3 expression of mature osteocyte markers in response to various physical, biochemical, and mechanical cues (e.g.,[21–25]). These types of studies were previously not possible due to the limitations of the other osteocyte-related cell lines. However, to date, IDG-SW3 osteocyte maturation has not yet been achieved and fully characterized in a 3D environment.

Three-dimensional, rather than two-dimensional, environments more accurately resemble the native tissue networking of cells.[26,27] Various studies have shown that osteocyte differentiation is significantly improved when cultured in 3D.[28–31] For example, primary human osteoblasts cultured on a biphasic calcium phosphate porous scaffold showed up-regulation of several osteocyte-related genes within two weeks of culture including *Dmp1* and *Phex*.[28] The expression of these genes was either low or undetectable in 2D cultures. Pre-osteoblastic MC3T3-E1 cells were shown to differentiate towards an osteocyte phenotype *in vitro*, but only after migrating into a 3D collagen hydrogel.[31] These studies indicate that osteocytes will maintain their *in vivo* phenotype, but only if cultured in 3D. To relate findings from *in vitro* studies to the *in vivo* environment, 3D culture systems are important. Some studies have established 3D cultures for osteoblasts and early osteocytes using scaffolds such as collagen type I hydrogels or microbeads (e.g.[13,32–34]), but there are few 3D models that support mature osteocyte differentiation using late

osteocyte cell lines, and, to date, there are no known 3D tunable hydrogel systems that support IDG-SW3 culture.

The goal of this study is to develop and characterize a hydrogel system that supports the transition from osteoblasts to osteocytes in a 3D environment. A poly(ethylene glycol) (PEG) hydrogel based on the thiol-norbornene photoclick chemistry was chosen for its cytocompatibility, tunability, and ease with which peptides are incorporated.[35] Specifically, cell adhesion peptides and matrix metalloproteinase (MMP)-sensitive crosslinks were introduced into the hydrogel. Given the tight polymer mesh of the hydrogel, cell-mediated degradation is important for the extension of cellular processes, such as dendrites, and formation of cell-cell contacts.[36] Moreover, studies have reported that incorporating MMP-sensitive crosslinks into a hydrogel enhanced osteogenesis,[37,38] supported ECM deposition,[37,38] and was biocompatible in a subcutaneous implant.[38] To develop this hydrogel system, this study focused on three aims. The first aim was to identify a MMP-sensitive hydrogel, which would support IDG-SW3 cell-mediated degradation. To this end, several MMPs were investigated for their known roles in bone development and homeostasis and include MMP 2,9,13 and 14.[39] The second aim was to assess IDG-SW3 differentiation within the MMP-sensitive degradable hydrogel and compare to a non-degradable hydrogel and 2D culture on tissue culture polystyrene (TCPS). The final aim examined the effect of cell encapsulation density on cellular morphology and bone ECM deposition. In particular, cell density has been identified as a key regulator of osteoblast-to-osteocyte differentiation[30,40,41] and will influence cell-cell contacts as well as the amount of total ECM deposited. Overall, this study identified a promising hydrogel for IDG-SW3 culture in 3D that can be degraded by the encapsulated IDG-SW3 cells and which supports bone extracellular matrix deposition and mature osteocyte differentiation.

2.3 Experimental Section

2.3.1 2D Cell Culture

IDG-SW3 cells (Kerafast, Inc., Boston, MA) are engineered with GFP expression under the control of the dentin matrix acidic phosphoprotein 1 (DMP1) promoter. The cells are also engineered to proliferate and remain immortal under interferon-gamma (INF-γ) at 33°C. When INF-γ is removed from the culture, and the cells are cultured in osteogenic media at 37°C, they revert to their *in vivo* phenotype of late osteoblasts and are capable of differentiating to osteocytes [20]. IDG-SW3 cells were expanded in culture medium consisting of Modified Essential Medium (MEM) α containing L-glutamine and deoxyribonucleosides (Gibco) supplemented with 10% FBS (Atlanta Biologicals), 30 U/ml recombinant mouse interferon-gamma (INF-γ) (Peprotech), and penicillin/streptomycin/ amphotericin B (PSF, Invitrogen). The cells were seeded at a density of 3000 cells/cm^2 on to T-225 tissue culture polystyrene flasks that were coated with rat-tail collagen type-1 (Sigma-Aldrich). The cells were expanded in a regulated incubator at 33°C with 5% CO_2. Medium was replaced thrice weekly. Cells were treated with trypsin and passaged at ~80-90% confluency.

To induce osteogenesis, cells were plated on collagen type I-coated surfaces at 80,000 cells/cm^2 and cultured under osteogenic conditions and at 37°C. This process involved the removal of IFN-γ from the culture medium, and the introduction of 50 mg/mL of ascorbic acid and 4 mM β-glycerophosphate to the culture medium.

2.3.2 3D Hydrogel Formation and Culture

An 8-arm PEG with terminal amines (20,000 g/mol; JenKem Technology USA, Plano, TX) was functionalized with norbornenes by reacting 5-norbornene-2-carboxylic acid (Sigma-Aldrich, St. Louis, MO) with 2-(1H-7-azabenzotriazol-1-yl)-1,1,3,3-tetramethyl uranium

hexafluorophosphate methanaminium (Chem-Impex International, Inc., Wool Dale, IL), and N,N-diisopropylethylamine (Chem-Impex) in dimethylformamide (DMF)/ dichloromethane (DCM) (Sigma-Aldrich). The reaction was carried out overnight at room temperature under inert atmosphere. The product was precipitated in diethyl ether (Sigma-Aldrich), filtered, dialyzed, and lyophilized. The extent of conjugation of norbornene to each arm of the 8-arm PEG-amine was determined to be 92% using ^{1}H NMR by comparing the protons across the carbon-carbon double bond in the norbornene to the methylene protons in PEG. Two different crosslinkers were used: a non-degradable PEG-dithiol (1000 g/mol; Sigma-Aldrich) and an MMP-sensitive peptide with the amino acid sequence GCGPLG-LWARCG (GenScript) containing two cysteines. CRGDS (GenScript), which contains one cysteine for tethering, was also introduced as the cell adhesion peptide.

For cell encapsulation studies, MMP-sensitive, degradable hydrogels were formed from a precursor solution consisting of 6.5% (w/w) 8-arm PEG-norbornene, MMP-sensitive peptide at 0.65:1 thiol:ene ratio, 2 mM CRDGS, and 0.05% (w/w) photoinitiator, 1-(4-(2- Hydroxyethoxy)-phenyl)-2-hydroxy-2-methyl-1-propane-1-one (I2959; BASF, Tarrytown, NY), in phosphate-buffered saline (PBS). Non-degradable hydrogels were formed from a precursor solution consisting of 7% (w/w) 8-arm PEG-norbornene, PEG dithiol (1000 g/mol) at 0.5:1 thiol:ene, 2 mM CRGDS, and 0.05% (w/w) photoinitiator in PBS. The non-degradable hydrogel formulation was chosen to achieve a compressive modulus that was close to the MMP-sensitive hydrogel, with an acellular compressive modulus of 10 (1) kPa and 8 (1) kPa for the non-degradable and MMP-sensitive hydrogel formulations, respectively. Murine IDG-SW3 cells were encapsulated into the MMP-sensitive and non-degradable hydrogels at cell concentrations of (1) low, $2x10^{6}$ cells/mL, (2) medium, $20x10^{6}$ cells/mL, and (3) high, $80x10^{6}$ cells/mL. All hydrogels were

photopolymerized for 10 minutes with 352 nm light at 5–10 mW/cm^2 in molds that were 3 mm in diameter and 3 mm in height and immediately cultured in osteogenic differentiation media.

2.3.3 Acellular Hydrogel Degradation

Acellular, MMP-sensitive, degradable hydrogels were formed from a precursor solution consisting of 4.5% (w/w) 8-arm PEG-norbornene, MMP-sensitive peptide at 0.65:1 thiol:ene ratio, and 0.05% I2959 in PBS using the same molds and photopolymerization method as described above. A lower concentration of 8-arm PEG-norbornene was chosen to shorten the time of degradation. A solution of 10 nM MMP-13 or 11.1 nM MMP-2 (Calbiochem, EMD Millipore) was prepared in a buffer consisting of 50mM (4-(2-hydroxyethyl)-1-piperazineethanesulfonic acid) (Corning), 10mM $CaCl_2$ (Thermo Fisher Scientific), 20% glycerol (Mallinckrodt Chemicals), and 0.005% BRIJ-35 (Alfa Aesar). Hydrogels were placed initially in this buffer but without MMP and allowed to swell to equilibrium at 37˚C for 48 hours. After equilibrium swelling, the buffer solution was replaced with new buffer solution containing either MMP-13 or MMP-2 and incubated at 37 ˚C. Every 24 hours for 3 days, the enzyme solution was refreshed, and samples were collected, weighed, tested for compressive modulus, and then lyophilized.

2.3.4 GFP Expression

GFP-expressing DMP-1 was monitored over culture time up to 30 days by fluorescence microscopy (EVOS FL Imaging System; Life Technologies) and image acquisition using a camera (Sony ICX445 monochrome CCD camera) in the 2D cultures. At day 28, intact hydrogels were imaged by confocal microscopy (Zeiss LSM 5 Pascal system using a Zeiss Axiovert microscope). In the 2D culture experiment, the corresponding bright field images were also acquired.

2.3.5 Gene Expression

In the 2D experiment for the first study of the paper (Figure 2.1), samples were collected at days 1, 4, 14, 21 and 35, and the cells were lysed directly in the well plates with TRK lysis buffer (Omega) and stored at -80°C. In the 2D experiment for the second study of the paper (Figure 2.3), samples were collected at days 1, 7, 14, and 28. In the 3D culture experiments, samples were collected at days 1, 7, 14, and 28, placed in TRK lysis buffer (Omega) and stored at -80°C. Samples were disrupted using a tissue lyser (Qiagen), and RNA was isolated using E.Z.N.A. microelute kit (Omega) per the manufacturer instructions. The amount of pure RNA was quantified using a Nanodrop instrument (ND-1000, Thermo Scientific) with A260/280 greater than 1.90. Purified RNA was reverse transcribed into cDNA using a High Capacity cDNA Reverse Transcription Kit (Applied Biosystems) per the manufacturer instructions. Samples were analyzed by qPCR with Fast SYBR Green Master Mix (Applied Biosystems) on a 7500 Fast system (Applied Biosystems). Custom primers were designed using Primer Express 3.0 software (Applied Biosystems) and were evaluated for efficiency. Primer sequences, efficiencies, and accession numbers are listed in Table 2.1. Data are presented as relative expression (RE) to the housekeeping gene L32 given by

$$Relative\ Expression\ (RE) = E_{HKG}^{C_{t(HKG)}} / E_{GOI}^{C_{t(GOI)}}$$

where *E* is the true primer efficiency, HKG is the housekeeping gene, GOI is the gene of interest, and C_t is the cycle number where the sample crosses the threshold. Data are also presented as normalized expression (NE) given by

$$NE = (E_{GOI})^{\Delta C_{t,GOI}(control-sample)} / (E_{HKG})^{\Delta C_{t,HKG}(control-sample)}$$

where the gene expression of the sample is normalized to a control, as described in the text.

Table 2.1: Primer sequences, accession numbers, and efficiencies for each gene used in this study.

Gene	Forward Primer	Reverse Primer	Accession #	Efficiency
L32	CCATCTGTTTT ACGGCATCATG	TGAACTTCTTGG TCCTCTTTTTGA	NM_172086	1.83
Dmp1	GCTTCTCTGA GATCCCTCTTCG	GCGATTCCTC TACCCTCTCT	NM_016779.2	1.97
Phex	CAACGTTCC GCGGTCAATAC	GTGTTGCTTGGT CCAGCTTC	NM_011077.2	1.88
Mmp2	AACGGTCGGG AATACAGCAG	GTAAACAAGGC TTCATGGGGG	NM_008610.3	1.91
Mmp9	GCCGACTTT TGTGGTCTTCC	TACAAGTATGC CTCTGCCAGC	NM_013599.4	1.96
Mmp13	GGAGCCCTG ATGTTTCCCAT	GTCTTCATCGC CTGGACCATA	NM_008607.2	1.88
Mmp14	GCCCTCTGTC CCAGATAAGC	ACCATCGCTCC TTGAAGACA	NM_008608.4	2.00

2.3.6 Alkaline Phosphatase Activity

Hydrogel specimens were removed from culture at 1, 14 and 28 days and rinsed in PBS for 1 hour, lysed in deionized water (diH_2O), frozen in liquid nitrogen, and stored at -80°C. Samples were disrupted using a tissue lyser (Qiagen), then subjected to freeze-thaw-sonicate cycles to lyse the cells. DNA content was measured using a Quant-iT PicoGreen dsDNA Assay Kit (Thermo Fisher Scientific) by fluorescence with an excitation at 485 nm and emission at 520 nm according manufacturer specifications. Alkaline phosphatase activity was determined by measuring the number of moles of p-nitrophenol phosphate catalyzed to p-nitrophenol, which was measured by absorbance at 450 nm using a spectrophotometer.

2.3.7 Cell Viability and Morphology in 3D Hydrogels

The viability and morphology of encapsulated IDG-SW3 cells were assessed using a live/dead assay based on Calcein AM (Corning), which stains the cytosol of live cells, and ethidium homodimer (Corning), which enters the nucleus of compromised cells and stains DNA.

Hydrogels were incubated with 4 μM Calcein AM and 2 μM ethidium homodimer for 10 minutes. The GFP expression could not be distinguished from the cytosolic stain of Calcein, but the latter will stain all live cells. Qualitative assessment of dead cells was not affected by GFP expression. Intact hydrogels were imaged by confocal microscopy (Zeiss LSM 5 Pascal system using a Zeiss Axiovert microscope).

2.3.8 Immunohistochemistry and Histology

Hydrogel specimen were removed from culture at day 28, fixed immediately in 4% paraformaldehyde at 4°C for 24 hours, dehydrated, paraffin embedded, and sectioned to 10 μm thickness. For connexin 43 staining, sections were treated with an antigen retrieval (Retrivagen A, BD Biosciences), blocked for 2 hours at room temperature with 10% normal goat serum, 2% bovine serum albumin, and 0.25% triton X-100 in PBS. Sections were then treated with the primary antibody to connexin 43 (ab11370, Abcam) at 1:1000 overnight at 4°C. An Alexa Fluor 546 goat anti-rabbit secondary (4 μg/mL; Life Technologies) was applied for 1 hour at room temperature. Sections were also stained with von Kossa and counterstained with nuclear red, according to standard protocols and imaged using light microscopy (Zeiss Axioskop 40) with either a 20x or 40x objective and a digital camera (Diagnostic Instruments, MN 14.2 Color Mosaic) using SPOT Software v. 4.6. For collagen type I, sections were enzyme treated with pepsin (280 kU), protease (400 U) and 0.25% trypsin and EDTA for 1 hour at 37°C. Sections were treated for antigen retrieval as described above and then blocked with 1% BSA and permeabilized with 1% BSA 0.25% Triton-X-100. Sections were treated with primary anti-collagen type I (Abcam ab34710) at 1:50 overnight at 4°C followed by treatment with Alexa Fluor 546 goat anti-rabbit secondary (4 μg/mL; Life Technologies) for 1 hour at room temperature. Both connexin 43 and collagen type I stained sections were counterstained with 4,6-diamidino-2-phenylindole (DAPI) for nucleus

detection and then imaged by confocal microscopy (Nikon A1R Confocal System) with a 40x or 60x objective and NIS-Elements Confocal software.

The immunohistochemistry microscopy images for connexin 43 and collagen type I were quantitated using Image J. For each image (n = 3 per group for connexin 43, n = 9 per group for collagen I), the blue (DAPI) channel and red (connexin 43 or collagen I) channel were converted to binary using the same threshold value for each respective channel. The number of nuclei per image was counted using Analyze Particles with the size range of 10 – infinity μm^2. The percent total area of red connexin 43 or collagen I staining were calculated using Analyze Particles with the size range of 0 – infinity μm^2.

2.3.9 Biochemical Assays

Hydrogel specimens were removed from culture at 28 days and subsequently rinsed in PBS for 1 hour, lysed in diH_2O, frozen in liquid nitrogen, and stored at -80°C. Samples were disrupted using a tissue lyser (Qiagen) and subjected to freeze-thaw-sonicate cycles. A known amount of sample was measured for calcium content using the Calcium (CPC) Liquicolor® Assay (Stanbio) according to manufacturer specifications, with absorbance measured at 540 nm. Hydroxyproline, an amino acid in high abundance in collagen, was measured. A known amount of sample was hydrolyzed in 6 M hydrochloric acid for 3 hours at 120°C, prior to being reacted with 4-(dimethylamino)benzaldehyde in a chloramine-T/oxidation buffer for 90 min. Absorbance was measured at 570 nm using a spectrophotometer and normalized to a baseline at 620 nm.

2.3.10 Mechanical Testing of 3D Hydrogel Constructs

Mechanical testing was conducted on a Mechanical Testing System Insight II (MTS; Eden Prairie, MN) in unconfined compression acellular hydrogels were tested in their swollen state with

a 2 N load cell. Testing was performed with the top platen out-of-contact with the hydrogel and then a constant displacement rate of 1.2 mm/min until an approximate 50% strain (based on the initial height of the hydrogel) was reached. The point of contact was determined using MATLAB. The compressive modulus was calculated from the slope of the linear region of the engineering stress-strain curve between 10 and 15% strain.

For mechanical testing of cellular hydrogels, the specimens were removed from culture at days 14, 21 and 28 for mechanical assessment. A 2 mN pre-load was used to establish consistent contact with each sample. Hydrogels were then compressed at a constant displacement rate of 0.5 mm/min to 15% strain. The compressive modulus was calculated as described above between 10 and 15% strain.

2.3.11 Statistical Analysis

Statistical analysis was performed using Real Statistics add-in for Excel. ANOVAs were performed with $\alpha = 0.05$ where factors included time, culture condition, and/or cell encapsulation density as described in the results. If significant interactions between factors were observed, follow-up one-way ANOVAs were performed holding each factor constant. Post-hoc analysis was performed using Tukey's HSD and $\alpha = 0.05$. In comparisons that were limited to two groups, a Student's t-test was performed assuming independent samples and equal variances. *P*-values from the one-way ANOVAs are provided to indicate the level of significance with $p < 0.05$ being considered statistically significant. Data were confirmed to follow a normal distribution and exhibit homogeneous variance. All numerical results are presented as mean with standard deviation listed parenthetically in the text. Graphical results are presented as mean with standard deviation as error bars. The sample size was n = 3 unless otherwise noted.

2.4 Results

2.4.1 IDG-SW3 Differentiation In 2D Culture and MMP Gene Expression Profiles

IDG-SW3 cells were cultured in 2D on collagen-coated TCPS and analyzed over the course of a 35-day study using the study design in Figure 2.1A. Differentiation was confirmed by GFP expression indicating activity by the DMP-1 promoter. Brightfield images and corresponding fluorescent microscopy images are shown over time (Figure 2.1B). The cells were confluent by day 7 and remained confluent through the experiment. There was minimal expression of GFP detected on days 7 and 10. Qualitatively by day 14, GFP was noticeable in a small number of cells. By day 21, GFP was more prevalent and remained consistent at day 30.

Relative expression for genes encoding matrix degradative enzymes *Mmp2*, *Mmp9*, *Mmp13*, and *Mmp14* was assessed as a function of culture time (Figure 2.1C). Comparing MMP type at each time-point revealed a dynamic pattern of *Mmp* expression. At day 1, relative expression for *Mmp2* was highest ($p < 0.001$) when compared to the other three MMPs, which continued through day 21. *Mmp9* and *Mmp13* relative expression levels were not different from each other and were the lowest of the MMPs at day 1. By day 35, *Mmp2* and *Mmp13* relative expressions were not significantly different from each other, but both were higher ($p < 0.001$) than *Mmp9* and *Mmp14*.

Relative expression for each MMP type was normalized to its expression level prior to the initiation of differentiation (i.e., day 1) and shown as a function of culture time (Figure 2.1D). Normalized expression levels increased from day 1 to 4 by 1.7-fold ($p = 0.005$) for *Mmp2*, 1.9-fold ($p < 0.001$) for *Mmp9*, and 1.8-fold ($p = 0.025$) for *Mmp14*. By day 35, *Mmp2* and *Mmp14* normalized expression levels returned to levels that were not significantly different from their day 1 values. *Mmp9* levels remained elevated, but no further increase was observed after day 4. On the

contrary, *Mmp13* normalized expression exhibited a distinctly different expression profile than the other MMPs. *Mmp13* expression significantly increased at each time point resulting in a 200-fold increase ($p < 0.001$) from day 1 to day 35. Collectively, these results demonstrate that *Mmp2* expression is high in the IDG-SW3 cells prior to osteocyte differentiation and is maintained during differentiation. In contrast, *Mmp13* expression is low prior to differentiation and increases with osteocyte differentiation.

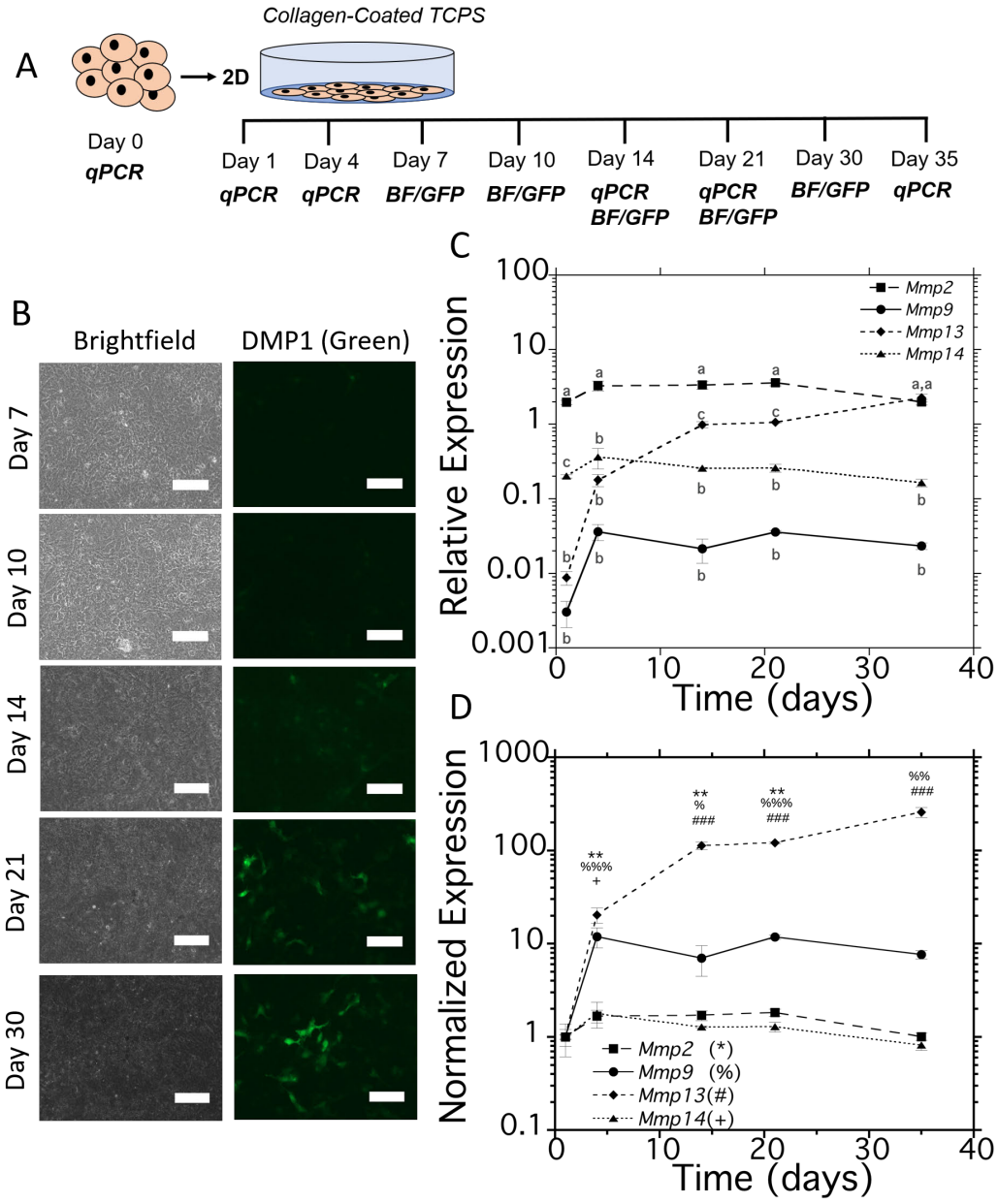

Figure 2.1: A) Schematic of 2D experiment. B) Brightfield fluorescence images and fluorescent microscopy images depicting the expression of DMP-1 (green) in IDG-SW3 cells cultured on collagen type-1 coated tissue culture polystyrene on days 7, 10, 14, 21, and 30 of osteogenic differentiation. Scale bar is 150 μm. C) Relative and D) Normalized gene expression of *Mmp2*, *Mmp9*, *Mmp13*, and *Mmp14* genes expressed in IDG-SW3 cells cultured on collagen type-1 coated tissue culture polystyrene on days 1, 4, 14, 21, and 35 of osteogenic differentiation. For RE, letter symbols denote significance between MMPs at each time point. For normalized expression, symbols represent significance from day 1 for a given MMP and are shown in the legend for each MMP.

2.4.2 Acellular Characterization of an MMP-Sensitive PEG Hydrogel.

MMP-sensitive PEG hydrogels were formed via the photoclick reaction between thiols and norbornene functionalized monomers (Figure 2.2A, B). We chose the peptide sequence GPLG-LWAR for the crosslinker because it was previously identified for its specificity for MMP-13.[42] Degradation occurs via an enzyme-catalyzed hydrolysis of the peptide bond. Acellular hydrogels exposed to exogenous MMP-2 and MMP-13 was assessed by the compressive modulus (Figure 2.2C). The compressive modulus decreased ($p < 0.001$) in the first day for both MMP-2 and MMP-13 exogenous treatment. The hydrogels exposed to MMP-2 degraded more rapidly by day 2, as shown by the lower ($p = 0.025$) modulus as compared to MMP-13. However, by day 3, hydrogels exposed to MMP-2 and MMP-13 were not significantly different.

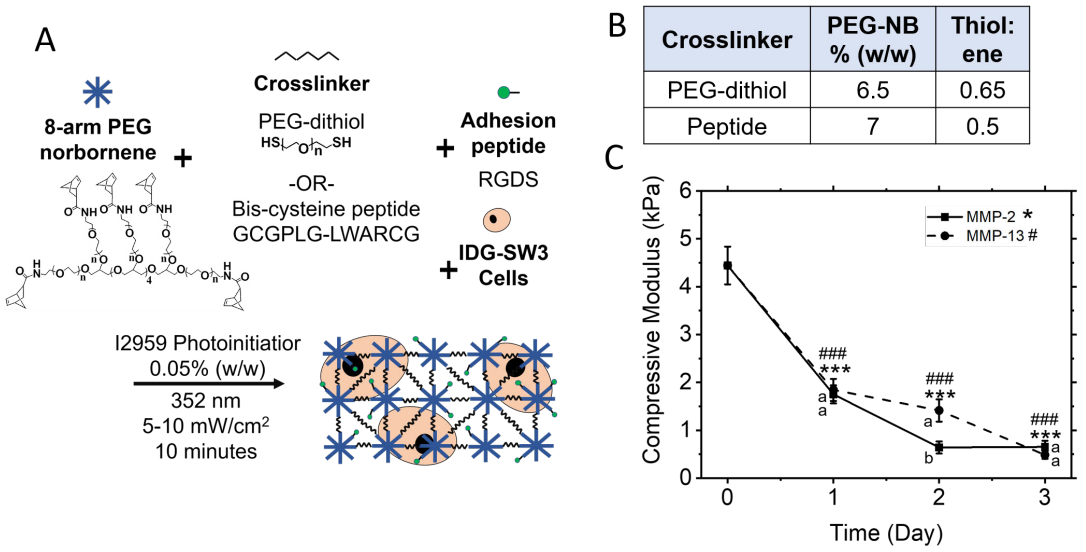

Figure 2.2: A) Schematic of hydrogel formation and cell encapsulation by a photoclickable thiol:norbornene reaction. Non-degradable hydrogels were formed by reacting monomers of eight-arm PEG-norbornene (PEG-NB) with crosslinkers of PEG-dithiol. MMP-sensitive hydrogels were formed by reacting PEG-NB with a bis-cysteine peptide sequence shown. Both non-degradable and MMP-sensitive hydrogels had the same molar concentration of RGDS and weight percent of I2959 Photoinitiator. B) The PEG-NB weight percent and thiol:ene molar ratio used to form the hydrogels. C) Compressive modulus of acellular MMP-sensitive hydrogels when exposed to exogenous MMP treatment for 3 days. Symbols represent significance from day 0 and are shown in legend for each MMP treatment; one symbol $p<0.05$; two symbols $p<0.01$; three symbols $p<0.001$. Letter symbols denote significance between MMP treatment each day.

2.4.3 IDG-SW3 Differentiation in 3D MMP-Sensitive Hydrogels.

IDG-SW3 cells were cultured under three conditions: (1) 2D collagen-coated TCPS, (2) 3D non-degradable hydrogels, and (3) 3D MMP-sensitive hydrogels. The study design is shown in Figure 2.3A. The high cell encapsulation density ($80x10^6$ cells/mL) was used for this study. The effect of culture condition on osteocyte differentiation over time was assessed by alkaline phosphatase activity, expression of the osteocytic genes, *Dmp1* and *Phex*, and GFP expression associated with DMP1 (Figure 2.3B-E).

Alkaline phosphatase (ALP) activity was assessed as a function of time and culture condition (Figure 2.3B). Considering time as the only factor, ALP activity in 2D culture increased ($p < 0.001$) from day 1 to 14 and then decreased ($p = 0.025$) by day 28 where mean ALP levels were greater ($p = 0.06$) than levels from day 1. Similar findings were observed for ALP activity from the 3D culture in non-degradable hydrogels, but day 28 levels were not different from day 1. In MMP-sensitive hydrogels, ALP activity also reached its highest level at day 14 when compared to day 1 ($p < 0.001$) and day 28 ($p < 0.009$) with levels remaining higher ($p = 0.03$) than day 1 at day 28. At day 14, ALP activity was 2.4- ($p = 0.01$) and 3.7- ($p = 0.003$) fold higher in the MMP-sensitive hydrogels compared to the 2D culture and 3D culture in non-degradable hydrogels, respectively. There were no differences between the 2D culture and the 3D culture in non-degradable hydrogels at any time point. Although the magnitude of ALP activity was lower at day 28, similar trends were observed between culture conditions as in day 14.

Dmp1 expression is normalized to that of the pre-encapsulated cells (Figure 2.3C). Considering time as the only factor, *Dmp1* levels in 2D culture increased ($p = 0.001$) with time resulting in a 2200-fold change from day 1 to 28. In 3D culture non-degradable hydrogels, *Dmp1* levels increased ($p < 0.001$) from day 1 to 14 and then decreased ($p < 0.001$) from day 14 to 28 to

levels that were not significantly different from day 1. For the MMP-sensitive hydrogels, *Dmp1* levels increased ($p < 0.001$) by 2500-fold from day 1 to 28. Considering culture condition as the only factor, *Dmp1* normalized levels at day 28 were 2.9- ($p = 0.016$) and 8.1- ($p = 0.004$) fold higher in the MMP-sensitive hydrogel compared to the 2D culture and 3D culture non- degradable hydrogels, respectively.

Phex expression is also shown as normalized to that of the pre-encapsulated cells (Figure 2.3D). Considering time as the only factor, *Phex* levels in 2D culture increased ($p = 0.015$) from day 1 to 14, but by day 28 were not significantly different from day 1. In 3D culture non-degradable hydrogels, *Phex* levels increased ($p = 0.005$) from day 1 to 14 and then decreased ($p = 0.049$) from day 14 to 28 to levels that were not significantly different from day 1. For the MMP-sensitive hydrogels, *Phex* levels increased ($p < 0.001$) by 140-fold from day 1 to 28. Considering culture condition as the only factor, *Phex* levels at day 28 were 3.2- ($p = 0.005$) and 3.8- ($p = 0.004$) fold higher in the MMP-sensitive hydrogel compared to the 2D culture and 3D culture non-degradable hydrogels, respectively.

Activity of the DMP-1 promoter was confirmed by the presence of GFP in the cells in 3D culture in the non-degradable and the MMP-sensitive hydrogels (Figure 2.3E). At day 28, a few cells expressed GFP in the non-degradable hydrogel, while many cells expressed GFP in the MMP-sensitive hydrogel. Qualitatively, there appeared to be more GFP+ cells in the MMP-sensitive hydrogel, but quantification was not performed. Collectively, these results along with gene expression and ALP activity demonstrate that osteocyte differentiation is improved in the MMP-sensitive hydrogels over 3D culture in non-degradable hydrogels and the 2D cultures.

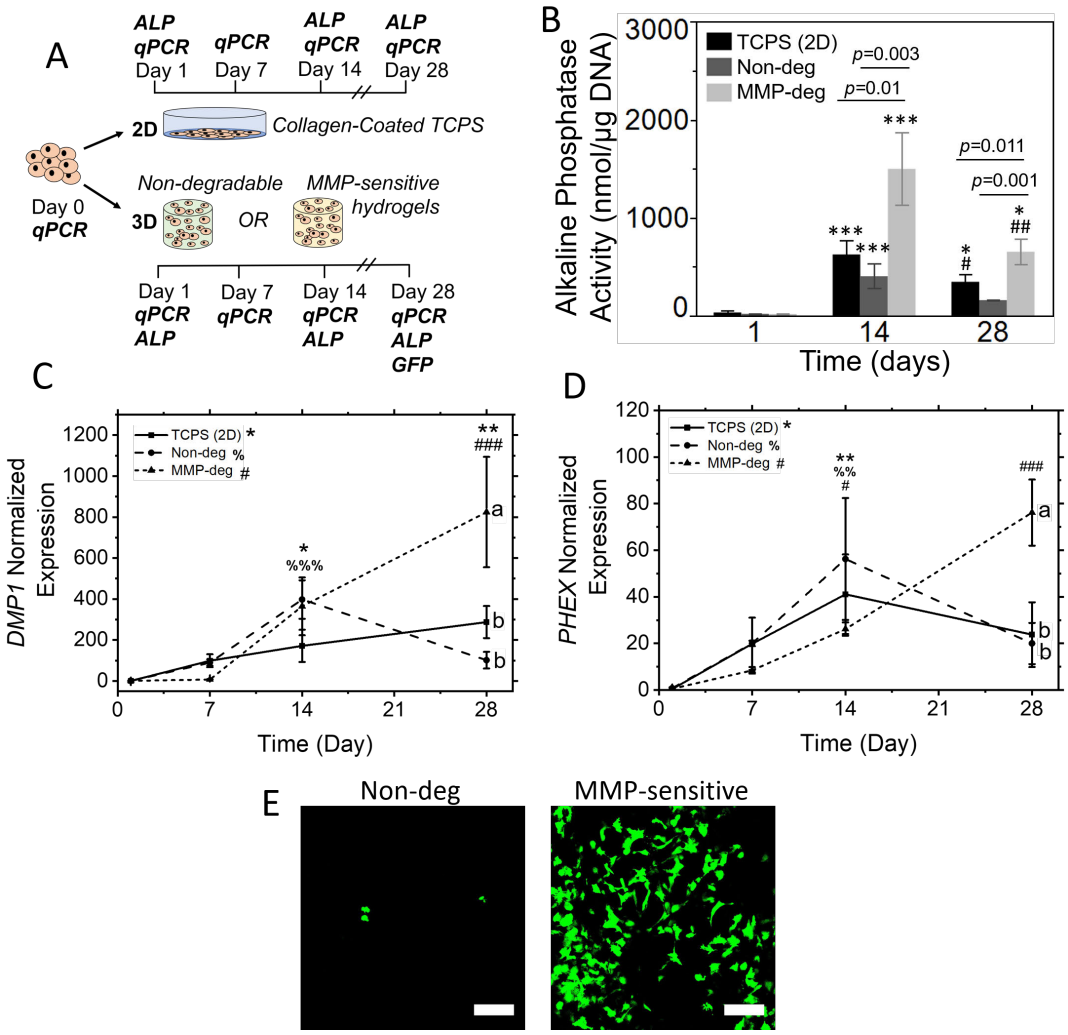

Figure 2.3 A) Schematic showing study outline. The high encapsulation density ($80x10^6$ cells/ml) was used in this study. Abbreviations are as follows: ALP = Alkaline Phosphatase Assay, qPCR = quantitative Polymerase Chain Reaction, GFP = DMP-1 Green Fluorescent Protein positive imaging. B) ALP Activity as a function of culture condition. * is difference from day 1, # is difference from day 14. one symbol is $p<0.05$, two symbols is $p<0.01$, three symbols is $p<0.001$. C&D) Normalized gene expression for (C) *Dmp1* and (D) *Phex* expressed in IDG-SW3 cells at days 1, 7, 14 and 28 in osteogenic differentiation media and encapsulated at high cell seeding density in MMP-deg (dotted) hydrogels, Non-deg (dashed) hydrogels and collagen type-1 coated tissue-culture polystyrene (solid). Normalized expression is the relative expression that is normalized to the Day 0 trypsin-treated cells prior to adding in differentiation media and encapsulating in hydrogels. Symbols represent significance from day 1 for a given culture condition; one symbol $p<0.05$; two symbols $p<0.01$; three symbols $p<0.001$; symbols are shown in legend for each condition. Letter symbols denote significance between culture conditions at Day 28 (a's are statistically different from b's; b's are not statistically different from each other). E) Confocal images depicting live IDG-SW3 cells at day 28 expressing DMP-1 GFP (green) cultured in osteogenic differentiation media and encapsulated at high cell seeding density in non-degradable PEG (left) and MMP-sensitive (right) hydrogels. Scale bar is 150 µm.

2.4.4 The Effect of IDG-SW3 Cell Encapsulation Density and Hydrogel Type on Osteocyte Morphology and Bone ECM Deposition

After confirming that IDG-SW3 cells underwent osteocyte differentiation in the MMP-sensitive hydrogels, we next investigated if cell density within the hydrogels influenced differentiation and bone ECM deposition (study design in Figure 2.4). The effect of cell encapsulation density and hydrogel type (MMP-sensitive vs non-degradable) was assessed for cellular morphology that included formation of dendrite-like processes and connexin 43 staining, matrix mineralization, collagen deposition, and compressive modulus.

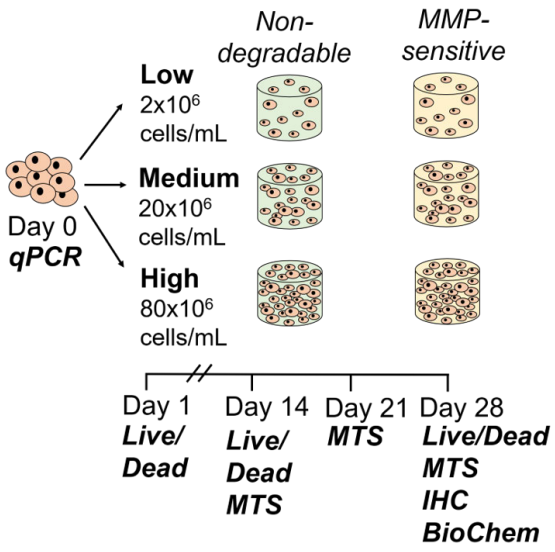

Figure 2.4: Schematic showing study outline. Abbreviations are as follows: qPCR = quantitative Polymerase Chain Reaction, MTS = Mechanical Testing System compressive modulus, IHC = immunohistochemistry, Biochemical assays = calcium and hydroxyproline, Histology = von Kossa.

Cellular morphology was evaluated as a function of time (day 1, 14, and 28) and cell encapsulation density (low, medium and high) in non-degradable and MMP-sensitive hydrogels (Figure 2.5). At day 1, cells retained a round morphology after encapsulation with increased cell numbers evident at increased cell encapsulation densities. With time, cells retained the round

morphology at the low cell encapsulation density in the non-degradable hydrogels. On the contrary, in the medium and high cell encapsulation density, there was evidence of short dendritic-like cellular processes developing by day 14 in the non-degradable hydrogels. In the MMP-sensitive hydrogels, dendritic-like cellular processes extending into the hydrogel were observable across all cell densities by day 14. There were few dead cells observed in the confocal microscopy images for the low and medium cell encapsulation density. However, there were dead cells present in the high cell encapsulation at day 1 after encapsulation (see also Figure 7.1, which shows the dead cells only). Thus, the apparent decrease in live cells for the high cell encapsulation density could be attributed to the initial cell death after encapsulation. It is worth noting that there was no apparent overlap between green cells and those staining as dead cells. Thus, any GFP+ cells that overlap with the calcein stained cells are expected to be limited to live cells.

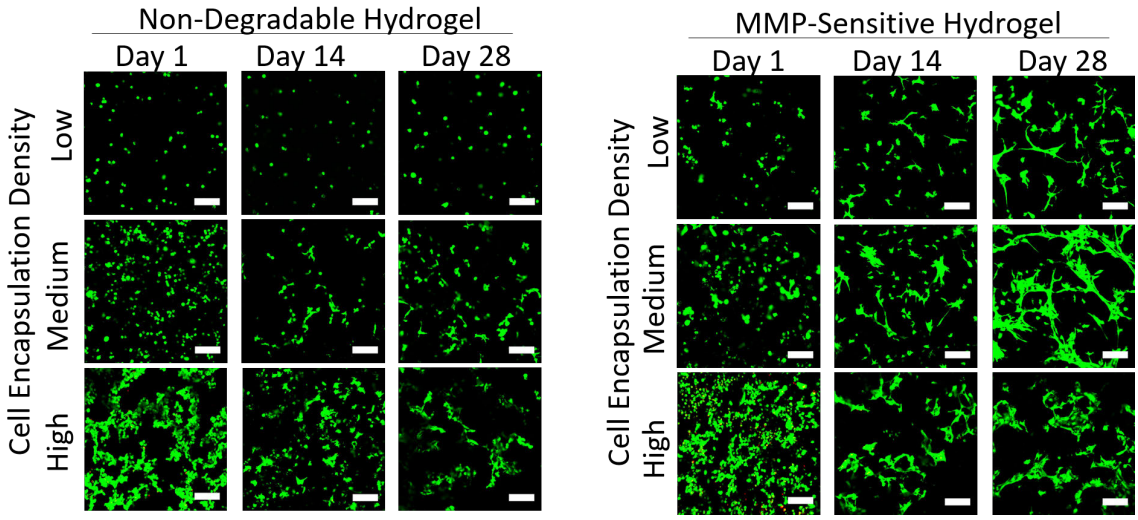

Figure 2.5: Confocal images depicting live, stained by Calcein AM (green), and dead, stained by ethidium homodimer (red), IDG-SW3 cells at days 1, 14 and 28 in osteogenic differentiation media encapsulated at low, medium, and high cell seeding densities in MMP-sensitive and non-degradable PEG hydrogels. Note that any GFP staining would overlap. Scale bar is 150 μm.

The presence of connexin 43 was investigated by immunohistochemistry as a function of cell encapsulation density in the non-degradable and MMP-sensitive hydrogels (Figure 2.6). Positive staining for connexin 43 was evident by punctate staining near the encapsulated cells (Figure 2.6A). There was little to minimal staining in the non-degradable hydrogels at low encapsulation cell density. With medium and high cell encapsulation density there was some evidence of connexin 43 in the non-degradable hydrogels. On the contrary, there was greater positive staining for connexin 43 in the MMP-sensitive hydrogels for all three cell encapsulation densities. The images were quantified by amount of connexin 43 per cell as measured by positive staining area (%) per nuclei for each condition (Figure 2.6B). Connexin 43 on a per cell basis was affected by hydrogel type (p = 0.0076), indicating an overall higher amount of connexin 43 in the MMP-sensitive hydrogels over the non-degradable gels; although pair-wise comparisons were not statistically significant. Cell encapsulation density did not affect the amount of connexin 43 staining on a per cell basis.

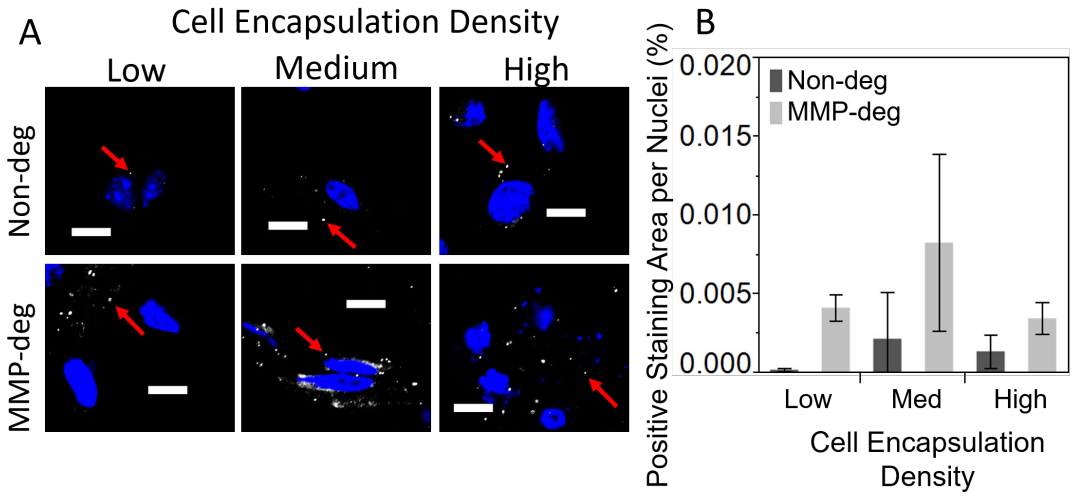

Figure 2.6: A) Representative microscopy images of IDG-SW3 cells at day 28, for connexin 43 (white, indicated by arrows) and nuclei counterstained with DAPI (blue) cultured in osteogenic differentiation media and encapsulated at low, medium, and high cell seeding densities in non-degradable PEG (top) and MMP-sensitive (bottom) hydrogels. Scale bar is 10 μm. B) Semi-quantitative analysis of positive staining area (%) per nuclei for connexin 43.

Mineralization was quantified by calcium content (Figure 2.7A) and its spatial distribution assessed by von Kossa staining (Figure 2.7B) at day 28 of differentiation. Calcium content was affected by hydrogel type ($p < 0.001$) and cell encapsulation density ($p < 0.001$) with no significant interaction between the two factors. Calcium content increased ($p < 0.001$) with increasing cell encapsulation density and was consistently higher ($p < 0.001$) in the MMP-sensitive hydrogel compared to the non-degradable hydrogel. Spatially, there was minimal staining in the low cell encapsulation density in the non-degradable hydrogels. There was mineralization present in all other experimental groups with mineralization predominantly being localized to regions near the cells.

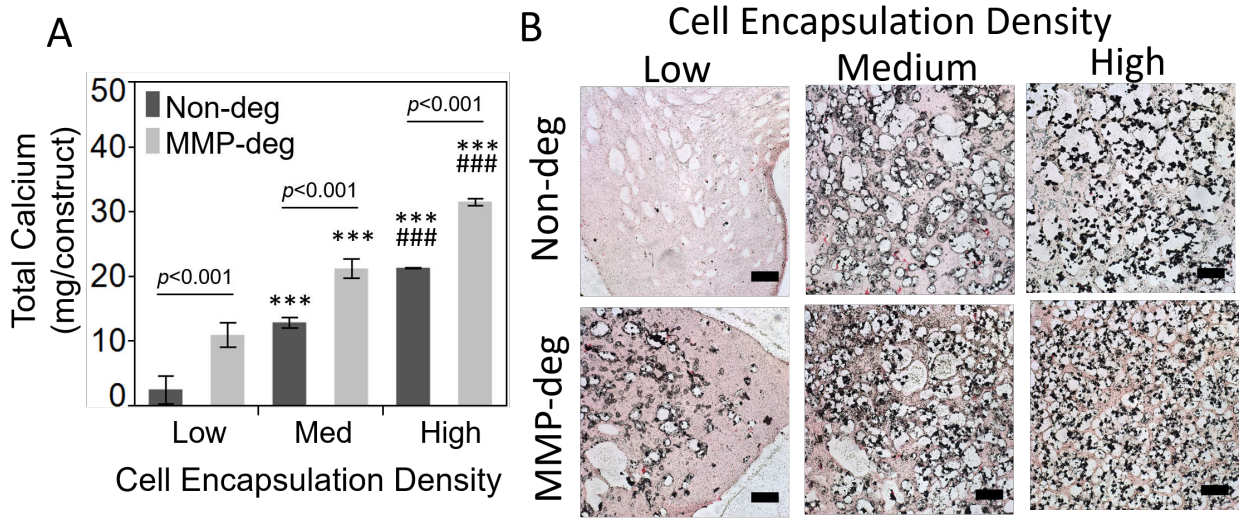

Figure 2.7: Assessment of mineral content in IDG-SW3 cells encapsulated MMP-degradable and non-degradable PEG hydrogels at low, medium, and high cell seeding densities at day 28 of osteogenic differentiation. A) Calcium content; p-values are shown for pairwise comparisons between hydrogel and from low (Indicated by *) and from medium (indicated by #) for the same hydrogel. One symbol is $p < 0.05$, two symbols is $p < 0.01$, and three symbols is $p < 0.001$. B) Representative microscopy images of IDG-SW3 cells for mineralization by von Kossa staining (black) with nuclei counterstained with methyl red (red). Scale bar is 100 μm.

IDG-SW3 cells have been shown to produce a mineralized collagen matrix,[20] therefore total collagen content was quantified by hydroxyproline, an amino acid in high abundance in collagen (Figure 2.8A) and the spatial distribution of collagen type 1 (the major collagen type found in bone)[43] assessed by immunohistochemistry (Figure 2.8B) at day 28 of differentiation. The immunohistochemistry images were analyzed to quantify the amount of collagen I per cell as measured by positive staining area per nuclei (Figure 2.8C). Considering the non-degradable hydrogel only, total collagen content (i.e., Figure 2.8A) was not different between the low and medium but was higher ($p < 0.01$) in the high cell encapsulation density condition. Similarly, considering only the MMP-sensitive hydrogel, total collagen content was not different between the low and medium but was higher ($p < 0.01$) in the high cell encapsulation density condition. Comparing the two hydrogels, total collagen content was 3.2- ($p = 0.004$) and 2.9-fold ($p = 0.006$) higher in the MMP-sensitive hydrogels compared to the non-degradable hydrogels for the medium and high cell encapsulation density conditions, respectively. Collagen type I was spatially restricted to regions in and near the encapsulated cells in all conditions (Figure 2.8B). However, there were differences in the amount of collagen I staining per cell (i.e., Figure 2.8C). Considering only non-degradable hydrogels, the high encapsulation density showed greater collagen I per cell when compared to either low ($p = 0.005$) or medium ($p = 0.007$) cell encapsulation densities. Considering only the MMP-sensitive hydrogels, the amount of collagen I per cell was not affected by cell encapsulation density. This result suggests that the increased total collagen content in Figure 2.8A is due to a higher cell number. Comparing the two hydrogel types, the amount of collagen I per cell was 4.1-fold higher ($p = 0.0114$) for low and 4.2-fold higher ($p = 0.0026$) for medium cell encapsulation densities in the MMP-sensitive hydrogels. At high cell encapsulation density, there was no difference in the amount of collagen I per cell between the hydrogel types.

However, there was more total collagen deposited in the MMP-sensitive hydrogels, which could be due to an increase in cell proliferation, although this was not measured.

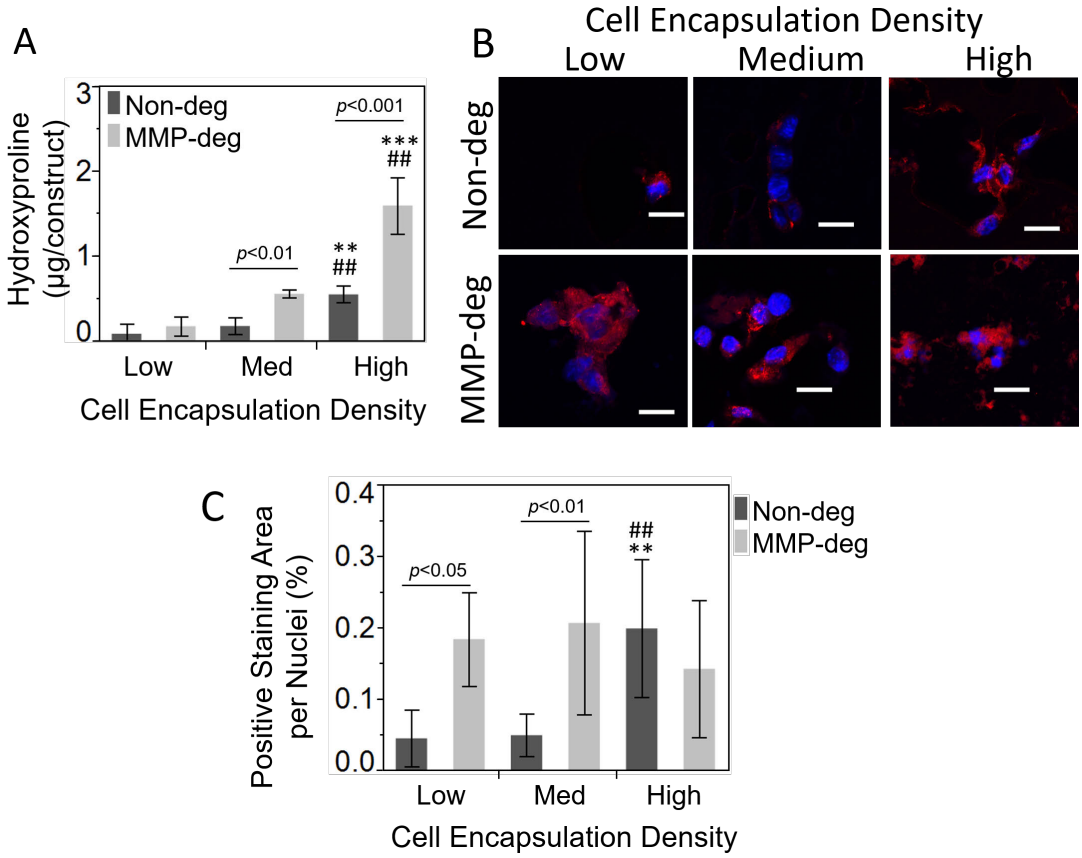

Figure 2.8: Assessment of collagen content in IDG-SW3 cells encapsulated MMP-degradable and non-degradable PEG hydrogels at low, medium, and high cell seeding densities at day 28 of osteogenic differentiation. A) Hydroxyproline content. B) Representative microscopy images of IDG-SW3 cells for collagen type I (red) with nuclei counterstained with DAPI. Scale bar length is 20 µm. C) Quantitative analysis of positive staining area (%) per nuclei for collagen I in the immunohistochemistry images. *P*-values are shown for pairwise comparisons between hydrogel and from low (indicated by *) and from medium (indicated by #) for the same hydrogel. One symbol is $p < 0.05$, two symbols is $p < 0.01$, and three symbols is $p < 0.001$.

The compressive modulus of the hydrogels was measured over time as a function of hydrogel type and cell encapsulation density (Figure 2.9). The non-degradable hydrogels maintained their compressive modulus with an average equilibrium modulus of 10.9 kPa over the

duration of the 28 days for all three cell encapsulation densities. In the MMP-sensitive hydrogels, the modulus remained low for the low cell encapsulation density and did not change with time. For the medium cell encapsulation density, the modulus of the MMP-sensitive hydrogels decreased (p = 0.006) with time resulting in a modulus of 1.3 kPa by day 28. On the contrary, the modulus for the high cell encapsulation density in the MMP-sensitive hydrogels increased (p < 0.001) with time resulting in a modulus of 4 kPa at day 14 and increasing (p < 0.001) to 14 kPa by day 28.

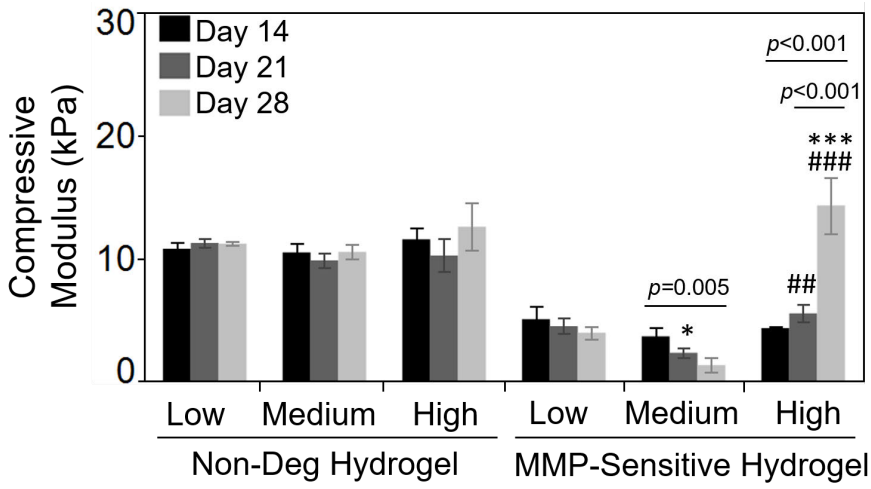

Figure 2.9: Compressive modulus measurements of IDG-SW3 encapsulated MMP-sensitive and non-degradable PEG hydrogels at low, medium and high cell seeding densities at days 14, 21 and 28 of osteogenic differentiation. *P*-values for MMP-13 sensitive hydrogels denote significance from day 1.

Collectively, these results demonstrate that the MMP-sensitive hydrogel led to enhanced dendritic-like cellular processes and increased positive staining for connexin 43. Further, the high cell encapsulation density in the MMP-sensitive hydrogels improved collagenous matrix mineralization when compared to the lower MMP-sensitive encapsulation densities and all encapsulation densities in the non-degradable hydrogels.

2.5 Discussion

This study identified an MMP-sensitive hydrogel that is susceptible to degradation by MMP-2, MMP-13 and IDG-SW3 cells and supports osteoblast to osteocyte differentiation of IDG-SW3 cells. As compared to the non-degradable hydrogel, the MMP-sensitive hydrogel led to increased osteocyte differentiation and bone extracellular matrix deposition. Overall, a high cell encapsulation density combined with the MMP-sensitive hydrogel is a promising 3D culture system that supports the osteoblast to osteocyte transition of IDG-SW3 cells.

In this work, we confirmed that throughout osteocyte differentiation IDG-SW3 cells express MMPs of type 2, 9, 13, and 14 at the gene level. These four MMPs have been identified as playing an important role in skeletal development.[39] Herein, *Mmp2* expression maintained consistently higher expression throughout differentiation. *Mmp14* and *Mmp9* mirrored the temporal expression pattern of *Mmp2*, but at lower levels, and with *Mmp9* at the lowest expression. Studies have reported that mice lacking MMP-14[44] or MMP-2[45] had aberrant bone formation. MMP-9 has been shown to be involved in apoptosis and angiogenesis[46] and important in endochondral ossification.[47] Thus, the IDG-SW3 osteoblast to osteocyte transition may require MMP-2 and MMP-14, but not MMP-9.

The temporal expression pattern of *Mmp13* was uniquely different from the other three MMP types during IDG-SW3 osteoblast to osteocyte transition. While its expression was initially low compared to *Mmp2* and *Mmp14*, a 200-fold increase occurred during differentiation from day 1 to day 35. Studies have reported that mice lacking MMP-13 displayed defects in remodeling and ECM organization in the perilacunar space in bone[48] In a separate *in vitro* study, upregulation of *Mmp13* correlated to DMP-1 expression during migration of differentiating osteocytes in a dense

collagen matrix.[49] Further, MLO-A5 cells, which do not express the osteocyte marker DMP-1, expressed low *Mmp13* levels during their differentiation period.[50] Thus, it is possible that MMP-13 plays a critical role in the formation of the LCN and late stage osteocyte differentiation.

Based on the *Mmp2* and *Mmp13* expression profiles of IDG-SW3 cells during osteocyte differentiation in the established 2D culture, we chose an MMP-sensitive peptide crosslinker that was originally identified for its susceptibility to MMP-13,[42] but which we confirmed was also susceptible to MMP-2. IDG-SW3 cell-mediated hydrogel degradation was also confirmed by evidence of cell spreading. Extension of cellular processes was more pronounced within the MMP-sensitive hydrogel than in the non-degradable PEG hydrogel. This result is consistent with previous findings whereby a MMP inhibitor prevented cell spreading within similar MMP-sensitive PEG based hydrogels.[38] Bulk hydrogel degradation in the MMP-sensitive hydrogels was also evident, which indicates that cell-secreted enzymes diffused through the hydrogel and subsequently cleaved crosslinks in the bulk. This was particularly evident in the medium cell density condition where the hydrogel construct modulus decreased from days 14 to 28, which indicates bulk degradation. Although the exact MMP type or types used by IDG-SW3 cells during differentiation to degrade the MMP-sensitive hydrogel was not identified, the MMP-sensitive hydrogel formed with the peptide crosslinker, GCGPLG-LWARCG, supported the formation of dendritic-like cellular processes, which are important for osteocyte differentiation and a critical first step to forming the LCN of mature bone.

IDG-SW3 cells were derived from long bone chips and are capable of expressing osteoblast markers, producing a mineralized collagen matrix, as well as expressing early to late osteocyte markers.[20] To investigate the osteoblast to osteocyte transition of IDG-SW3 cells in this 3D hydrogel, this study assessed both osteoblast and osteocyte characteristics with the goal of

identifying culture conditions that enhance osteocyte differentiation while supporting a bone ECM deposition. Osteocyte differentiation of the IDG-SW3 cells was most pronounced in the MMP-sensitive hydrogel. ALP is an osteoblast marker that is downregulated as osteoblasts differentiate towards osteocytes.[51,52] Regardless of the culture environment, ALP increased in the first 14 days of culture, and by day 28 ALP decreased to levels that were either similar to day 1 or lower than day 14. These results indicated a shift towards an osteocyte phenotype. IDG-SW3 cells in the MMP-sensitive hydrogels showed the highest expression of the osteocyte genes, *Dmp1* and *Phex*[19] and showed greater number of DMP1-GFP-positive cells by day 28. *In vitro* and *in vivo*, DMP-1 controls phosphate metabolism during osteocyte differentiation and is important for the organization of the osteocyte LCN.[53,54] PHEX, which is a membrane-bound endoprotease, binds DMP-1 to control phosphate homeostasis and ultimately mineralization.[55] The temporal profiles of *Dmp1* and *Phex* expressions increased over the 28 days in the MMP-sensitive hydrogels but declined between 14 and 28 days in the non-degradable hydrogel.

Another hallmark of the osteoblast-to-osteocyte transition is dendrite formation.[7] IDG-SW3 cells showed thin cellular processes that extend from the cell body wall, which may be an early form of osteocyte dendrite formation. There was evidence of short cellular processes in the non-degradable hydrogels at medium and high cell encapsulation densities by day 28. However, the cellular processes were longer and more pronounced in the MMP-sensitive hydrogels at all cell densities, likely due to cell-mediated hydrogel degradation. While dendrites that formed were less numerous than osteocyte LCN in bone tissue, the dendrites appeared to extend towards neighboring cells. In the non-degradable hydrogels, extension of these processes is only possible if they can extend through the mesh of the hydrogel. Our observations suggest that the hydrogel mesh restricted the development of the dendrite-like processes in the non-degradable hydrogels,

which may have limited osteocyte differentiation in the non-degradable hydrogels. Yet, the evidence of cell-mediated degradation in the MMP-degradable hydrogels suggests that the MMP-degradation created space for more abundant dendrite formation and therefore enhanced osteocyte differentiation.

Connexin 43 staining was observed in both hydrogel types at day 28, and was greater in the MMP-sensitive hydrogels. In bone, connexin 43 is expressed by both osteoblasts and osteocytes and acts not only as a gap junction between cells, but also functions as an unopposed hemichannel. Hemichannels are located on the cell membrane, and unlike gap junctions, they do not require cell-to-cell connections.[58] Punctate staining for connexin 43 was observed and localized to cells, which is consistent with previous connexin 43 immunohistochemical staining.[56,57] Further studies are needed to confirm whether the observed connexin 43 is associated with hemichannels or gap junctions. Given that connexin 43 staining was similar regardless of cell density, the former role may dominate in this system. Connexin 43 is necessary for osteoblast and osteocyte survival and function[58] and thus we postulate that it is likely present and playing a role in IDG-SW3 differentiation. The greater amount of connexin 43 staining in the MMP-sensitive hydrogels correlates to the observed greater prevalence of cellular processes and higher expression levels for osteocyte genes *Dmp1* and *Phex*. Taken together, we hypothesize that the continued ability to extend cellular processes in the MMP-sensitive hydrogels by day 28 improved osteocyte differentiation, but that differentiation was impaired when growth of cellular processes was restricted in the non-degradable hydrogels. This observation suggests that the formation of cellular processes was critical to osteocyte differentiation and that degradable hydrogels facilitated formation of osteocyte networks *in vitro*. However, additional studies are needed to confirm this hypothesis.

Mineralization and collagen were also present in both hydrogel types at day 28, but to a greater amount in the MMP-sensitive hydrogels. ALP activity, which plays a role in bone mineralization, was also highest in the MMP-sensitive hydrogels,[52] and collagen can serve as a nucleation site for mineralization.[59] Collagen I is the most abundant collagen type found in bone, and contributes approximately 20-25% of the composition of bone.[43] Osteocytes are known for orchestrating osteoblast bone-forming activity,[60] but osteocytes themselves can also deposit new bone matrix directly around osteocyte lacunae.[61] The exact characteristics that define osteocytes, as compared to their parent osteoblast population, are still being elucidated.[62,63] Due to the restricted transport of large ECM molecules, such as collagen, through the crosslinks of the hydrogel,[64] deposition was limited to the pericellular region in this study, which also closely resembles osteocyte perilacunar modeling. In the MMP-sensitive hydrogel, this region can grow providing increasingly more space for more ECM to deposit, which is supported at the low and medium cell densities by the higher amount of collagen type I positive staining per nuclei. Longer studies are needed to determine if this deposition of bone ECM would continue to replace hydrogel beyond the perilacunar space. In this study, osteocyte differentiation and bone ECM deposition were both enhanced in the MMP-sensitive hydrogel. Similarly, the pre-osteoblastic cell line MC3T3-E1 has shown higher amounts of *Dmp1* and *Phex* expression concomitant with mineralization in a collagen gel.[65] Thus, it is possible that the ability to mineralize is a quality important to both osteoblasts and osteocytes *in vitro*, and that the presence of bone ECM may be necessary for osteocyte differentiation.

The cell encapsulation density was varied to investigate its impact on cellular morphology and bone ECM deposition. For the MMP-sensitive hydrogels, the formation of cellular processes and the positive staining of connexin 43 per cell were similar with different cell concentrations,

indicating no effect on these osteocyte characteristics. Similarly, the spatial deposition of mineral around the cells and the collagen I staining on a per cell basis were similar across all cell densities in the MMP-sensitive hydrogels. On the other hand, the total amount of calcium and hydroxyproline content increased with cell density and, therefore, a higher number of cells.[64] Moreover, from day 14 to day 28 the compressive modulus tripled for the MMP-sensitive hydrogels with high cell encapsulation density which is attributed to a greater amount of ECM in the hydrogel. In the non-degradable hydrogels, cell encapsulation density had a greater effect on osteocyte characteristics. The hydrogels with low cell density performed poorly with minimal signs of cellular processes or connexin 43 and a lack of mineral deposits. On the contrary, the hydrogels with medium and high cell densities supported osteocyte characteristics albeit to a lesser degree than the MMP-sensitive hydrogels, which was supported by the quantitative analysis of the connexin 43 and collagen type I staining per cell. Overall, these results indicate that for the MMP-sensitive hydrogel, cell density does not have a significant impact on the formation of dendritic-like processes, expression of connexin 43, and bone ECM deposition. Rather, higher cell concentrations produce overall more mineralized collagen matrix, which leads to increases in the construct compressive modulus over time. The formation of a mineralized matrix, or osteoid, may be necessary to continue IDG-SW3 osteocyte differentiation into mature osteocytes, but cell density may not be a critical factor. Additional studies are needed to determine the long-term effect of differences in cell density.

There are several limitations of this study. Notably, there were several differences in hydrogel formulation. First, a PEG-dithiol crosslinker was chosen for the non-degradable hydrogel to ensure stability of the hydrogel. We have observed (unpublished observations) that scrambled peptide sequences can be broadly susceptible to degradation by collagenases. Second, the

formulation of the hydrogel was varied due to differences in crosslinker reactivity, which led to differences in the PEG-NB concentration and thus slight differences in the crosslinked structure. Third, there were small differences in the modulus between the non-degradable and MMP-sensitive hydrogel (8 vs 10 kPa). It is possible that differences in the crosslink chemistry, formulation and/or modulus could have impacted the cells, but which was not tested in this study. We assessed ALP activity at discrete time points and therefore may have missed the timing of optimal activity, which typically peaks between 14 and 21 days. We also assessed gene expression at discrete time points and thus may have not captured the true trends in differentiation. Although, the IDG-SW3 cells were confirmed to differentiate in 2D and 3D in differentiation medium in the first part of this study, we did not investigate differentiation markers in the study with cell encapsulation density. Thus, it is possible the cell encapsulation density may have altered the timing of differentiation. This study focused on IDG-SW3 cells given their known ability to differentiate into mature osteocytes. Future studies should investigate whether this promising MMP-sensitive hydrogel could support osteocyte differentiation of other cell types, which do not readily differentiate into mature osteocytes, such as MLO-Y4, MLO-A5, and MC3T3-E1.

2.6 Conclusions

This study provides insight into the importance of 3D culture conditions on IDG-SW3 osteocyte differentiation. We show that an MMP-sensitive hydrogel promotes osteoblast to osteocyte differentiation by the enhanced expression of mature osteocytic genes, formation of dendritic-like cellular processes, positive staining for connexin 43, and a mineralized collagen matrix. An IDG-SW3 cell-laden hydrogel promotes bone ECM deposition around the cells as they differentiate from osteoblasts into osteocytes, thus mimicking aspects of *in vivo* bone formation, but in a highly controlled environment. The combination of IDG-SW3 cells with an MMP-

sensitive hydrogel offers a more realistic *in vitro* culture system when compared to the traditional 2D culture on TCPS for the study of osteoblast to osteocyte differentiation. Moreover, once the cells have differentiated into osteocytes, formed dendrite-like processes, and are embedded in a mineralized collagen matrix, this platform can be used to investigate for example, the effects of drug treatment, hormone levels, or mechanical loading on osteocytes.

2.7 Acknowledgements

The authors thank Prof. Corey Neu for use of his Nikon A1R Confocal System. Research reported in this publication was supported by the National Institute of Arthritis and Musculoskeletal and Skin Diseases of the National Institutes of Health under Award Numbers 1R21AR069791-01A1. RW was supported on an NIH/NIA National Institute of Aging Integrative Physiology of Aging Training Grant under Award T32AG000279-16A1. The content is solely the responsibility of the authors and does not necessarily represent the official views of the National Institutes of Health.

2.8 Abbreviations

MMP, matrix metalloproteinase; 2D, two-dimensional; 3D, three-dimensional, LCN, lacuno-canalicular network; TCPS, tissue culture polystyrene; PEG, poly(ethylene glycol); ECM, extracellular matrix; INF-γ, interferon-gamma; MEM, Modified Essential Medium, FBS, fetal bovine serum; PSF, penicillin/streptomycin/ amphotericin B; PBS, phosphate buffered saline; GFP, green fluorescent protein; DMP1, dentin matrix acidic phosphoprotein 1; qPCR, quantitative Polymerase Chain Reaction; RE, relative expression; NE, normalized expression; HKG, housekeeping gene; GOI, gene of interest; IHC, immunohistochemistry; DAPI, 4,6-diamidino-2-phenylindole ALP, alkaline phosphatase; MTS, Mechanical Testing System; ANOVA, analysis of variance.

2.9 References

1. Bellido, T. Osteocyte-Driven Bone Remodeling. *Calcified Tissue International* **94**, 25–34 (2014).
2. Bonewald, L. F. The Role of the Osteocyte in Bone and Nonbone Disease. *Endocrinol Metab Clin North Am* **46**, 1–18 (2017).
3. Burger, E. H. & Klein-Nulend, J. Mechanotransduction in bone - role of the lacuno-canalicular network. *Faseb Journal* **13**, S101–S112 (1999).
4. Bonewald, L. F. Osteocytes as dynamic multifunctional cells. *Annals of the New York Academy of Sciences* **1116**, 281–90 (2007).
5. Dallas, S. L. & Bonewald, L. F. Dynamics of the Transition from Osteoblast to Osteocyte. *Annals of the New York Academy of Sciences* **1192**, 437–443 (2010).
6. Bonewald, L. F. The amazing osteocyte. *Journal of Bone and Mineral Research* **26**, 229–238 (2011).
7. Palumbo, C., Palazzini, S. & Marotti, G. Morphological study of intercellular junctions during osteocyte differentiation. *Bone* **11**, 401–406 (1990).
8. Knothe Tate, M. L., Adamson, J. R., Tami, A. E. & Bauer, T. W. The osteocyte. *Int J Biochem Cell Biol* **36**, 1–8 (2004).
9. Fowler, T. W. *et al.* Glucocorticoid suppression of osteocyte perilacunar remodeling is associated with subchondral bone degeneration in osteonecrosis. *Scientific Reports* **7**, 44618 (2017).
10. Lara-Castillo, N. *et al.* In vivo mechanical loading rapidly activates β-catenin signaling in osteocytes through a prostaglandin mediated mechanism. *Bone* **76**, 58–66 (2015).
11. Robling, A. G. *et al.* Mechanical Stimulation of Bone in Vivo Reduces Osteocyte Expression of Sost/Sclerostin. *Journal of Biological Chemistry* **283**, 5866–5875 (2008).
12. Lewis, K. J. *et al.* Osteocyte calcium signals encode strain magnitude and loading frequency in vivo. *Proceedings of the National Academy of Sciences* **114**, 11775–11780 (2017).
13. Tanaka, T. *et al.* Analysis of Ca2+ response of osteocyte network by three-dimensional time-lapse imaging in living bone. *Journal of Bone and Mineral Metabolism; Tokyo* **36**, 519–528 (2018).
14. Kalajzic, I. *et al.* In vitro and in vivo approaches to study osteocyte biology. *Bone* **54**, 296–306 (2013).
15. Stern, A. R. *et al.* Isolation and culture of primary osteocytes from the long bones of skeletally mature and aged mice. *BioTechniques* **52**, 361–73 (2012).
16. Barragan-Adjemian, C. *et al.* Mechanism by which MLO-A5 Late Osteoblasts/Early Osteocytes Mineralize in Culture: Similarities with Mineralization of Lamellar Bone. *Calcif Tissue Int* **79**, 340–353 (2006).

17. Rath, A. L. *et al.* Correlation of cell strain in single osteocytes with intracellular calcium, but not intracellular nitric oxide, in response to fluid flow. *Journal of Biomechanics* **43**, 1560–1564 (2010).

18. Kato, Y., Windle, J. J., Koop, B. A., Mundy, G. R. & Bonewald, L. F. Establishment of an osteocyte-like cell line, MLO-Y4. *Journal of bone and mineral research : the official journal of the American Society for Bone and Mineral Research* **12**, 2014–23 (1997).

19. Paic, F. *et al.* Identification of differentially expressed genes between osteoblasts and osteocytes. *Bone* **45**, 682–692 (2009).

20. Woo, S. M., Rosser, J., Dusevich, V., Kalajzic, I. & Bonewald, L. F. Cell line IDG-SW3 replicates osteoblast-to-late-osteocyte differentiation in vitro and accelerates bone formation in vivo. *Journal of bone and mineral research : the official journal of the American Society for Bone and Mineral Research* **26**, 2634–46 (2011).

21. Lindberg, I. *et al.* FGF23 is endogenously phosphorylated in bone cells. *Journal of bone and mineral research : the official journal of the American Society for Bone and Mineral Research* **30**, 449–54 (2015).

22. Ito, N., Findlay, D. M., Anderson, P. H., Bonewald, L. F. & Atkins, G. J. Extracellular phosphate modulates the effect of 1α,25-dihydroxy vitamin D3 (1,25D) on osteocyte like cells. *The Journal of steroid biochemistry and molecular biology* **136**, 183–6 (2013).

23. Fujita, K., Xing, Q., Khosla, S. & Monroe, D. G. Mutual enhancement of differentiation of osteoblasts and osteocytes occurs through direct cell-cell contact. *Journal of cellular biochemistry* **115**, 2039–44 (2014).

24. St John, H. C. *et al.* The osteoblast to osteocyte transition: epigenetic changes and response to the vitamin D3 hormone. *Molecular endocrinology (Baltimore, Md.)* **28**, 1150–65 (2014).

25. Xu, H. *et al.* Impact of flow shear stress on morphology of osteoblast-like IDG-SW3 cells. *Journal of Bone and Mineral Metabolism* **36**, 529–536 (2018).

26. Baker, B. M. & Chen, C. S. Deconstructing the third dimension - how 3D culture microenvironments alter cellular cues. *Journal of Cell Science* **125**, 3015–3024 (2012).

27. Bao, M., Xie, J. & Huck, W. T. S. Recent Advances in Engineering the Stem Cell Microniche in 3D. *Advanced Science* **5**, 1800448 (2018).

28. Boukhechba, F. *et al.* Human Primary Osteocyte Differentiation in a 3D Culture System. *Journal of Bone and Mineral Research* **24**, 1927–1935 (2009).

29. Zujur, D. *et al.* Three-dimensional system enabling the maintenance and directed differentiation of pluripotent stem cells under defined conditions. *Science Advances* **3**, e1602875 (2017).

30. Mc Garrigle, M. J., Mullen, C. A., Haugh, M. G., Voisin, M. C. & McNamara, L. M. Osteocyte differentiation and the formation of an interconnected cellular network in vitro. *European Cells & Materials* **31**, 323–340 (2016).

31. Uchihashi, K., Aoki, S., Matsunobu, A. & Toda, S. Osteoblast migration into type I collagen gel and differentiation to osteocyte-like cells within a self-produced mineralized matrix: A novel system for analyzing differentiation from osteoblast to osteocyte. *Bone* **52**, 102–110 (2013).

32. Kurata, K., Heino, T. J., Higaki, H. & Väänänen, H. K. Bone Marrow Cell Differentiation Induced by Mechanically Damaged Osteocytes in 3D Gel-Embedded Culture. *Journal of Bone and Mineral Research* **21**, 616–625 (2006).

33. Sun, Q. *et al.* Ex vivo replication of phenotypic functions of osteocytes through biomimetic 3D bone tissue construction. *Bone* **106**, 148–155 (2018).

34. Lee, K. Y., Alsberg, E. & Mooney, D. J. Degradable and injectable poly(aldehyde guluronate) hydrogels for bone tissue engineering. *Journal of Biomedical Materials Research* **56**, 228–233 (2001).

35. Fairbanks, B. D. *et al.* A Versatile Synthetic Extracellular Matrix Mimic via Thiol-Norbornene Photopolymerization. *Advanced Materials* **21**, 5005–5010 (2009).

36. McKinnon, D. D., Kloxin, A. M. & Anseth, K. S. Synthetic hydrogel platform for three-dimensional culture of embryonic stem cell-derived motor neurons. *Biomaterials Science* **1**, 460 (2013).

37. Sridhar, B. V. *et al.* Development of a Cellularly Degradable PEG Hydrogel to Promote Articular Cartilage Extracellular Matrix Deposition. *Advanced Healthcare Materials* **4**, 702–713 (2015).

38. Amer, L. D. & Bryant, S. J. The In Vitro and In Vivo Response to MMP-Sensitive Poly(Ethylene Glycol) Hydrogels. *Annals of Biomedical Engineering* **44**, 1959–1969 (2016).

39. Silva Paiva, K. B. & Granjeiro, J. M. Bone tissue remodeling and development: Focus on matrix metalloproteinase functions. *Archives of Biochemistry and Biophysics* **561**, 74–87 (2014).

40. Mullen, C. A., Haugh, M. G., Schaffler, M. B., Majeska, R. J. & McNamara, L. M. Osteocyte differentiation is regulated by extracellular matrix stiffness and intercellular separation. *Journal of the Mechanical Behavior of Biomedical Materials* **28**, 183–194 (2013).

41. Kim, K., Dean, D., Mikos, A. G. & Fisher, J. P. Effect of Initial Cell Seeding Density on Early Osteogenic Signal Expression of Rat Bone Marrow Stromal Cells Cultured on Cross-Linked Poly(propylene fumarate) Disks. *Biomacromolecules* **10**, 1810–1817 (2009).

42. Deng, S. J. *et al.* Substrate specificity of human collagenase 3 assessed using a phage-displayed peptide library. *The Journal of biological chemistry* **275**, 31422–7 (2000).

43. Burr, D. B. & Akkus, O. Bone Morphology and Organization. in *Basic and Applied Bone Biology* 3–25 (Elsevier, 2014). doi:10.1016/B978-0-12-416015-6.00001-0.

44. Holmbeck, K. *et al.* MT1-MMP-deficient mice develop dwarfism, osteopenia, arthritis, and connective tissue disease due to inadequate collagen turnover. *Cell* **99**, 81–92 (1999).

45. Mosig, R. A. *et al.* Loss of MMP-2 disrupts skeletal and craniofacial development and results in decreased bone mineralization, joint erosion and defects in osteoblast and osteoclast growth. *Human Molecular Genetics* **16**, 1113–1123 (2007).

46. Vandooren, J., Van den Steen, P. E. & Opdenakker, G. Biochemistry and molecular biology of gelatinase B or matrix metalloproteinase-9 (MMP-9): The next decade. *Critical Reviews in Biochemistry and Molecular Biology* **48**, 222–272 (2013).

47. Vu, T. H. *et al.* MMP-9/Gelatinase B Is a Key Regulator of Growth Plate Angiogenesis and Apoptosis of Hypertrophic Chondrocytes. *Cell* **93**, 411–422 (1998).

48. Tang, S. Y., Herber, R.-P., Ho, S. P. & Alliston, T. Matrix metalloproteinase-13 is required for osteocytic perilacunar remodeling and maintains bone fracture resistance. *Journal of bone and mineral research : the official journal of the American Society for Bone and Mineral Research* **27**, 1936–50 (2012).

49. Robin, M. *et al.* Involvement of 3D osteoblast migration and bone apatite during in vitro early osteocytogenesis. *Bone* **88**, 146–156 (2016).

50. Prideaux, M. *et al.* MMP and TIMP temporal gene expression during osteocytogenesis. *Gene Expression Patterns* **18**, 29–36 (2015).

51. Kaur, K., Das, S. & Ghosh, S. Regulation of Human Osteoblast-to-Osteocyte Differentiation by Direct-Write 3D Microperiodic Hydroxyapatite Scaffolds. *ACS Omega* **4**, 1504–1515 (2019).

52. Golub, E. E. & Boesze-Battaglia, K. The role of alkaline phosphatase in mineralization. *Current opinion in Orthopaedics* **18**, 444–448 (2007).

53. Lu, Y. *et al.* The biological function of DMP-1 in osteocyte maturation is mediated by its. *J Bone Miner Res* **26**, 331–340 (2011).

54. Qin, C., D'Souza, R. & Feng, J. Q. Dentin Matrix Protein 1 (DMP1): New and Important Roles for Biomineralization and Phosphate Homeostasis. *J Dent Res* **86**, 1134–1141 (2007).

55. Rowe, P. S. N. The chicken or the egg: PHEX, FGF23 and SIBLINGs unscrambled. *Cell Biochemistry and Function* **30**, 355–375 (2012).

56. Langhorst, H. *et al.* The IgCAM CLMP regulates expression of Connexin43 and Connexin45 in intestinal and ureteral smooth muscle contraction in mice. *Disease Models & Mechanisms* **11**, dmm032128 (2018).

57. Balla, P. *et al.* Prognostic Impact of Reduced Connexin43 Expression and Gap Junction Coupling of Neoplastic Stromal Cells in Giant Cell Tumor of Bone. *PLOS ONE* **10**, e0125316 (2015).

58. Plotkin, L. I. Connexin 43 and Bone: Not Just a Gap Junction Protein. *Actual osteol* **7**, 79–90 (2011).

59. Zhang, W., Huang, Z.-L., Liao, S.-S. & Cui, F.-Z. Nucleation Sites of Calcium Phosphate Crystals during Collagen Mineralization. *Journal of the American Ceramic Society* **86**, 1052–1054 (2003).

60. Bellido, T., Plotkin, L. I. & Bruzzaniti, A. Bone Cells. in *Basic and Applied Bone Biology* 27–45 (Elsevier, 2014). doi:10.1016/B978-0-12-416015-6.00002-2.

61. Qing, H. *et al.* Demonstration of osteocytic perilacunar/canalicular remodeling in mice during lactation. *J Bone Miner Res* **27**, 1018–1029 (2012).

62. Qing, H. & Bonewald, L. F. Osteocyte remodeling of the perilacunar and pericanalicular matrix. *International journal of oral science* **1**, 59 (2009).

63. Yee, C. S., Schurman, C. A., White, C. R. & Alliston, T. Investigating Osteocytic Perilacunar/Canalicular Remodeling. *Curr Osteoporos Rep* **17**, 157–168 (2019).

64. Bryant, S. J. & Vernerey, F. J. Programmable Hydrogels for Cell Encapsulation and Neo-Tissue Growth to Enable Personalized Tissue Engineering. *Adv Healthc Mater* **7**, 1–13 (2018).

65. Uchihashi, K., Aoki, S., Matsunobu, A. & Toda, S. Osteoblast migration into type I collagen gel and differentiation to osteocyte-like cells within a self-produced mineralized matrix: A novel system for analyzing differentiation from osteoblast to osteocyte. *Bone* **52**, 102–110 (2013).

3. Osteocyte Differentiation and Dendrite Formation in poly(ethylene glycol) Hydrogels with Tunable Physical and Biochemical Cues

Rachel L. Wilmoth, Virginia L. Ferguson, Stephanie J. Bryant

3.1 Abstract

In vivo, osteocytes reside within a highly interconnected 3D environment known as the lacunocanalicular network, characterized by dendrites extending outward from the cell body that form gap junctions with neighboring cells. Osteocytes use the lacunocanalicular network for communication, signaling, and mechanotransduction. This study sought to understand how some of the tunable physical and biochemical factors in a 3D hydrogel culture system affect both osteocyte differentiation and dendrite formation. In this study, OCY454 cells were cultured in poly(ethylene glycol) hydrogels with immobilized transforming growth factor-β3 and RGD in chemically defined media. Physical factors, (*i.e.*, hydrogel crosslinking density and degradability with matrix-metalloproteinase sensitive crosslinks) and biochemical factors (*i.e.*, collagen I and hydroxyapatite) were varied to assess osteocyte differentiation and dendrite formation. Osteocyte differentiation gene expression (*Dmp1* and *Sost*) were enhanced in 3D, degradable hydrogels. Degradability was essential for dendrite formation and the addition of collagen and hydroxyapatite further increased dendrite formation. In hydrogels with RGD but no collagen or hydroxyapatite, osteocyte differentiation (*Dmp1* and *Sost*) and dendrite formation both increased with increasing crosslinking densities. Together, this study demonstrates that a poly(ethylene glycol) hydrogel needs degradable crosslinks to support dendrite formation, that modulus regulates differentiation and dendrite formation together, and that addition of bone matrix components increases dendrite formation via biochemical signaling.

3.2 Introduction

Osteocytes make up over 95% of the total bone cells and reside within the mineralized collagenous matrix of bone in a highly interconnected cellular network that is comparable in size and connectivity to the neural network. Osteocyte cell bodies are encased within lacunae, which are small, rounded cavities in the bone matrix.[1] Each cell body develops dendrites that extend outward to form connexin 43 gap junctions with neighboring cell dendrites.[2–4] The dendrites extend through small channels called canaliculi.[5] Together, this network is called the lacunocanalicular network (LCN).

The LCN is vital to osteocyte mechanobiology and intracellular communication. Being mechanosensitive cells that regulate bone homeostasis, osteocytes use the fluid movement in the annular space (between the cell body/dendrites and lacunae/canaliculi walls) of the LCN to sense changes in mechanical loading to bone.[3] Osteocytes are more sensitive to changes in fluid flow in their dendrites as compared to the cell body.[6–8] This difference may be attributed to higher fluid velocities within annular space of the canaliculi versus the lacunae,[9] but may also be due to the mechanosensing mechanisms on the dendrites. To this point, the integrins that tether the osteocyte cytoskeleton to the surrounding matrix, vary between the cell body and the dendrite. On the cell body, integrins with the β1 subunit form large focal adhesions containing vinculin and paxillin, but on the dendrites, integrins with the β3 subunit form atypical, smaller focal adhesions that co-localize with specialized pannexin-1 ion channels.[10,11] Osteocytes depend on both β1 and β3 integrins to sense and respond to mechanical loads,[12–14] but to study the contributions of each *in vitro* relies on a 3D system that enables dendrite formation. Osteocytes also use gap junctions that dendrites form with other dendrites of neighboring cells to amplify a signaling response by sharing secondary messengers, such as 3,5'-cyclic adenosine monophosphate (cAMP).[15] Thus, studying

osteocyte mechanobiology and signaling *in vitro* with a 3D environment that fosters dendrite formation will retain more relevance to *in vivo* conditions because of the unique mechanotransduction and gap junctional communication that dendrites facilitate.

The LCN is vital to osteocyte mechanobiology, yet most studies of osteocyte mechanobiology to date culture cells in two-dimensional (2D) environments, which lack the characteristics of the 3D LCN.[16] While osteocytes form dendrites in 3D collagen gels, [17–19] collagen gels are limited in their tunability of matrix stiffness and result in gel contraction that densifies the collagen matrix. Synthetic hydrogels offer a higher degree of tunability of stiffness and allow for control over the types of biological cues that are incorporated into a 3D culture environment. For example, the elastic modulus of hydrogels can be easily tuned by varying the crosslinking density, by means of changing the monomer concentration or the amount of crosslinker.[20] Modulus and crosslinking density are both important factors in osteocyte differentiation and cell spreading.[21–24] Chemically crosslinked hydrogels result in a tight polymer mesh (on the order of 1-10 nm),[25,26] which is smaller than the diameter of an osteocyte dendrite (100-150 nm).[1] The polymer mesh has been shown to limit cellular spreading and extracellular matrix (ECM) growth.[25–27] While the mesh size increases with hydrogel degradation, the hydrogel typically has to reach its point of reverse gelation, which is when the hydrogel transitions from a solid to a liquid, to allow cell spreading or ECM growth.[28] To overcome this limitation, hydrogels have been engineered with metalloproteinase (MMP)-sensitive crosslinks, which allows the cells to locally degrade the hydrogel, providing regions for cells to extend their processes without needing the bulk hydrogel to reach reverse gelation. In designing a synthetic-based hydrogel to promote dendrite formation, a degradable hydrogel will be a key requirement. Other studies have shown that incorporation of MMP-sensitive crosslinks into a hydrogel enhances osteogenesis,[37,38]

ECM deposition,[29,30] and maturation of osteocyte differentiation.[31] Another advantage to synthetic hydrogels is the ability to incorporate biochemical cues in a highly controlled manner to improve differentiation and cell spreading outcomes. For example, tethered RGD increases cell spreading as it provides attachment sites for integrin binding.[32] Growth factors such as transforming growth factor-β (TGF-β) increase the number of dendrites per osteocyte *in vivo* and *in vitro* when exogenously applied.[33] Immobilization of TGF-β via modification and tethering to the hydrogel avoids diffusion out of the hydrogel and increases chondrocyte differentiation,[34,35] and is thus a promising technique to increase osteocyte dendrite formation.

In vivo, osteocytes form their dendritic connections during the osteoblast-to-osteocyte differentiation period. When osteoblasts are encased in newly formed bone (consisting of collagen I and mineral), they extend dendritic protrusions outward, which may require E11 protein expression.[36] Eventually, deeply embedded in bone, osteocytes reside within their cell-mediated LCN and express markers of mature osteocytes such DMP1 and sclerostin. Thus, differentiation may depend on dendrite extension, and dendrite extension in hydrogels may be influenced by physical (*e.g.*, elastic modulus) and biochemical (*e.g.*, collagen I) factors. Therefore, this study sought to investigate the influence of controlled physical and biochemical factors on OCY454 osteocyte differentiation and dendrite extension in a 3D hydrogel. Poly(ethylene glycol) (PEG) hydrogels were chosen as the base chemistry, due to their cytocompatibility, bioinertness, and the ability to control their properties and incorporate biochemical factors with ease.[37] The hydrogels were formed with matrix metalloproteinase (MMP)-sensitive crosslinks to impart degradability, cell adhesion peptides RGD to support cell-hydrogel interactions, and tethered TGF-β3. This study has two main objectives. The first objective was to investigate physical and biochemical factors that influence dendrite formation in a 3D hydrogel. This objective aimed to test two hypotheses.

First, we hypothesized that degradable hydrogels are required for dendrite extension and will increase mature osteocyte differentiation. To test this hypothesis, we compared the MMP-sensitive hydrogels to non-degradable hydrogels. Second, we hypothesized that a lower crosslinking density and addition of biochemical cues would increase the extent of dendrite formation and the differentiation in degradable hydrogels. To test this hypothesis, we compared hydrogels formed with varying crosslinking density and bone extracellular matrix biochemical cues (collagen I and hydroxyapatite). All hydrogels were cultured in chemically defined media to avoid the use of serum. The second objective was to determine if osteocytes when cultured in a hydrogel permitting dendrite extension would respond to a common mechanobiology signaling molecule in bone, Prostaglandin E2 (PGE_2).[38] Osteocyte gene expression was assessed for key anabolic and catabolic genes associated with PGE_2 signaling and compared to a non-degradable hydrogel. The overall study outline is shown in Figure 3.1.

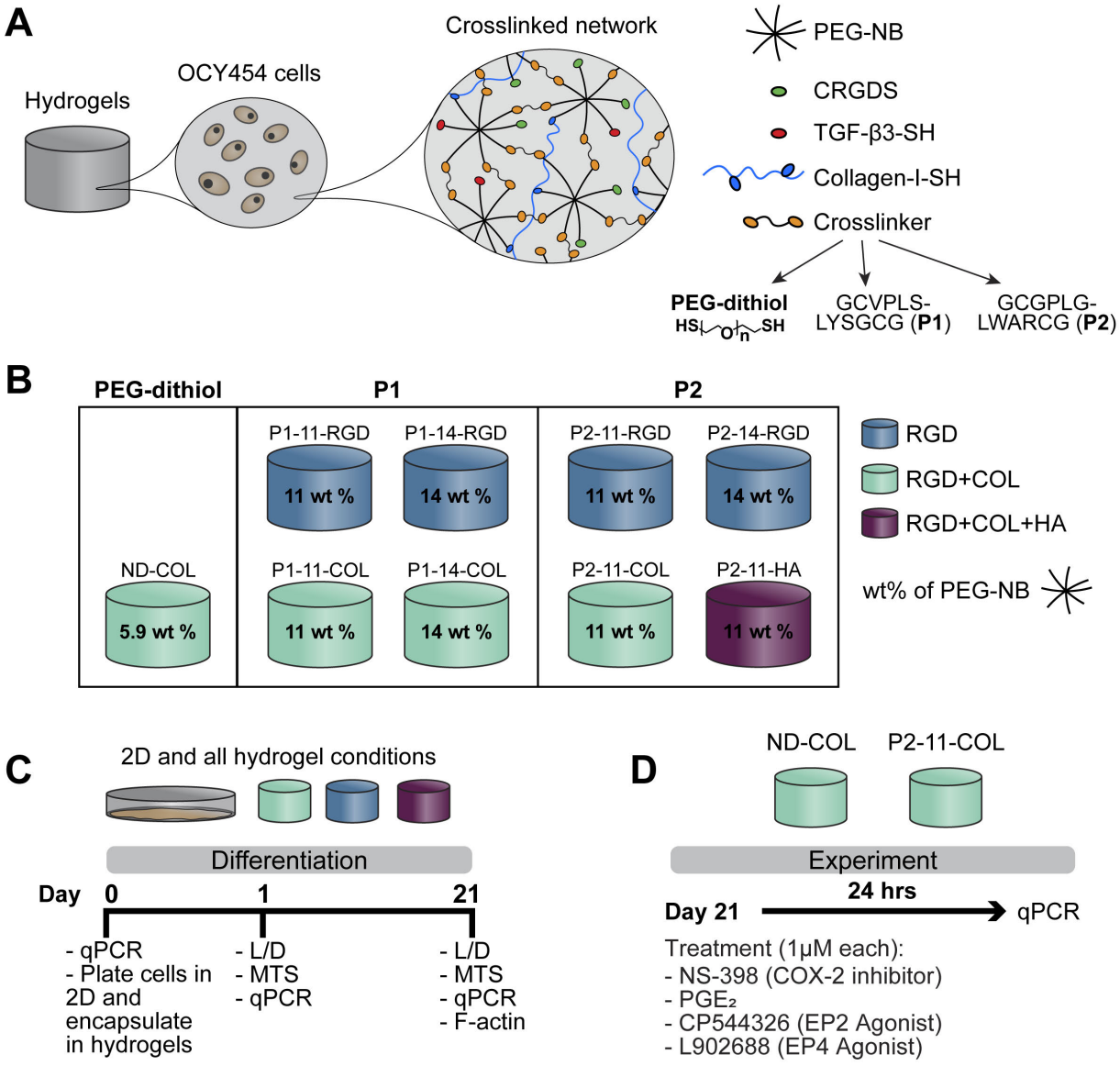

Figure 3.1: (A) Schematic of Ocy454 cells encapsulated in a crosslinked hydrogel. PEG-norbornene (PEG-NB) was crosslinked using three different crosslinkers, a non-degradable PEG-dithiol or one of two MMP-degradable crosslinkers (GCVPLS-LYSGCG, P1 or GCGPLG-LWARCG, P2). All networks also tethered in CRGDS and thiolated TGF-β3 (TGF-β3-SH), while some also included thiolated Collagen-I (Collagen-I-SH). (B) Schematic of the hydrogel formulations used in this study, sorted in columns by crosslinker type, colored by the attachment additions, and labeled by PEG-NB wt% (g/g). Each hydrogel condition was abbreviated into an acronym, which is labeled above each condition (*e.g.*, ND-COL, P1-11-COL, etc.) (C) Schematic of the study outline used to evaluate osteocyte differentiation and dendrite extension in each hydrogel condition over a 21-day differentiation period. Abbreviations: L/D = Live/Dead, MTS = Mechanical Testing, qPCR = quantitative polymerase chain reaction, F-actin = staining and imaging of F-actin. (D) Schematic of the study outline used to evaluate the effect of PGE2 or EP2/EP4 Agonist treatment on gene expression in two hydrogel conditions.

3.3 Methods

3.3.1 Macromer Synthesis

An 8-arm PEG (20000 g/mol, JenKem Technology) was synthesized as previously described[31] with 92% conjugation of norbornene to each arm of the PEG as confirmed using ^{1}H NMR. Collagen type I from rat tail (4 mg/ml, Sigma-Alridch) was thiolated by mixing neutralized collagen with Traut's reagent (2-iminothiolane, 2IT, Thermo-Fisher) in phosphate-buffered saline (PBS) at a molar ratio of 0.5:1 [2IT]:[Collagen] for a minimum of 2 hours on ice.[39] Similarly, TGF-β3 (Peprotech) dissolved in 10mM citric acid was thiolated by mixing with 2IT in PBS at a molar ratio of 4:1 [2IT]:[TGF-β3] for 1 hour at room temperature as previously described.[34] For calculating total thiols, we assumed 5 thiols per collagen molecule[39] and 1 thiol per TGF-β3 molecule.

3.3.2 Hydrogel Fabrication

The hydrogel formulations and their abbreviations used in this study are shown in Table 3.1. Thiolated TGF-β3 (TGF-β3-SH) and CRGDS were pre-tethered to the PEG norbornene (PEG-NB) by combining PEG-NB, CRGDS (GenScript), TGF-β3-SH, and 0.05 wt% (g/g) photoinitiator, 1-(4-(2- Hydroxyethoxy)-phenyl)-2-hydroxy-2-methyl-1-propane-1-one (I2959; BASF), in PBS to obtain final precursor concentrations of 4 mM CRGDS and 50 nM TGF-β3. The PEG-NB wt% used in this study included 5.9, 11, or 14 wt% (g/g), but the [crosslinking thiol]:[ene] ratio was kept constant at 0.8 to maintain the same percentage of crosslinks to be cleaved before reverse gelation.[40] In degradable hydrogels, PEG-NB wt% was either 11 or 14%. Because the thiol of the PEG-dithiol crosslinker is more reactive than the cysteine on the degradable crosslinkers, the PEG-NB wt% in the ND hydrogel was lowered to 5.9% to adjust for this difference. A precursor solution

of the PEG-NB with the pre-tethered CRGDS and TGF-β3 was combined with either a non-degradable PEG-dithiol crosslinker (1012 g/mol, Sigma-Aldrich) or an MMP-degradable crosslinker containing the sequence GCGPLG-LWARCG (1189 g/mol, Genscript) or GCVPLS-LYSGCG (1155 g/mol, Genscript) at a [crosslinker thiol]:[NB ene] molar ratio of 0.8:1, along with 0.05 wt% (g/g) I2959 in PBS. For collagen or hydroxyapatite (HA) hydrogels, thiolated collagen I or HA nanoparticles (<200 nm size, Sigma-Aldrich, 677418) were added to the precursor solution to obtain 0.1 wt% (g/g) collagen or 1 wt% (g/g) HA. OCY454 cells were encapsulated into the precursor solution at a concentration of 80 million cells/mL and photopolymerized in 3 mm diameter x 3 mm height molds for 8 minutes with 352 nm light at 1.5-2.1 mW/cm^2. The wt% (g/g) for each component was calculated based on the weight of all components.

Table 3.1: Hydrogel formulations and their abbreviations used in this study.

Hydrogel abbreviation	Cross-linker type	PEG-NB wt% (g/g)	thiol:ene	TGF-β3 (nM)	CRGDS (mM)	Collagen I wt% (g/g)	Hydroxy-apatite wt% (g/g)
ND	PEG-dithiol	5.9	0.8	50	4	0.1	0
P1-11-RGD	P1	11	0.8	50	4	0	0
P1-14-RGD	P1	14	0.8	50	4	0	0
P1-11-COL	P1	11	0.8	50	4	0.1	0
P1-14-COL	P1	14	0.8	50	4	0.1	0
P2-11-RGD	P2	11	0.8	50	4	0	0
P2-14-RGD	P2	14	0.8	50	4	0	0
P2-11-COL	P2	11	0.8	50	4	0.1	0
P2-11-HA	P2	11	0.8	50	4	0.1	1

The MMP-degradable sequences are termed P1 (GCVPLS-LYSGCG) and P2 (GCGPLG-LWARCG).

3.3.3 Cell Culture

OCY454 cells were expanded at 33˚C and 5% CO_2 on collagen type I-coated tissue culture polystyrene in growth media which consisted of alpha MEM (Gibco) with 1% Antibiotic-Antimycotic (Gibco) and 10% FBS (Atlanta Biologicals). At the start of the experiment, cells were either plated on collagen-coated polystyrene (2D) or encapsulated in hydrogels and then cultured in osteogenic media at 37˚C and 5% CO_2 on a shaker plate. Osteogenic media for 2D samples consisted of alpha MEM with 1% Antibiotic-Antimycotic, 10% FBS, 50 mg/ml ascorbic acid (Sigma-Aldrich) and 4 mM β-glycerophosphate (Sigma-Aldrich). 3D samples were cultured in chemically defined osteogenic media, which we have previously observed increases degradation in MMP-degradable hydrogels with TGF-β3. The chemically defined medium replaced the 10% FBS with 1% ITS+ Premix (Corning).

3.3.4 Live/Dead Imaging

On days 1 and 21, samples (n = 3) were stained with 4 μM Calcein AM (Corning) for 40 minutes and and 2uM ethidium homodimer (Corning) for 10 minutes in defined differentiation media on a shaker plate. Samples were rinsed in PBS and immediately imaged using a Leica DM6 CFS stellaris upright confocal (Leica Microsystems) with LAS X software (V4.1.1.23273).

3.3.5 Mechanical Testing

Immediately after Live/Dead imaging, the samples (n = 3) were subjected to unconfined compression using a mechanical testing system Insight II (MTS) with a 5N load cell. The top platen started out-of-contact with the hydrogel and then applied a constant displacement rate of 1.2 mm/min until approximately 50% strain (based on initial height of the hydrogel) was reached. The point of contact was determined using custom MATLAB code and the true modulus was calculated from the slope of the linear true-stress/true-strain curve from 10-15% strain.

3.3.6 Gene expression

Pre-encapsulated cells (day 0), 2D cultures (day 1 and 21), and 3D hydrogels (day 1 and 21) were collected for RNA extraction (n = 4 except P2-11-COL n = 8)). Pre-encapsulated cells and 2D samples were immediately lysed in Qiazol, flash-frozen, and stored at -80˚C. 3D samples were collected and immediately flash-frozen and stored at -80˚C. 3D samples were later homogenized in Qiazol using a tissue lyser (Qiagen). RNA was isolated from all samples using QIA shredder columns (Qiagen), phase lock gel tubes (Quantabio), and the miRNeasy Micro Kit (Qiagen). RNA was quantified using a Nanodrop instrument (ND-1000, Thermo Scientific) and 260/280 and 260/230 values were confirmed to be between 1.8 and 2.2. RNA was converted to cDNA using a High Capacity cDNA Reverse Transcription Kit (Applied Biosystems) at 1000ng per reaction. Each sample was diluted to 2.5-5 ng/μL and analyzed by real-time quantitative polymerase chain reaction (qPCR) using custom primers (Table 3.2) and SYBR Green Master Mix (Applied Biosystems) with a 7500 Fast PCR Machine (Applied Biosystems). Gene expression was analyzed with the Pfaffl method[41] using the housekeeping gene L32 to obtain the relative expression (RE) and normalizing to an experimental control to obtain the normalized expression (NE).

Table 3.2: Custom primer sequences and their calculated efficiencies for each gene

Gene	Protein	Efficiency	Forward	Reverse
Dmp1	DMP1	2.1	GCTTCTCTGAGA TCCCTCTTCG	GCGATTCCTCTAC CCTCTCT
Gja1	Cx43	2	GAGTTCCACCAC TTTGGCGT	GTGGAGTAGGCTT GGACCTT
L32	L32	2.01	CCATCTGTTTTA CGGCATCATG	TGAACTTCTTGGT CCTCTTTTTGA
Panx1	Pannexin 1	2.12	TGGACCTAAGAG ACGGACCT	GCTCCACGATTGG GTACTTG
Pdpn	E11	2.01	GGGATGAAACGC AGACAAC	CAATGAAGATCCC TCCGACG
Ptger1 [42]	EP1	2.14	TTTATTAGCCTT GGGCCTCGTGGA	ATTGCACACTAAT GCCGCAAGGAG
Ptger2 [42]	EP2	1.99	GATGAAGCAACC AGAGCAGAC	CAGAGAGGACTCC CACATGAA
Ptger3 [42]	EP3	2.05	GGTCATCCTCGT GTACCTGTC	GTCATGGTTAGCC CGAAGAA
Ptger4 [42]	EP4	2.07	GCCCTCTCCTGC CAATATAAC	TTTCAACACTTTG GCCTGAAC
Ptges	mPGES1	2.17	TACAGGAGTGAC CCAGATGT	GGAATGAGTACAC GAAGCCG
Sost	Sclerostin	2.09	GGCAAGCCTTCA GGAATGATG	TCTTTGGCGTCAT AGGGATGG
Tnfrsf11b	OPG	2.09	AGAAGCCACGCA AAAGTGTG	TTCACTTTGGTCCC AGGCAA
Tnfsf11	RANKL	2.18	CCATTTGCACAC CTCACCATC	CGTGGTACCAAGA GGACAGAG

3.3.7 Fluorescent Staining and Imaging

After 21 days of culture in osteogenic media, hydrogels (n = 3 except P2-11-COL n = 6) were fixed in 4% paraformaldehyde (Electron Microscopy Sciences) for 24 hours at 4˚C, rinsed in PBS, then stored in PBS at 4˚C for 1-3 weeks. Samples were permeabilized in 0.5% Triton X-100 (VWR) in PBS for 5 min on a shaker plate at room temperature (RT), rinsed twice, and blocked in 5% Bovine Serum Albumin (BSA, Sigma-Aldrich) in PBS for 1 hour on a shaker plate at RT. After rinsing twice, F-actin was stained using Phalloidin (Texas Red, Thermo-Fisher used at 1:80 dilution in PBS with 0.1% Triton X-100 and 3% BSA) for 6 hours on a shaker plate at RT. Samples

were rinsed twice and the nuclei were stained with DAPI (supplier, used at 1:500 dilution in PBS) for 10 min on a shaker plate at RT. Samples were rinsed twice and stored in PBS at 4˚C until imaging.

Confocal images were acquired using a Leica DM6 CFS stellaris upright confocal (Leica Microsystems) with LAS X software (V4.1.1.23273) with a 25x and 63x water immersion objective. Maximum intensity projections were generated for image quantification from 20 slices of the z-stacks taken with the 63x objective with 0.6 μm spacing in between slices, for a total depth of 12 μm per image. Dendritic cells were defined as cells that show F-actin connections to other cells or protrusions outwards from the cell while spherical cells were defined as having no F-actin connections to neighboring cells or protrusions (Figure 3.6A). The number of dendritic and spherical nuclei in each image was counted using NIH ImageJ software. Three hydrogels per condition were imaged, and the mean number and percentage of dendritic nuclei per image (n=5 images per sample) were calculated.

3.3.8 Prostaglandin E2 and Agonist Treatment

After 21 days of culture, osteogenic media was replaced with media containing either PGE_2 (1 μM, Cayman Chemical), CP544326 (1 μM, EP2 agonist, Cayman Chemical), L902688 (1 μM, EP4 agonist, Cayman Chemical), or NS-398 (1 μM, COX-2 inhibitor, Cayman Chemical). Hydrogels from the P2-11-COL and ND conditions were treated (n=4 per treatment). The final solvent (DMSO or methanol) concentration was 0.002% (v/v) for all treatments. Following 24 hours of incubation at 37˚C and 5% CO_2 on a shaker plate, samples were collected and flash-frozen for qPCR analysis.

3.3.9 Statistics

All statistics were analyzed using JMP Pro 14.1.0. Data were analyzed using one- or two-way analysis of variance (ANOVA) with a significance level of 0.05 where factors included time, culture condition, and treatment. For two-way ANOVAs, if the interaction term was significant, separate one-way ANOVAs were run for each individual effect. For significant effects from the ANOVA, Tukey's post hoc analysis was performed. The data were confirmed to have homogeneous variance and normal distribution. Outliers were removed using Grubb's outlier test. Graphical results are presented as a bar plot (mean and standard deviation error bars) or box plot including all points. When statistical significance is shown in figures with symbols, one symbol represents $p < 0.05$.

3.4 Results

3.4.1 Cell viability

To assess cell viability, hydrogel samples were stained for Live/Dead imaging on days 1 and 21 of culture in osteogenic media (Figure 3.2). Cell viability remained high at both time points in all hydrogel conditions. On day 1, cells regardless of hydrogel condition were rounded with no noticeable cell spreading. On day 21, many cells remained rounded, but there were regions that had form cell aggregates, which showed some evidence of cell spreading.

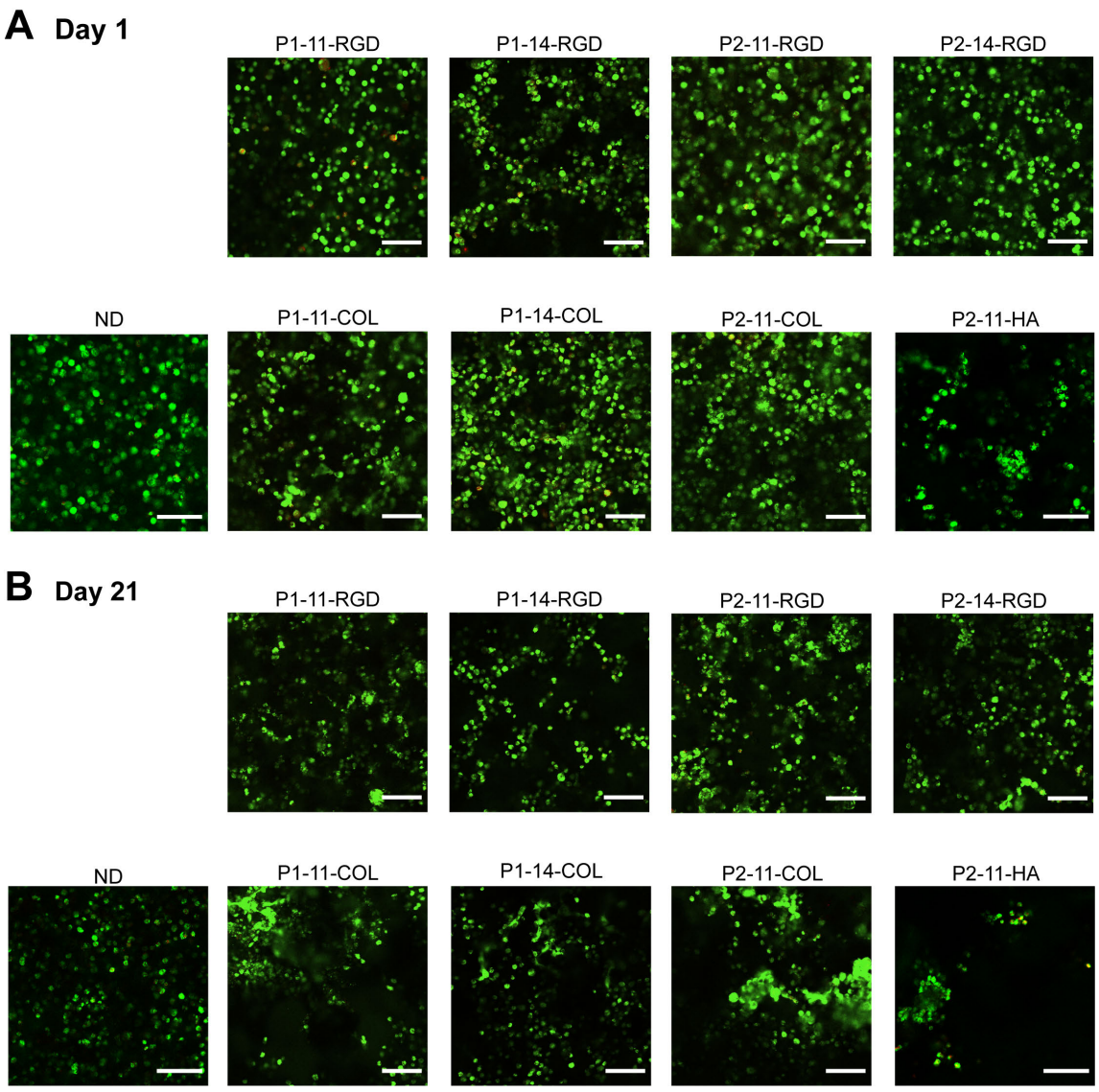

Figure 3.2: Representative Live/Dead images of each hydrogel condition on day 1 (A) or day 21 (B). Scale bar is 100 μm.

3.4.2 Mechanical properties of cell-laden hydrogels

On days 1 and 21 of culture, hydrogel samples (n = 3 per condition) were tested in unconfined compression to obtain the elastic modulus (Figure 3.3) of the different hydrogel formulations (Figure 3.1B). The mean and standard deviation of elastic moduli for each condition and day are compiled into Table 7.1. The initial modulus (day 1) of the ND hydrogels (2.5 ± 0.1

kPa) was significantly lower than all other hydrogel conditions except P1-11-RGD and P1-14-COL. The hydrogel with the highest modulus was the P2-14-RGD (13.2 ± 0.8 kPa). The P2 hydrogels were stiffer than the P1 hydrogels, changing the modulus by +50%, +32%, and +30% from P1 to P2 in the 11-RGD, 14-RGD, and 11-COL hydrogels, respectively. Increasing from 11 to 14 wt% in the RGD hydrogels changed the modulus by +51% and +36% in the P1 and P2 hydrogels, respectively. Interestingly, from 11 to 14 wt% in the P1-COL hydrogel, the modulus changed by -32%. Similarly, adding collagen to the P1-14 hydrogel decreased the modulus by -53%. Adding hydroxyapatite (HA) to the P2-11-COL hydrogel did not change the modulus.

Over the 21-day differentiation period, a few conditions showed significant changes in modulus: ND, P1-14-COL, and P2-11-COL. The ND hydrogels changed +64% while the P1-14-COL and P2-11-COL hydrogels both changed by -34% and -43%, respectively. The P1-11-RGD hydrogels exhibited the largest mean increase in modulus by +162% but was not statistically significant.

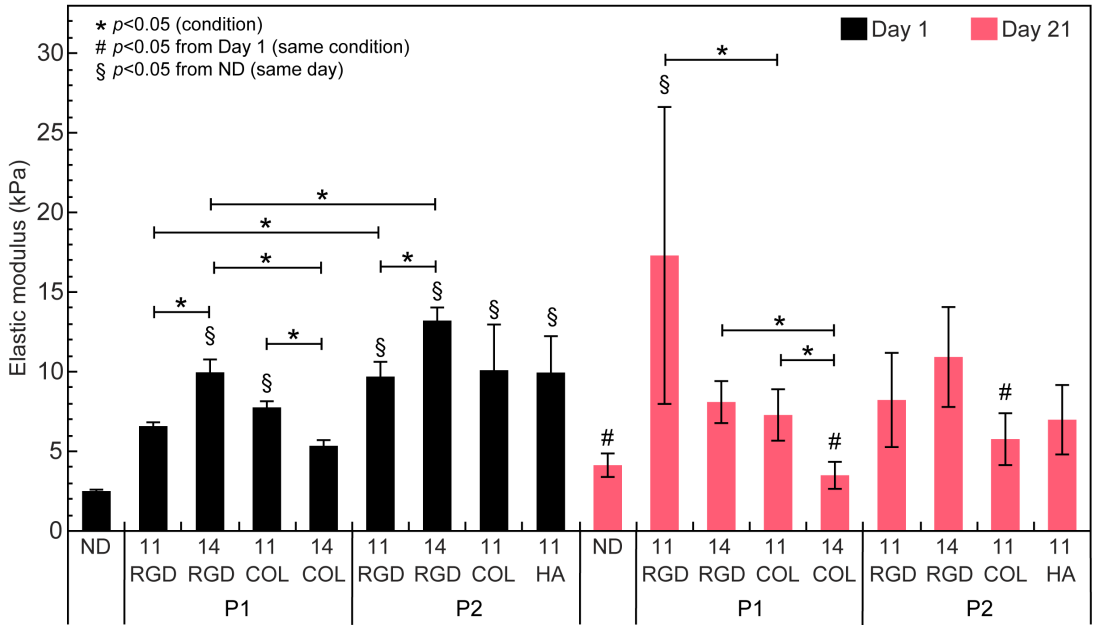

Figure 3.3: Elastic modulus calculated from the true-stress, true-strain curve for each hydrogel condition after 1 and 21 days of culture. Data are presented as the mean with standard deviation as error bars (n = 3).

3.4.3 Osteocyte Differentiation

To assess the differentiation after 21 days of culture, the gene expression for two key osteocyte differentiation markers, *Dmp1* and *Sost*, was measured. For *Dmp1*, a marker of early-to-late osteocyte differentiation, the NE of 2D and ND significantly increased from day 0 (58-fold for 2D and 8-fold for ND). The NE of ND was significantly lower from 2D by 7-fold. Within all hydrogels, there was a significant effect of crosslinker type (non-degradable vs. degradable, p = 0.005). Within the degradable hydrogels, there was also a significant effect of attachment type (RGD vs. RGD+COL, p = 0.016). Within P1, all conditions significantly increased from day 0, while the collagen conditions were higher than 2D and ND. Increasing the wt% significantly increased the NE in the RGD conditions within P1 (3-fold). Within the same wt%, adding collagen significantly increased the NE at 11% (6-fold) and was trending towards significance at 14% (2-fold, p = 0.054). Within P2, all conditions significantly increased from day 0, while the 14-RGD and 11-COL conditions were also significantly higher than 2D and ND. Increasing the wt% significantly increased the NE in the RGD conditions (2.5-fold). There was no significant difference between any of the P2, 11 wt% conditions. There was no significant effect of degradable crosslinker type (P1 vs. P2).

For *Sost*, a marker of mature osteocyte differentiation, the NE of 2D did not change from day 0, but the NE of ND significantly increased from day 0 by 154-fold. The NE of ND also significantly increased from 2D by 214-fold. Within all hydrogels, the effect of crosslinker type was not significant (non-degradable vs. degradable). In P1, all conditions significantly increased from day 0 and was higher than 2D and increasing the wt% had no effect. At 14 wt%, adding collagen significantly increased the NE (1.6-fold). Within P2, all conditions significantly increased from day 0 and from 2D. Increasing the wt% increased the NE in the RGD conditions (1.3-fold, p = 0.08). There was no significant difference between any of the P2, 11 wt% conditions. There was

only a significant effect of degradable crosslinker type with the 14-RGD conditions, where the P2 condition was 1.6-fold higher than the P1 condition.

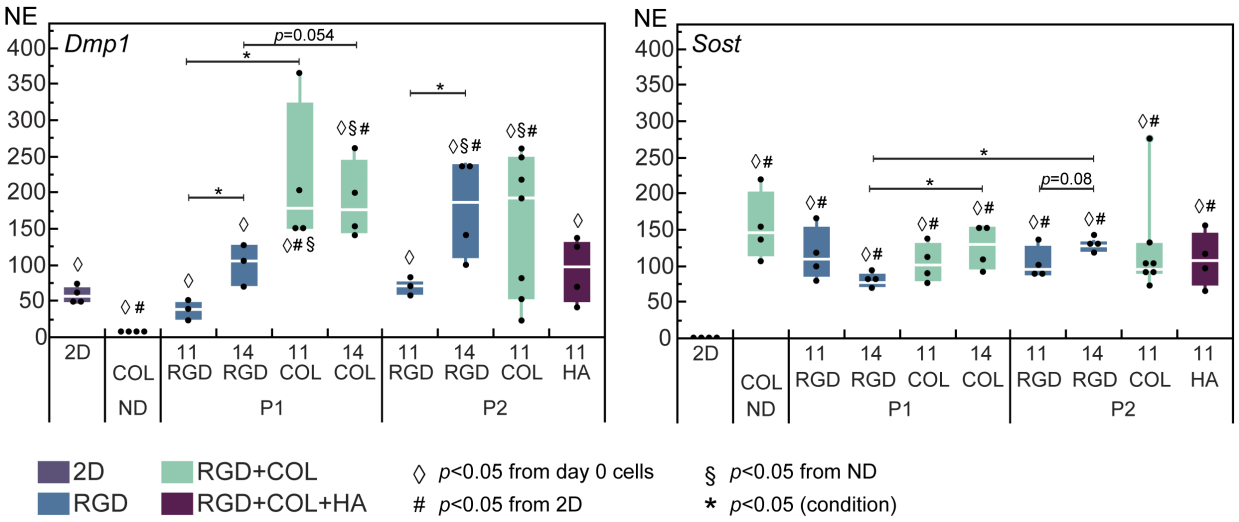

Figure 3.4: Normalized expression (NE) to the day 0 pre-encapsulated cells of *Dmp1* and *Sost* as measured in each hydrogel condition after 21 days of differentiation (n = 4-8).

3.4.4 Dendrite formation after 21 days of differentiation

After 21 days of culture, cells were assessed by staining for F-actin and imaging with confocal microscopy. Qualitatively, there were regions observed in all hydrogel conditions with only spherical cells (Figure 7.2). However, there were also regions of cell aggregates in all hydrogels with varying degrees of dendritic protrusions and connections (Figure 3.5). Image quantification was performed on the cell aggregate regions (175 μm x 175 μm), and the number (#) and percentage (%) of the dendritic cells per image were assessed (Figure 3.6A-C). A dendritic cell was defined by at least one protrusion. The mean, standard deviation, and maximum for the # and % of dendritic cells for each condition (from all images taken) are shown in Table 3.3.

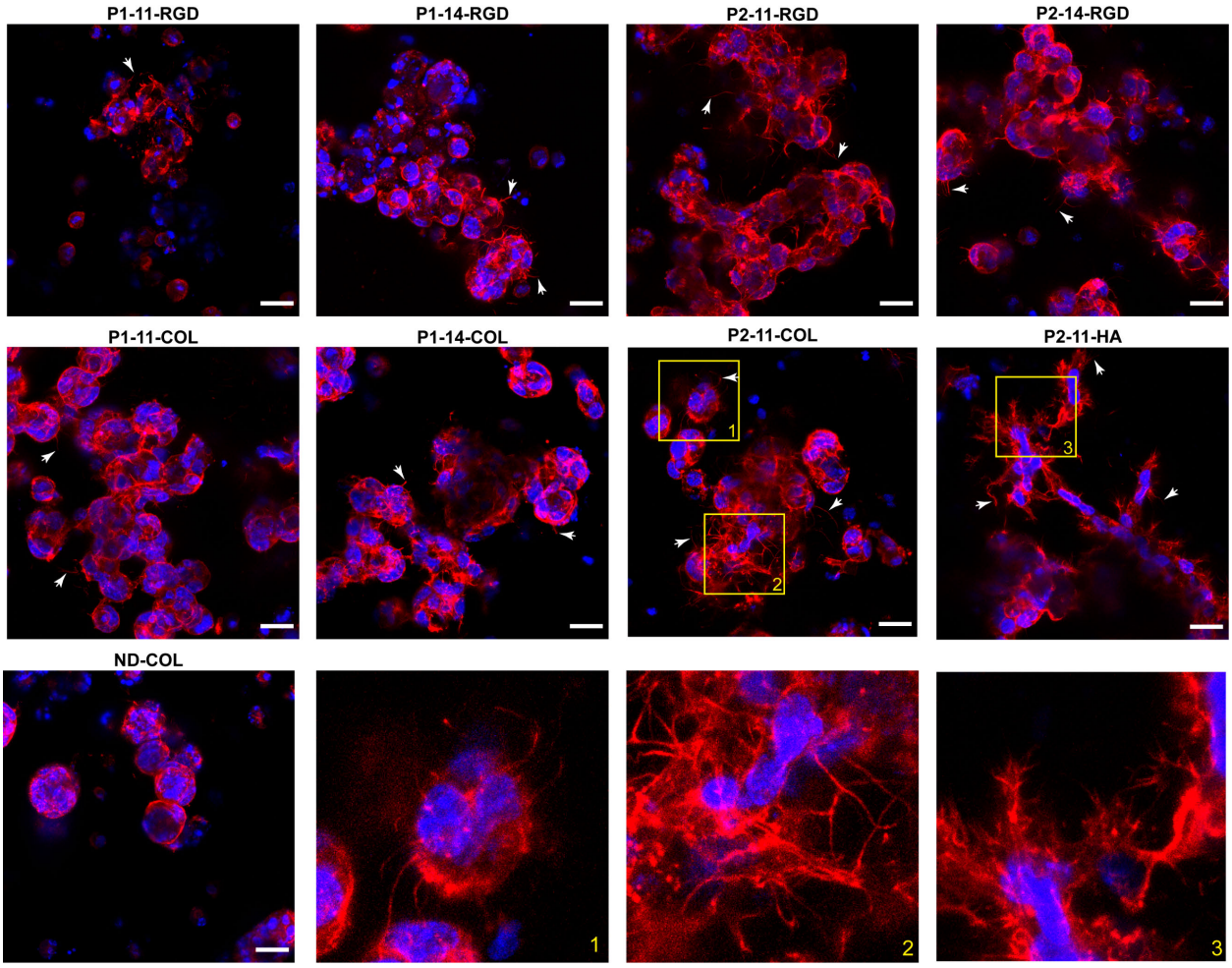

Figure 3.5: Representative images of cell aggregates in each hydrogel condition with a few dendrites per image denoted with an arrow. F-actin was stained with Phalloidin (red) and nuclei were stained with DAPI (blue). Images were taken with a 63X objective and are maximum intensity projections of 12 μm depth, with 0.6 μm spacing in between slices. Scale bar is 20 μm and image size is 175 μm x 175 μm. The lower right three panels zoom in on regions 1-3 labeled in the P2-11-COL and P2-11-HA images.

All hydrogels with collagen were significantly higher in # and % of dendritic nuclei as compared to the ND hydrogels. P2-14-RGD also had higher # and % as compared to ND, and P1-14-RGD had higher %. There is a clear trend of increasing number and percentage of dendritic cells with increasing wt% in the P1-RGD, P2, RGD, and P1-COL hydrogels (although not statistically significant). Collagen also increased the # and % of dendritic cells. In P1, the % of

dendritic cells significantly increased when collagen was added. The only significant difference between degradable crosslinkers was the increase in # of dendritic nuclei in P2 as compared to P1 in the 11-COL hydrogels. Adding HA did not have a significant effect compared to the P2-11-COL hydrogel.

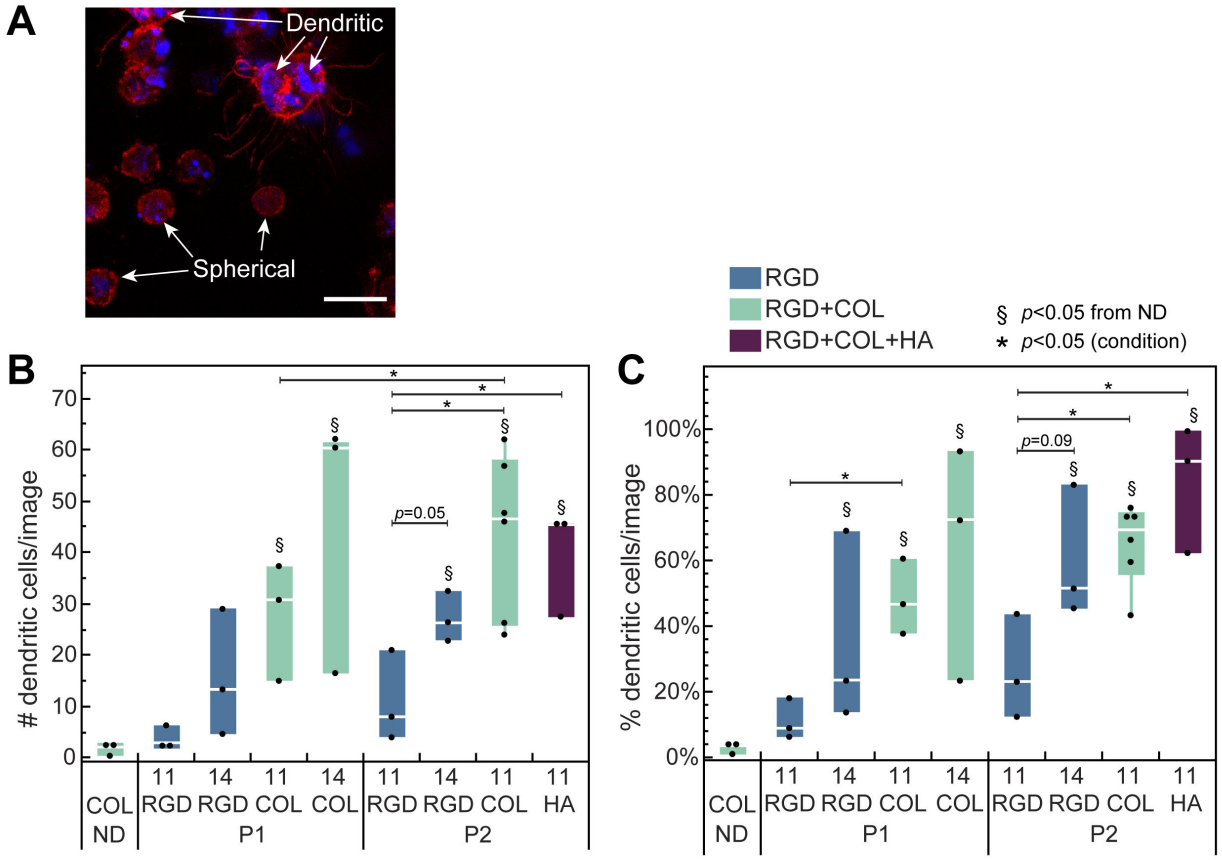

Figure 3.6: (A) Sample image denoting nuclei of dendritic and spherical cells with arrows. Mean number (B) and percentage (C) of dendritic nuclei per image for each sample (n = 5 images per sample) and condition (n = 3-6 samples per condition). In each image, the number of dendritic nuclei was counted (B) and then divided by the total number of nuclei in that image (C).

By qualitative and quantitative assessment, the dendrite formation within the degradable hydrogels spanned a larger range than in the ND hydrogels. All conditions had regions in the hydrogel with no dendritic cells (i.e., 0 for the # and % of dendritic cells). Yet, the maximum

values for each condition differed. There were regions that reached a maximum percentage of dendritic cells of 16% for ND, but 100% with collagen. Figure 3.5B and Figure 3.5C represent the mean # and % of dendrites assessed per sample. Dot plots of the same data are provided in Figure 7.3. These quantitative results support the qualitative finding that the range of dendrite formation throughout the ND hydrogels was much lower than in the degradable hydrogels.

Table 3.3: The mean, standard deviation (S.D.), and maximum for the number (#) and percentage (%) of dendritic cells for all the images that were quantified. All conditions had a minimum of 0 for # and % of dendritic cells.

	# dendritic cells			**% dendritic cells**		
	Mean	S.D.	Maximum	Mean	S.D.	Maximum
ND	2	4	11	3%	6%	16%
P1-11-RGD	3	6	18	10%	16%	49%
P1-14-RGD	17	20	55	39%	42%	95%
P1-11-COL	25	30	108	49%	40%	100%
P1-14-COL	44	38	121	60%	44%	100%
P2-11-RGD	14	20	53	31%	40%	98%
P2-14-RGD	27	23	68	58%	37%	100%
P2-11-COL	45	37	161	65%	39%	100%
P2-HA	41	38	132	76%	37%	100%

3.4.5 Dendrite extension gene expression after 21 days

The gene expression for three genes that are associated with osteocyte dendrite extension was measured after 21 days: *Gja1*, *Panx1,* and *Pdpn* (Figure 3.7). *Gja1* encodes for the protein connexin 43, which form gap junctions in osteocytes. *Panx1* encodes pannexin-1, an ion channel that forms on dendrites *in vivo,* and *Pdpn* encodes E11, a protein that is expressed by early osteocytes during dendrite formation *in vivo.*

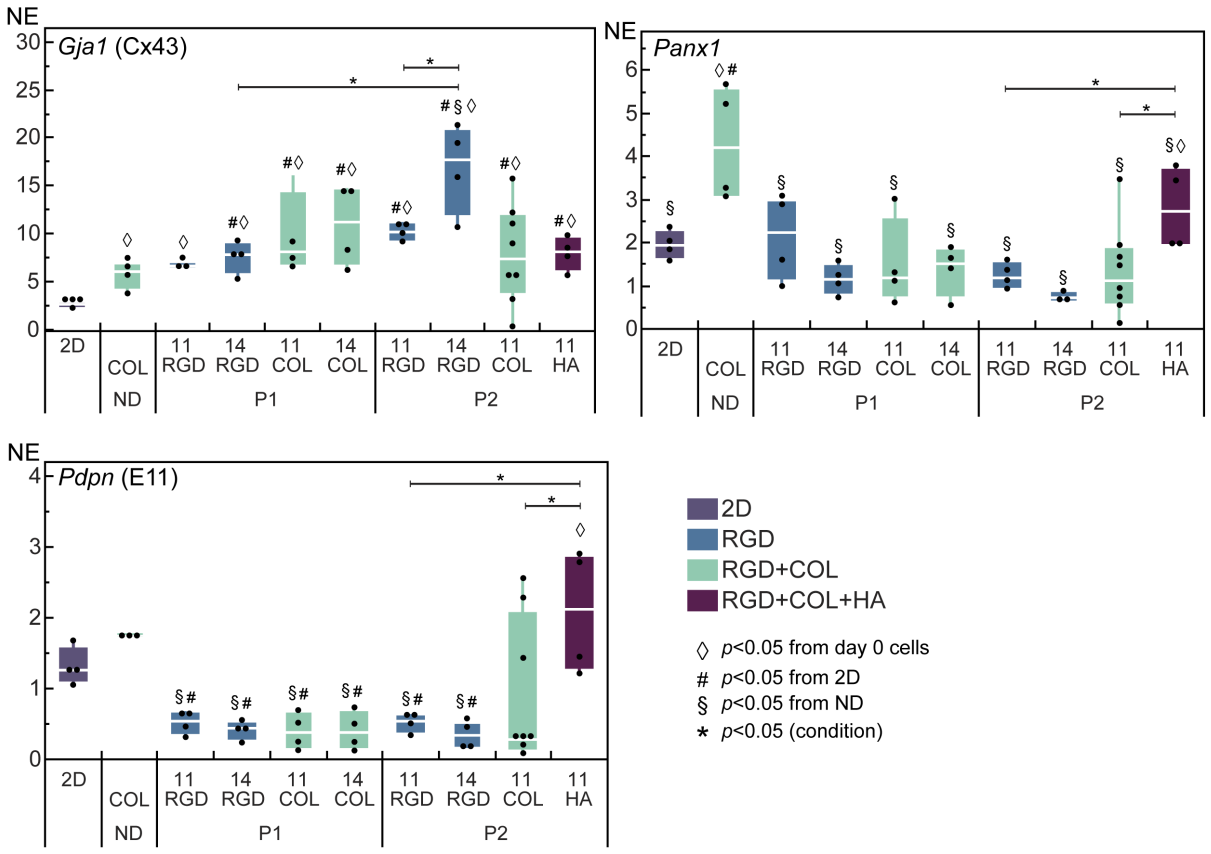

Figure 3.7: Normalized expression (NE) to the day 0 pre-encapsulated cells of *Gja1*, *Panx1*, and *Pdpn* as measured in each hydrogel condition after 21 days of differentiation (n = 4-8).

For *Gja1*, which encodes the gap junction protein connexin 43, the NE of 2D did not change from day 0. The NE of ND significantly increased from day 0 (6-fold) but was not significantly different than 2D. Within all hydrogels, there was no effect of crosslinker type (non-degradable vs. degradable). In the degradable hydrogels, there was also no effect of attachment type (RGD vs. RGD+COL). Within P1, all conditions significantly increased from day 0, while the collagen conditions and 14-RGD also increased from 2D. Increasing the wt% or adding collagen did not significantly change the NE in the P1 hydrogels. Within P2, all conditions significantly increased from day 0 and were higher than 2D, while the 14-RGD condition also significantly increased from ND. Increasing the wt% significantly increased the NE in the RGD conditions (1.6-fold).

There was no significant difference between any of the P2, 11 wt% conditions. There was only a significant effect of degradable crosslinker type with the 14-RGD conditions, where the P2 condition was 2-fold higher than the P1 condition.

For *Panx1*, encoding a protein that comprises atypical focal adhesions in the dendrites of osteocytes, the NE of 2D did not change from day 0. The NE of ND significantly increased from day 0 (4-fold) and significantly increased from 2D (2-fold). Within all hydrogels, there was a significant effect of crosslinker type (non-degradable vs. degradable, p = 0.0001). In the degradable hydrogels, there was no effect of attachment type (RGD vs. RGD+COL). Within P1, all conditions significantly decreased from ND, did not change from day 0 or 2D. There was no effect of wt% or adding collagen within P1. In P2, all conditions significantly decreased from ND, and all but HA were unchanged from day 0 or 2D. The HA condition significantly increased from 2D (1.5-fold). There was no effect of wt% or adding collagen in P2, but adding HA significantly increased the NE as compared to the P2-11-COL condition (2-fold) and P2-11-RGD (2.2-fold). There was no significant effect of degradable crosslinker type (P1 vs. P2).

For *Pdpn*, which is expressed in early osteocytes extending dendrites, the NE of 2D did not change from day 0. The NE of ND significantly also did not change from day 0 or from 2D. Within all hydrogels, there was a significant effect of crosslinker type (non-degradable vs. degradable, p = 0.026). In the degradable hydrogels, there was no effect of attachment type (RGD vs. RGD+COL). Within P1, all conditions significantly decreased from ND and from 2D. There was no effect of wt% or adding collagen within P1. In P2, all RGD conditions significantly decreased from ND and from 2D. The 11-COL and HA conditions were both unchanged from 2D and ND. The HA condition significantly increased from day 0 (2-fold). There was no effect of wt% or adding collagen in P2, but adding HA significantly increased the NE as compared to the P2-11-

COL condition (2-fold) and P2-11-RGD (4-fold). There was no significant effect of degradable crosslinker type (P1 vs. P2).

3.4.6 Gene expression after treatment with PGE_2 and EP agonists

After 21 days of differentiation, the gene expression for the genes that encode all four EP receptors EP1-4 (*Ptger1, Ptger2, Ptger3, Ptger4*) were measured in two conditions: ND and P2-11-COL (Figure 3.8A). All four genes were present, and there was no significant difference in the RE values comparing the two conditions. However, there were significant differences in RE between the genes. In both conditions, *Ptger1* was significantly lower than all other genes. Additionally, in the P2 hydrogel *Pger2* and *Ptger4* were significantly higher than *Ptger3*. In both hydrogels, there was no significant difference between *Ptger2* and *Ptger4* expression.

On day 21, hydrogels from two conditions (ND and P2-11-COL, n=4 per treatment) were treated with PGE_2, a rapid response to mechanical loading in osteocytes.[38] NS-398 was added to the base samples, which inhibits COX-2, an intracellular enzyme that is involved in the biosynthesis of PGE_2.[43] Agonists for EP2 (EP2A, CP544326) and EP4 (EP4A, L902688) were investigated, as EP2 and EP4 are the two cell-surface receptors for PGE_2 that induce anabolic effects in bone.[44–46] Following 24-hours of treatment, samples were collected and the expression of five genes important to anabolic, catabolic, or PGE_2 signaling was measured (*Gja1, Ptges, Tnfrsf11b, Tnfsf11,* and *Sost*) and normalized to the RE of the NS-treated samples within each hydrogel condition to obtain the NE (Figure 3.8B). In the ND hydrogels, the expression of these five genes was also measured in samples that were treated in media alone (Figure 7.4). There was no significant difference in gene expression between the NS-treated and untreated samples, indicating that endogenous PGE_2 lacked a significant effect.

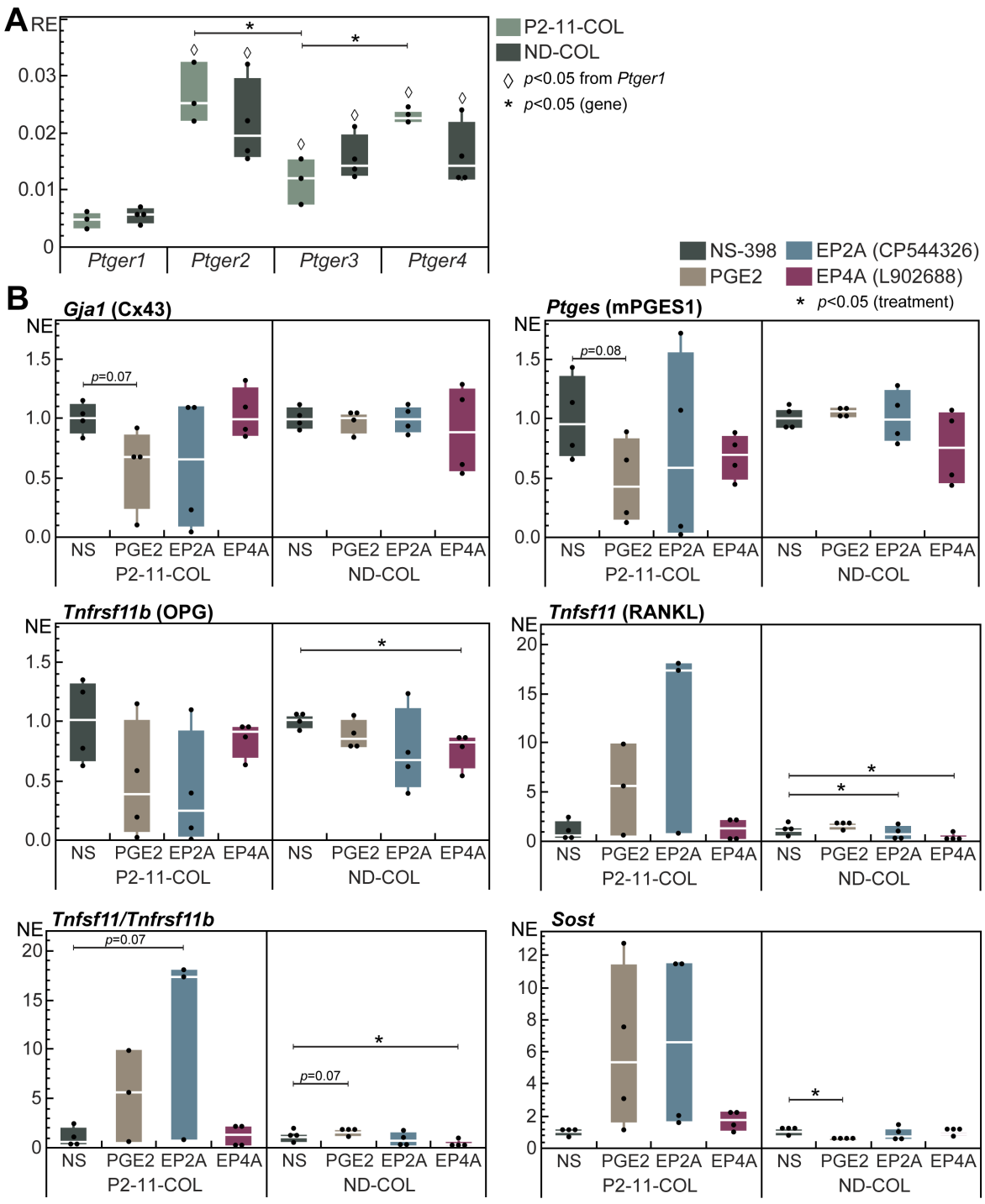

Figure 3.8: (A) Relative expression (RE) of *Ptger1*, *Ptger2*, *Ptger3*, and *Ptger4* in the P2-11-COL and ND-COL hydrogels after 21 days of differentiation (n = 4). (B) Gene expression of *Gja1*, *Ptges*, *Tnfrsf11b*, *Tnsfsf11*, and *Sost* was measured in P2-11-COL or ND-COL hydrogels after 24-hours of incubation in 1 μM NS-398, PGE2, CP544326, or L902688 (n = 4). RE was normalized to the NS-398 treated samples to obtain the normalized expression (NE).

Treatment did not significantly change *Gja1* or *Ptges* expression. In the P2 hydrogel, PGE_2 treatment reduced the *Gja1* NE by 1.7-fold and was trending towards significance ($p = 0.07$). Also, PGE_2 reduced the *Ptges* NE by 2-fold in the P2 hydrogel and was trending towards significance ($p = 0.08$).

Treatment significantly changed the *Tnfrsf11b*, *Tnfsf11,* and *Sost* expression in only the ND hydrogel. EP4A treatment significantly reduced the *Tnfrsf11b* expression in the ND hydrogel by 1.3-fold and had no effect in the P2 hydrogel. PGE_2 treatment did not significantly alter the *Tnfsf11* expression in the ND hydrogel, but both EP2A and EP4A treatment did. EP2A reduced the NE by 2-fold and EP4A reduced the NE by 4-fold, both compared to NS. In the ND hydrogel, PGE_2 treatment increased the *Tnfrsf11b/Tnfsf11* ratio by 1.5-fold, trending towards significance ($p = 0.07$). The EP4A treatment significantly reduced the *Tnfrsf11b/Tnfsf11* ratio by 2.7-fold compared to NS ($p = 0.03$) only in the ND hydrogel. With PGE_2 treatment, *Sost* NE was reduced by 1.6-fold ($p = 0.008$).

3.5 Discussion

This study investigated the effects of physical and biochemical factors of a hydrogel on osteocyte differentiation and dendrite extension in 3D culture. To achieve extensive dendrite formation in 3D hydrogels, degradability was necessary. Further, dendrite formation and differentiation were stimulated by increasing the modulus and adding biochemical cues, indicating that both physical and biochemical cues regulate osteocyte behavior. Together, this work shows that osteocytes express mature osteocyte markers and form dendritic connections in degradable PEG hydrogels, enabling a platform to study osteocyte mechanobiology with relevance to *in vivo* conditions in a highly tunable system.

Extensive dendrite formation was observed only in degradable hydrogels. Osteocyte dendrites *in vivo* are estimated to have a diameter of 100 nm,[1] which is much larger than the 1-10 nm mesh size of these PEG hydrogels. Therefore, cell-mediated degradation allows for dendrite extension. Interestingly, *Dmp1* was also enhanced in degradable hydrogels but there was no difference in *Sost* expression between the non-degradable and degradable conditions. This suggests that the 3D environment may play a larger role in dominating mature osteocyte markers such as *Sost* while degradability dominates the dendrite formations and earlier osteocyte markers *Dmp1*.

There was little difference between the degradable (P1 vs. P2) crosslinkers in the RGD hydrogels. However, in the hydrogels with collagen, the P2 crosslinker significantly increased the number of dendrites at 11 wt%. The P1 crosslinker has been shown to be degradable by MMP-2 and MMP-14,[47] while the P2 crosslinker has been shown to be degradable by MMP-2 and MMP-13.[31] The non-specific nature of these degradable crosslinkers and the few differences observed between suggests that any differences in the rate of degradation was not enough to have an impact on dendrites.

The PEG-NB wt% was varied between 11 and 14% within the degradable hydrogels to affect the crosslinking density of the hydrogel network. Increasing the PEG-NB wt% increased the elastic modulus in the RGD hydrogels, which is expected when [crosslinking thiols]:[ene] is constant and indicates increased crosslinking density.[20] In these RGD hydrogels, increasing the modulus also upregulated the *Dmp1* expression. The *Dmp1* expression did not change between the two RGD hydrogels with different crosslinkers that were both approximately 10 kPa (P1-14-RGD and P2-11-RGD), further indicating a connection between modulus and osteocyte differentiation. Increasing the modulus also slightly increased the number and percentage of dendrites in the P2-

RGD hydrogels. The few dendrites in the non-degradable hydrogels indicates that the polymer mesh must degrade for dendrite formation. However, more dendrite formation in initially stiffer hydrogels suggests that the stiffness is involved in mechanotransduction events that increase osteocyte differentiation and dendrite extension together despite a higher crosslinking density that the cells must degrade to form dendrites. Cultured osteoblasts in 2D increase cell spreading with increased modulus,[22] and stiffness provides traction for cell spreading on 2D substrates.[21,22] Yet, mesenchymal stem cells in non-degradable 3D hydrogels show no effect of stiffness on cell spreading.[21] Rather, in that study, osteogenic differentiation was enhanced in the 10-20 kPa range which was modulated in part by integrin-RGD binding, but not cell morphology. Thus, the results from this study are consistent with previous studies that show modulus regulating differentiation, but our findings also suggest that an initially stiffer hydrogel increases dendrite extension in 3D hydrogels which may be a result of higher traction combined with cell-mediated degradation.

Adding hydroxyapatite (HA) particles or collagen did not change the initial modulus, and therefore the crosslinking density. The finding that the HA particles did not alter the modulus is supported by previous work using the same low concentration in degradable hydrogels.[48] The collagen molecules can likely bind to multiple PEG-NB molecules due to the difference in size and multiple thiols per collagen molecule. Yet, any crosslinking that did occur was undetectable by the modulus measurements, indicating that any effect on cellular behavior that the collagen induced was likely via biochemical signaling rather than physical crosslinking. Dendrite formation was increased by the addition of the collagen and HA, compared to the hydrogels with only RGD. RGD provides cell attachment sites for αv integrin binding[21] and *in vivo*, osteocyte cell dendrites express integrin αv.[10,49] It is possible that the αv integrin binding affinity to other peptide sequences unique to collagen I may have increased the dendrite extension in the hydrogels with collagen. It

is also possible that the cell-collagen interaction in the hydrogels with collagen mimicked aspects of the cell-matrix interaction that occurs when osteoblasts are surrounded by unorganized collagen I *in vivo*, which stimulates dendrite extension. The HA hydrogel was not significantly different than the HA+COL hydrogel, indicating that the increased dendrite formation was dominated by the collagen biochemical signaling effects rather than HA effects. Interestingly, the osteocyte differentiation markers of *Dmp1* and *Sost* were unchanged by the addition of collagen and HA, indicating that these extracellular matrix cues stimulated dendrite formation unrelated to gene expression changes. This suggests that dendrite formation may be independent of differentiation gene expression changes, or that one may precede the other.

None of the genes that were selected for relevance to dendrite extension *in vivo* (*Gja1*, *Panx1*, and *Pdpn*) investigated in this study showed any difference between the RGD and RGD+COL hydrogels, but dendrite formation was enhanced in RGD+COL hydrogels. This indicates that the day 21 expression of these genes does not directly relate to the day 21 dendrites. The hydrogel with HA was not significantly different than the same hydrogel without HA (P2-11-COL) in number or percentage of dendrites. Yet, the gene expression of *Panx1* and *Pdpn* were both upregulated with HA. This further supports the conclusion that these genes do not indicate the cell dendrites as assessed by the fluorescent microscopy.

We identified one hydrogel condition that had a high number and percentage of dendrites, P2-11-COL, which showed a different osteocyte response to PGE_2 as compared to the ND hydrogel. Osteocytes rapidly produce PGE_2 in response to mechanical loading,[50,51] and PGE_2 induces an overall anabolic response on bone[52,53] by regulating both osteoblasts and osteoclasts.[54–56] In previous work, we showed that dimensionality, which affects differentiation, also affects the osteocyte response to PGE_2. Here, we hypothesized that the degradable environment, which affects

osteocyte differentiation and dendrite formation, would also affect the response to PGE_2. Further, we treated with agonists for EP2 and EP4, the two cell surface receptors for PGE_2 responsible for anabolic signaling.[44–46] The gene expression response to PGE_2 varied between hydrogel types: the P2 hydrogels were highly variable and not significant. We attribute the variability in the P2 hydrogel to larger range of dendrite formations that were observed. In the ND hydrogel, *Sost* expression decreased with PGE_2 treatment, which aligns with previous studies.[57,58] Additionally, *Tnfsf11* expression decreased with both EP2 and EP4 agonist treatment, but not with PGE_2. This indicates that *Tnfsf11* expression is regulated by intracellular signaling pathways that EP2 and EP4 activate, but activation of EP1 and/or EP3 may inhibit the effects of EP2/EP4. The decrease in *Tnfsf11/Tnfrsf11b* and *Sost* both indicate anabolic signaling, aligning with our previous study (Chapter 4).

3.6 Conclusion

In conclusion, this study varied physical (crosslinking density, degradability) and biochemical (collagen, hydroxyapatite) factors in a tunable 3D hydrogel with tethered TGF-β3 and RGD to study osteocyte differentiation and dendrite formation. The results of this study indicate that degradability is necessary for dendrite formation and that a small amount of collagen (0.1 wt%) can increase dendrites independent of differentiation gene expression. Additionally, modulus affects dendrite formation and differentiation gene expression together. Taken together, this study shows that dendrites form in 3D degradable hydrogels, which enables the study of osteocyte mechanobiology and signaling *in vitro* in an environment and with a cell phenotype that more accurately resembles osteocytes *in vivo* than 2D cultures.

3.7 Acknowledgements

Jennifer Coulombe provided statistical advice. We thank Professor Sarah Calve for the use of her Leica DM6 CFS stellaris upright confocal. The research reported in this publication was supported by the National Institute of Arthritis and Musculoskeletal and Skin Diseases of the National Institutes of Health under the Award 1R21AR069791-01A1. RW was supported on an NIH/NIA National Institute of Aging Integrative Physiology of Aging Training Grant under Award T32AG000279-16A1. The content in this publication is solely the responsibility of the authors and does not necessarily represent the official views of the NIH.

3.8 References

1. You, L.-D., Weinbaum, S., Cowin, S. C. & Schaffler, M. B. Ultrastructure of the osteocyte process and its pericellular matrix. *Anat. Rec.* **278A**, 505–513 (2004).

2. Bellido, T., Plotkin, L. I. & Bruzzaniti, A. Bone Cells. in *Basic and Applied Bone Biology* 27–45 (Elsevier, 2014). doi:10.1016/B978-0-12-416015-6.00002-2.

3. Hemmatian, H., Bakker, A. D., Klein-Nulend, J. & van Lenthe, G. H. Aging, Osteocytes, and Mechanotransduction. *Curr Osteoporos Rep* **15**, 401–411 (2017).

4. Ribeiro-Rodrigues, T. M., Martins-Marques, T., Morel, S., Kwak, B. R. & Girão, H. Role of connexin 43 in different forms of intercellular communication – gap junctions, extracellular vesicles and tunnelling nanotubes. *J Cell Sci* **130**, 3619–3630 (2017).

5. Price, C., Zhou, X., Li, W. & Wang, L. Real-Time Measurement of Solute Transport Within the Lacunar-Canalicular System of Mechanically Loaded Bone: Direct Evidence for Load-Induced Fluid Flow. *J Bone Miner Res* **26**, 277–285 (2011).

6. Wu, D., Ganatos, P., Spray, D. C. & Weinbaum, S. On the electrophysiological response of bone cells using a Stokesian fluid stimulus probe for delivery of quantifiable localized picoNewton level forces. *J Biomech* **44**, 1702–1708 (2011).

7. Wu, D., Schaffler, M. B., Weinbaum, S. & Spray, D. C. Matrix-dependent adhesion mediates network responses to physiological stimulation of the osteocyte cell process. *PNAS* **110**, 12096–12101 (2013).

8. Burra, S. *et al.* Dendritic processes of osteocytes are mechanotransducers that induce the opening of hemichannels. *PNAS* **107**, 13648–13653 (2010).

9. Fritton, S. P. & Weinbaum, S. Fluid and Solute Transport in Bone: Flow-Induced Mechanotransduction. *Annual Review of Fluid Mechanics* **41**, 347–374 (2009).

10. Qin, L., Liu, W., Cao, H. & Xiao, G. Molecular mechanosensors in osteocytes. *Bone Res* **8**, 23 (2020).

11. Cabahug-Zuckerman, P. *et al.* Potential role for a specialized β3 integrin-based structure on osteocyte processes in bone mechanosensation. *J Orthop Res* **36**, 642–652 (2018).

12. Litzenberger, J. B., Tang, W. J., Castillo, A. B. & Jacobs, C. R. Deletion of β1 Integrins from Cortical Osteocytes Reduces Load-Induced Bone Formation. *Cel. Mol. Bioeng.* **2**, 416–424 (2009).

13. Haugh, M. G., Vaughan, T. J. & McNamara, L. M. The role of integrin α(V)β(3) in osteocyte mechanotransduction. *J Mech Behav Biomed Mater* **42**, 67–75 (2015).

14. Thi, M. M., Suadicani, S. O., Schaffler, M. B., Weinbaum, S. & Spray, D. C. Mechanosensory responses of osteocytes to physiological forces occur along processes and not cell body and require αVβ3 integrin. *PNAS* **110**, 21012–21017 (2013).

15. Gupta, A. *et al.* Communication of cAMP by connexin43 gap junctions regulates osteoblast signaling and gene expression. *Cellular Signalling* **28**, 1048–1057 (2016).

16. Zhang, C., Bakker, A. D., Klein-Nulend, J. & Bravenboer, N. Studies on Osteocytes in Their 3D Native Matrix Versus 2D In Vitro Models. *Current Osteoporosis Reports* **17**, 207–216 (2019).

17. Bernhardt, A., Weiser, E., Wolf, S., Vater, C. & Gelinsky, M. Primary Human Osteocyte Networks in Pure and Modified Collagen Gels. *Tissue Engineering Part A* **25**, 1347–1355 (2019).

18. Bernhardt, A., Österreich, V. & Gelinsky, M. Three-Dimensional Co-culture of Primary Human Osteocytes and Mature Human Osteoclasts in Collagen Gels. *Tissue Engineering Part A* ten.tea.2019.0085 (2019) doi:10.1089/ten.tea.2019.0085.

19. Skottke, Gelinsky, & Bernhardt. In Vitro Co-culture Model of Primary Human Osteoblasts and Osteocytes in Collagen Gels. *IJMS* **20**, 1998 (2019).

20. Anseth, K. S., Bowman, C. N. & Brannon-Peppas, L. Mechanical properties of hydrogels and their experimental determination. *Biomaterials* **17**, 1647–1657 (1996).

21. Huebsch, N. *et al.* Harnessing traction-mediated manipulation of the cell/matrix interface to control stem-cell fate. *Nature Materials* **9**, 518–526 (2010).

22. Mullen, C. A., Vaughan, T. J., Billiar, K. L. & McNamara, L. M. The Effect of Substrate Stiffness, Thickness, and Cross-Linking Density on Osteogenic Cell Behavior. *Biophysical Journal* **108**, 1604–1612 (2015).

23. Mullen, C. A., Haugh, M. G., Schaffler, M. B., Majeska, R. J. & McNamara, L. M. Osteocyte differentiation is regulated by extracellular matrix stiffness and intercellular separation. *Journal of the Mechanical Behavior of Biomedical Materials* **28**, 183–194 (2013).

24. Mc Garrigle, M., Haugh, M., Voisin, M. & McNamara, L. Osteocyte differentiation and the formation of an interconnected cellular network in vitro. *European Cells and Materials* **31**, 323–340 (2016).

25. McKinnon, D. D., Kloxin, A. M. & Anseth, K. S. Synthetic hydrogel platform for three-dimensional culture of embryonic stem cell-derived motor neurons. *Biomaterials Science* **1**, 460 (2013).

26. Nicodemus, G. D., Skaalure, S. C. & Bryant, S. J. Gel structure has an impact on pericellular and extracellular matrix deposition, which subsequently alters metabolic activities in chondrocyte-laden PEG hydrogels. *Acta Biomaterialia* **7**, 492–504 (2011).

27. Liao, H. *et al.* Influence of hydrogel mechanical properties and mesh size on vocal fold fibroblast extracellular matrix production and phenotype. *Acta Biomaterialia* **4**, 1161–1171 (2008).

28. Schneider, M. C. *et al.* Local Heterogeneities Improve Matrix Connectivity in Degradable and Photoclickable Poly(ethylene glycol) Hydrogels for Applications in Tissue Engineering. *ACS Biomater. Sci. Eng.* **3**, 2480–2492 (2017).

29. Sridhar, B. V. *et al.* Development of a Cellularly Degradable PEG Hydrogel to Promote Articular Cartilage Extracellular Matrix Deposition. *Advanced Healthcare Materials* **4**, 702–713 (2015).

30. Amer, L. D. & Bryant, S. J. The In Vitro and In Vivo Response to MMP-Sensitive Poly(Ethylene Glycol) Hydrogels. *Annals of Biomedical Engineering* **44**, 1959–1969 (2016).

31. Aziz, A. H., Wilmoth, R. L., Ferguson, V. L. & Bryant, S. J. IDG-SW3 Osteocyte Differentiation and Bone Extracellular Matrix Deposition Are Enhanced in a 3D Matrix Metalloproteinase-Sensitive Hydrogel. *ACS Appl. Bio Mater.* **3**, 1666–1680 (2020).

32. Hersel, U., Dahmen, C. & Kessler, H. RGD modified polymers: biomaterials for stimulated cell adhesion and beyond. *Biomaterials* **24**, 4385–4415 (2003).

33. Liu, W. *et al.* TGF-β1 facilitates cell–cell communication in osteocytes via connexin43- and pannexin1-dependent gap junctions. *Cell Death Discov.* **5**, 141 (2019).

34. Schneider, M. C., Chu, S., Randolph, M. A. & Bryant, S. J. An in vitro and in vivo comparison of cartilage growth in chondrocyte-laden matrix metalloproteinase-sensitive poly(ethylene glycol) hydrogels with localized transforming growth factor β3. *Acta Biomaterialia* **93**, 97–110 (2019).

35. Park, J. S., Woo, D. G., Yang, H. N., Na, K. & Park, K.-H. Transforming growth factor β-3 bound with sulfate polysaccharide in synthetic extracellular matrix enhanced the biological

activities for neocartilage formation in vivo. *Journal of Biomedical Materials Research Part A* **91A**, 408–415 (2009).

36. Zhang, K. *et al.* E11/gp38 Selective Expression in Osteocytes: Regulation by Mechanical Strain and Role in Dendrite Elongation. *Mol. Cell. Biol.* **26**, 4539–4552 (2006).

37. Fairbanks, B. D. *et al.* A Versatile Synthetic Extracellular Matrix Mimic via Thiol-Norbornene Photopolymerization. *Advanced Materials* **21**, 5005–5010 (2009).

38. Kitase, Y. *et al.* Mechanical induction of PGE2 in osteocytes blocks glucocorticoid-induced apoptosis through both the β-catenin and PKA pathways. *Journal of Bone and Mineral Research* **25**, 2657–2668 (2010).

39. Holmes, R. *et al.* Thiol-Ene Photo-Click Collagen-PEG Hydrogels: Impact of Water-Soluble Photoinitiators on Cell Viability, Gelation Kinetics and Rheological Properties. *Polymers* **9**, 226 (2017).

40. M. Schultz, K. & S. Anseth, K. Monitoring degradation of matrix metalloproteinases-cleavable PEG hydrogels via multiple particle tracking microrheology. *Soft Matter* **9**, 1570–1579 (2013).

41. Michael Pfaffl. A new mathematical model for relative quantification in real-time RT-PCR. *Nucleic Acids Research* **29**, 2002–2007 (2001).

42. Cao Xian *et al.* Angiotensin II–Dependent Hypertension Requires Cyclooxygenase 1–Derived Prostaglandin E2 and EP1 Receptor Signaling in the Subfornical Organ of the Brain. *Hypertension* **59**, 869–876 (2012).

43. Swartzlander, M. D. *et al.* Immunomodulation by mesenchymal stem cells combats the foreign body response to cell-laden synthetic hydrogels. *Biomaterials* **41**, 79–88 (2015).

44. Yoshida, K. *et al.* Stimulation of bone formation and prevention of bone loss by prostaglandin E EP4 receptor activation. *Proc Natl Acad Sci U S A* **99**, 4580–4585 (2002).

45. Paralkar, V. M. *et al.* An EP2 receptor-selective prostaglandin E2 agonist induces bone healing. *Proceedings of the National Academy of Sciences* **100**, 6736–6740 (2003).

46. Li, M. *et al.* A Novel, Non-Prostanoid EP2 Receptor-Selective Prostaglandin E2 Agonist Stimulates Local Bone Formation and Enhances Fracture Healing. *Journal of Bone and Mineral Research* **18**, 2033–2042 (2003).

47. Aziz, A. H. & Bryant, S. J. A comparison of human mesenchymal stem cell osteogenesis in poly(ethylene glycol) hydrogels as a function of MMP-sensitive crosslinker and crosslink density in chemically defined medium. *Biotechnology and Bioengineering* **116**, 1523–1536 (2019).

48. Carles-Carner, M., Saleh, L. S. & Bryant, S. J. The effects of hydroxyapatite nanoparticles embedded in a MMP-sensitive photoclickable PEG hydrogel on encapsulated MC3T3-E1 pre-osteoblasts. *Biomed. Mater.* **13**, 045009 (2018).

49. McNamara, L. M., Majeska, R. J., Weinbaum, S., Friedrich, V. & Schaffler, M. B. Attachment of Osteocyte Cell Processes to the Bone Matrix. *The Anatomical Record* **292**, 355–363 (2009).

50. Kamel, M. A., Picconi, J. L., Lara-Castillo, N. & Johnson, M. L. Activation of B-catenin signaling in MLO-Y4 osteocytic cells versus 2T3 osteoblastic cells by fluid flow shear stress and PGE2: Implications for the study of mechanosensation in bone. *Bone* **47**, 872–881 (2010).

51. Cheng, B. *et al.* PGE2 is essential for gap junction-mediated intercellular communication between osteocyte-like MLO-Y4 cells in response to mechanical strain. *Endocrinology* **142**, 3464–3473 (2001).

52. Jee, W. S. S. & Ma, Y. F. The in vivo anabolic actions of prostaglandins in bone. *Bone* **21**, 297–304 (1997).

53. Ke, H. Z. *et al.* Prostaglandin E2 increases bone strength in intact rats and in ovariectomized rats with established osteopenia. *Bone* **23**, 249–255 (1998).

54. Collins, D. A. & Chambers, T. J. Effect of prostaglandins E1, E2, and F2α on osteoclast formation in mouse bone marrow cultures. *Journal of Bone and Mineral Research* **6**, 157–164 (1991).

55. Liu, X.-H., Kirschenbaum, A., Yao, S. & Levine, A. C. Interactive Effect of Interleukin-6 and Prostaglandin E2 on Osteoclastogenesis via the OPG/RANKL/RANK System. *Annals of the New York Academy of Sciences* **1068**, 225–233 (2006).

56. Suzuki, H. *et al.* The role of autonomously secreted PGE2 and its autocrine/paracrine effect on bone matrix mineralization at the different stages of differentiating MC3T3-E1 cells. *Biochemical and Biophysical Research Communications* **524**, 929–935 (2020).

57. Galea, G. L. *et al.* Sost down-regulation by mechanical strain in human osteoblastic cells involves PGE2 signaling via EP4. *FEBS Letters* **585**, 2450–2454 (2011).

58. Genetos, D. C., Yellowley, C. E. & Loots, G. G. Prostaglandin E2 Signals Through PTGER2 to Regulate Sclerostin Expression. *PLoS ONE* **6**, e17772 (2011).

4. A 3D, *in* vitro, Enzyme-Degradable Hydrogel Reveals that Dimensionality Alters Osteocyte Gene Expression Response to Prostaglandin E2

Rachel L. Wilmoth, Sadhana Sharma, Virginia L. Ferguson, Stephanie J. Bryant

4.1 Abstract

Prostaglandin E_2 (PGE_2) is a key signaling molecule that osteocytes produce in response to mechanical loading. Yet, the effect of PGE_2 autocrine signaling on osteocytes is not fully understood. This work characterizes the effect of PGE_2 on osteocyte gene expression of common signaling molecules in two culture environments: the commonly used 2D tissue culture plastic vs. a 3D enzyme-degradable hydrogel that promotes mature osteocyte differentiation. Encapsulated IDG-SW3 osteocytes in 3D expressed 100-fold elevated levels of *Sost*, a mature osteocyte marker, as compared to 2D after 35 days, suggesting that the cells differentiated into mature osteocytes to a greater extent in 3D as compared to 2D. Additionally, PGE_2 induced an anabolic response as indicated by the increased levels of *Gja1* and *Sost* and decreased *Tnfsf11/Tnfrsf11b* ratio only in 3D. Further, in 3D we showed that EP4, a cell surface receptor for PGE_2, is not necessary for the mature osteocyte response to PGE_2 in all genes investigated except *Tnfsf11* (encoding for RANKL). This study demonstrates that dimensionality of the osteocyte culture *in vitro* significantly affects osteocyte gene expression in response to PGE_2.

4.2 Introduction

Osteocytes maintain bone homeostasis by responding to mechanical and hormonal cues. In response to these external cues, osteocytes direct the anabolic and catabolic activity in bone by secreting molecules that regulate the activity of bone-forming osteoblasts or bone-resorbing osteoclasts.[1] One signaling molecule that osteocytes produce in response to mechanical loading is Prostaglandin E2 (PGE_2).[2,3] PGE_2 induces significant increases in bone mass and strength[4,5] and increases local repair after fracture when administered *in vivo*.[6] *In vitro*, addition of PGE_2 increases osteoblast mineralization.[7] Yet, PGE_2 also increases osteoclast recruitment and differentiation.[8,9] These prior studies indicate that PGE_2 has an anabolic (*i.e.*, bone forming) effect in response to mechanical loading by regulating both osteoblast and osteoclast activity.

Although it is established that PGE_2 is secreted by osteocytes to regulate osteoblast and osteoclast activity, the role of PGE_2 autocrine signaling on osteocytes is unclear. It is challenging to isolate the effects of PGE_2 on osteocytes *in vivo* because PGE_2 affects osteoblast and osteoclast activity as well. Thus, osteocyte PGE_2 signaling has largely been studied *in vitro* and in 2D cultures of either osteoblasts[2,7,9–17] or MLO-Y4 osteocyte-like cells.[2,3,15,18–20] These studies have been fundamental in increasing our understanding of the role of PGE_2 signaling in bone. Yet, the stage of differentiation affects cell behavior, such as the production of PGE_2,[7] in osteoblasts and osteocytes.[2,21] Newer osteocyte-like cell lines have been developed in the last decade, such as the IDG-SW3 cells, which express mature osteocyte markers (*e.g. Sost*) that osteoblasts and MLO-Y4 cells lack.[22] Our previous work has shown that IDG-SW3 cells develop a more mature osteocyte phenotype in 3D as compared to 2D.[23] In this study we investigated if the dimensionality (i.e., 2D vs. 3D), which greatly impacts osteocyte differentiation,[23–25] also affects the osteocyte response to PGE_2. We hypothesized that the anabolic response to PGE_2 would be higher in 3D.

In this study, we addressed three main questions. First, is the osteocyte response to PGE_2 time-dependent? Osteocytes have been shown to respond to mechanical loading at the gene and protein level after both 1 and 24 hours *in vivo*[26,27] and *in vitro.*[28] Because PGE_2 is produced in response to mechanical loading, we investigated the time-dependence of the osteocyte response to PGE_2 after 1 and 24 hours. Second, how does the dimensionality of the culture environment (i.e., 2D vs. 3D) affect the osteocyte response to PGE_2? Third, using our 3D system we asked if EP4, one of the cell surface receptors for PGE_2, is necessary for the osteocyte response to PGE_2. *In vivo* studies have identified EP4 as the key EP receptor responsible for anabolic activity.[29–32] To answer these three questions, osteocytes were cultured in 2D on collagen coated standard tissue culture plastic or encapsulated in an enzyme-sensitive poly(ethylene glycol) hydrogel that supports osteocyte maturation.[23] Osteocyte response to PGE_2 was assessed by gene expression for key PGE_2-signaling, catabolic, and anabolic genes.

4.3 Materials and Methods

4.3.1 2D Cell Culture

IDG-SW3 cells (Kerafast, Inc.) were grown in the same conditions as previously reported.[23] For the 2D studies, IDG-SW3 cells were plated on rat-tail collagen type I (Sigma-Aldrich) coated 6-well plates at 80,000 cells/cm^2. Proliferation media was replaced with differentiation media, which removes IFN- γ and adds 50 mg/ml ascorbic acid (Sigma-Aldrich) and 4mM β-glycerophosphate (Sigma-Aldrich). For differentiation, cells were cultured for 35 days at 37°C with 5% CO_2.

4.3.2 3D Hydrogel Fabrication and Culture

For 3D studies, IDG-SW3 cells were encapsulated in enzyme-sensitive hydrogels as previously reported [23] and shown in Figure 4.1A. In brief, an 8-arm PEG (20000 g/mol, JenKem Technology) was functionalized with norbornenes and confirmed to reach 92% conjugation of norbornene to each arm of PEG with ^{1}H NMR using established protocols.[23] Hydrogels were formed from a precursor solution of 6.5% (w/w) 8-arm PEG-norbornene, enzyme-sensitive crosslinker containing the sequence GCGPLG-LWARCG (GenScript) at 0.65:1 thiol:norbornene ratio, 2mM CRGDS (GenScript) for cell adhesion, and 0.05% (w/w) photoinitiator, 1-(4-(2-Hydroxyethoxy)-phenyl)-2-hydroxy-2-methyl-1-propane-1-one (I2959; BASF), in phosphate-buffered saline (PBS). IDG-SW3 cells were encapsulated into the precursor solution at 80x10^6 cells/ml, photopolymerized for 8 minutes with 352 nm light at 1.5-2.1 mW/cm^2 in molds that were 3 mm in diameter and 3 mm in height. After photopolymerization, hydrogels were immediately cultured in differentiation media at 37°C with 5% CO_2. On days 1 and 35 of differentiation, three hydrogels were assessed for cell viability by incubating with 4 μM Calcein AM (Corning) and 2 μM ethidium homodimer (Corning) for 40 and 10 minutes, respectively. Calcein AM stains the

cytosol of cells while ethidium homodimer stains the DNA in the nucleus of dead cells. Stained hydrogels were imaged by confocal microscopy immediately (Zeiss LSM 5 Pascal system using a Zeiss Axiovert microscope).

4.3.3 Prostaglandin E_2 Treatment

After 35 days of differentiation, 2D and 3D samples were treated with Prostaglandin E_2 (PGE_2, Cayman Chemical) at concentrations of 0, 5, and 1000 nM. 2D samples were collected for RT-qPCR after both 1 and 24 hours of PGE_2 treatment while all 3D samples were collected after 24 hours. Some of the 3D samples were also treated with 5 μM AH 23848 (Cayman Chemical), an EP4 inhibitor.[10,33] With inhibitor studies, samples were pre-incubated with the inhibitor for 30 minutes.

4.3.4 RNA Extraction and Gene Expression

RNA was extracted using a miRNeasy Micro Kit (QIAgen, USA) with QIA shredder columns (Qiagen) and phase lock gel tubes (Quantabio), as described in detail elsewhere.[34] 2D samples were lysed directly in the well plates with Qiazol. 3D samples were snapped frozen in liquid nitrogen and homogenized in Qiazol using a tissue lyser (TissueLyser II, Qiagen). Isolated RNA was quantified using a Nanodrop instrument (ND-1000, Thermo Scientific) and reverse transcribed into cDNA (50-100 ng) using a High Capacity cDNA Reverse Transcription Kit (Applied Biosystems). The gene expression of key PGE_2-signaling, catabolic, and anabolic genes that were analyzed in response to PGE2 are shown in Table 4.1.

Table 4.1: Osteocyte PGE_2-, catabolic-, or anabolic-signaling genes measured in study.

Gene Name	Protein Name	Category	Function
Gja1	Connexin 43 (CX43)	PGE_2 signaling	PGE_2 release mechanism [18]
Ptgs2	Cyclooxygenase-2 (COX-2)	PGE_2 signaling	Enzyme involved in PGE_2 synthesis [35] Involved in bone resorption [36] and formation [37]
Ptger1	EP1	PGE_2 signaling	PGE_2 receptor [38] ↓ activation leads to bone formation [39]
Ptger2	EP2	PGE_2 signaling	PGE_2 receptor [38] ↑ activation leads to bone formation [40]
Ptger3	EP3	PGE_2 signaling	PGE_2 receptor [38]
Ptger4	EP4	PGE_2 signaling	PGE_2 receptor [38] ↑ activation leads to bone formation [29–32]
Il6	IL-6	Catabolic signaling	↑ leads to bone resorption [9,12,41,42]
Tnfrsf11b	Osteoprotegerin (OPG)	Catabolic signaling	↓ leads to bone resorption [43]
Tnfsf11	Receptor activator of nuclear factor kappa B ligand (RANKL)	Catabolic signaling	↑ leads to bone resorption [43–47]
Bglap	Osteocalcin (OCN)	Anabolic signaling	↓ leads to bone formation [48,49]
Sost	Sclerostin (SOST)	Anabolic signaling	↓ leads to bone formation [50] ↑ leads to bone resorption [51]

Each sample was analyzed by quantitative real-time polymerase chain reaction (RT-qPCR) on a 7500 Fast System (Applied Biosystems) using custom primers (Table 4.2) and SYBR Green Master Mix (Applied Biosystems). Gene expression for each gene of interest (GOI) was analyzed following Pfaffl method[52] using primer efficiency (E) relative to the housekeeping gene (HKG), ribosomal protein L32. The gene expression data are presented as normalized expression (NE) by:

$$NE = (E_{GOI})^{\Delta C_{t,GOI}(control-sample)} / (E_{HKG})^{\Delta C_{t,HKG}(control-sample)}$$

where C_t is the cycle threshold and the control is specified in the text and figures.

Table 4.2: Custom primer sequences and their calculated efficiencies (E) for each gene used.

Gene	Forward Primer	Reverse Primer	E
Phex	CAACGTTCCGCGGTCAATAC	GTGTTGCTTGGTCCAGCTTC	2.04
Dmp1	GCTTCTCTGAGATCCCTCTTCG	GCGATTCCTCTACCCTCTCT	1.98
Gja1	GAGTTCCACCACTTTGGCGT	GTGGAGTAGGCTTGGACCTT	1.97
Ptgs2	TTCTTTGCCCAGCACTTCAC	GGCGCAGTTTATGTTGTCTG	1.98
Ptger1 [53]	TTTATTAGCCTTGGGCCTCGTGGA	ATTGCACACTAATGCCGCAAGGAG	1.83
Ptger2 [53]	GATGAAGCAACCAGAGCAGAC	CAGAGAGGACTCCCACATGAA	1.97
Ptger3 [53]	GGTCATCCTCGTGTACCTGTC	GTCATGGTTAGCCCGAAGAA	1.89
Ptger4 [53]	GCCCTCTCCTGCCAATATAAC	TTTCAACACTTTGGCCTGAAC	1.96
Il6	TCGGAGGCTTAATTACACATGTTC	TGCCATTGCACAACTCTTTTCT	1.95
Tnfrsf11b	AGAAGCCACGCAAAAGTGTG	TTCACTTTGGTCCCAGGCAA	2.12
Tnsfsf11	CCATTTGCACACCTCACCATC	CGTGGTACCAAGAGGACAGAG	2.11
Bglap	CAGACACCATGAGGAGGACCATCTT	GATAGCTCGTCACAAGCAGG	2.18
Sost	GGTGGCAAGCCTTCAGGAAT	GGACACATCTTTGGCGTCAT	1.91
L32	CCATCTGTTTTACGGCATCATG	TGAACTTCTTGGTCCTCTTTTTGA	1.91

4.3.5 Statistical Analysis

Statistical analysis was performed using JMP Pro 14.1.0. Data were analyzed using two-way analysis of variance (ANOVA) with a significance level of 0.05 where factors included PGE_2 concentration, time, culture condition, or inhibitor presence. When an interaction term was significant, separate one-way ANOVAs tested each main effect separately. If a main effect was significant, Tukey's post hoc analysis was performed. The data were confirmed to have homogeneous variance and normal distribution. Graphical results are presented as the mean with standard deviation as error bars. Statistical significance is shown in figures with a (*) or (#) symbol representing $p < 0.05$ and denoted in the figure. The sample size was n = 3 unless noted otherwise.

4.4 Results

4.4.1 Cell viability and differentiation over a 35-day culture period

IDG-SW3 cells were cultured in 2D and 3D conditions for 35 days using the study design shown in Figure 4.1A-B. Qualitative assessment of viability of cells encapsulated in 3D hydrogels on days 1 and 35 showed high cell viability at all time points (Figure 7.5). On day 1, cells demonstrated a rounded morphology, but by day 35, cells developed a morphology consistent with three-dimensional spreading in enzyme-degradable hydrogels.[23]

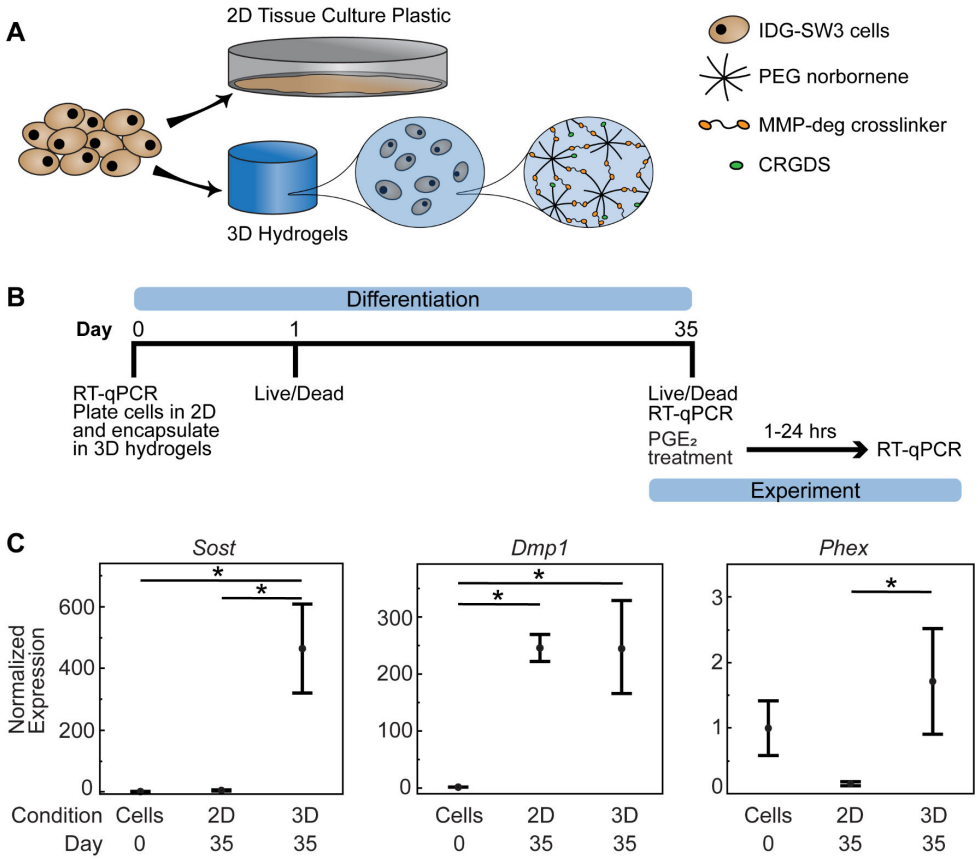

Figure 4.1: (A) Schematic of culture environments used: 2D tissue culture plastic and 3D MMP-degradable hydrogels. (B) Timeline used in study. IDG-SW3 cells were either plated on 2D tissue culture plastic or encapsulated in 3D hydrogels on day 0 and then cultured for a differentiation period of 35 days. On day 35, samples were treated with PGE2 for 1- or 24-hours, after which samples were collected for RT-qPCR (C) Gene expression levels for osteocyte markers *Sost, Dmp1,* and *Phex* from day 0 to day 35 in 2D and 3D (n = 3). The gene expression was normalized to the day 0 pre-plated/pre-encapsulated cells to obtain the normalized expression. Statistical significance was determined by a one-way ANOVA with PGE_2 as the effect followed by Tukey's post hoc. Symbols denote significance ($p < 0.05$) from post hoc Tukey's test.

Samples were collected for RT-qPCR on days 0 (pre-seeded/pre-encapsulated cells) and 35 (2D and 3D samples) to assess the maturation state of the IDG-SW3 cells through osteocyte-marker genes of *Sost*, *Dmp1*, and *Phex* (Figure 4.1C). The gene expression was normalized to the day 0 pre-encapsulated condition within each gene to obtain the normalized expression. The expression of *Sost* in 3D on day 35 was 465-fold higher than day 0 and 100-fold higher than day 35 2D samples ($p < 0.0001$). The 2D day 35 condition was 5-fold higher than day 0 but was not

significant from the post hoc test. However, using an independent comparison (student's t-test) the 2D and day 0 expression levels were significantly different ($p < 0.022$). The expression of *Dmp1* on day 35 was 246-fold higher in 2D and 247-fold higher in 3D than day 0 ($p < 0.002$), with no significant difference between the 2D and 3D conditions on day 35. The expression of *Phex* was 11-fold higher in 3D than 2D on day 35 ($p < 0.025$), but neither 3D nor 2D were significantly different from day 0. These results confirm that the IDG-SW3 cells differentiated into a more mature osteocyte phenotype in our 3D system as compared to collagen-coated 2D tissue culture polystyrene. However, the 5-fold increase in *Sost* and 246-fold increase in *Dmp1* in 2D as compared to day 0 confirm that the IDG-SW3 cells do differentiate in 2D over 35 days, just to a lesser extent than in 3D.

4.4.2 PGE_2 response is time-dependent

To comprehend the time-dependence of the osteocyte response to PGE_2 treatment, we incubated IDG-SW3 cells with PGE_2 (0 or 1000 nM) for 1 or 24 hours in a 2D culture environment. After treatment, gene expression (of the genes outlined in Table 4.1) was analyzed and the NE was calculated by normalizing to the untreated (0 nM), 1-hour treatment (Figure 4.2).

All genes except *Tnfs11* and *Gja1* elicited a significant response to PGE_2 in 2D. Several genes increased expression in response to PGE_2 after 1 hour treatment (*Ptger1*, *Ptger2*, *Ptger4*, *Ptgs2*, and *Il6*). However, after 24 hours treatment, the response to PGE_2 was variable, as illustrated by increasing expression of *Ptger2* and *Ptger3*, and decreasing expression of *Bglap*, *Ptger1*, and *Tnfrsf11b*. Only *Ptger1* and *Ptger2* responded to PGE_2 treatment at both time points. Interestingly, *Ptger1* expression increased in response to PGE_2 after 1 hour, but decreased after 24 hours, while *Ptger2* expression increased at both time points.

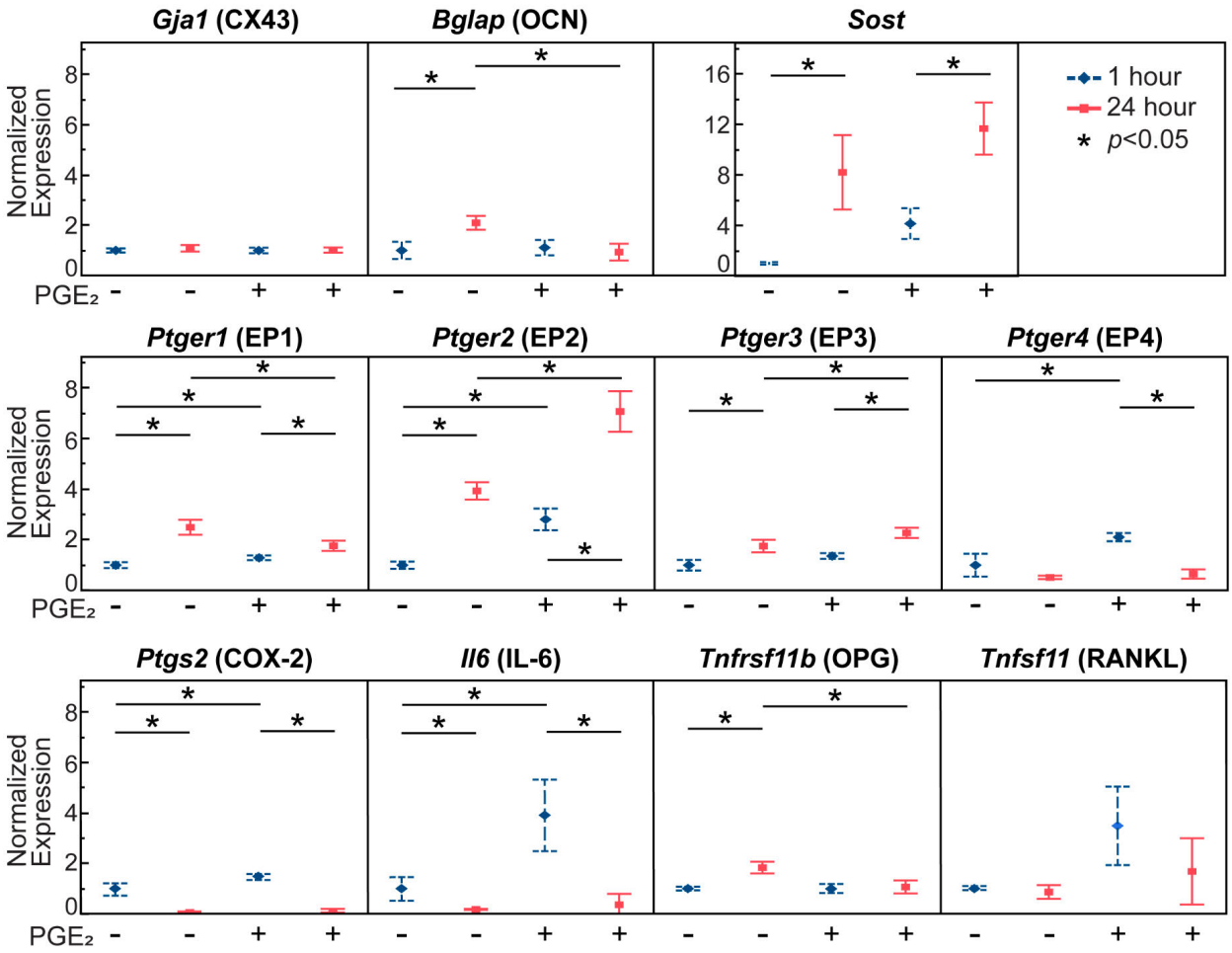

Figure 4.2: Gene expression in 2D culture after 1 and 24 hours of PGE_2 treatment. After 35 days of differentiation, IDG-SW3 cells in 2D were treated with 0 or 1000 nM of PGE_2 for 1 (blue) or 24 (red) hours (n = 3). The gene expression was normalized to the 0 nM, 1 hour condition to obtain the normalized expression. Statistical significance was determined by a two-way ANOVA with PGE_2 and time as main effects followed by Tukey's post hoc. Symbols denote significance ($p < 0.05$) from post hoc Tukey's test.

The gene expression was not consistently higher for either 1 or 24 hours at the same PGE_2 concentration. With 0 nM PGE_2, the gene expression was higher after 24 hours (compared to 1 hour) for most genes (*Bglap*, *Sost*, *Ptger1*, *Ptger2*, *Ptger3*, and *Tnfrsf11b*). The expression was higher after 1 hour (compared to 24 hours) for two genes (*Ptgs2* and *Il6*), and no different between the time-points for two genes (*Ptger4* and *Tnfs11*). At 1000 nM PGE_2, the gene expression was higher at 24 hours for three genes (*Ptger1*, *Ptger2*, *Ptger3*), higher at 1 hour for three genes

(*Ptger4*, *Ptgs2*, *Il6*), and no different for three genes (*Bglap*, *Tnfrsf11b*, and *Tnfsf11*). The differences observed between 1 and 24 hours are attributed to the media exchange at the onset of the experiment, which can influence the cell response.[54] To avoid confounding factors, the following studies assessed the 24-hour time point for PGE_2 treatment.

4.4.3 PGE_2 response is environment dependent (i.e., 2D vs. 3D)

The osteocyte response to PGE_2 (0, 5, or 1000 nM) was assessed using our 3D environment and compared to the response in 2D. Samples were incubated with PGE_2 for 24 hours, after which samples were collected to measure gene expression (Figure 4.3 and Figure 7.6).

The environment played a role in the IDG-SW3 basal expression levels (0 nM PGE_2). *Sost* and all four of the *Ptger* genes showed higher expression in 3D, ranging from ~5-fold (*Ptger1*) to ~35-fold (*Ptger4*) to ~100-150-fold (*Sost*, *Ptger2*, and *Ptger3*). *Gja1*, *Bglap*, and *Tnfrsf11b* showed the opposite, with higher expression in 2D, while the difference between 2D and 3D was not significant for *Ptgs2*, *Il6*, and *Tnfsf11*.

The cell response to PGE_2 was also mediated by the environment. *Sost* and all four of the *Ptger* genes decreased with increasing levels of PGE_2 in 3D, with no significant change in 2D, except for *Ptger4*, which increased slightly in 2D in response to PGE_2. *Ptgs2* expression showed similar trends between 2D and 3D, although the increase in response to PGE_2 was only significant in 3D. *Blgap* expression also showed similar (but decreasing) trends in response to PGE_2 between 2D and 3D, but only the 2D changes were significant. Interestingly, *Tnfrsf11b* and *Tnfsf11* expression were slightly higher in 2D (but only significant for *Tnfrsf11b*), but the response to PGE_2 for both genes was only significant in 3D. In 3D, *Tnfrsf11b* expression increased in response to PGE_2 while *Tnfsf11* expression decreased. *Gja1* expression was non-monotonic in that at 0nM, expression was higher in 2D, but at 1000 nM, expression was higher in 3D. Additionally, the *Gja1*

expression in response to PGE_2 did not change significantly in 2D but increased significantly in 3D.

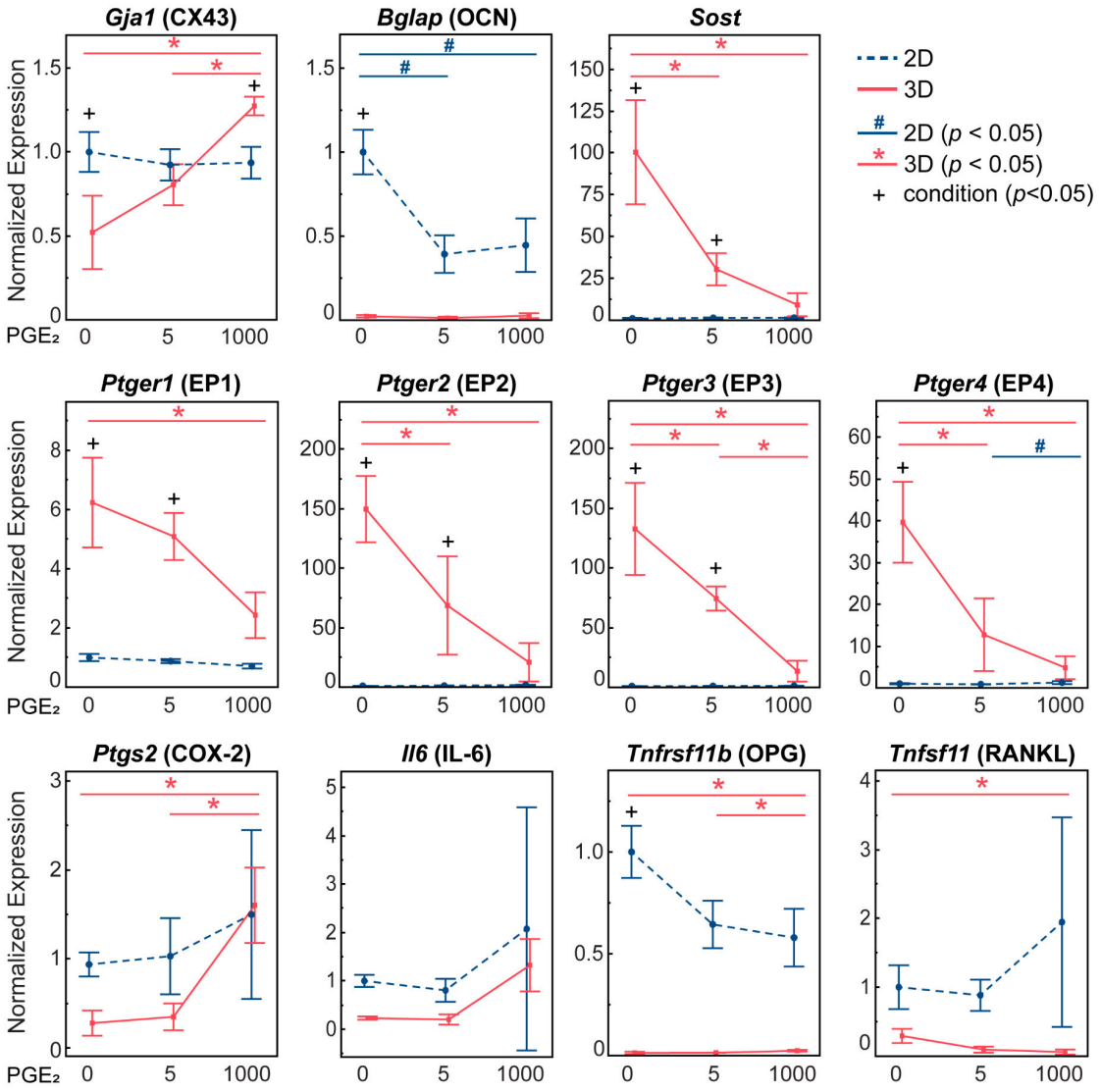

Figure 4.3: Gene expression in 2D and 3D after 24 hours of PGE_2 treatment. After 35 days of differentiation, IDG-SW3 cells in 2D (blue) and 3D (red) were treated with 0, 5, or 1000 nM of PGE_2 for 24 hours (n = 3). The gene expression was normalized to the 0 nM, 2D condition to obtain the normalized expression. Statistical significance was determined by a two-way ANOVA with PGE_2 concentration and environment (2D vs. 3D) as main effects followed by Tukey's post hoc. Symbols denote significance ($p < 0.05$) from post hoc Tukey's test and are color-coded by condition (# for 2D, * for 3D). + symbols denote significance from post hoc for condition.

4.4.4 PGE_2 response does not require EP4 signaling in most genes

To evaluate one mechanism by which PGE_2 induces gene expression changes in mature osteocytes, 3D samples with PGE_2 (1000 nM) were incubated with and without an EP4 inhibitor (AH 23848). Samples were incubated for 24 hours, after which samples were collected for gene expression analysis. RE values were normalized to the no inhibitor, untreated (0 nM PGE_2) control within each gene (Figure 4.4).

For *Sost* and *Ptger1-4*, inhibiting EP4 had no effect on the PGE_2-induced change in gene expression. However, inhibiting EP4 caused the *Tnfsf11* expression to decrease ~2-fold from the PGE_2-treated, no inhibitor samples, bringing the expression to levels from a 3-fold reduction to a 2-fold reduction from the control (0 nM PGE_2).

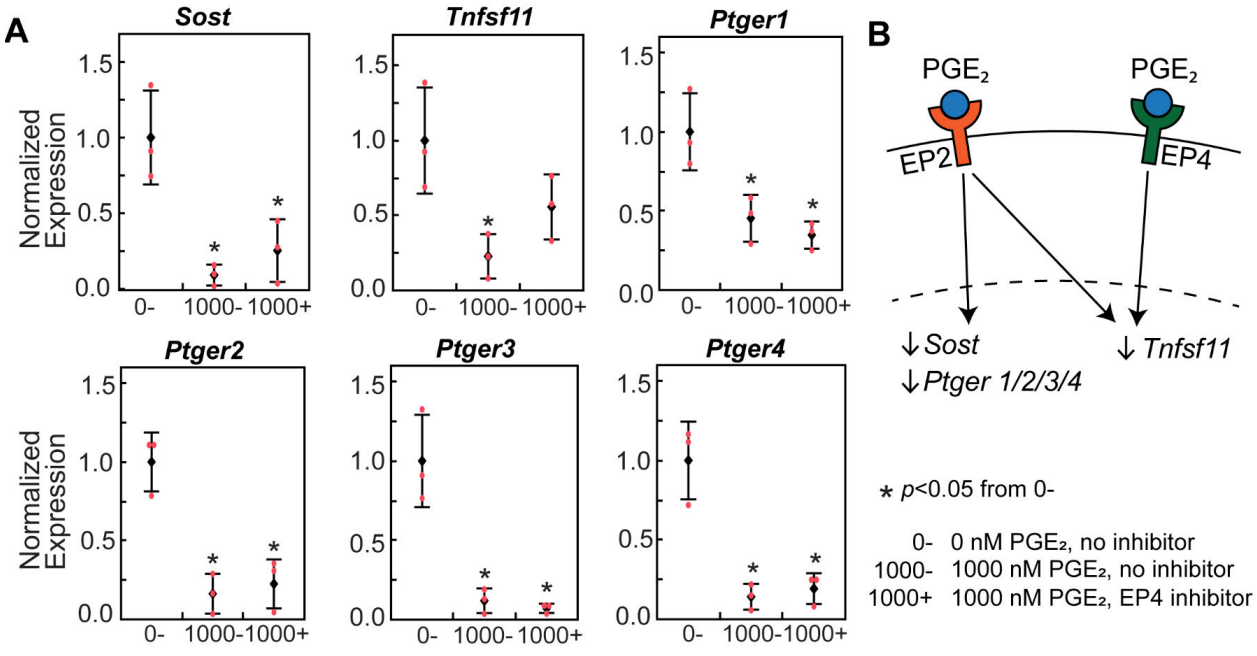

Figure 4.4: Gene expression when treated with PGE_2 and an EP4 inhibitor. (A) After 35 days of differentiation, IDG-SW3 cells in 3D were treated with 1000 nM of PGE_2 for 24 hours with (1000+) and without (1000-) an EP4 inhibitor (n = 3). The gene expression was normalized to the no inhibitor, 0 nM PGE_2 condition to obtain the normalized expression. Statistical significance was determined by a one-way ANOVA between conditions followed by Tukey's post hoc. Symbols denote significance ($p < 0.05$) from post hoc Tukey's test. (B) Hypothesized mechanism by which PGE_2 induces gene expression changes in osteocytes.

4.5 Discussion

This study utilized a novel, 3D, enzyme-degradable hydrogel to demonstrate that the dimensionality (*i.e.,* 3D vs. 2D) affects the osteocyte gene expression response to PGE_2 in IDG-SW3 cells. We first confirmed that the IDG-SW3 cells differentiate into mature osteocytes to a greater extent in 3D as compared to 2D after 35 days. We established that PGE_2 treatment induced an anabolic gene expression response in 3D, but not 2D. Additionally, we demonstrated that the dimensionality alters the initial expression levels of all four EP receptor genes. Using the 3D system, we also showed that the PGE_2-induced changes in gene expression do not require PGE_2 binding to the EP4 receptor in all genes except *Tnfsf11*.

Our previous study demonstrated that IDG-SW3 cells express elevated levels of mature osteocyte markers and deposit elevated levels of bone matrix in the 3D enzyme-degradable hydrogel as compared to 2D and non-degradable hydrogel culture conditions after 28 days.[23] Additionally, cells in the 3D enzyme-degradable hydrogel showed enhanced amounts of cellular spreading, which may be required for mature osteocyte differentiation.[55] In this study, we measured the gene expression of three mature osteocyte markers after 35 days: *Sost*, *Dmp1*, and *Phex*. *Sost* and *Phex* were substantially elevated in 3D as compared to 2D after 35 days, while *Dmp1* was equally high in 2D and 3D as compared to day 0. *Dmp1* is expressed in early osteocytes, while *Sost* is expressed by mature osteocytes. These findings confirmed the results from our previous study that although the cells differentiate to some extent in 2D, a 3D environment may be necessary to achieve mature osteocyte differentiation *in vitro*.

Overall, the 3D response to PGE_2 indicates anabolic signaling. *Tnfsf11* decreased while *Tnfrsf11b* increased, which together decreased the *Tnfsf11*/*Tnfrsf11b* ratio, a common indicator of osteoclast regulation.[56] A decrease in the secreted protein levels of RANKL/OPG ratio decreases

osteoclast recruitment and differentiation, thus decreasing bone resorption.[43] Interestingly, our finding at the gene level is opposite to a previous study that cultured osteoblasts in 2D and found that PGE_2 treatment increased protein levels of RANKL and decreased protein levels of OPG.[9] The decrease in *Sost* expression in 3D is consistent with previous studies[10,11,57] and also indicated an anabolic response, as sclerostin (encoded by *Sost*) is an inhibitory regulator of osteoblast activity.[50,56,58] Additionally, *Gja1* increased in 3D, which aligns with previous studies[28] and is a key indicator of the osteocyte anabolic response to mechanical loading.[3] None of the anabolic responses observed in 3D were observed in 2D, further indicating that the dimensionality altered the gene expression response to PGE_2. Osteocytes and osteoblasts respond differently to mechanical loading stimuli[2,15,59,60] in part due to cell morphology differences,[15] and osteocytes grown in 2D vs. 3D show morphology differences.[61,62] This, in combination with our finding that the 2D environment does not support mature osteocyte differentiation, suggests that the increased anabolic response in 3D may be a combined effect of the differentiation and morphology that is achieved in 3D.

Gene expression for the EP receptors was investigated because PGE_2 can bind to any one of the four EP receptors. Upon binding to a receptor, intracellular signaling cascades are initialized that eventually regulate gene expression of other key signaling molecules such as *Sost*, *Bglap*, or *Gja1*.[10,28,38] In this study, the genes for all four EP receptors ranged from 6-fold to 150-fold higher in 3D than in 2D. Previously, osteoblasts cultured in 2D did not express detectable levels of *Ptger1* and *Ptger3*.[10] These findings indicate that the initial (0 nM PGE_2) gene expression levels for the EP receptors may be regulated by the environment (3D vs. 2D) or may increase as osteoblasts differentiate to early and mature osteocytes, which is enhanced in 3D.

Interestingly, the expression of the EP receptors in response to PGE_2 in this study contrasted previously published 2D studies. Herein, genes for all four EP receptors decreased in 3D when treated with PGE_2. In an earlier study, MLO-Y4 cells cultured in 2D showed no change in *Ptger1, Ptger3,* and *Ptger 4,* but an increase in *Ptger2* expression after 24 hours of treatment with equivalent PGE_2 as this study (1000 nM).[28] When subjected to fluid flow in this same study, MLO-Y4 cells showed similar results, indicating that treatment with PGE_2 influences the gene expression levels of the EP receptors similar to that of mechanical stimulation. In another study, Saos2 osteoblasts cultured in 2D did not express *Ptger1* or *Ptger3,* while *Ptger2* and *Ptger4* increased with applied strain.[10] In our current study, the 2D response to PGE_2 was not significant for any EP receptors except *Ptger4,* where expression slightly, but significantly, increased ~2-fold from 5 to 1000 nM PGE_2. The 2D response was more in line with the previous MLO-Y4 and osteoblast studies showing an increase in either *Ptger2* or *Ptger4* with applied strain or PGE_2.[10,28] It is likely that the PGE_2-induced reduction of *Ptger* gene expression only in 3D is a combined effect of the difference in initial *Ptger* levels and osteocyte differentiation between 3D and 2D in this study.

By inhibiting EP4, we showed that EP4 signaling is not required for the gene expression osteocyte response to PGE_2 in all genes except *Tnfsf11*. In our study, when treated with PGE_2, *Tnfsf11* significantly decreased, but the EP4 inhibitor dampened this effect and resulted in no significant difference from the untreated samples. This indicates that PGE_2 binds to the EP4 receptor to induce a reduction in *Tnfsf11* expression. Although the EP4-inhibited NE was not statistically different than the untreated NE, it did still show a 2-fold reduction, which suggests that part of the PGE_2-induced reduction of *Tnfsf11* signals through another EP receptor. EP2 and EP4 activation both increase intracellular 3,5'-cyclic adenosine monophosphate (cAMP) while

EP3 decreases intracellular cAMP and EP1 increases intracellular Ca^{2+}.[38] cAMP activates protein kinase A (PKA)-mediated phosphorylation of glycogen synthase kinase-3β (GSK-3β).[28,57,63] The cAMP/PKA pathway has been shown to be dominated by EP2,[64] whereas GSK-3β can also be phosphorylated in a phosphatidylinositol 3-kinase (PI3K)-dependent mechanism, which only couples to EP4.[38,63] Therefore, we hypothesize that the reduction of *Tnfsf11* was likely mediated by both EP2 (cAMP/PKA/GSK-3β) and EP4 (PI3K/GSK-3β), and that *Tnfsf11* expression depends more heavily on the PI3K pathway than any other genes investigated in this study (Figure 4.4B). It is possible that there were contributions from EP1 or EP3 or that there was crosstalk with another pathway, such as the canonical Wnt pathway[65] to reduce *Tnfsf11* expression, but because we see the expression changing with the EP4 inhibitor, it was likely activated by both EP2 and EP4.

The results from this study indicate that the reduction in *Sost* and *Ptger1-4* do not require EP4 activation. Previous conflicting studies have shown that osteoblasts in 2D decrease *Sost* expression in response to PGE_2 through exclusively EP2[11] or exclusively EP4 signaling.[10] EP2 and EP4 agonists both stimulate anabolic effects in bone,[31,40,66] and sclerostin (encoded by *Sost*) reduction stimulates bone formation.[50,56,58] Taken together, it is likely that the PGE_2-induced *Sost* reduction signals primarily through EP2 in osteocytes, but further studies using inhibitors for EP's 1, 2, and 3 are also needed to confirm this hypothesis (Figure 4.4B). The finding that *Ptger* expression does not require EP4 activation is partially supported by a study showing that *Ptger2* expression increased in MLO-Y4 cells in response to PGE_2 via EP2 stimulation.[28] Therefore, it is likely that the reduction in *Ptger* expression is regulated by EP2. Another consideration is that EP4 quickly desensitizes from PGE_2 in part due to rapid internalization that EP2 does not undergo.[63] Thus, any gene expression changes that are driven by either EP2 or EP4 may be dominated by EP2, further explaining why EP4 inhibition had little effect in this study.

4.6 Conclusion

In conclusion, this study showed that the dimensionality affects the cellular response to PGE_2 treatment via gene expression. We confirmed that culturing IDG-SW3 osteocytes in a 3D enzyme-degradable hydrogel enhances mature osteocyte differentiation as compared to 2D cultures on collagen-coated polystyrene. When treated with PGE_2, some of the genes show an opposite response in 3D as compared to previous work using 2D cultures, and the anabolic response in our 3D system was not evident in our 2D cultures. Additionally, we showed that EP4 is not required for the PGE_2-induced gene expression changes in any genes except *Tnfsf11* in mature osteocytes. These results demonstrate that 3D *in vitro* culture systems that enhance mature osteocyte differentiation are necessary to study osteocyte signaling, as the results in 2D did not produce similar results to 3D. Osteocyte signaling drives bone degeneration and homeostasis – thus 3D *in vitro* models will enable the effect of different treatments (*e.g.*, drug treatments, hormone levels, or inflammatory mediators) on osteocyte signaling to be studied during bone degenerative diseases such as osteoarthritis.

4.7 Acknowledgements

Dr. Kristine Fischenich and Jennifer Coulombe provided statistical advice. The research reported in this publication was supported by the National Institute of Arthritis and Musculoskeletal and Skin Diseases of the National Institutes of Health under the Award 1R21AR069791-01A1. RW was supported on an NIH/NIA National Institute of Aging Integrative Physiology of Aging Training Grant under Award T32AG000279-16A1. The content in this publication is solely the responsibility of the authors and does not necessarily represent the official views of the NIH.

4.8 References

1. Schaffler, M. B., Cheung, W.-Y., Majeska, R. & Kennedy, O. Osteocytes: Master Orchestrators of Bone. *Calcified Tissue International* **94**, 5–24 (2014).

2. Kamel, M. A., Picconi, J. L., Lara-Castillo, N. & Johnson, M. L. Activation of B-catenin signaling in MLO-Y4 osteocytic cells versus 2T3 osteoblastic cells by fluid flow shear stress and PGE2: Implications for the study of mechanosensation in bone. *Bone* **47**, 872–881 (2010).

3. Cheng, B. *et al.* PGE2 is essential for gap junction-mediated intercellular communication between osteocyte-like MLO-Y4 cells in response to mechanical strain. *Endocrinology* **142**, 3464–3473 (2001).

4. Jee, W. S. S. & Ma, Y. F. The in vivo anabolic actions of prostaglandins in bone. *Bone* **21**, 297–304 (1997).

5. Ke, H. Z. *et al.* Prostaglandin E2 increases bone strength in intact rats and in ovariectomized rats with established osteopenia. *Bone* **23**, 249–255 (1998).

6. Dekel, S., Lenthall, G. & Francis, M. J. O. Release of Prostaglandins from Bone and Muscle After Tibial Fracture. *British Editorial Society of Bone and Joint Surgery* **63-B**, 185–189 (1981).

7. Suzuki, H. *et al.* The role of autonomously secreted PGE2 and its autocrine/paracrine effect on bone matrix mineralization at the different stages of differentiating MC3T3-E1 cells. *Biochemical and Biophysical Research Communications* **524**, 929–935 (2020).

8. Collins, D. A. & Chambers, T. J. Effect of prostaglandins E1, E2, and F2α on osteoclast formation in mouse bone marrow cultures. *Journal of Bone and Mineral Research* **6**, 157–164 (1991).

9. Liu, X.-H., Kirschenbaum, A., Yao, S. & Levine, A. C. Interactive Effect of Interleukin-6 and Prostaglandin E2 on Osteoclastogenesis via the OPG/RANKL/RANK System. *Annals of the New York Academy of Sciences* **1068**, 225–233 (2006).

10. Galea, G. L. *et al.* Sost down-regulation by mechanical strain in human osteoblastic cells involves PGE2 signaling via EP4. *FEBS Letters* **585**, 2450–2454 (2011).

11. Genetos, D. C., Yellowley, C. E. & Loots, G. G. Prostaglandin E2 Signals Through PTGER2 to Regulate Sclerostin Expression. *PLoS ONE* **6**, e17772 (2011).

12. Kumei, Y. *et al. Microgravity induces prostaglandin E2 and interleukin-6 production in normal rat osteoblasts: role in bone demineralization*. (Elsevier, 1996).

13. Lee, C. M., Genetos, D. C., You, Z. & Yellowley, C. E. Hypoxia regulates PGE2 release and EP1 receptor expression in osteoblastic cells. *Journal of Cellular Physiology* **212**, 182–188 (2007).

14. Liu, X.-H. *et al.* Prostaglandin E2 modulates components of the Wnt signaling system in bone and prostate cancer cells. *Biochemical and Biophysical Research Communications* **394**, 715–720 (2010).

15. McGarry, J. G., Klein-Nulend, J. & Prendergast, P. J. The effect of cytoskeletal disruption on pulsatile fluid flow-induced nitric oxide and prostaglandin E2 release in osteocytes and osteoblasts. *Biochemical and Biophysical Research Communications* **330**, 341–348 (2005).

16. Bakker, A. D., Soejima, K., Klein-Nulend, J. & Burger, E. H. The production of nitric oxide and prostaglandin E2 by primary bone cells is shear stress dependent. *Journal of Biomechanics* **34**, 671–677 (2001).

17. Smalt, R., Mitchell, F. T., Howard, R. L. & Chambers, T. J. Induction of NO and prostaglandin E2 in osteoblasts by wall-shear stress but not mechanical strain. *American Journal of Physiology-Endocrinology And Metabolism* **273**, E751–E758 (1997).

18. Cherian, P. P. *et al.* Mechanical strain opens connexin 43 hemichannels in osteocytes: a novel mechanism for the release of prostaglandin. *Molecular biology of the cell* **16**, 3100–3106 (2005).

19. Kitase, Y. *et al.* Mechanical induction of PGE2 in osteocytes blocks glucocorticoid-induced apoptosis through both the β-catenin and PKA pathways. *Journal of Bone and Mineral Research* **25**, 2657–2668 (2010).

20. Zhang, J.-N. *et al.* The role of the sphingosine-1-phosphate signaling pathway in osteocyte mechanotransduction. *Bone* **79**, 71–78 (2015).

21. Westbroek, I. *et al.* Differential Stimulation of Prostaglandin G/H Synthase-2 in Osteocytes and Other Osteogenic Cells by Pulsating Fluid Flow. *Biochemical and Biophysical Research Communications* **268**, 414–419 (2000).

22. Woo, S. M., Rosser, J., Dusevich, V., Kalajzic, I. & Bonewald, L. F. Cell line IDG-SW3 replicates osteoblast-to-late-osteocyte differentiation in vitro and accelerates bone formation in vivo. *J Bone Miner Res* **26**, 2634–2646 (2011).

23. Aziz, A. H., Wilmoth, R. L., Ferguson, V. L. & Bryant, S. J. IDG-SW3 Osteocyte Differentiation and Bone Extracellular Matrix Deposition Are Enhanced in a 3D Matrix Metalloproteinase-Sensitive Hydrogel. *ACS Appl. Bio Mater.* **3**, 1666–1680 (2020).

24. Sun, Q. *et al.* Ex vivo replication of phenotypic functions of osteocytes through biomimetic 3D bone tissue construction. *Bone* **106**, 148–155 (2018).

25. Boukhechba, F. *et al.* Human Primary Osteocyte Differentiation in a 3D Culture System. *Journal of Bone and Mineral Research* **24**, 1927–1935 (2009).

26. Robling, A. G. *et al.* Mechanical Stimulation of Bone in Vivo Reduces Osteocyte Expression of Sost/Sclerostin. *Journal of Biological Chemistry* **283**, 5866–5875 (2008).

27. Lara-Castillo, N. *et al.* In vivo mechanical loading rapidly activates β-catenin signaling in osteocytes through a prostaglandin mediated mechanism. *Bone* **76**, 58–66 (2015).

28. Cherian, P. P. *et al.* Effects of Mechanical Strain on the Function of Gap Junctions in Osteocytes Are Mediated through the Prostaglandin EP2 Receptor. *Journal of Biological Chemistry* **278**, 43146–43156 (2003).

29. Miyaura, C. *et al.* Impaired Bone Resorption to Prostaglandin E2 in Prostaglandin E Receptor EP4-knockout Mice. *Journal of Biological Chemistry* **275**, 19819–19823 (2000).

30. Machwate, M. *et al.* Prostaglandin Receptor EP4 Mediates the Bone Anabolic Effects of PGE2. *Mol Pharmacol* **60**, 36–41 (2001).

31. Yoshida, K. *et al.* Stimulation of bone formation and prevention of bone loss by prostaglandin E EP4 receptor activation. *Proc Natl Acad Sci U S A* **99**, 4580–4585 (2002).

32. Tanaka, M. *et al.* Prostaglandin E2 receptor (EP4) selective agonist (ONO-4819.CD) accelerates bone repair of femoral cortex after drill-hole injury associated with local upregulation of bone turnover in mature rats. *Bone* **34**, 940–948 (2004).

33. Ma, X., Kundu, N., Rifat, S., Walser, T. & Fulton, A. M. Prostaglandin E Receptor EP4 Antagonism Inhibits Breast Cancer Metastasis. *Cancer Res* **66**, 2923–2927 (2006).

34. Patel, D., Sharma, S., Screen, H. R. C. & Bryant, S. J. Effects of cell adhesion motif, fiber stiffness, and cyclic strain on tenocyte gene expression in a tendon mimetic fiber composite hydrogel. *Biochemical and Biophysical Research Communications* **499**, 642–647 (2018).

35. Swartzlander, M. D. *et al.* Immunomodulation by mesenchymal stem cells combats the foreign body response to cell-laden synthetic hydrogels. *Biomaterials* **41**, 79–88 (2015).

36. Wei, X. *et al.* Fibroblasts Express RANKL and Support Osteoclastogenesis in a COX-2-Dependent Manner After Stimulation With Titanium Particles. *Journal of Bone and Mineral Research* **20**, 1136–1148 (2005).

37. Forwood, M. R. Inducible cyclo-oxygenase (COX-2) mediates the induction of bone formation by mechanical loading in vivo. *Journal of Bone and Mineral Research* **11**, 1688–1693 (1996).

38. Sugimoto, Y. & Narumiya, S. Prostaglandin E Receptors. *Journal of Biological Chemistry* **282**, 11613–11617 (2007).

39. Zhang, M. *et al.* EP1−/− mice have enhanced osteoblast differentiation and accelerated fracture repair. *Journal of Bone and Mineral Research* **26**, 792–802 (2011).

40. Paralkar, V. M. *et al.* An EP2 receptor-selective prostaglandin E2 agonist induces bone healing. *Proceedings of the National Academy of Sciences* **100**, 6736–6740 (2003).

41. Wu, Q., Zhou, X., Huang, D., Ji, Y. & Kang, F. IL-6 Enhances Osteocyte-Mediated Osteoclastogenesis by Promoting JAK2 and RANKL Activity ***In Vitro***. *Cellular Physiology and Biochemistry* **41**, 1360–1369 (2017).

42. Zhou, M., Li, S. & Pathak, J. L. Pro-inflammatory Cytokines and Osteocytes. *Curr Osteoporos Rep* **17**, 97–104 (2019).

43. Cao, J., Venton, L., Sakata, T. & Halloran, B. P. Expression of RANKL and OPG correlates with age-related bone loss in male C57BL/6 mice. *J. Bone Miner. Res.* **18**, 270–277 (2003).

44. Cabahug-Zuckerman, P. *et al.* Osteocyte Apoptosis Caused by Hindlimb Unloading is Required to Trigger Osteocyte RANKL Production and Subsequent Resorption of Cortical and Trabecular Bone in Mice Femurs. *Journal of Bone and Mineral Research* **31**, 1356–1365 (2016).

45. Nakashima, T. *et al.* Evidence for osteocyte regulation of bone homeostasis through RANKL expression. *Nature Medicine* **17**, 1231–1234 (2011).

46. Xiong, J. *et al.* Osteocytes, not Osteoblasts or Lining Cells, are the Main Source of the RANKL Required for Osteoclast Formation in Remodeling Bone. *PLoS One* **10**, (2015).

47. Xiong, J. & O'Brien, C. A. Osteocyte RANKL: New insights into the control of bone remodeling. *J Bone Miner Res* **27**, 499–505 (2012).

48. Ducy, P., Desbois, C., Boyce, B. & Pinero, G. Increased bone formation in osteocalcin-deficient mice. *Nature (London)* **382**, 448–452 (1996).

49. Zoch, M. L., Clemens, T. L. & Riddle, R. C. New insights into the biology of osteocalcin. *Bone* **82**, 42–49 (2016).

50. Winkler, D. G. *et al.* Osteocyte control of bone formation via sclerostin,a novel BMP antagonist. *EMBO J* **22**, 6267–6276 (2003).

51. Wijenayaka, A. R. *et al.* Sclerostin Stimulates Osteocyte Support of Osteoclast Activity by a RANKL-Dependent Pathway. *PLoS One* **6**, (2011).

52. Michael Pfaffl. A new mathematical model for relative quantification in real-time RT-PCR. *Nucleic Acids Research* **29**, 2002–2007 (2001).

53. Cao Xian *et al.* Angiotensin II–Dependent Hypertension Requires Cyclooxygenase 1–Derived Prostaglandin E2 and EP1 Receptor Signaling in the Subfornical Organ of the Brain. *Hypertension* **59**, 869–876 (2012).

54. Masters, J. R. & Stacey, G. N. Changing medium and passaging cell lines. *Nat Protoc* **2**, 2276–2284 (2007).

55. Kaur, K., Das, S. & Ghosh, S. Regulation of Human Osteoblast-to-Osteocyte Differentiation by Direct-Write 3D Microperiodic Hydroxyapatite Scaffolds. *ACS Omega* **4**, 1504–1515 (2019).

56. Prideaux, M., Findlay, D. M. & Atkins, G. J. Osteocytes: The master cells in bone remodelling. *Current Opinion in Pharmacology* **28**, 24–30 (2016).

57. Gupta, A. *et al.* Communication of cAMP by connexin43 gap junctions regulates osteoblast signaling and gene expression. *Cellular Signalling* **28**, 1048–1057 (2016).

58. Poole, K. E. S. *et al.* Sclerostin is a delayed secreted product of osteocytes that inhibits bone formation. *The FASEB Journal* **19**, 1842–1844 (2005).

59. Ajubi, N. E. *et al.* Pulsating Fluid Flow Increases Prostaglandin Production by Cultured Chicken Osteocytes—A Cytoskeleton-Dependent Process. *Biochemical and Biophysical Research Communications* **225**, 62–68 (1996).

60. Klein-Nulend, J. *et al.* Sensitivity of osteocytes to biomechanical stress in vitro. *The FASEB Journal* **9**, 441–445 (1995).

61. Bernhardt, A., Weiser, E., Wolf, S., Vater, C. & Gelinsky, M. Primary Human Osteocyte Networks in Pure and Modified Collagen Gels. *Tissue Engineering Part A* **25**, 1347–1355 (2019).

62. Zhang, C., Bakker, A. D., Klein-Nulend, J. & Bravenboer, N. Studies on Osteocytes in Their 3D Native Matrix Versus 2D In Vitro Models. *Current Osteoporosis Reports* **17**, 207–216 (2019).

63. Regan, J. W. EP2 and EP4 prostanoid receptor signaling. *Life Sciences* **74**, 143–153 (2003).

64. Fujino, H., Xu, W. & Regan, J. W. Prostaglandin E2 Induced Functional Expression of Early Growth Response Factor-1 by EP4, but Not EP2, Prostanoid Receptors via the Phosphatidylinositol 3-Kinase and Extracellular Signal-regulated Kinases. *Journal of Biological Chemistry* **278**, 12151–12156 (2003).

65. Suzuki, A. *et al.* PTH/cAMP/PKA signaling facilitates canonical Wnt signaling via inactivation of glycogen synthase kinase-3β in osteoblastic Saos-2 cells. *Journal of Cellular Biochemistry* **104**, 304–317 (2008).

66. Li, M. *et al.* A Novel, Non-Prostanoid EP2 Receptor-Selective Prostaglandin E2 Agonist Stimulates Local Bone Formation and Enhances Fracture Healing. *Journal of Bone and Mineral Research* **18**, 2033–2042 (2003).

5. A 3D, Dynamically Loaded Hydrogel Model of the Osteochondral Unit to Study Osteocyte Mechanobiology

This chapter is published in full as: Wilmoth, R. L., Ferguson, V. L. & Bryant, S. J. A 3D, Dynamically Loaded Hydrogel Model of the Osteochondral Unit to Study Osteocyte Mechanobiology. *Advanced Healthcare Materials* **9**, 2001226 (2020).

5.1 Abstract

Osteocytes are mechanosensitive cells that orchestrate signaling in bone and cartilage across the osteochondral unit. The mechanisms by which osteocytes regulate osteochondral homeostasis and degeneration in response to mechanical cues remain unclear. This study introduces a novel 3D hydrogel bilayer composite designed to support osteocyte differentiation and bone matrix deposition in a bone-like layer and to recapitulate key aspects of the osteochondral unit's complex loading environment. The bilayer hydrogel was fabricated with a soft cartilage-like layer overlaying a stiff bone-like layer. The bone-like layer contained a stiff 3D-printed hydrogel structure infilled with a soft, degradable, cellular hydrogel. The IDG-SW3 cells embedded within the soft hydrogel matured into osteocytes and produced a mineralized collagen matrix. Under dynamic compressive strains, near-physiological levels of strain were achieved in the bone layer ($\leq 0.08\%$), while the cartilage layer borne the majority of the strains (>99%). Under loading, the model induced an osteocyte response, measured by prostaglandin E2, that was frequency, but not strain, dependent: a finding attributed to altered fluid flow within the composite. Overall, this new hydrogel platform provides a novel approach to study osteocyte mechanobiology *in vitro* in an osteochondral tissue-mimetic environment.

5.2 Main

Osteocytes are mechanosensitive cells that help to orchestrate signaling in bone and cartilage across the osteochondral unit. Yet the mechanisms by which osteocytes regulate osteochondral homeostasis and degeneration in response to normal and aberrant mechanical cues remain unclear.[1,2] Currently, we lack sufficient means of studying osteocyte mechanobiology both *in vivo* and *in vitro.* This study aimed to develop an *in vitro* platform to study osteocyte mechanobiology within a subchondral bone mimetic. Our novel platform uses a 3D hydrogel bilayer composite designed to support osteocyte differentiation and bone matrix deposition in a bone-like layer and to recapitulate key aspects of the osteochondral unit's complex loading environment with a specific focus on achieving near-physiological levels of strain. Overall, this new osteochondral model may help to elucidate how changes in mechanical and hormonal cues affect homeostatic and degenerative processes in osteochondral tissues.

Osteocytes play a key role in regulating osteochondral homeostasis and degeneration. In bone, osteocytes detect hormonal and mechanical cues and respond by secreting signaling molecules that direct bone-forming osteoblasts and bone-resorbing osteoclasts.[3–6] In subchondral bone, osteocytes also engage in crosstalk with chondrocytes that reside in articular cartilage across the osteochondral interface.[1,2] During the progression of osteoarthritis, bone and cartilage undergo property changes; for example, cartilage permeability increases,[7] which in turn increases the fluid flow in bone and cartilage.[8,9] Osteocytes detect increased fluid flow in subchondral bone and then secrete signaling molecules that affect chondrocyte, osteoblast, and osteoclast activities that further contribute to osteochondral degeneration.[1,2,10–13] A 3D *in vitro* model that recapitulates the strain and fluid flow of the osteochondral unit would enable key questions to be answered about the osteocyte's role in regulating osteochondral homeostasis and degeneration.

Currently, 3D *in vitro* osteocyte models that capture relevant mechanical cues are insufficient. The loading environment in bone and, in particular the osteochondral unit, experiences matrix strains, typically between 0.001% and 0.3%,[3,14] and interstitial fluid flow. Studying osteocyte mechanobiology *in vivo*[15–21] is challenging due to the difficulty in isolating and controlling the effects of different mechanical stimuli on cells. While *in vitro* studies in 2D culture allow for tighter control over mechanical stimuli (*e.g.*, fluid flow) and have advanced our knowledge of osteocyte mechanotransduction,[22–25] to date, these studies lack 3D aspects of the *in vivo* environment.[26] To this end, researchers developed 3D osteocyte culture models to improve upon the limitations of 2D cultures.[27–33] For example, one study achieved mature osteocyte differentiation in a 3D collagen gel but this culture system lacked mechanical cues.[34] Other studies revealed new effects of direct matrix strains on osteocytes in 3D [27,29,35] such as strain-induced osteocyte regulation of osteoblast bone formation.[27] These prior studies applied matrix strains ranging from 0.4-10%, which exceed physiological levels of strain in bone. Other studies incorporated fluid perfusion into 3D cultures[15,28,30,32,36,37] and revealed, for example, the link between fluid-induced shear and gene expression of proteins that regulate osteoblast bone formation (e.g., sclerostin).[28] However, 3D models that adequately capture both physiologically-relevant matrix strains and fluid perfusion are limited.

Here, we designed a bilayer composite hydrogel to mimic the osteochondral unit and control strain within the cellular niche where the osteocytes reside. While numerous studies have developed bilayer scaffolds for osteochondral defect repair models (e.g.[38–46]), few studies examine osteocytes in these scaffolds. A representative image of a histological section of human osteochondral tissue (Figure 5.1A) illustrates articular cartilage overlaying a thin interfacial calcified cartilage layer, underlying cortical subchondral bone plate, and subchondral trabecular

bone.[10,47,48] The osteochondral unit possesses a large mismatch in the compressive moduli between articular cartilage, ranging from 1-10 MPa,[49,50] and the subchondral bone, ranging from 1-10 GPa.[51,52] These disparate properties influence strain transfer from cartilage to bone during normal joint movement. To capture this difference, we fabricated a bilayer hydrogel with a soft cartilage-like layer overlaying a stiff bone-like layer. Because cells encapsulated in a 3D hydrogel, including bone cells, require soft and degradable hydrogels to form 3D interconnected cellular networks,[53] we introduced a stiff 3D-printed hydrogel structure into the bone layer to increase its composite modulus while maintaining a soft cellular niche. We designed the geometry of the 3D-printed structure to consist of vertical pillars which serve as stiff reinforcements to bear load, control strain and protect the cells within the cellular niche.[54] Rather than mimicking the modulus of bone, which is difficult to achieve in a 3D printed polymeric scaffold, we aimed to recapitulate the level of strain in bone with this osteochondral model. Discussed below are four aspects of this osteochondral model for the study of osteocyte mechanobiology: (1) fabrication of a bilayer hydrogel, (2) calculation of strain in each layer, (3) demonstration of osteocyte differentiation and bone matrix deposition, and (4) demonstration that loading induces an osteocyte response.

The bilayer composite was fabricated from poly(ethylene glycol) (PEG)-based hydrogels whose formulations were chosen to achieve functional differences in moduli that approach those of osteochondral tissues (Figure 5.1B). The 3D-printed structure was fabricated using stereolithography and a PEG diacrylate resin whose material compressive modulus was 31.1 (1.2) MPa (i.e., mean (SD)). This 3D-printed PEG structure was chosen for its stiff mechanical properties, hydrophilicity, and cytocompatibility.[54,55] The 3D-printed structure was infilled with IDG-SW3 osteocytes encapsulated in a soft and degradable PEG hydrogel that supports osteocyte differentiation.[56] PEG was chosen as the base synthetic chemistry for it tunability,

cytocompatibility, and ease of modifying with groups (e.g. norbornenes) that participate in thiol-ene click reactions and allow for facile incorporation of peptides (e.g. RGD) and peptide crosslinks. The hydrogel was made with crosslinks of matrix-metalloproteinase (MMP) sensitive peptides to enable cell-mediated degradation and tethered with RGD peptides to facilitate cell-hydrogel interactions. Over 35 days of static culture, the soft hydrogel supported cell viability (Figure 5.1C with live cells stained green by Calcein-AM and Figure 7.7) with dead cells stained red with ethidium homodimer) and cellular spreading (Figure 5.1C) with dendrite-like protrusions. The latter is important for creating an interconnected cellular system, known in bone as the lacunocanalicular network.[4] Some cell aggregation was observed, which is likely to have occurred prior to the encapsulation process,[57] but did not adversely affect cell viability. The compressive modulus of the acellular MMP-sensitive hydrogel was 8.8 (0.4) kPa, and after 35 days of differentiation the cell-laden hydrogel was 2.2 (0.2) kPa. The softer cell-laden hydrogel is attributed to several effects. At the time of encapsulation, cells can sequester crosslinker molecules prior to polymerization which lowers the effective crosslink density and hence stiffness.[58] After encapsulation, secretion of MMPs can lead to rapid degradation of the hydrogel before the cells have time to differentiate and deposit their own ECM.[57,59] The modulus of the 3D-printed structure infilled with the soft hydrogel (i.e. the bone layer shown in Figure 5.1B) was 2.4 (0.5) MPa. The cartilage layer was made from a PEG hydrogel containing non-degradable PEG-dithiol crosslinkers and a modulus of 2.9 (0.4) kPa.

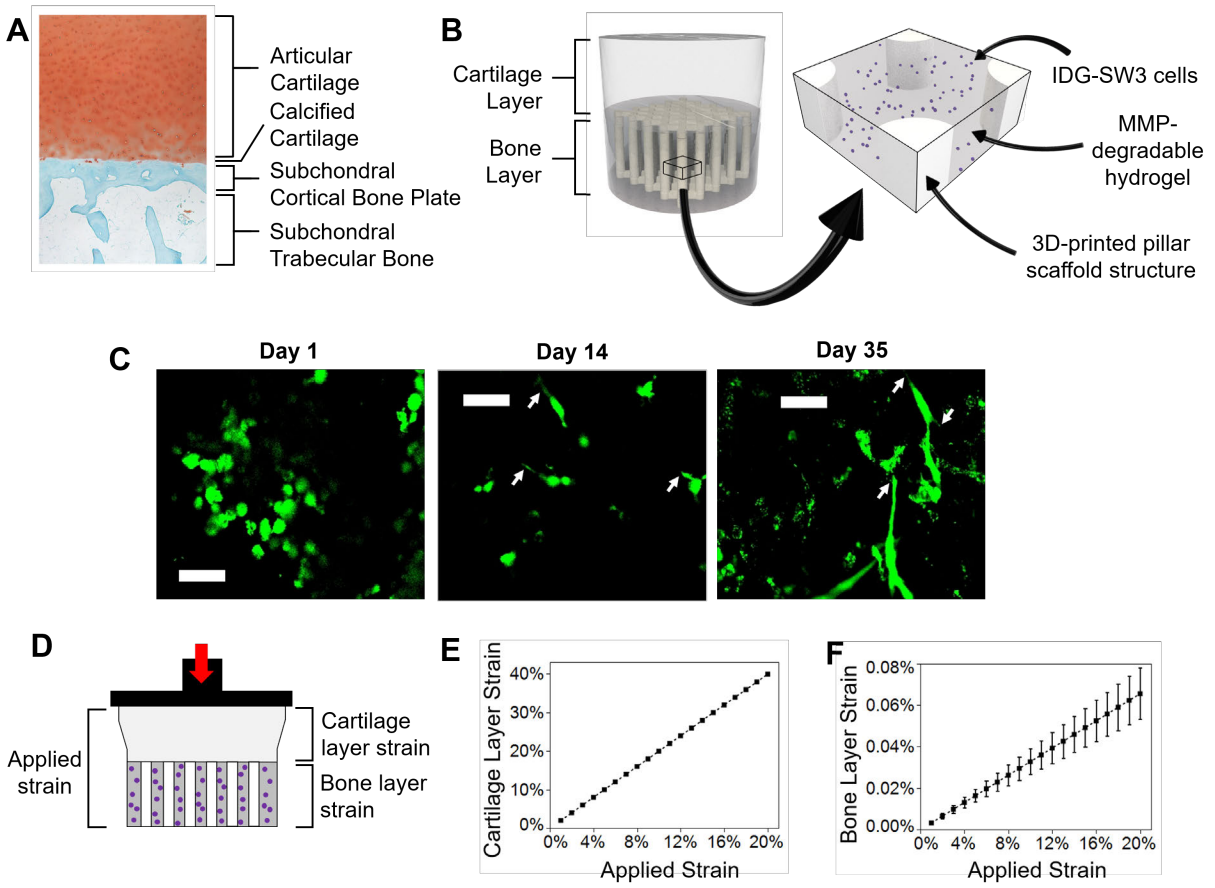

Figure 5.1 A bilayer composite hydrogel was designed to mimic the osteochondral unit and achieve near-physiological levels of strain in the bone layer. (A) Representative healthy human osteochondral tissue stained with Safranin-O Fast Green. (B) Schematic of the bilayer composite hydrogel. The cartilage layer is comprised of a soft, acellular, non-degradable hydrogel. An enlarged section shows the different components of the bone layer: IDG-SW3 cells (purple) encapsulated in a soft, MMP-degradable hydrogel, which is a continuous matrix infill of the 3D-printed pillar scaffold structure. (C) Representative images of live cells stained green by Calcein-AM, scale bar is 50 μm. Arrows denote dendrite-like cellular protrusions. (D) Schematic of the strain in each layer with an applied strain. (E) Cartilage and (F) bone layer strain as a function of applied strain (n=4).

We applied Hooke's Law to determine the relative transfer of strain to each layer when the bilayer composite is subjected to an applied compressive strain (Figure 5.1D). The strain in the cartilage layer was approximately twice the applied strain (Figure 5.1E): 20% applied strain resulted in 40 (0.012) % strain in the cartilage layer (Table 7.2). In contrast, strain in the bone layer

was minimal compared to the applied strain (Figure 5.1F): 20% applied strain resulted in 0.066 (0.012) % strain in the bone layer (Table 7.2). We applied strains of 5, 10, or 20% and in each case, the cartilage layer took on > 99% of the applied strain while strain in the bone layer was consistently ≤ 0.08%. These results confirm near-physiological strains were achieved within the bone layer.

We evaluated two requirements of the cellular niche within this bilayer composite: mature osteocyte differentiation and bone matrix deposition. The IDG-SW3 cell line was derived from murine long bone chips and was chosen for the ability to differentiate from osteoblasts to late osteocytes and deposit a mineralized collagen matrix.[60] Over a 35-day static culture (Figure 5.2A**),** IDG-SW3 cells differentiated from osteoblasts to osteocytes. Connexin 43 was observed by punctate staining in the hydrogel (Figure 5.2B), which is consistent with connexin 43 staining in a 2D culture control (Figure 5.2C) and typical for connexin 43 (negative control images included in Figure 7.8).[61,62] Connexin 43 comprises hemichannels and gap junctions along the cell membrane and is essential for osteocyte function, survival, and differentiation.[63–65] Concomitant, normalized expression (NE) of osteocyte-related genes *Dmp1* and *Sost*, as measured by qPCR, increased over culture time (Figure 5.2D). DMP1 plays a role in hydroxyapatite formation and lacunocanalicular formation[5] and marks the beginning of the osteoblast to osteocyte transition.[60,66–68] Sclerostin (encoded by *Sost*), expressed by mature osteocytes, regulates osteoblast-mediated bone formation.[5,69]The NE of *Dmp1* and *Sost* at day 35 was significantly higher than both day 0 pre-encapsulated cells (*Dmp1*: $p = 0.002$, *Sost*: $p = 0.009$) and day 1 encapsulated cells (*Dmp1*: $p = 0.002$, *Sost*: $p = 0.022$). Collectively, these results indicate that the statically-cultured IDG-SW3 cells in the bone layer differentiated toward a mature osteocyte phenotype.

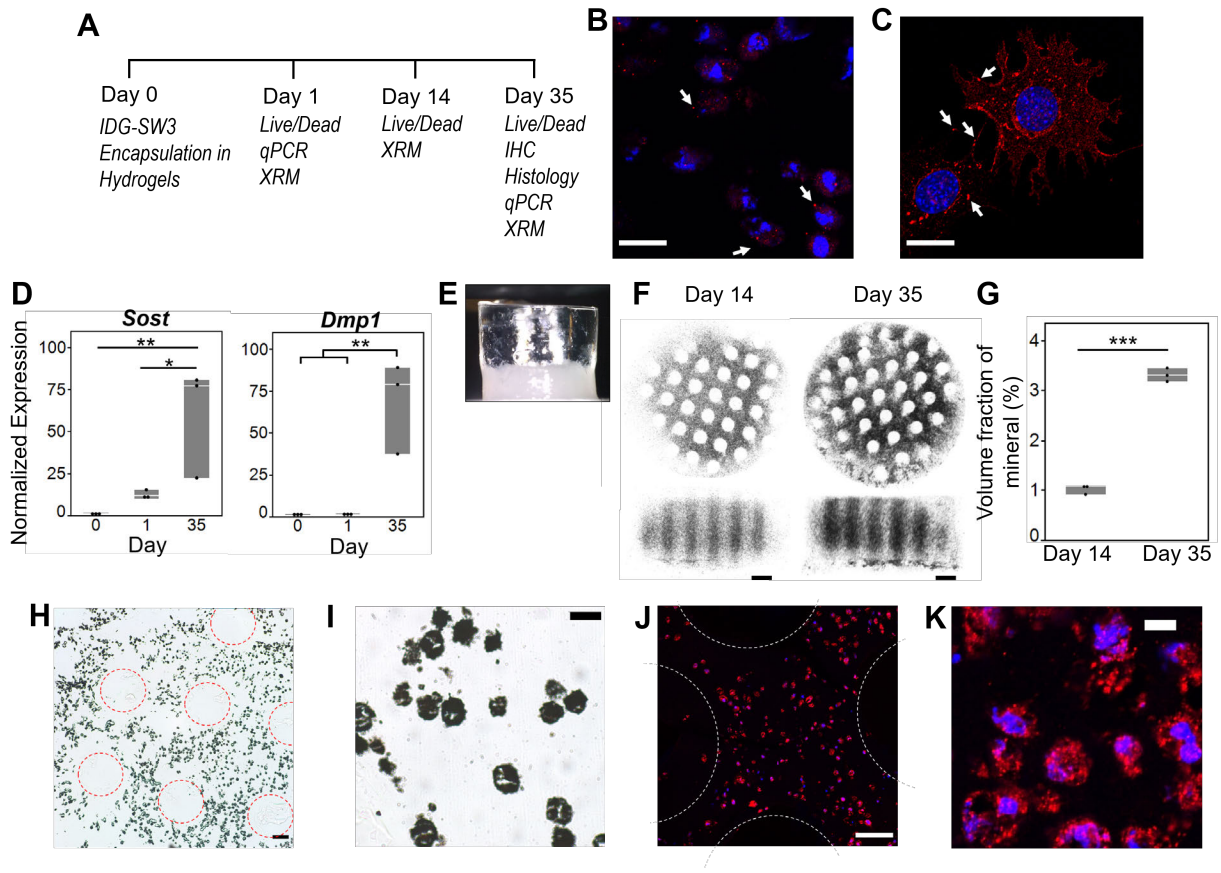

Figure 5.2: IDG-SW3 cells differentiated towards mature osteocytes and deposited bone matrix within the bilayer composite hydrogel. (A) Study design and corresponding assays at each time point. (B-C) Representative confocal microscopy images of Connexin 43 (red, denoted with arrows) counterstained with DAPI for nuclei (blue) on (B) day 35 within hydrogel by immunohistochemistry and (C) day 3 on collagen type I coated glass dish by immunocytochemistry, scale bar = 20 μm. (D) Normalized gene expression (to Day 0) of osteocyte-marker genes *Dmp1* and *Sost* on Days 0 (pre-encapsulated cells), 1, and 35 (n=3). (E) Photograph of bilayer composite at Day 35 depicting a translucent cartilage layer and opaque bone layer. (F) Representative 3D X-Ray Microscope (XRM) images show mineralization (black) on days 14 and 35. At day 1, there was no detectable mineral content and hence an image was not included. (G) Volume fraction of mineral content from the XRM images (n=3). (H-K) Representative images of day 35 Glycol methacrylate-embedded sections stained with von Kossa for mineralization (black) (H-I) and for collagen type I (red) and counterstained with DAPI for nuclei (blue) (J-K). Scale bar = 100 μm (H, J), 20 μm (I), 10 μm (K). In (H) and (J) 3D-printed pillar regions are outlined with dotted circles. Symbols denote significance from post hoc Tukey's test (D) or two-sided t-test (G): * $p<0.05$; ** $p<0.01$; *** $p<0.001$.

The deposition of bone matrix by the encapsulated osteocytes was also assessed after 35 days of differentiation in static culture. Matrix deposition was limited to the bottom layer, as evidenced by opaque coloration in images of the bilayer composite on day 35 (Figure 5.2E). Organic and inorganic components comprise bone matrix: the organic component includes mostly collagen type I while the inorganic component includes predominantly hydroxyapatite crystals, which are initially deposited as amorphous calcium phosphate.[47] The collagen serves as the organizational backbone for mineralization, following nucleation,[70] and binding[71–73] of hydroxyapatite crystals. We therefore assessed bone matrix deposition by 3D X-Ray microscopy (XRM) imaging and staining for calcium and collagen type I deposits in the bottom layer. XRM confirmed no detectable mineral content in the cartilage layer at any time point or in the bone layer on day 1. However, mineral was present through the bone layer by day 14 and further increased on day 35 (Figure 5.2F-G). The 3D printed pillars were visible by an absence of mineralization. Minimal difference was observed in the spatial distribution of deposited mineral, which suggests that the cellular-mediated mineral deposition was unimpacted by the 3D-printed structure. Calcium deposition was further confirmed by von Kossa staining of sections from glycol methacrylate (GMA)-embedded samples (Figure 5.2H-I). Collagen type 1 deposition was confirmed by immunohistochemical staining of sections from GMA-embedded samples (Figure 5.2J-K). GMA embedding limited extracellular staining; yet the positive staining for calcium and collagen type I within intracellular regions confirmed that the osteocytes produced bone matrix. Taken together, the bone layer of the composite hydrogel promoted both osteocyte differentiation and deposition of mineralized and collagenous matrix.

We next assessed the effect of loading on the osteocyte response by compressing the bilayer composite at varying applied strains (0, 5, 10, 20%) and frequencies (0.5, 1, 2 Hz) (Figure

5.3A). To determine whether osteocytes could sense and respond to an applied load in the 3D model, prostaglandin E_2 (PGE_2) was chosen as a measure of osteocyte response. PGE_2 is rapidly secreted by osteocytes, on the order of minutes,[74,75] in response to a mechanical stimulus (e.g., fluid flow[74,76] and compression[77]). Herein, PGE_2 was measured in the culture medium immediately after on hour of loading. Bilayer composite hydrogels were cultured between 35-43 days to first establish a bone matrix and mature osteocytes within the cellular niche. Then, on the final day of culture, hydrogels were dynamically loaded in a bioreactor for one hour. PGE_2 levels released into the culture medium immediately after loading were affected ($p < 0.0001$) by loading group (Figure 5.3B). We did not investigate loading of the infill hydrogel alone (i.e., without the stiff structure) due to its low modulus, which when placed in the bioreactor will lead to high tare strains imparted by the weight of the loading platens. All loading groups showed higher ($p < 0.05$) PGE_2 levels when compared to the unloaded group. Pair-wise comparisons between loading groups revealed several interesting findings. There was no significant effect of strain for comparisons within the same frequency. Here, bone layer strains were 0.033% and 0.066% (Table 7.2) for applied strains of 10 and 20%, respectively. This suggests that a difference in strain of 0.033% experienced by the osteocytes was insufficient to further influence PGE_2 levels. However, there were differences with loading frequencies. PGE_2 levels increased from 1 to 2 Hz frequency at both 10% ($p < 0.0001$) and 20% ($p = 0.0003$) applied strain. But an opposite effect was observed where PGE_2 levels decreased with increased frequency from 0.5 Hz to 1 Hz at 20% applied strain ($p = 0.0013$). These findings suggest that in this culture system and with IDG-SW3 cells, the osteocyte PGE_2 response is more sensitive to loading frequency than strain magnitude.

We next added an inhibitor of COX2, NS-398, which is required for PGE_2 synthesis,[78] to evaluate load-induced osteocyte synthesis of PGE_2 (Figure 5.3C). NS-398 was added to the media

in the unloaded control and for the condition with the highest PGE_2 concentration (10% strain, 2 Hz). In the absence of loading, osteocytes secreted low levels of PGE_2, which was further reduced (p = 0.001) by NS-398. NS-398 treatment abrogated (p = 0.0002) the load-induced PGE_2 levels, bringing the levels lower than the control samples without NS-398 (p < 0.05). These findings confirm that dynamic compressive loading, when applied to this composite hydrogel, induced PGE_2 synthesis by osteocytes.

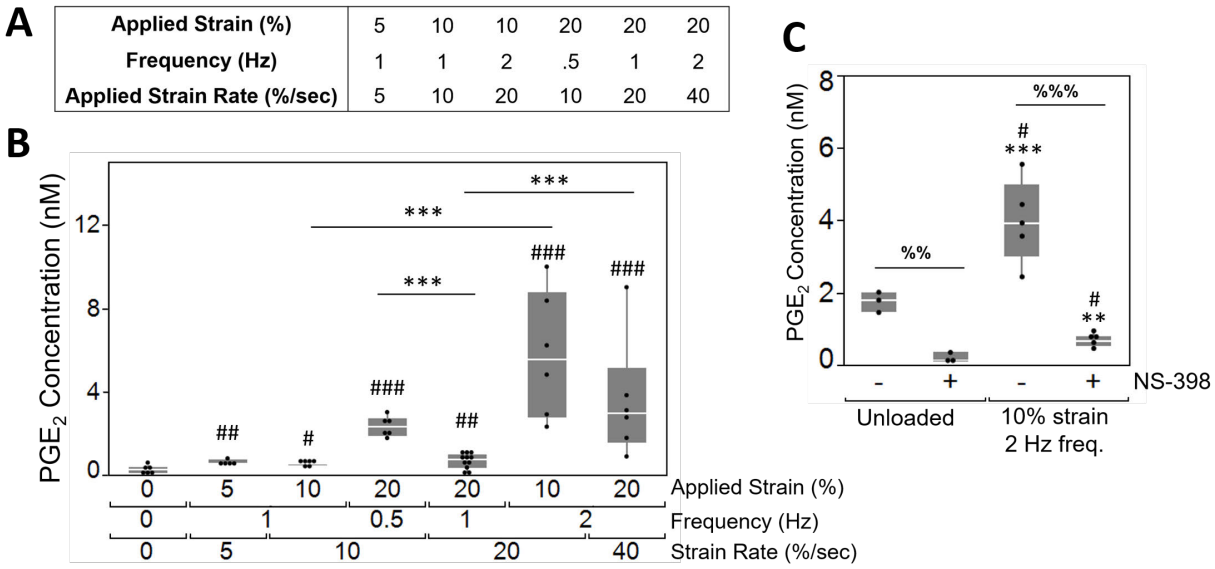

Figure 5.3 Osteocytes could sense and respond to loading within the bilayer composite hydrogel. (A) Experimental loading regimes. (B) PGE_2 concentration in the media directly after loading as a function of applied strain, frequency, and applied strain rate. Outliers were removed and experimental sample size of all groups was 6, except for the 20% applied strain/1 Hz frequency condition which represents a sample size of 12. Symbols denote significance of post hoc Tukey's test: # compared to unloaded condition; * between strain-matched or frequency-matched conditions. (C) PGE_2 in the media was analyzed directly after loading (n=5) or in unloaded controls (n=3) with or without NS-398, a COX2 inhibitor. Symbols denote significance of post hoc Tukey's test: # compared to unloaded -NS-398, * compared to unloaded +NS-398; % between NS-398 treatment within the same loading condition. Significance levels: one symbol p<0.05; two symbols p<0.01; three symbols p<0.001.

While dynamic loading frequency elicited an osteocyte response via PGE_2 production, the magnitude of applied strain had no effect. The applied strains that are translated to the bone layer are small, which is consistent with *in vitro* 2D studies that show bone cells are unaffected by cellular strains less than 0.5%.[79] Yet, tissue-level strains within bone range from 0.001-0.3% and rarely exceed 0.2%.[14] When bone is strained, fluid moves through the lacunocanalicular system and the elements that tether osteocytes to the canalicular walls are subjected to tension. This process amplifies the tissue-level strains on the cell's cytoskeleton by 10-100 fold.[11] Strain-amplification also occurs due to the softer pericellular matrix that surrounds osteocytes *in vivo*, where strain increases by 1.4-2.7×.[80] Thus, we postulate that osteocytes sense strain-induced mechanical cues when the environment leads to cellular strain amplification. In this study, we surmise that the effects dominated by frequency may be in part due to fluid flow-induced cellular strain amplification that occurs as fluid moves through the soft hydrogel and adjacent to the embedded osteocytes. Although the exact mechanisms remain to be determined, findings from this study indicate that osteocytes are more sensitive to fluid flow than physiologically relevant tissue-level strains, which is in agreement with computational models[11,81,82] and *in vitro* experiments[11,83].

Our findings also suggest that the bilayer composite hydrogel can generate fluid-induced flow in the bone layer despite the low strains that are transferred to the hydrogel. Increases in frequency during unconfined compression of cartilage amplify the velocity of interstitial fluid.[84] In our system, unconfined compression of the bilayer composite generated large strains (~10-40%) in the cartilage layer. As the cartilage layer hydrogel contains 98% water and PEG hydrogels exhibit poroelastic behavior,[85–87] fluid movement in the cartilage layer will be, in part, forced downward and into the bone layer when compressed.[38] This phenomenon is similar to fluid movement across the osteochondral interface between articular cartilage and subchondral bone

when the unit is compressed.[8] We expect the magnitude of fluid flow to be relatively low within the hydrogel (e.g., 1-10 nm second^{-1}[38]) based on previous computational modeling of bilayer hydrogels where the bone layer underwent ~1% strain. Contrarily, lacunocanalicular flow in bone is predicted to have velocities of ~300 nm second^{-1}.[88] This, in combination with the finding that strains did not affect load-induced PGE_2 synthesis by osteocytes, further points to the hypothesis that our 3D model may enable cellular strain amplification when subjected to frequency-induced small changes in fluid flow. While fluid flow magnitudes are difficult to determine, future studies will utilize experiments and computational modeling to evaluate this complex loading environment.

In conclusion, this study presents a new 3D model of the osteochondral unit to study the effects of simulated *in vivo* loading on osteocytes. Near-physiological levels of strain were achieved in the bone layer of the composite hydrogel. Further, the model induced an osteocyte response that was frequency, but not strain, dependent; we attribute the cellular response to altered fluid flow and possibly cellular strain amplification, which is observed *in vivo*. Our model will empower *in vitro* studies of osteocytes in a highly controlled system that mimics the mechanical environment of the osteochondral unit's subchondral bone plate. While this study used an MMP-sensitive PEG hydrogel, other hydrogels that support osteocyte differentiation could readily be infilled into the stiff 3D-printed structure and attain near-physiological levels of strain in the bone-like layer. Other environmental considerations that are known to influence osteocytes could be studied within this model, which include pH,[89] oxygen tension,[90] drug treatment,[91] hormone levels,[92,93] or inflammatory mediators.[94] Further, this unique model may generate new insights into the osteocyte's role in propagating osteoarthritis progression in response to the changes in fluid flow.[7,8] Even further, chondrocytes can be encapsulated the top layer and osteocyte-chondrocyte

crosstalk—a key part of osteochondral homeostasis and degeneration—can be investigated under different loading or inflammatory environments.

5.3 Experimental Section

Details of all methods are provided in the Supporting Information and all materials used are provided in Table 7.3. A custom-built stereolithography system[54] was used to 3D-print the stiff structure (Figure 7.9). A rectangular structure (3 mm x 3 mm x 1.5 mm) was designed with an array of 250 μm diameter pillars occupying 25% of the volume and resulting in a 75% void volume. A lattice on top and bottom connects the pillars and allows fluid flow between the layers. The resin was comprised of poly(ethylene glycol) diacrylate (700 g/mol) and pentaerythritol tetrakis(3-ercaptopropionate) mixed at a ratio of 99:1 by weight with 2-(2-hydroxyphenyl)-benzotriazole derivative (10 mg ml^{-1}, Tinuvin CarboProtect), Diphenyl-(2,4,6-trimethylbenzoyl)phosphine oxide (0.05 wt%, TPO) as a photoinitiator, and 2,20-Azobis(2-methylpropionitrile) (0.56 mg ml^{-1}, AIBN) for thermal post-curing. The structure was printed in 10 μm thick layers and each layer was exposed to 405 nm light for 12 seconds at an average intensity of 76 mW cm^{-2}. Post-printing, structures were briefly washed in 100% ethanol to remove the resin and then placed in an oven at a temperature of 105˚C under vacuum for 1 hour. The structures were soaked in 100% ethanol for 72 hours to remove any unreacted monomers within the material and then sterilized in 70% ethanol for 48 hours.

The bilayer hydrogel was fabricated by first infilling the 3D-printed structure with the MMP-sensitive cellular hydrogel containing IDG-SW3 cells (at a concentration of $80x10^6$ cells ml^{-1} of hydrogel precursor) and then forming an overlying acellular layer using established protocols.[95] The compressive modulus values were obtained by testing cylindrical samples in unconfined compression.[56] Throughout static culture, samples were stained using a Live/Dead

assay (Calcein-AM and ethidium homodimer) and imaged using confocal microscopy.[56] After 35 days of culture, samples were collected for: immunohistochemical and histological staining for connexin 43, collagen type I, and calcium[96]; RNA extraction and qPCR analysis; X-Ray Microscope imaging of mineralization; and dynamic loading using a custom bioreactor.[97–100] After loading, PGE_2 in the media was measured using a standard ELISA. Data were analyzed for statistical significance using either a two-tailed t-test (mineral fraction) or a one- or two-way analysis of variance followed by Tukey's post hoc analysis ($\alpha = 0.05$). Data are presented as mean (standard deviation) in the text, while graphical results are presented as box plots or as a mean with standard deviations as error bars.

5.4 Acknowledgments

The authors acknowledge technical support from Sadhana Sharma (hydrogel fabrication and culture), A. Camila Uzcategui (3D printing); Kristine Fischenich (XRM methods development and scanning, statistics advice), Sarah Schoonraad (immunohistochemistry methods development), Victor Crespo (single 3D-printed pillar modulus values); and Jennifer Coulombe (statistics advice). We thank Professor Corey Neu for the use of A1R Nikon Confocal System and Professor Vanessa Sherk for the use of the Leica HistoCore Autocut microtome. The research reported in this publication was supported by the National Institute of Arthritis and Musculoskeletal and Skin Diseases of the National Institutes of Health under the Award 1R21AR069791-01A1 and 1R01AR069060-01A1. RLW was supported on an NIH/NIA National Institute of Aging Integrative Physiology of Aging Training Grant under Award T32AG000279-16A1. The content in this publication is solely the responsibility of the authors and does not necessarily represent the official views of the NIH.

5.5 References

1. Findlay, D. M. & Kuliwaba, J. S. Bone–cartilage crosstalk: a conversation for understanding osteoarthritis. *Bone Research* **4**, 16028 (2016).

2. Funck-Brentano, T. & Cohen-Solal, M. Crosstalk between cartilage and bone: When bone cytokines matter. *Cytokine & Growth Factor Reviews* **22**, 91–97 (2011).

3. Schaffler, M. B., Cheung, W.-Y., Majeska, R. & Kennedy, O. Osteocytes: Master Orchestrators of Bone. *Calcified Tissue International* **94**, 5–24 (2014).

4. Bonewald, L. F. The amazing osteocyte. *Journal of Bone and Mineral Research* **26**, 229–238 (2011).

5. Klein-Nulend, J., Bakker, A. D., Bacabac, R. G., Vatsa, A. & Weinbaum, S. Mechanosensation and transduction in osteocytes. *Bone* **54**, 182–190 (2013).

6. Alliston, T. Biological Regulation of Bone Quality. *Current Osteoporosis Reports* **12**, 366–375 (2014).

7. Hwang, J. *et al.* Increased hydraulic conductance of human articular cartilage and subchondral bone plate with progression of osteoarthritis. *Arthritis & Rheumatism* **58**, 3831–3842 (2008).

8. Stender, M. E., Regueiro, R. A. & Ferguson, V. L. A poroelastic finite element model of the bone–cartilage unit to determine the effects of changes in permeability with osteoarthritis. *Computer Methods in Biomechanics and Biomedical Engineering* 1–13 (2016) doi:10.1080/10255842.2016.1233326.

9. Stender, M. E., Carpenter, R. D., Regueiro, R. A. & Ferguson, V. L. An evolutionary model of osteoarthritis including articular cartilage damage, and bone remodeling in a computational study. *Journal of Biomechanics* (2016) doi:10.1016/j.jbiomech.2016.09.024.

10. Burr, D. B. The importance of subchondral bone in osteoarthrosis: *Current Opinion in Rheumatology* **10**, 256–262 (1998).

11. Fritton, S. P. & Weinbaum, S. Fluid and Solute Transport in Bone: Flow-Induced Mechanotransduction. *Annual Review of Fluid Mechanics* **41**, 347–374 (2009).

12. Hemmatian, H., Bakker, A. D., Klein-Nulend, J. & van Lenthe, G. H. Aging, Osteocytes, and Mechanotransduction. *Curr Osteoporos Rep* **15**, 401–411 (2017).

13. Mazur, C. M. *et al.* Osteocyte dysfunction promotes osteoarthritis through MMP13-dependent suppression of subchondral bone homeostasis. *Bone Res* **7**, 34 (2019).

14. Fritton, S. P., McLeod, K. J. & Rubin, C. T. Quantifying the strain history of bone: spatial uniformity and self-similarity of low-magnitude strains. *Journal of biomechanics* **33**, 317–325 (2000).

15. Tanaka, T. *et al.* Analysis of Ca2+ response of osteocyte network by three-dimensional time-lapse imaging in living bone. *Journal of Bone and Mineral Metabolism; Tokyo* **36**, 519–528 (2018).

16. Lynch, M. E. *et al.* In vivo tibial compression decreases osteolysis and tumor formation in a human metastatic breast cancer model. *Journal of Bone and Mineral Research* **28**, 2357–2367 (2013).

17. Lara-Castillo, N. *et al.* In vivo mechanical loading rapidly activates β-catenin signaling in osteocytes through a prostaglandin mediated mechanism. *Bone* **76**, 58–66 (2015).

18. Lewis, K. J. *et al.* Osteocyte calcium signals encode strain magnitude and loading frequency in vivo. *Proceedings of the National Academy of Sciences* **114**, 11775–11780 (2017).

19. Robling, A. G. *et al.* Mechanical Stimulation of Bone in Vivo Reduces Osteocyte Expression of Sost/Sclerostin. *Journal of Biological Chemistry* **283**, 5866–5875 (2008).

20. Holguin, N., Brodt, M. D. & Silva, M. J. Activation of Wnt Signaling by Mechanical Loading Is Impaired in the Bone of Old Mice. *Journal of Bone and Mineral Research* **31**, 2215–2226 (2016).

21. Metzger, C. E. *et al.* Differential responses of mechanosensitive osteocyte proteins in fore- and hindlimbs of hindlimb-unloaded rats. *Bone* **105**, 26–34 (2017).

22. Rath, A. L. *et al.* Correlation of cell strain in single osteocytes with intracellular calcium, but not intracellular nitric oxide, in response to fluid flow. *Journal of Biomechanics* **43**, 1560–1564 (2010).

23. Liu, C. *et al.* Effects of cyclic hydraulic pressure on osteocytes. *Bone* **46**, 1449–1456 (2010).

24. Galea, G. L. *et al.* Sost down-regulation by mechanical strain in human osteoblastic cells involves PGE2 signaling via EP4. *FEBS Letters* **585**, 2450–2454 (2011).

25. Atkins, G. J. *et al.* Sclerostin is a locally acting regulator of late-osteoblast/preosteocyte differentiation and regulates mineralization through a MEPE-ASARM-dependent mechanism. *Journal of Bone and Mineral Research* **26**, 1425–1436 (2011).

26. Zhang, C., Bakker, A. D., Klein-Nulend, J. & Bravenboer, N. Studies on Osteocytes in Their 3D Native Matrix Versus 2D In Vitro Models. *Current Osteoporosis Reports* **17**, 207–216 (2019).

27. Vazquez, M. *et al.* A New Method to Investigate How Mechanical Loading of Osteocytes Controls Osteoblasts. *Front Endocrinol (Lausanne)* **5**, (2014).

28. Sun, Q. *et al.* Ex vivo replication of phenotypic functions of osteocytes through biomimetic 3D bone tissue construction. *Bone* **106**, 148–155 (2018).

29. Takemura, Y. *et al.* Mechanical loading induced osteocyte apoptosis and connexin 43 expression in three-dimensional cell culture and dental implant model. *Journal of Biomedical Materials Research Part A* **107**, 815–827 (2019).

30. Choudhary, S. *et al.* Hypoxic Three-Dimensional Cellular Network Construction Replicates Ex Vivo the Phenotype of Primary Human Osteocytes. *Tissue Engineering Part A* **24**, 458–468 (2018).

31. Kurata, K., Heino, T. J., Higaki, H. & Väänänen, H. K. Bone Marrow Cell Differentiation Induced by Mechanically Damaged Osteocytes in 3D Gel-Embedded Culture. *Journal of Bone and Mineral Research* **21**, 616–625 (2006).

32. Spatz, J. M. *et al.* The Wnt Inhibitor Sclerostin Is Up-regulated by Mechanical Unloading in Osteocytes in Vitro. *Journal of Biological Chemistry* **290**, 16744–16758 (2015).

33. Mc Garrigle, M., Haugh, M., Voisin, M. & McNamara, L. Osteocyte differentiation and the formation of an interconnected cellular network in vitro. *European Cells and Materials* **31**, 323–340 (2016).

34. Bernhardt, A., Weiser, E., Wolf, S., Vater, C. & Gelinsky, M. Primary Human Osteocyte Networks in Pure and Modified Collagen Gels. *Tissue Engineering Part A* **25**, 1347–1355 (2019).

35. Lynch, M. E. *et al.* Three-Dimensional Mechanical Loading Modulates the Osteogenic Response of Mesenchymal Stem Cells to Tumor-Derived Soluble Signals. *Tissue Engineering Part A* **22**, 1006–1015 (2016).

36. Wang, W., Sarazin, B. A., Kornilowicz, G. & Lynch, M. E. Mechanically-Loaded Breast Cancer Cells Modify Osteocyte Mechanosensitivity by Secreting Factors That Increase Osteocyte Dendrite Formation and Downstream Resorption. *Frontiers in Endocrinology* **9**, (2018).

37. You, L., Temiyasathit, S., Tao, E., Prinz, F. & Jacobs, C. R. 3D Microfluidic Approach to Mechanical Stimulation of Osteocyte Processes. *Cellular and Molecular Bioengineering* **1**, 103–107 (2008).

38. Aziz, A. H., Eckstein, K., Ferguson, V. L. & Bryant, S. J. The effects of dynamic compressive loading on human mesenchymal stem cell osteogenesis in the stiff layer of a bilayer hydrogel. *Journal of Tissue Engineering and Regenerative Medicine* **13**, 946–959 (2019).

39. Galperin, A. *et al.* Integrated Bi-Layered Scaffold for Osteochondral Tissue Engineering. *Advanced Healthcare Materials* **2**, 872–883 (2013).

40. Gan, D. *et al.* Mussel-Inspired Tough Hydrogel with In Situ Nanohydroxyapatite Mineralization for Osteochondral Defect Repair. *Advanced Healthcare Materials* **8**, 1901103 (2019).

41. Kim, B. J. *et al.* Restoration of articular osteochondral defects in rat by a bi-layered hyaluronic acid hydrogel plug with TUDCA-PLGA microsphere. *Journal of Industrial and Engineering Chemistry* **61**, 295–303 (2018).

42. Lin, D. *et al.* A viscoelastic PEGylated poly(glycerol sebacate)-based bilayer scaffold for cartilage regeneration in full-thickness osteochondral defect. *Biomaterials* **253**, 120095 (2020).

43. Liu, K., Liu, Y., Duan, Z., Ma, X. & Fan, D. A biomimetic bi-layered tissue engineering scaffolds for osteochondral defects repair. *Sci. China Technol. Sci.* (2020) doi:10.1007/s11431-020-1597-4.

44. Liu, X. *et al.* A Biomimetic Biphasic Osteochondral Scaffold with Layer-Specific Release of Stem Cell Differentiation Inducers for the Reconstruction of Osteochondral Defects. *Advanced Healthcare Materials* **n/a**, 2000076.

45. Steinmetz, N. J., Aisenbrey, E. A., Westbrook, K. K., Qi, H. J. & Bryant, S. J. Mechanical loading regulates human MSC differentiation in a multi-layer hydrogel for osteochondral tissue engineering. *Acta Biomaterialia* **21**, 142–153 (2015).

46. Zhu, X. *et al.* Biomimetic Bacterial Cellulose-Enhanced Double-Network Hydrogel with Excellent Mechanical Properties Applied for the Osteochondral Defect Repair. *ACS Biomater. Sci. Eng.* **4**, 3534–3544 (2018).

47. Burr, D. B. & Akkus, O. Bone Morphology and Organization. in *Basic and Applied Bone Biology* 3–25 (Elsevier, 2014). doi:10.1016/B978-0-12-416015-6.00001-0.

48. Lories, R. J. & Luyten, F. P. The bone–cartilage unit in osteoarthritis. *Nature Reviews Rheumatology* **7**, 43–49 (2011).

49. Chan, D. D. *et al.* In vivo articular cartilage deformation: noninvasive quantification of intratissue strain during joint contact in the human knee. *Scientific Reports* **6**, 19220 (2016).

50. Wahlquist, J. A. *et al.* Indentation mapping revealed poroelastic, but not viscoelastic, properties spanning native zonal articular cartilage. *Acta Biomaterialia* **64**, 41–49 (2017).

51. Choi, K., Kuhn, J. L., Ciarelli, M. J. & Goldstein, S. A. The elastic moduli of human subchondral, trabecular, and cortical bone tissue and the size-dependency of cortical bone modulus. *Journal of biomechanics* **23**, 1103–1113 (1990).

52. Hargrave-Thomas, E., van Sloun, F., Dickinson, M., Broom, N. & Thambyah, A. Multi-scalar mechanical testing of the calcified cartilage and subchondral bone comparing healthy vs early degenerative states. *Osteoarthritis and Cartilage* **23**, 1755–1762 (2015).

53. Aziz, A. H. & Bryant, S. J. A comparison of human mesenchymal stem cell osteogenesis in poly(ethylene glycol) hydrogels as a function of MMP-sensitive crosslinker and crosslink density in chemically defined medium. *Biotechnology and Bioengineering* **116**, 1523–1536 (2019).

54. Uzcategui, A. C., Muralidharan, A., Ferguson, V. L., Bryant, S. J. & McLeod, R. R. Understanding and Improving Mechanical Properties in 3D printed Parts Using a Dual-Cure Acrylate-Based Resin for Stereolithography. *Adv. Eng. Mater.* **20**, 1800876 (2018).

55. Aisenbrey, E. A. *et al.* A Stereolithography-Based 3D Printed Hybrid Scaffold for In Situ Cartilage Defect Repair. *Macromolecular Bioscience* **18**, 1700267 (2018).

56. Aziz, A. H., Wilmoth, R. L., Ferguson, V. L. & Bryant, S. J. IDG-SW3 Osteocyte Differentiation and Bone Extracellular Matrix Deposition Are Enhanced in a 3D Matrix Metalloproteinase-Sensitive Hydrogel. *ACS Appl. Bio Mater.* **3**, 1666–1680 (2020).

57. Schneider, M. C. *et al.* Local Heterogeneities Improve Matrix Connectivity in Degradable and Photoclickable Poly(ethylene glycol) Hydrogels for Applications in Tissue Engineering. *ACS Biomater. Sci. Eng.* **3**, 2480–2492 (2017).

58. Chu, S., Maples, M. M. & Bryant, S. J. Cell encapsulation spatially alters crosslink density of poly(ethylene glycol) hydrogels formed from free-radical polymerizations. *Acta Biomaterialia* **109**, 37–50 (2020).

59. Aisenbrey, E. A. & Bryant, S. J. A MMP7-sensitive photoclickable biomimetic hydrogel for MSC encapsulation towards engineering human cartilage. *Journal of Biomedical Materials Research Part A* **106**, 2344–2355 (2018).

60. Woo, S. M., Rosser, J., Dusevich, V., Kalajzic, I. & Bonewald, L. F. Cell Line IDG-SW3 Replicates Osteoblast-to-Late-Osteocyte Differentiation in vitro and Accelerates Bone Formation in vivo. *J Bone Miner Res* **26**, 2634–2646 (2011).

61. Langhorst, H. *et al.* The IgCAM CLMP regulates expression of Connexin43 and Connexin45 in intestinal and ureteral smooth muscle contraction in mice. *Disease Models & Mechanisms* **11**, dmm032128 (2018).

62. Balla, P. *et al.* Prognostic Impact of Reduced Connexin43 Expression and Gap Junction Coupling of Neoplastic Stromal Cells in Giant Cell Tumor of Bone. *PLOS ONE* **10**, e0125316 (2015).

63. Plotkin, L. I. Connexin 43 and Bone: Not Just a Gap Junction Protein. *Actual osteol* **7**, 79–90 (2011).

64. Gramsch, B. *et al.* Enhancement of Connexin 43 Expression Increases Proliferation and Differentiation of an Osteoblast-like Cell Line. *Experimental Cell Research* **264**, 397–407 (2001).

65. Buo, A. M. & Stains, J. P. Gap junctional regulation of signal transduction in bone cells. *FEBS Letters* **588**, 1315–1321 (2014).

66. Paic, F. *et al.* Identification of differentially expressed genes between osteoblasts and osteocytes. *Bone* **45**, 682–692 (2009).

67. Uchihashi, K., Aoki, S., Matsunobu, A. & Toda, S. Osteoblast migration into type I collagen gel and differentiation to osteocyte-like cells within a self-produced mineralized matrix: A novel system for analyzing differentiation from osteoblast to osteocyte. *Bone* **52**, 102–110 (2013).

68. Kalajzic, I. *et al.* Dentin matrix protein 1 expression during osteoblastic differentiation, generation of an osteocyte GFP-transgene. *Bone* **35**, 74–82 (2004).

69. Galea, G. L., Lanyon, L. E. & Price, J. S. Sclerostin's role in bone's adaptive response to mechanical loading. *Bone* **96**, 38–44 (2017).

70. Zhang, W., Huang, Z.-L., Liao, S.-S. & Cui, F.-Z. Nucleation sites of calcium phosphate crystals during collagen mineralization. *Journal of the American Ceramic Society* **86**, 1052–1054 (2003).

71. Magne, D., Weiss, P., Bouler, J.-M., Laboux, O. & Daculsi, G. Study of the Maturation of the Organic (Type I Collagen) and Mineral (Nonstoichiometric Apatite) Constituents of a Calcified Tissue (Dentin) as a Function of Location: A Fourier Transform Infrared Microspectroscopic Investigation. *Journal of Bone and Mineral Research* **16**, 750–757 (2001).

72. Jiao, K. *et al.* Complementarity and Uncertainty in Intrafibrillar Mineralization of Collagen. *Advanced Functional Materials* **26**, 6858–6875 (2016).

73. Niu, L.-N. *et al.* Collagen intrafibrillar mineralization as a result of the balance between osmotic equilibrium and electroneutrality. *Nat Mater* **16**, 370–378 (2017).

74. Kamel, M. A., Picconi, J. L., Lara-Castillo, N. & Johnson, M. L. Activation of B-catenin signaling in MLO-Y4 osteocytic cells versus 2T3 osteoblastic cells by fluid flow shear stress and PGE2: Implications for the study of mechanosensation in bone. *Bone* **47**, 872–881 (2010).

75. Cheng, B. *et al.* PGE2 is essential for gap junction-mediated intercellular communication between osteocyte-like MLO-Y4 cells in response to mechanical strain. *Endocrinology* **142**, 3464–3473 (2001).

76. Westbroek, I. *et al.* Differential Stimulation of Prostaglandin G/H Synthase-2 in Osteocytes and Other Osteogenic Cells by Pulsating Fluid Flow. *Biochemical and Biophysical Research Communications* **268**, 414–419 (2000).

77. Klein-Nulend, J. *et al.* Sensitivity of osteocytes to biomechanical stress in vitro. *The FASEB Journal* **9**, 441–445 (1995).

78. Swartzlander, M. D. *et al.* Immunomodulation by mesenchymal stem cells combats the foreign body response to cell-laden synthetic hydrogels. *Biomaterials* **41**, 79–88 (2015).

79. You, J. *et al.* Substrate deformation levels associated with routine physical activity are less stimulatory to bone cells relative to loading-induced oscillatory fluid flow. *J. Biomech. Eng.* **122**, 387–393 (2000).

80. Rath Bonivtch, A., Bonewald, L. F. & Nicolella, D. P. Tissue strain amplification at the osteocyte lacuna: A microstructural finite element analysis. *Journal of Biomechanics* **40**, 2199–2206 (2007).

81. You, L., Cowin, S. C., Schaffler, M. B. & Weinbaum, S. A model for strain amplification in the actin cytoskeleton of osteocytes due to fluid drag on pericellular matrix. *Journal of biomechanics* **34**, 1375–1386 (2001).

82. Han, Y., Cowin, S. C., Schaffler, M. B. & Weinbaum, S. Mechanotransduction and strain amplification in osteocyte cell processes. *Proceedings of the national academy of sciences* **101**, 16689–16694 (2004).

83. Smalt, R., Mitchell, F. T., Howard, R. L. & Chambers, T. J. Induction of NO and prostaglandin E2 in osteoblasts by wall-shear stress but not mechanical strain. *American Journal of Physiology-Endocrinology And Metabolism* **273**, E751–E758 (1997).

84. Kim, Y.-J., Bonassar, L. J. & Grodzinsky, A. J. The role of cartilage streaming potential, fluid flow and pressure in the stimulation of chondrocyte biosynthesis during dynamic compression. *Journal of Biomechanics* **28**, 1055–1066 (1995).

85. Chan, E. P., Deeyaa, B., Johnson, P. M. & Stafford, C. M. Poroelastic relaxation of polymer-loaded hydrogels. *Soft Matter* **8**, 8234 (2012).

86. Rakovsky, A., Marbach, D., Lotan, N. & Lanir, Y. Poly(ethylene glycol)-based hydrogels as cartilage substitutes: Synthesis and mechanical characteristics. *J. Appl. Polym. Sci.* **112**, 390–401 (2009).

87. Bush, B. G., Shapiro, J. M., DelRio, F. W., Cook, R. F. & Oyen, M. L. Mechanical measurements of heterogeneity and length scale effects in PEG-based hydrogels. *Soft Matter* **11**, 7191–7200 (2015).

88. Goulet, G. C., Cooper, D. M. L., Coombe, D. & Zernicke, R. F. Influence of cortical canal architecture on lacunocanalicular pore pressure and fluid flow. *Computer Methods in Biomechanics and Biomedical Engineering* **11**, 379–387 (2008).

89. Ishihara, Y. *et al.* Hormonal, pH, and Calcium Regulation of Connexin 43–Mediated Dye Transfer in Osteocytes in Chick Calvaria. *Journal of Bone and Mineral Research* **23**, 350–360 (2008).

90. Lee, C. M., Genetos, D. C., You, Z. & Yellowley, C. E. Hypoxia regulates PGE2 release and EP1 receptor expression in osteoblastic cells. *Journal of Cellular Physiology* **212**, 182–188 (2007).

91. Tamplen, M. *et al.* Treatment with anti-Sclerostin antibody to stimulate mandibular bone formation. *Head & Neck* **40**, 1453–1460 (2018).

92. Fowler, T. W. *et al.* Glucocorticoid suppression of osteocyte perilacunar remodeling is associated with subchondral bone degeneration in osteonecrosis. *Scientific Reports* **7**, 44618 (2017).

93. Sharma, D. *et al.* Alterations in the osteocyte lacunar–canalicular microenvironment due to estrogen deficiency. *Bone* **51**, 488–497 (2012).

94. Pathak, J. L. *et al.* Systemic Inflammation Affects Human Osteocyte-Specific Protein and Cytokine Expression. *Calcif Tissue Int* **98**, 596–608 (2016).

95. Aziz, A. H. *et al.* Mechanical characterization of sequentially layered photo-clickable thiol-ene hydrogels. *Journal of the Mechanical Behavior of Biomedical Materials* **65**, 454–465 (2017).

96. Aziz, A. H. & Bryant, S. J. A comparison of human mesenchymal stem cell osteogenesis in poly(ethylene glycol) hydrogels as a function of MMP-sensitive crosslinker and crosslink density in chemically defined medium. *Biotechnology and Bioengineering* **0**,.

97. Nicodemus, G. D. & Bryant, S. J. The role of hydrogel structure and dynamic loading on chondrocyte gene expression and matrix formation. *Journal of Biomechanics* **41**, 1528–1536 (2008).

98. Nicodemus, G. D. & Bryant, S. J. Mechanical loading regimes affect the anabolic and catabolic activities by chondrocytes encapsulated in PEG hydrogels. *Osteoarthritis and Cartilage* **18**, 126–137 (2010).

99. Villanueva, I., Hauschulz, D. S., Mejic, D. & Bryant, S. J. Static and dynamic compressive strains influence nitric oxide production and chondrocyte bioactivity when encapsulated in PEG hydrogels of different crosslinking densities. *Osteoarthritis and Cartilage* **16**, 909–918 (2008).

100. Steinmetz, N. J. & Bryant, S. J. The effects of intermittent dynamic loading on chondrogenic and osteogenic differentiation of human marrow stromal cells encapsulated in RGD-modified poly(ethylene glycol) hydrogels. *Acta Biomaterialia* **7**, 3829–3840 (2011).

5.6 Supplementary Methods

5.6.1 Infilling Support Structure to Form a Bilayer Hydrogel

The bilayer hydrogel was fabricated by first infilling the 3D-printed structure with the MMP-sensitive cellular hydrogel containing IDG-SW3 cells, and then forming an acellular layer on top, using established protocols.[1] The cellular and acellular hydrogels were formed from precursor solutions of 8-arm PEG-norbornene, synthesized from 8-arm PEG amine following

established protocols.[2] The precursor solution for the cellular hydrogel consisted of PEG-norbornene (6.5% w/w, 20k MW), MMP-sensitive crosslinker containing the peptide sequence GCGPLG-LWARCG at a 0.65 thiol:ene ratio, CRGDS (2mM), and photoinitiator, 1-(4-(2-Hydroxyethoxy)-phenyl)-2-hydroxy-2-methyl-1-propane-1-one (0.05% w/w I2959) in phosphate-buffered saline (PBS). Murine IDG-SW3 cells were suspended in the precursor solution ($80x10^6$ cells ml^{-1}). A volume of 33 μl of the cell-laden precursor solution was infilled into the scaffold structure in a 1ml syringe-mold and was polymerized for 8 minutes with 352 nm light at 5–10 mW cm^{-2}. The precursor solution for the acellular hydrogel consisted of PEG-norbornene (2% w/w 10k MW), PEG-dithiol crosslinker (3.4k MW) at a 1 thiol:ene ratio, and I2959 photoinitiator (0.05% w/w) in PBS. A volume of 44 μl of the precursor solution was deposited on top the 3D printed structure with the infilled polymerized cellular layer and then photopolymerized for 5 minutes as described above. After polymerization, bilayer composite hydrogels were cultured at 37˚C with 5% CO_2 in osteogenic medium consisting of Modified Essential Medium (MEM) α containing L-glutamine and deoxyribonucleosides supplemented with FBS (10%), ascorbic acid (50 mg ml^{-1}), β-glycerophosphate (4 mM), and penicillin/streptomycin (1%).

On days 1, 14, and 35 of culture, samples (n = 3) were removed from culture and stained using a Live/Dead assay. Samples were incubated with Calcein AM (4 μM) for 20 minutes and eithidium homodimer (2 μM) for 10 minutes and immediately imaged by confocal microscopy (Zeiss LSM 5 Pascal system using a Zeiss Axiovert microscope).

5.6.2 Mechanical Characterization

The cellular and acellular hydrogel components of the bilayer composite hydrogel were mechanically tested using a Mechanical Testing Insight II to obtain the bulk true compressive modulus. Hydrogels of 3 mm diameter by 3 mm height were made for both the acellular (n = 3)

and cellular MMP-degradable (n = 5) hydrogels. The cellular hydrogels were cultured for 35 days before compression testing. Testing was performed using a 2N load cell with the top platen out-of-contact with the hydrogel and then a constant displacement rate of 1.2 mm min^{-1} until an approximate 50% strain (based on the initial height of the hydrogel) was reached. The point of contact was determined using MATLAB. The true compressive modulus was calculated from the slope of the linear region of the true stress-strain curve between 10 and 15% strain. The 3D-printed infilled (n = 6) structures were tested with a 5N load cell and a 0.25 N pre-load to calculate the height of the structure. The true compressive modulus was calculated from the linear portion of the true stress-strain curve up until buckling. Any structures that had visible pillar misalignment (*i.e.* pillars at an angle) were excluded from the analysis. To test the modulus of the 3D-printed resin, single pillars were printed, tested, and analyzed in the same way as the entire structure (n = 7). Every sample was tested in unconfined compression and in its swollen state.

5.6.3 Assessment of Matrix Deposition using Histology and X-Ray Microscope Imaging

Samples were removed from culture and fixed in 4% paraformaldehyde (PFA) for 24 hours at 4˚C. Histology samples (n = 3) from Days 1 and 35 were embedded in glycol methacrylate using the Technovit 7100 kit. Sections (5 μm) were stained for Collagen I and Connexin 43 and counterstained with DAPI using established immunohistochemistry (IHC) protocols. Sections (5 μm) were also stained by von Kossa to identify calcium deposits using established protocols.[3] Collagen I and Connexin 43 stained sections were imaged using a Nikon A1R Confocal System and the von Kossa stained sections were imaged using a light microscope (Zeiss Axioskop 40) with a digital camera (Diagnostic Instruments, MN 14.2 Color Mosaic). Following fixation, nano-CT samples (n = 3) from days 1, 14, and 35 were imaged using a Zeiss Xradia 520 Versa X-Ray Microscope (XRM). Each sample was scanned with a 4x objective, LE3 filter, and power and

voltage settings of 3 W and 40 kV, respectively. The pixel size of the scans was 4.17 μm. Images were analyzed using Dragonfly Pro and segmented using Otsu methods. The volume fraction of mineral content was calculated by determining the volume of mineral particles in each sample and normalized to the sample size. The total volume of each sample was not affected by time (Figure 7.10).

2D control samples were seeded with IDG-SW3 cells at a concentration of 20,000 cells cm^{-2} on collagen type I-coated glass-bottom petri dishes. Cells were cultured up to 3 days in osteogenic medium and fixed in 4% PFA for 20 minutes at room temperature. Samples were stained for collagen type I and DAPI using established immunocytochemistry protocols and imaged using a Nikon A1R Confocal System.

5.6.4 Gene Expression

RNA was extracted from samples (n = 3) via tissue homogenization and the miRNeasy Mini Kit, and reverse transcribed into cDNA using a High Capacity cDNA Reverse Transcription Kit. Quantitative real-time polymerase chain reaction (RT-qPCR) using custom primers (Table 7.4) was conducted using SYBR Green Master Mix.

Gene expression was analyzed using the true efficiency following the Pfaffl method,[4] normalized to the housekeeping gene L32 to obtain the relative expression, and normalized to the day 0 pre-encapsulated cells for normalized expression (NE).

5.6.5 Mechanical Loading using a Custom Bioreactor

A custom bioreactor was used to compress bilayer hydrogels during culture.[5–8] After a differentiation period (35-43 days), each sample (n = 5-6) was loaded for 1 hour at 5, 10, or 20 % applied strain with a frequency of 0.5, 1, or 2 Hz (Figure 5.3) with or without NS-398 (5 μM), a cyclooxygenase 2 (COX2) inhibitor. A baseline unloaded group (n = 3) was included as a control.

Directly after the 1 hour of loading, samples were removed from the bioreactor, and 200 μl of media was removed from each well for PGE_2 analysis using a standard ELISA kit. There was no significant effect of day (35 vs. 43, $p = 1$ for unloaded, $p = 0.963$ for 20%, 1 Hz) between the repeated measures (Figure 7.11); thus, all samples were graphed and statistically analyzed together.

5.6.6 Statistical Analysis

Statistics was performed using JMP Pro 14.1.0. To analyze the effect of time on gene expression, a one-way analysis of variance (ANOVA) was run with the effect of time. Post-hoc Tukey's test was used. For this analysis, distribution was confirmed to be normal, but sample size was small (n=3) and variances were not always equal. To analyze the effect of time on the volume fraction of mineral, the two-tailed t-test was used. To analyze the cellular release of PGE_2 as a function of loading, the PGE_2 concentration data was log-transformed to meet the normal distribution criteria. A one-way ANOVA was run with the effect of loading regime, and the data was confirmed to have homogeneous variance. Post-hoc analysis was performed using Tukey's test to compare pairs, and significant *p*-values between loading regimes that share common loading condition (*i.e.* strain or frequency) are shown in the figure. To analyze the effect of loading and NS-398 on PGE_2 release, the interaction term was significant of the two-way ANOVA and thus single effects were analyzed with post-hoc analysis using Tukey's test if the single effect was significant. The data from the loading experiment with NS-398 was confirmed to have homogeneous variance and normal distribution.

5.7 References from Supplementary Methods

1. Aziz, A. H. *et al.* Mechanical characterization of sequentially layered photo-clickable thiol-ene hydrogels. *Journal of the Mechanical Behavior of Biomedical Materials* **65**, 454–465 (2017).

2. Aziz, A. H., Eckstein, K., Ferguson, V. L. & Bryant, S. J. The effects of dynamic compressive loading on human mesenchymal stem cell osteogenesis in the stiff layer of a bilayer hydrogel. *Journal of Tissue Engineering and Regenerative Medicine* **0**,.

3. Aziz, A. H. & Bryant, S. J. A comparison of human mesenchymal stem cell osteogenesis in poly(ethylene glycol) hydrogels as a function of MMP-sensitive crosslinker and crosslink density in chemically defined medium. *Biotechnology and Bioengineering* **0**,.

4. Michael Pfaffl. A new mathematical model for relative quantification in real-time RT-PCR. *Nucleic Acids Research* **29**, 2002–2007 (2001).

5. Nicodemus, G. D. & Bryant, S. J. The role of hydrogel structure and dynamic loading on chondrocyte gene expression and matrix formation. *Journal of Biomechanics* **41**, 1528–1536 (2008).

6. Nicodemus, G. D. & Bryant, S. J. Mechanical loading regimes affect the anabolic and catabolic activities by chondrocytes encapsulated in PEG hydrogels. *Osteoarthritis and Cartilage* **18**, 126–137 (2010).

7. Villanueva, I., Hauschulz, D. S., Mejic, D. & Bryant, S. J. Static and dynamic compressive strains influence nitric oxide production and chondrocyte bioactivity when encapsulated in PEG hydrogels of different crosslinking densities. *Osteoarthritis and Cartilage* **16**, 909–918 (2008).

8. Steinmetz, N. J. & Bryant, S. J. The effects of intermittent dynamic loading on chondrogenic and osteogenic differentiation of human marrow stromal cells encapsulated in RGD-modified poly(ethylene glycol) hydrogels. *Acta Biomaterialia* **7**, 3829–3840 (2011).

6. Conclusions and Future Directions

6.1 Significance

Osteocytes are difficult to study *in vivo* and *in vitro*. *In vivo,* osteocytes are entombed within the heavily mineralized matrix of bone. Additionally, we lack a transgenic mouse model that specifically targets osteocytes without negative side effects.[1,2] Therefore, most of our current understanding of osteocyte mechanobiology and signaling is from *in vitro* culture. *In vitro,* primary osteocytes de-differentiate into osteoblasts when cultured in 2D.[3] Additionally, I showed in Chapter 4 that cells from one osteocyte-like cell line, IDG-SW3, upregulate the gene *Sost* (which is indicative of mature osteocyte differentiation) 5-fold in 2D culture and 465-fold in the 3D hydrogel after 35 days (compared to day 0). The 5-fold increase in *Sost* expression in 2D aligns with previous work by others culturing IDG-SW3 cells in 2D.[4] In Chapter 3, I showed a similar result with *Sost* expression using the OCY454 cell line: in 2D there was no significant change in expression, but culturing these osteocyte-like cells in 3D upregulated *Sost* expression by 120-fold (compared to day 0). This work showed that although osteocyte-like cell lines differentiate to some extent in 2D, a 3D environment may be necessary to achieve mature osteocyte differentiation *in vitro*.

In Chapter 4, I showed that the dimensionality (2D vs. 3D), which significantly affects differentiation, also significantly impacts the osteocyte response to a common signaling molecule in response to mechanical loading, Prostaglandin E2 (PGE_2). To date, most *in vitro* studies of osteocyte PGE_2 signaling have largely used *in vitro,* 2D cultures of either osteoblasts[5–15] or MLO-Y4 osteocyte-like cells.[5,13,16–19] I showed that the IDG-SW3 cells cultured in 3D express gene markers for anabolic signaling, a well-documented response to PGE_2 in bone.[20,21] This same

anabolic response was not observed in 2D. Further, I showed that the gene expression for all four PGE_2 cell-surface receptors, EP1-4, (*Ptger1, Ptger2, Ptger3, Ptger4*) were upregulated in 3D as compared to 2D. Previous studies showed that neither *Ptger1* nor *Ptger3* were detectable in 2D cultures of osteoblasts.[8] These findings indicate that gene expression levels for the EP receptors may be regulated by the environment (2D vs. 3D) or may increase as osteoblasts differentiate to early and mature osteocytes. Additionally, all four EP receptor genes decreased in 3D when treated with PGE_2, but not in 2D (Chapter 4). In an earlier study, MLO-Y4 cells cultured in 2D showed no change in *Ptger1, Ptger3*, and *Ptger 4*, but an increase in *Ptger2* expression after 24 hours of treatment with equivalent PGE_2 as I used.[22] It is likely that the PGE_2-induced reduction of *Ptger* gene expression only in 3D in Chapter 4 is a combined effect of the difference in initial *Ptger* levels and stage of osteocyte differentiation between 3D and 2D. Together, these findings indicate that studying osteocyte signaling in response to PGE_2 in 2D cultures yields different results than 3D cultures. It is likely that other signaling molecules that play a role in osteocyte mechanobiology, such as Wnt, influence the osteocyte anabolic response differently between 2D and 3D. Since the 3D cultures support mature osteocytes to a greater extent than the 2D cultures, *in vitro* studies of osteocyte signaling appear to require growth in 3D environments to mimic a mature osteocyte response.

Several groups have recently developed promising 3D culture systems that improve mature osteocyte differentiation and incorporate aspects of mechanical loading in 3D.[23–29] Most of these 3D cultures use collagen gels or mineral beads as a scaffold to mimic a certain characteristic of the *in vivo* bone matrix. Yet, these types of 3D scaffolds are subject to lack of tunability. This dissertation develops a 3D osteocyte culture system that enhances osteocyte differentiation using a poly(ethylene glycol) (PEG) hydrogel. Utilizing the tunability of the PEG hydrogel, I

incorporated degradable crosslinks, which increased osteocyte differentiation and bone matrix deposition, and were necessary for dendrite formation (Chapters 2.4 and 3.4). Incorporating TGF-β3, collagen type I, hydroxyapatite, and RGD into the degradable PEG network and culturing in chemically defined medium further increased dendrite formation and mature osteocyte differentiation (Chapter 3.4). This is the first PEG hydrogel-based 3D scaffold that has been developed that achieves mature osteocyte differentiation and dendrite formation.

To mimic the mechanical environment of subchondral bone, I incorporated the degradable PEG hydrogel into a bilayer composite design that uses a stiff, 3D-printed scaffold to control the strains in the bone layer. I incorporated an acellular, soft cartilage-like layer to mimic the elastic modulus mismatch between articular cartilage and subchondral bone within the osteochondral unit. When loaded in compression, this model achieved physiologically relevant strains (*i.e.*, 0.001-0.3%)[30,31] and interstitial fluid flow in the subchondral bone layer. Together, this work developed a 3D, *ex vivo* model of subchondral bone.

The utility of this system is extensive. Different growth factors, proteoglycans, or proteins could be tethered to the PEG network to investigate their impact on osteocyte differentiation or dendrite extension. Osteocyte signaling mechanisms due to inflammatory mediators or increased fluid flow during osteoarthritic degeneration could be investigated. Understanding the role that osteocytes play in osteoarthritis progression could inform new drug treatments to treat or slow the disease. Since bone is an endocrine organ in its ability to regulate phosphate levels, osteocytes in this hydrogel could be treated with different hormones or drugs; the osteocyte response could inform how endocrine signaling affects bone metabolism.

6.2 Major Conclusions

Osteocyte differentiation is enhanced in 3D PEG hydrogels as compared to collagen-coated 2D tissue culture polystyrene. In this dissertation, IDG-SW3 and OCY454 cells were used and both cell lines showed increased osteocyte markers such as *Dmp1, Phex,* and *Sost* after extended culture in 3D (Chapter 2-4). Additionally, the osteocyte response to Prostaglandin E2 (PGE_2) is affected by dimensionality (2D vs. 3D). The anabolic response in 3D was not observed in 2D. Also, in 3D the gene expression for all EP receptors decreases, which is a response that is not seen in 2D (Chapter 4). We also showed that *Tnfsf11* (gene encoding the regulatory protein Receptor activator of nuclear factor kappa-β ligand, RANKL) is downregulated in mature osteocytes (IDG-SW3 and OCY454) in response to PGE_2 (Chapters 3 and 4). This finding at the gene level is opposite to a previous study that cultured osteoblasts in 2D and found that PGE_2 treatment increased protein levels of RANKL.[7] By using an EP4 inhibitor and EP2 and EP4 agonists, we showed that the downregulation of *Tnfsf11* is mediated by PGE_2 binding to EP2 and EP4 (Chapters 3 and 4).

Some osteocyte differentiation markers are enhanced in degradable hydrogels as compared to non-degradable. OCY454 osteocyte dendrite formation (a morphological indicator of mature osteocyte differentiation) requires degradable hydrogels and is further enhanced in hydrogels with TGF-β3, RGD, collagen type I, and hydroxyapatite (Chapter 3). IDG-SW3 cells increased expression of *Dmp1* and *Phex* (Chapter 2) and OCY454 cells showed increased expression of *Dmp1* in degradable hydrogels as compared to non-degradable (Chapter 3). Degradable hydrogels also enhance bone matrix deposition (collagen type I, mineralization) in IDG-SW3 cells (Chapter 2). With higher cell densities (*i.e.*, 80 million cells/mL), the total matrix deposition increases,

indicating that these cells need a higher cell density to replace hydrogel with neotissue (Chapter 2).

A bilayer composite hydrogel was designed to generate bone-level strains and fluid-induced flow in a bone layer. IDG-SW3 cells encapsulated in a soft, degradable hydrogel was infilled into a 3D-printed stiff scaffold. This composite hydrogel created a bone layer that includes: (1) a soft, cellular niche that enhances cell spreading, osteocyte differentiation, and bone matrix deposition, and (2) a stiff scaffold that controls the strain. I also incorporated a soft, acellular, cartilage-like layer on top of the stiff bone layer to mimic the modulus mismatch between articular cartilage and subchondral bone. When compressed, the cartilage layer bore ~600x more strain that the bone layer, resulting in physiologically relevant strain in the bone layer (*i.e.*, 0.001-0.3%).[30,31] For example, a total strain of 10% or 20% resulted in approximately 0.033% or 0.066% bone layer strain and approximately 20% or 40% cartilage layer strain. When I loaded this structure in dynamic compression, increasing the strain (*i.e.*, 10% to 20%) had no effect on PGE_2 production by IDG-SW3 osteocytes. Thus, we concluded that the applied strains that are translated to the bone layer are small, which is consistent with *in vitro* 2D studies that show bone cells are unaffected by cellular strains less than 0.5% *in vitro*.[32] Yet, increasing the frequency of loading from 1 to 2 Hz increased the PGE_2 production. Increases in frequency during unconfined compression of cartilage have been shown to amplify the velocity of interstitial fluid.[33] In our bilayer system, unconfined compression of the total structure generated large strains (~10-40%) in the cartilage layer. The cartilage layer hydrogel is 98% water and PEG hydrogels exhibit poroelastic behavior.[34–36] Thus, when compressed, fluid from the cartilage layer will be, in part, forced downward into the bone layer.[37] This is similar to fluid movement between articular cartilage and subchondral bone when the osteochondral unit is compressed.[38] We expect this fluid flow to be relatively low: previous

computational modeling of a bilayer hydrogel with higher strains (~1%) predicted low magnitude fluid flows in the bone layer (e.g., 1-10 nm second[137]). Contrarily, in bone, lacunocanalicular flow is predicted flow at ~300 nm second.[139] This, in combination with the finding that strains did not affect PGE_2 synthesis by osteocytes, points to the conclusion that our 3D model may enable cellular strain amplification when subjected to frequency-induced small changes in fluid flow.

6.3 Future Directions

In this dissertation, I developed a degradable PEG hydrogel that enhances osteocyte differentiation, bone matrix deposition, and dendrite formation. This work identified several biochemical and physical cues that facilitate dendrite formation, with the goal of developing a lacunocanalicular network (LCN) *in vitro.* Yet, further work is needed to establish a more elaborate LCN that is observed *in vivo.* There are several potential directions including higher collagen concentrations. I saw that incorporating 0.1 wt% collagen type I increased some osteocyte differentiation markers and dendrite formation. At this low concentration, the collagen likely affected the dendrite formation via biochemical signaling rather than as a crosslinker. Higher concentrations of collagen could potentially further increase dendrite formation, as the collagen may provide a biochemical cue that stimulates osteocyte dendrite formation. Further, increasing the hydroxyapatite concentration (beyond the 1 wt% used in this dissertation) may also increase osteocyte differentiation or dendrite formation, as it increases osteogenesis in osteoblasts in a similar hydrogel model.[40] Additionally, investigating the impact of other growth factors, proteoglycans, or proteins on dendrite formation may show that osteocytes need other biochemical cues for extensive LCN development. For example, perlecan is a proteoglycan that constitutes most of the pericellular matrix in bone[41] and it may impact osteocyte dendrite formation. Another direction could be investigating dendrite extension with higher elastic modulus hydrogels. Other

studies have shown that osteogenic differentiation is enhanced in the 12-20 kPa range.[42] In Aim 2, the highest initial modulus was 13.3 kPa. Therefore, increasing the modulus to include 20 kPa in hydrogels with TGF-β3, collagen I, hydroxyapatite, and RGD as well may increase osteocyte differentiation and/or dendrite formation.

In hydrogels, a high cell density may be required for cell viability and communication *in vitro* due to the small mesh size of the initial polymer network that limits communication until degradation occurs. In Chapter 3, I used one cell concentration, 80 million cells/mL to investigate dendrite formation with OCY454 cells. Although this cell concentration was shown in Chapter 2 to increase matrix deposition and elastic modulus over 28 days in IDG-SW3 cells, we never investigated the impact of cell density on dendrite formation. *In vivo*, osteocyte density is 5-6 million cells/mL in young mice.[43] There likely exists a balance between spacing the cells out (to achieve longer dendrite formations) and spacing them closer (to allow for early communication via cell-mediated degradation of the polymer network). Varying the cell density (*e.g.*, 5, 10, 15, 20, 50, 80 million cells/mL) may show some tradeoff between cell viability and dendrite extension in the PEG hydrogel.

In Chapter 3, the degradable hydrogels were highly variable in dendrite assessment outcomes, depending on the image. For example, in most of the hydrogels with collagen added, the minimum and maximum percentage of dendritic cells were 0% and 100%. This indicates that the cells were still in the transition period of replacing hydrogel with ECM. Culturing these hydrogels longer may eventually result in a more complete LCN development and less (or even no) regions with 0% dendritic cells. If attained, this may also produce a more homogenous response to PGE_2 than we observed in Chapter 3.

This dissertation used IDG-SW3 and OCY454 cells which are newer (developed in the last 6-8 years) osteocyte cell lines that express mature osteocyte markers (*e.g., Sost*) after extended culture. However, in 2019, an even newer cell line was developed: OMGFP66. These cells display a highly dendritic morphology that resembles the LCN in 2D.[44] Incorporating these cells into the PEG hydrogel may yield even more dendritic formations than I achieved with the OCY454 cells. Additionally, primary osteocytes may develop a more mature phenotype (differentiation markers and dendrite extension) earlier than the OCY454 cells did in this dissertation. Further, if a Sost-cre mouse is developed, then primary osteocytes (or a cell line derived from the mouse) could develop a mature osteocyte phenotype earlier than the OCY454 cells.

In Chapter 5 of this dissertation, I focused on developing a bilayer design that achieves relevant biological and mechanical cues only in the subchondral bone. Now, the system can be broadened. For example, incorporating chondrocytes into the top layer would enable investigation into chondrocyte-osteocyte crosstalk during osteoarthritis. Alternatively, this design could be used to investigate the osteocyte response to any biological treatment when the osteocytes are cultured in a 3D environment with physiologically relevant mechanical loading. Static cultures do not properly mimic the *in vivo* mechanical environment where osteocytes are subjected to different mechanical cues. Thus, this system could be used to treat osteocytes with hormones, drugs, or inflammatory mediators in a physiologically relevant environment with mechanical loading. The bilayer scaffold developed in this dissertation uses a pillar design for the stiff scaffold to reinforce the bone layer. This design leads to heterogeneity in mechanical loading – some regions likely are subjected to low fluid flow whereas some (underneath a hole in the lattice) likely are subjected to higher fluid flow. Using a more homogenous design may lead to more uniform fluid flow. One idea is to mimic the trabecular structure of bone.

Overall, this dissertation focused on developing a 3D culture system for osteocytes, but *in vivo* osteocytes communicate with other cell types such as osteoblasts. To study osteocyte-osteoblast signaling, a bilayer hydrogel could be made by encapsulating osteocytes in one layer and osteoblasts in another layer. A treatment (such as PGE_2) could be applied, and the osteocyte and osteoblast communication could be assessed. For example, when treating with PGE_2, does osteocyte production of sclerostin increase, and do the osteoblasts in turn increase collagen production and mineralization? If certain ligand receptors (*e.g.,* EP2 or EP4) or intracellular signaling mechanisms (*e.g.,* GSK-3β) are inhibited, how does the osteocyte and osteoblast response change? Alternatively, osteocytes in the 3D hydrogel could be subjected to mechanical loading or PGE_2, and the media could be collected and then applied to osteoblast cultures. This would investigate the osteocyte-produced anabolic effect on osteoblasts in response to loading or PGE_2 in a more tightly controlled experiment.

Finally, if a Sost-transgenic mouse is developed, then further double transgenic mice could be used to study osteocyte mechanobiology *in vivo.* For example, a double Sost-transgenic, EP2-knockout mouse could investigate the impact of EP2 activation in only osteocytes on bone formation or resorption. Current methods do not isolate knockout models to osteocytes alone due to the lack of a Sost-transgenic mouse.

6.4 References

1. Robling, A. G. & Bonewald, L. F. The Osteocyte: New Insights. *Annual Review of Physiology* **82**, 485–506 (2020).

2. Maurel, D. B. *et al.* Characterization of a novel murine Sost ER T2 Cre model targeting osteocytes. *Bone Research* **7**, 1–13 (2019).

3. Sawa, N., Fujimoto, H., Sawa, Y., Yamashita, J. Alternating Differentiation and Dedifferentiation between Mature Osteoblasts and Osteocytes. *Scientific Reports (Nature Publisher Group); London* **9**, 1–9 (2019).

4. Woo, S. M., Rosser, J., Dusevich, V., Kalajzic, I. & Bonewald, L. F. Cell line IDG-SW3 replicates osteoblast-to-late-osteocyte differentiation in vitro and accelerates bone formation in vivo. *J Bone Miner Res* **26**, 2634–2646 (2011).

5. Kamel, M. A., Picconi, J. L., Lara-Castillo, N. & Johnson, M. L. Activation of B-catenin signaling in MLO-Y4 osteocytic cells versus 2T3 osteoblastic cells by fluid flow shear stress and PGE2: Implications for the study of mechanosensation in bone. *Bone* **47**, 872–881 (2010).

6. Suzuki, H. *et al.* The role of autonomously secreted PGE2 and its autocrine/paracrine effect on bone matrix mineralization at the different stages of differentiating MC3T3-E1 cells. *Biochemical and Biophysical Research Communications* **524**, 929–935 (2020).

7. Liu, X.-H., Kirschenbaum, A., Yao, S. & Levine, A. C. Interactive Effect of Interleukin-6 and Prostaglandin E2 on Osteoclastogenesis via the OPG/RANKL/RANK System. *Annals of the New York Academy of Sciences* **1068**, 225–233 (2006).

8. Galea, G. L. *et al.* Sost down-regulation by mechanical strain in human osteoblastic cells involves PGE2 signaling via EP4. *FEBS Letters* **585**, 2450–2454 (2011).

9. Genetos, D. C., Yellowley, C. E. & Loots, G. G. Prostaglandin E2 Signals Through PTGER2 to Regulate Sclerostin Expression. *PLoS ONE* **6**, e17772 (2011).

10. Kumei, Y. *et al. Microgravity induces prostaglandin E2 and interleukin-6 production in normal rat osteoblasts: role in bone demineralization*. (Elsevier, 1996).

11. Lee, C. M., Genetos, D. C., You, Z. & Yellowley, C. E. Hypoxia regulates PGE2 release and EP1 receptor expression in osteoblastic cells. *Journal of Cellular Physiology* **212**, 182–188 (2007).

12. Liu, X.-H. *et al.* Prostaglandin E2 modulates components of the Wnt signaling system in bone and prostate cancer cells. *Biochemical and Biophysical Research Communications* **394**, 715–720 (2010).

13. McGarry, J. G., Klein-Nulend, J. & Prendergast, P. J. The effect of cytoskeletal disruption on pulsatile fluid flow-induced nitric oxide and prostaglandin E2 release in osteocytes and osteoblasts. *Biochemical and Biophysical Research Communications* **330**, 341–348 (2005).

14. Bakker, A. D., Soejima, K., Klein-Nulend, J. & Burger, E. H. The production of nitric oxide and prostaglandin E2 by primary bone cells is shear stress dependent. *Journal of Biomechanics* **34**, 671–677 (2001).

15. Smalt, R., Mitchell, F. T., Howard, R. L. & Chambers, T. J. Induction of NO and prostaglandin E2 in osteoblasts by wall-shear stress but not mechanical strain. *American Journal of Physiology-Endocrinology And Metabolism* **273**, E751–E758 (1997).

16. Cheng, B. *et al.* PGE2 is essential for gap junction-mediated intercellular communication between osteocyte-like MLO-Y4 cells in response to mechanical strain. *Endocrinology* **142**, 3464–3473 (2001).

17. Cherian, P. P. *et al.* Mechanical strain opens connexin 43 hemichannels in osteocytes: a novel mechanism for the release of prostaglandin. *Molecular biology of the cell* **16**, 3100–3106 (2005).

18. Kitase, Y. *et al.* Mechanical induction of PGE2 in osteocytes blocks glucocorticoid-induced apoptosis through both the β-catenin and PKA pathways. *Journal of Bone and Mineral Research* **25**, 2657–2668 (2010).

19. Zhang, J.-N. *et al.* The role of the sphingosine-1-phosphate signaling pathway in osteocyte mechanotransduction. *Bone* **79**, 71–78 (2015).

20. Jee, W. S. S. & Ma, Y. F. The in vivo anabolic actions of prostaglandins in bone. *Bone* **21**, 297–304 (1997).

21. Ke, H. Z. *et al.* Prostaglandin E2 increases bone strength in intact rats and in ovariectomized rats with established osteopenia. *Bone* **23**, 249–255 (1998).

22. Cherian, P. P. *et al.* Effects of Mechanical Strain on the Function of Gap Junctions in Osteocytes Are Mediated through the Prostaglandin EP2 Receptor. *Journal of Biological Chemistry* **278**, 43146–43156 (2003).

23. Vazquez, M. *et al.* A New Method to Investigate How Mechanical Loading of Osteocytes Controls Osteoblasts. *Front Endocrinol (Lausanne)* **5**, (2014).

24. Sun, Q. *et al.* Ex vivo replication of phenotypic functions of osteocytes through biomimetic 3D bone tissue construction. *Bone* **106**, 148–155 (2018).

25. Takemura, Y. *et al.* Mechanical loading induced osteocyte apoptosis and connexin 43 expression in three-dimensional cell culture and dental implant model. *Journal of Biomedical Materials Research Part A* **107**, 815–827 (2019).

26. Choudhary, S. *et al.* Hypoxic Three-Dimensional Cellular Network Construction Replicates Ex Vivo the Phenotype of Primary Human Osteocytes. *Tissue Engineering Part A* **24**, 458–468 (2018).

27. Kurata, K., Heino, T. J., Higaki, H. & Väänänen, H. K. Bone Marrow Cell Differentiation Induced by Mechanically Damaged Osteocytes in 3D Gel-Embedded Culture. *Journal of Bone and Mineral Research* **21**, 616–625 (2006).

28. Spatz, J. M. *et al.* The Wnt Inhibitor Sclerostin Is Up-regulated by Mechanical Unloading in Osteocytes in Vitro. *Journal of Biological Chemistry* **290**, 16744–16758 (2015).

29. Mc Garrigle, M., Haugh, M., Voisin, M. & McNamara, L. Osteocyte differentiation and the formation of an interconnected cellular network in vitro. *European Cells and Materials* **31**, 323–340 (2016).

30. Fritton, S. P., McLeod, K. J. & Rubin, C. T. Quantifying the strain history of bone: spatial uniformity and self-similarity of low-magnitude strains. *Journal of biomechanics* **33**, 317–325 (2000).

31. Schaffler, M. B., Cheung, W.-Y., Majeska, R. & Kennedy, O. Osteocytes: Master Orchestrators of Bone. *Calcified Tissue International* **94**, 5–24 (2014).

32. You, J. *et al.* Substrate deformation levels associated with routine physical activity are less stimulatory to bone cells relative to loading-induced oscillatory fluid flow. *J. Biomech. Eng.* **122**, 387–393 (2000).

33. Kim, Y.-J., Bonassar, L. J. & Grodzinsky, A. J. The role of cartilage streaming potential, fluid flow and pressure in the stimulation of chondrocyte biosynthesis during dynamic compression. *Journal of Biomechanics* **28**, 1055–1066 (1995).

34. Chan, E. P., Deeyaa, B., Johnson, P. M. & Stafford, C. M. Poroelastic relaxation of polymer-loaded hydrogels. *Soft Matter* **8**, 8234 (2012).

35. Rakovsky, A., Marbach, D., Lotan, N. & Lanir, Y. Poly(ethylene glycol)-based hydrogels as cartilage substitutes: Synthesis and mechanical characteristics. *J. Appl. Polym. Sci.* **112**, 390–401 (2009).

36. Bush, B. G., Shapiro, J. M., DelRio, F. W., Cook, R. F. & Oyen, M. L. Mechanical measurements of heterogeneity and length scale effects in PEG-based hydrogels. *Soft Matter* **11**, 7191–7200 (2015).

37. Aziz, A. H., Eckstein, K., Ferguson, V. L. & Bryant, S. J. The effects of dynamic compressive loading on human mesenchymal stem cell osteogenesis in the stiff layer of a bilayer hydrogel. *Journal of Tissue Engineering and Regenerative Medicine* **13**, 946–959 (2019).

38. Stender, M. E., Regueiro, R. A. & Ferguson, V. L. A poroelastic finite element model of the bone–cartilage unit to determine the effects of changes in permeability with osteoarthritis. *Computer Methods in Biomechanics and Biomedical Engineering* 1–13 (2016) doi:10.1080/10255842.2016.1233326.

39. Goulet, G. C., Cooper, D. M. L., Coombe, D. & Zernicke, R. F. Influence of cortical canal architecture on lacunocanalicular pore pressure and fluid flow. *Computer Methods in Biomechanics and Biomedical Engineering* **11**, 379–387 (2008).

40. Carles-Carner, M., Saleh, L. S. & Bryant, S. J. The effects of hydroxyapatite nanoparticles embedded in a MMP-sensitive photoclickable PEG hydrogel on encapsulated MC3T3-E1 pre-osteoblasts. *Biomed. Mater.* **13**, 045009 (2018).

41. Wang, B. *et al.* Perlecan-Containing Pericellular Matrix Regulates Solute Transport and Mechanosensing Within the Osteocyte Lacunar-Canalicular System. *Journal of Bone and Mineral Research* **29**, 878–891 (2014).

42. Huebsch, N. *et al.* Harnessing traction-mediated manipulation of the cell/matrix interface to control stem-cell fate. *Nature Materials* **9**, 518–526 (2010).

43. Tiede-Lewis, L. M. & Dallas, S. L. Changes in the osteocyte lacunocanalicular network with aging. *Bone* **122**, 101–113 (2019).

44. Wang, K. *et al.* A Novel Osteogenic Cell Line That Differentiates Into GFP-Tagged Osteocytes and Forms Mineral With a Bone-Like Lacunocanalicular Structure. *Journal of Bone and Mineral Research* **34**, 979–995 (2019).

7. Bibliography

7.1 Chapter 1 References

1. Fuchs, R. K., Thompson, W. R. & Warden, S. J. Bone biology. in *Bone Repair Biomaterials* 15–52 (Elsevier, 2019). doi:10.1016/B978-0-08-102451-5.00002-0.

2. Burr, D. B. & Akkus, O. Bone Morphology and Organization. in *Basic and Applied Bone Biology* 3–25 (Elsevier, 2014). doi:10.1016/B978-0-12-416015-6.00001-0.

3. Boskey, A. L. & Robey, P. G. The Regulatory Role of Matrix Proteins in Mineralization of Bone. in *Osteoporosis* 235–255 (Elsevier, 2013). doi:10.1016/B978-0-12-415853-5.00011-X.

4. Qing, H. & Bonewald, L. F. Osteocyte remodeling of the perilacunar and pericanalicular matrix. *International journal of oral science* **1**, 59 (2009).

5. Yee, C. S., Schurman, C. A., White, C. R. & Alliston, T. Investigating Osteocytic Perilacunar/Canalicular Remodeling. *Curr Osteoporos Rep* **17**, 157–168 (2019).

6. Qing, H. *et al.* Demonstration of osteocytic perilacunar/canalicular remodeling in mice during lactation. *J Bone Miner Res* **27**, 1018–1029 (2012).

7. Burr, D. B. The importance of subchondral bone in osteoarthrosis: *Current Opinion in Rheumatology* **10**, 256–262 (1998).

8. Goldring, S. R. & Goldring, M. B. Changes in the osteochondral unit during osteoarthritis: structure, function and cartilage–bone crosstalk. *Nature Reviews Rheumatology* (2016) doi:10.1038/nrrheum.2016.148.

9. Findlay, D. M. & Kuliwaba, J. S. Bone–cartilage crosstalk: a conversation for understanding osteoarthritis. *Bone Research* **4**, 16028 (2016).

10. Funck-Brentano, T. & Cohen-Solal, M. Crosstalk between cartilage and bone: When bone cytokines matter. *Cytokine & Growth Factor Reviews* **22**, 91–97 (2011).

11. Hwang, J. *et al.* Increased hydraulic conductance of human articular cartilage and subchondral bone plate with progression of osteoarthritis. *Arthritis & Rheumatism* **58**, 3831–3842 (2008).

12. Stender, M. E., Regueiro, R. A. & Ferguson, V. L. A poroelastic finite element model of the bone–cartilage unit to determine the effects of changes in permeability with osteoarthritis. *Computer Methods in Biomechanics and Biomedical Engineering* 1–13 (2016) doi:10.1080/10255842.2016.1233326.

13. Stender, M. E., Carpenter, R. D., Regueiro, R. A. & Ferguson, V. L. An evolutionary model of osteoarthritis including articular cartilage damage, and bone remodeling in a computational study. *Journal of Biomechanics* (2016) doi:10.1016/j.jbiomech.2016.09.024.

14. Fritton, S. P. & Weinbaum, S. Fluid and Solute Transport in Bone: Flow-Induced Mechanotransduction. *Annual Review of Fluid Mechanics* **41**, 347–374 (2009).

15. Hemmatian, H., Bakker, A. D., Klein-Nulend, J. & van Lenthe, G. H. Aging, Osteocytes, and Mechanotransduction. *Curr Osteoporos Rep* **15**, 401–411 (2017).

16. Mazur, C. M. *et al.* Osteocyte dysfunction promotes osteoarthritis through MMP13-dependent suppression of subchondral bone homeostasis. *Bone Res* **7**, 34 (2019).

17. Beck, K. & Brodsky, B. Supercoiled Protein Motifs: The Collagen Triple-Helix and the alpha-Helical Coiled Coil. 13.

18. Marini, J. C. *et al.* Consortium for osteogenesis imperfecta mutations in the helical domain of type I collagen: regions rich in lethal mutations align with collagen binding sites for integrins and proteoglycans. *Human Mutation* **28**, 209–221 (2007).

19. Blank, R. D. & Boskey, A. L. Genetic Collagen Diseases: Influence of Collagen Mutationson Structure and Mechanical Behavior. in *Collagen: Structure and Mechanics* (ed. Fratzl, P.) 447–474 (Springer US, 2008). doi:10.1007/978-0-387-73906-9_16.

20. Traub, W., Arad, T., Vetter, U. & Weiner, S. Ultrastructural studies of bones from patients with osteogenesis imperfecta. *Matrix Biology* **14**, 337–345 (1994).

21. Vetter, U., Eanes, E. D., Kopp, J. B., Termine, J. D. & Robey, P. G. Changes in apatite crystal size in bones of patients with osteogenesis imperfecta. *Calcif Tissue Int* **49**, 248–250 (1991).

22. Boskey, A. L. Amorphous Calcium Phosphate: The Contention of Bone. *J Dent Res* **76**, 1433–1436 (1997).

23. Combes, C. & Rey, C. Amorphous calcium phosphates: Synthesis, properties and uses in biomaterials. *Acta Biomaterialia* **6**, 3362–3378 (2010).

24. Dey, A. *et al.* The role of prenucleation clusters in surface-induced calcium phosphate crystallization. *Nature Materials* **9**, 1010–1014 (2010).

25. Mahamid, J. *et al.* Mapping amorphous calcium phosphate transformation into crystalline mineral from the cell to the bone in zebrafish fin rays. *Proceedings of the National Academy of Sciences* **107**, 6316–6321 (2010).

26. Nollet, M. *et al.* Autophagy in osteoblasts is involved in mineralization and bone homeostasis. *Autophagy* **10**, 1965–1977 (2014).

27. Anderson, H. C. Matrix vesicles and calcification. *Curr Rheumatol Rep* **5**, 222–226 (2003).

28. Zhang, W., Huang, Z.-L., Liao, S.-S. & Cui, F.-Z. Nucleation sites of calcium phosphate crystals during collagen mineralization. *Journal of the American Ceramic Society* **86**, 1052–1054 (2003).

29. Magne, D., Weiss, P., Bouler, J.-M., Laboux, O. & Daculsi, G. Study of the Maturation of the Organic (Type I Collagen) and Mineral (Nonstoichiometric Apatite) Constituents of a Calcified Tissue (Dentin) as a Function of Location: A Fourier Transform Infrared Microspectroscopic Investigation. *Journal of Bone and Mineral Research* **16**, 750–757 (2001).

30. Jiao, K. *et al.* Complementarity and Uncertainty in Intrafibrillar Mineralization of Collagen. *Advanced Functional Materials* **26**, 6858–6875 (2016).

31. Niu, L.-N. *et al.* Collagen intrafibrillar mineralization as a result of the balance between osmotic equilibrium and electroneutrality. *Nat Mater* **16**, 370–378 (2017).

32. Bellido, T., Plotkin, L. I. & Bruzzaniti, A. Bone Cells. in *Basic and Applied Bone Biology* 27–45 (Elsevier, 2014). doi:10.1016/B978-0-12-416015-6.00002-2.

33. Franz-Odendaal, T. A., Hall, B. K. & Witten, P. E. Buried alive: How osteoblasts become osteocytes. *Developmental Dynamics* **235**, 176–190 (2006).

34. Palumbo, C., Palazzini, S., Zaffe, D. & Marotti, G. Osteocyte Differentiation in the Tibia of Newborn Rabbit: An Ultrastructural Study of the Formation of Cytoplasmic Processes. *Acta Anatomica* **137**, 350–358 (1990).

35. Dallas, S. L. & Bonewald, L. F. Dynamics of the transition from osteoblast to osteocyte. *Ann. N. Y. Acad. Sci.* **1192**, 437–443 (2010).

36. Noble, B. S. The osteocyte lineage. *Archives of Biochemistry and Biophysics* **473**, 106–111 (2008).

37. Bonewald, L. F. Osteocyte Biology. in *Osteoporosis* 209–234 (Elsevier, 2013). doi:10.1016/B978-0-12-415853-5.00010-8.

38. Bonewald, L. F. The amazing osteocyte. *Journal of Bone and Mineral Research* **26**, 229–238 (2011).

39. You, L.-D., Weinbaum, S., Cowin, S. C. & Schaffler, M. B. Ultrastructure of the osteocyte process and its pericellular matrix. *Anat. Rec.* **278A**, 505–513 (2004).

40. Ribeiro-Rodrigues, T. M., Martins-Marques, T., Morel, S., Kwak, B. R. & Girão, H. Role of connexin 43 in different forms of intercellular communication – gap junctions, extracellular vesicles and tunnelling nanotubes. *J Cell Sci* **130**, 3619–3630 (2017).

41. Price, C., Zhou, X., Li, W. & Wang, L. Real-Time Measurement of Solute Transport Within the Lacunar-Canalicular System of Mechanically Loaded Bone: Direct Evidence for Load-Induced Fluid Flow. *J Bone Miner Res* **26**, 277–285 (2011).

42. Dallas, S. L. & Moore, D. S. Using confocal imaging approaches to understand the structure and function of osteocytes and the lacunocanalicular network. *Bone* **138**, 115463 (2020).

43. Qin, L., Liu, W., Cao, H. & Xiao, G. Molecular mechanosensors in osteocytes. *Bone Res* **8**, 23 (2020).

44. Burra, S., Nicolella, D. P. & Jiang, J. X. Dark horse in osteocyte biology. *Commun Integr Biol* **4**, 48–50 (2011).

45. Wang, B. *et al.* Perlecan-Containing Pericellular Matrix Regulates Solute Transport and Mechanosensing Within the Osteocyte Lacunar-Canalicular System. *Journal of Bone and Mineral Research* **29**, 878–891 (2014).

46. McNamara, L. M., Majeska, R. J., Weinbaum, S., Friedrich, V. & Schaffler, M. B. Attachment of Osteocyte Cell Processes to the Bone Matrix. *The Anatomical Record* **292**, 355–363 (2009).

47. Geoghegan, I. P., Hoey, D. A. & McNamara, L. M. Integrins in Osteocyte Biology and Mechanotransduction. *Curr Osteoporos Rep* **17**, 195–206 (2019).

48. Wijeratne, S. S. *et al.* Single molecule force measurements of perlecan/HSPG2: A key component of the osteocyte pericellular matrix. *Matrix Biology* **50**, 27–38 (2016).

49. Thompson, W. R. *et al.* Perlecan/Hspg2 deficiency alters the pericellular space of the lacunocanalicular system surrounding osteocytic processes in cortical bone. *J Bone Miner Res* **26**, 618–629 (2011).

50. Cabahug-Zuckerman, P. *et al.* Potential role for a specialized β3 integrin-based structure on osteocyte processes in bone mechanosensation. *J Orthop Res* **36**, 642–652 (2018).

51. Buo, A. M. & Stains, J. P. Gap junctional regulation of signal transduction in bone cells. *FEBS Letters* **588**, 1315–1321 (2014).

52. Gupta, A. *et al.* Communication of cAMP by connexin43 gap junctions regulates osteoblast signaling and gene expression. *Cellular Signalling* **28**, 1048–1057 (2016).

53. Schaffler, M. B., Cheung, W.-Y., Majeska, R. & Kennedy, O. Osteocytes: Master Orchestrators of Bone. *Calcified Tissue International* **94**, 5–24 (2014).

54. Rath Bonivtch, A., Bonewald, L. F. & Nicolella, D. P. Tissue strain amplification at the osteocyte lacuna: A microstructural finite element analysis. *Journal of Biomechanics* **40**, 2199–2206 (2007).

55. Smalt, R., Mitchell, F. T., Howard, R. L. & Chambers, T. J. Induction of NO and prostaglandin E2 in osteoblasts by wall-shear stress but not mechanical strain. *American Journal of Physiology-Endocrinology And Metabolism* **273**, E751–E758 (1997).

56. Yu, K. *et al.* Mechanical loading disrupts osteocyte plasma membranes which initiates mechanosensation events in bone. *J Orthop Res* **36**, 653–662 (2018).

57. Malone, A. M. D. *et al.* Primary cilia mediate mechanosensing in bone cells by a calcium-independent mechanism. *Proc Natl Acad Sci U S A* **104**, 13325–13330 (2007).

58. Litzenberger, J. B., Tang, W. J., Castillo, A. B. & Jacobs, C. R. Deletion of β1 Integrins from Cortical Osteocytes Reduces Load-Induced Bone Formation. *Cel. Mol. Bioeng.* **2**, 416–424 (2009).

59. Haugh, M. G., Vaughan, T. J. & McNamara, L. M. The role of integrin α(V)β(3) in osteocyte mechanotransduction. *J Mech Behav Biomed Mater* **42**, 67–75 (2015).

60. Thi, M. M., Suadicani, S. O., Schaffler, M. B., Weinbaum, S. & Spray, D. C. Mechanosensory responses of osteocytes to physiological forces occur along processes and not cell body and require αVβ3 integrin. *PNAS* **110**, 21012–21017 (2013).

61. Wu, D., Ganatos, P., Spray, D. C. & Weinbaum, S. On the electrophysiological response of bone cells using a Stokesian fluid stimulus probe for delivery of quantifiable localized picoNewton level forces. *J Biomech* **44**, 1702–1708 (2011).

62. Wu, D., Schaffler, M. B., Weinbaum, S. & Spray, D. C. Matrix-dependent adhesion mediates network responses to physiological stimulation of the osteocyte cell process. *PNAS* **110**, 12096–12101 (2013).

63. Burra, S. *et al.* Dendritic processes of osteocytes are mechanotransducers that induce the opening of hemichannels. *PNAS* **107**, 13648–13653 (2010).

64. Robling, A. G., Fuchs, R. K. & Burr, D. B. Mechanical Adaptation. in *Basic and Applied Bone Biology* 175–204 (Elsevier, 2014). doi:10.1016/B978-0-12-416015-6.00009-5.

65. Kamel, M. A., Picconi, J. L., Lara-Castillo, N. & Johnson, M. L. Activation of B-catenin signaling in MLO-Y4 osteocytic cells versus 2T3 osteoblastic cells by fluid flow shear stress and PGE2: Implications for the study of mechanosensation in bone. *Bone* **47**, 872–881 (2010).

66. Cheng, B. *et al.* PGE2 is essential for gap junction-mediated intercellular communication between osteocyte-like MLO-Y4 cells in response to mechanical strain. *Endocrinology* **142**, 3464–3473 (2001).

67. Galea, G. L. *et al.* Sost down-regulation by mechanical strain in human osteoblastic cells involves PGE2 signaling via EP4. *FEBS Letters* **585**, 2450–2454 (2011).

68. Sugimoto, Y. & Narumiya, S. Prostaglandin E Receptors. *Journal of Biological Chemistry* **282**, 11613–11617 (2007).

69. Cherian, P. P. *et al.* Effects of Mechanical Strain on the Function of Gap Junctions in Osteocytes Are Mediated through the Prostaglandin EP2 Receptor. *Journal of Biological Chemistry* **278**, 43146–43156 (2003).

70. Cherian, P. P. *et al.* Mechanical Strain Opens Connexin 43 Hemichannels in Osteocytes: A Novel Mechanism for the Release of Prostaglandin. *MBoC* **16**, 3100–3106 (2005).

71. Westbroek, I. *et al.* Differential Stimulation of Prostaglandin G/H Synthase-2 in Osteocytes and Other Osteogenic Cells by Pulsating Fluid Flow. *Biochemical and Biophysical Research Communications* **268**, 414–419 (2000).

72. Klein-Nulend, J. *et al.* Sensitivity of osteocytes to biomechanical stress in vitro. *The FASEB Journal* **9**, 441–445 (1995).

73. Genetos, D. C., Yellowley, C. E. & Loots, G. G. Prostaglandin E2 Signals Through PTGER2 to Regulate Sclerostin Expression. *PLoS ONE* **6**, e17772 (2011).

74. Liu, X.-H., Kirschenbaum, A., Yao, S. & Levine, A. C. Interactive Effect of Interleukin-6 and Prostaglandin E2 on Osteoclastogenesis via the OPG/RANKL/RANK System. *Annals of the New York Academy of Sciences* **1068**, 225–233 (2006).

75. Kumei, Y. *et al. Microgravity induces prostaglandin E2 and interleukin-6 production in normal rat osteoblasts: role in bone demineralization*. (Elsevier, 1996).

76. Wu, Q., Zhou, X., Huang, D., Ji, Y. & Kang, F. IL-6 Enhances Osteocyte-Mediated Osteoclastogenesis by Promoting JAK2 and RANKL Activity ***In Vitro***. *Cellular Physiology and Biochemistry* **41**, 1360–1369 (2017).

77. Zhou, M., Li, S. & Pathak, J. L. Pro-inflammatory Cytokines and Osteocytes. *Curr Osteoporos Rep* **17**, 97–104 (2019).

78. Cao, J., Venton, L., Sakata, T. & Halloran, B. P. Expression of RANKL and OPG correlates with age-related bone loss in male C57BL/6 mice. *J. Bone Miner. Res.* **18**, 270–277 (2003).

79. Cabahug-Zuckerman, P. *et al.* Osteocyte Apoptosis Caused by Hindlimb Unloading is Required to Trigger Osteocyte RANKL Production and Subsequent Resorption of Cortical and Trabecular Bone in Mice Femurs. *Journal of Bone and Mineral Research* **31**, 1356–1365 (2016).

80. Nakashima, T. *et al.* Evidence for osteocyte regulation of bone homeostasis through RANKL expression. *Nature Medicine* **17**, 1231–1234 (2011).

81. Xiong, J. *et al.* Osteocytes, not Osteoblasts or Lining Cells, are the Main Source of the RANKL Required for Osteoclast Formation in Remodeling Bone. *PLoS One* **10**, (2015).

82. Xiong, J. & O'Brien, C. A. Osteocyte RANKL: New insights into the control of bone remodeling. *J Bone Miner Res* **27**, 499–505 (2012).

83. Ducy, P., Desbois, C., Boyce, B. & Pinero, G. Increased bone formation in osteocalcin-deficient mice. *Nature (London)* **382**, 448–452 (1996).

84. Zoch, M. L., Clemens, T. L. & Riddle, R. C. New insights into the biology of osteocalcin. *Bone* **82**, 42–49 (2016).

85. Winkler, D. G. *et al.* Osteocyte control of bone formation via sclerostin,a novel BMP antagonist. *EMBO J* **22**, 6267–6276 (2003).

86. Wijenayaka, A. R. *et al.* Sclerostin Stimulates Osteocyte Support of Osteoclast Activity by a RANKL-Dependent Pathway. *PLoS One* **6**, (2011).

87. Jee, W. S. S. & Ma, Y. F. The in vivo anabolic actions of prostaglandins in bone. *Bone* **21**, 297–304 (1997).

88. Ke, H. Z. *et al.* Prostaglandin E2 increases bone strength in intact rats and in ovariectomized rats with established osteopenia. *Bone* **23**, 249–255 (1998).

89. Suzuki, H. *et al.* The role of autonomously secreted PGE2 and its autocrine/paracrine effect on bone matrix mineralization at the different stages of differentiating MC3T3-E1 cells. *Biochemical and Biophysical Research Communications* **524**, 929–935 (2020).

90. Yoshida, K. *et al.* Stimulation of bone formation and prevention of bone loss by prostaglandin E EP4 receptor activation. *Proc Natl Acad Sci U S A* **99**, 4580–4585 (2002).

91. Paralkar, V. M. *et al.* An EP2 receptor-selective prostaglandin E2 agonist induces bone healing. *Proceedings of the National Academy of Sciences* **100**, 6736–6740 (2003).

92. Li, M. *et al.* A Novel, Non-Prostanoid EP2 Receptor-Selective Prostaglandin E2 Agonist Stimulates Local Bone Formation and Enhances Fracture Healing. *Journal of Bone and Mineral Research* **18**, 2033–2042 (2003).

93. Regan, J. W. EP2 and EP4 prostanoid receptor signaling. *Life Sciences* **74**, 143–153 (2003).

94. Castellone, M. D., Teramoto, H., Williams, B. O., Druey, K. M. & Gutkind, J. S. Prostaglandin E2 Promotes Colon Cancer Cell Growth Through a Gs-Axin-b-Catenin Signaling Axis. **310**, 8 (2005).

95. Kitase, Y. *et al.* Mechanical induction of PGE2 in osteocytes blocks glucocorticoid-induced apoptosis through both the β-catenin and PKA pathways. *Journal of Bone and Mineral Research* **25**, 2657–2668 (2010).

96. Fujino, H., Xu, W. & Regan, J. W. Prostaglandin E2 Induced Functional Expression of Early Growth Response Factor-1 by EP4, but Not EP2, Prostanoid Receptors via the Phosphatidylinositol 3-Kinase and Extracellular Signal-regulated Kinases. *Journal of Biological Chemistry* **278**, 12151–12156 (2003).

97. Nishigaki, N., Negishi, M. & Ichikawa, A. Two Gs-coupled prostaglandin E receptor subtypes, EP2 and EP4, differ in desensitization and sensitivity to the metabolic inactivation of the agonist. *Mol Pharmacol* **50**, 1031–1037 (1996).

98. Waclawik, A., Jabbour, H. N., Blitek, A. & Ziecik, A. J. Estradiol-17β, Prostaglandin E2 (PGE2), and the PGE2 Receptor Are Involved in PGE2 Positive Feedback Loop in the Porcine Endometrium. *Endocrinology* **150**, 3823–3832 (2009).

99. Maurel, D. B. *et al.* Characterization of a novel murine Sost ER T2 Cre model targeting osteocytes. *Bone Research* **7**, 1–13 (2019).

100. Rath Stern, A. *et al.* Isolation and culture of primary osteocytes from the long bones of skeletally mature and aged mice. *BioTechniques* **52**, (2012).

101. Torreggiani, E. *et al.* Preosteocytes/Osteocytes Have the Potential to Dedifferentiate Becoming a Source of Osteoblasts. *PLoS One* **8**, (2013).

102. Sawa, N., Fujimoto, H., Sawa, Y., Yamashita, J. & Link to external site, this link will open in a new window. Alternating Differentiation and Dedifferentiation between Mature Osteoblasts and Osteocytes. *Scientific Reports (Nature Publisher Group); London* **9**, 1–9 (2019).

103. Divieti Pajevic, P. New and Old Osteocytic Cell Lines and 3D Models. *Curr Osteoporos Rep* (2020) doi:10.1007/s11914-020-00613-3.

104. Kato, Y., Windle, J. J., Koop, B. A., Mundy, G. R. & Bonewald, L. F. Establishment of an Osteocyte-like Cell Line, MLO-Y4. *Journal of Bone and Mineral Research* **12**, 2014–2023 (1997).

105. Robling, A. G. & Bonewald, L. F. The Osteocyte: New Insights. *Annual Review of Physiology* **82**, 485–506 (2020).

106. Bodine, P. V., Vernon, S. K. & Komm, B. S. Establishment and hormonal regulation of a conditionally transformed preosteocytic cell line from adult human bone. *Endocrinology* **137**, 4592–4604 (1996).

107. Kato, Y. *et al.* Establishment of an osteoid preosteocyte-like cell MLO-A5 that spontaneously mineralizes in culture. *Journal of Bone and Mineral Research* **16**, 1622–1633 (2001).

108. Barragan-Adjemian, C. *et al.* Mechanism by which MLO-A5 Late Osteoblasts/Early Osteocytes Mineralize in Culture: Similarities with Mineralization of Lamellar Bone. *Calcif Tissue Int* **79**, 340–353 (2006).

109. Woo, S. M., Rosser, J., Dusevich, V., Kalajzic, I. & Bonewald, L. F. Cell line IDG-SW3 replicates osteoblast-to-late-osteocyte differentiation in vitro and accelerates bone formation in vivo. *J Bone Miner Res* **26**, 2634–2646 (2011).

110. Spatz, J. M. *et al.* The Wnt Inhibitor Sclerostin Is Up-regulated by Mechanical Unloading in Osteocytes in Vitro. *Journal of Biological Chemistry* **290**, 16744–16758 (2015).

111. Xu, L. H., Shao, H., Ma, Y.-H. V. & You, L. OCY454 Osteocytes as an in Vitro Cell Model for Bone Remodeling Under Mechanical Loading. *Journal of Orthopaedic Research* **0**,.

112. Wang, K. *et al.* A Novel Osteogenic Cell Line That Differentiates Into GFP-Tagged Osteocytes and Forms Mineral With a Bone-Like Lacunocanalicular Structure. *Journal of Bone and Mineral Research* **34**, 979–995 (2019).

113. Zhang, C., Bakker, A. D., Klein-Nulend, J. & Bravenboer, N. Studies on Osteocytes in Their 3D Native Matrix Versus 2D In Vitro Models. *Current Osteoporosis Reports* **17**, 207–216 (2019).

114. Vazquez, M. *et al.* A New Method to Investigate How Mechanical Loading of Osteocytes Controls Osteoblasts. *Front Endocrinol (Lausanne)* **5**, (2014).

115. Sun, Q. *et al.* Ex vivo replication of phenotypic functions of osteocytes through biomimetic 3D bone tissue construction. *Bone* **106**, 148–155 (2018).

116. Takemura, Y. *et al.* Mechanical loading induced osteocyte apoptosis and connexin 43 expression in three-dimensional cell culture and dental implant model. *Journal of Biomedical Materials Research Part A* **107**, 815–827 (2019).

117. Choudhary, S. *et al.* Hypoxic Three-Dimensional Cellular Network Construction Replicates Ex Vivo the Phenotype of Primary Human Osteocytes. *Tissue Engineering Part A* **24**, 458–468 (2018).

118. Kurata, K., Heino, T. J., Higaki, H. & Väänänen, H. K. Bone Marrow Cell Differentiation Induced by Mechanically Damaged Osteocytes in 3D Gel-Embedded Culture. *Journal of Bone and Mineral Research* **21**, 616–625 (2006).

119. Fritton, S. P., McLeod, K. J. & Rubin, C. T. Quantifying the strain history of bone: spatial uniformity and self-similarity of low-magnitude strains. *Journal of biomechanics* **33**, 317–325 (2000).

120. Brolese, E., Buser, D., Kuchler, U., Schaller, B. & Gruber, R. Human bone chips release of sclerostin and FGF-23 into the culture medium: an in vitro pilot study. *Clinical Oral Implants Research* **26**, 1211–1214 (2015).

121. Chan, M. E. *et al.* A Trabecular Bone Explant Model of Osteocyte–Osteoblast Co-Culture for Bone Mechanobiology. *Cel. Mol. Bioeng.* **2**, 405–415 (2009).

122. Takai, E., Mauck, R. L., Hung, C. T. & Guo, X. E. Osteocyte Viability and Regulation of Osteoblast Function in a 3D Trabecular Bone Explant Under Dynamic Hydrostatic Pressure. *Journal of Bone and Mineral Research* **19**, 1403–1410 (2004).

123. Bernhardt, A., Weiser, E., Wolf, S., Vater, C. & Gelinsky, M. Primary Human Osteocyte Networks in Pure and Modified Collagen Gels. *Tissue Engineering Part A* **25**, 1347–1355 (2019).

124. Mullen, C. A., Vaughan, T. J., Billiar, K. L. & McNamara, L. M. The Effect of Substrate Stiffness, Thickness, and Cross-Linking Density on Osteogenic Cell Behavior. *Biophysical Journal* **108**, 1604–1612 (2015).

125. Huebsch, N. *et al.* Harnessing traction-mediated manipulation of the cell/matrix interface to control stem-cell fate. *Nature Materials* **9**, 518–526 (2010).

126. Aisenbrey, E. A. & Bryant, S. J. The role of chondroitin sulfate in regulating hypertrophy during MSC chondrogenesis in a cartilage mimetic hydrogel under dynamic loading. *Biomaterials* **190–191**, 51–62 (2019).

127. Holmes, R. *et al.* Thiol-Ene Photo-Click Collagen-PEG Hydrogels: Impact of Water-Soluble Photoinitiators on Cell Viability, Gelation Kinetics and Rheological Properties. *Polymers* **9**, 226 (2017).

128. Boukhechba, F. *et al.* Human Primary Osteocyte Differentiation in a 3D Culture System. *Journal of Bone and Mineral Research* **24**, 1927–1935 (2009).

129. Carles-Carner, M., Saleh, L. S. & Bryant, S. J. The effects of hydroxyapatite nanoparticles embedded in a MMP-sensitive photoclickable PEG hydrogel on encapsulated MC3T3-E1 pre-osteoblasts. *Biomed. Mater.* **13**, 045009 (2018).

130. Fairbanks, B. D. *et al.* A Versatile Synthetic Extracellular Matrix Mimic via Thiol-Norbornene Photopolymerization. *Advanced Materials* **21**, 5005–5010 (2009).

131. Hoyle, C. E. & Bowman, C. N. Thiol-Ene Click Chemistry. *Angewandte Chemie International Edition* **49**, 1540–1573 (2010).

132. McKinnon, D. D., Kloxin, A. M. & Anseth, K. S. Synthetic hydrogel platform for three-dimensional culture of embryonic stem cell-derived motor neurons. *Biomaterials Science* **1**, 460 (2013).

133. Sridhar, B. V. *et al.* Development of a Cellularly Degradable PEG Hydrogel to Promote Articular Cartilage Extracellular Matrix Deposition. *Advanced Healthcare Materials* **4**, 702–713 (2015).

134. Amer, L. D. & Bryant, S. J. The In Vitro and In Vivo Response to MMP-Sensitive Poly(Ethylene Glycol) Hydrogels. *Annals of Biomedical Engineering* **44**, 1959–1969 (2016).

135. Schneider, M. C. *et al.* Local Heterogeneities Improve Matrix Connectivity in Degradable and Photoclickable Poly(ethylene glycol) Hydrogels for Applications in Tissue Engineering. *ACS Biomater. Sci. Eng.* **3**, 2480–2492 (2017).

136. Klein-Nulend, J., Bakker, A. D., Bacabac, R. G., Vatsa, A. & Weinbaum, S. Mechanosensation and transduction in osteocytes. *Bone* **54**, 182–190 (2013).

137. Spyropoulou, A., Karamesinis, K. & Basdra, E. K. Mechanotransduction pathways in bone pathobiology. *Biochimica et Biophysica Acta (BBA) - Molecular Basis of Disease* **1852**, 1700–1708 (2015).

138. Cisternas, M. G. *et al.* Alternative Methods for Defining Osteoarthritis and the Impact on Estimating Prevalence in a US Population-Based Survey. *Arthritis Care & Research* **68**, 574–580 (2016).

139. Mc Garrigle, M. J., Mullen, C. A., Haugh, M. G., Voisin, M. C. & McNamara, L. M. Osteocyte differentiation and the formation of an interconnected cellular network in vitro. *European Cells & Materials* **31**, 323–340 (2016).

140. Mullen, C. A., Haugh, M. G., Schaffler, M. B., Majeska, R. J. & McNamara, L. M. Osteocyte differentiation is regulated by extracellular matrix stiffness and intercellular separation. *Journal of the Mechanical Behavior of Biomedical Materials* **28**, 183–194 (2013).

141. Kim, K., Dean, D., Mikos, A. G. & Fisher, J. P. Effect of Initial Cell Seeding Density on Early Osteogenic Signal Expression of Rat Bone Marrow Stromal Cells Cultured on Cross-Linked Poly(propylene fumarate) Disks. *Biomacromolecules* **10**, 1810–1817 (2009).

142. Aziz, A. H. & Bryant, S. J. A comparison of human mesenchymal stem cell osteogenesis in poly(ethylene glycol) hydrogels as a function of MMP-sensitive crosslinker and crosslink density in chemically defined medium. *Biotechnology and Bioengineering* **116**, 1523–1536 (2019).

143. Kaur, K., Das, S. & Ghosh, S. Regulation of Human Osteoblast-to-Osteocyte Differentiation by Direct-Write 3D Microperiodic Hydroxyapatite Scaffolds. *ACS Omega* **4**, 1504–1515 (2019).

144. Liu, W. *et al.* TGF-β1 facilitates cell–cell communication in osteocytes via connexin43- and pannexin1-dependent gap junctions. *Cell Death Discov.* **5**, 141 (2019).

145. Lee, C. M., Genetos, D. C., You, Z. & Yellowley, C. E. Hypoxia regulates PGE2 release and EP1 receptor expression in osteoblastic cells. *Journal of Cellular Physiology* **212**, 182–188 (2007).

146. Liu, X.-H. *et al.* Prostaglandin E2 modulates components of the Wnt signaling system in bone and prostate cancer cells. *Biochemical and Biophysical Research Communications* **394**, 715–720 (2010).

147. McGarry, J. G., Klein-Nulend, J. & Prendergast, P. J. The effect of cytoskeletal disruption on pulsatile fluid flow-induced nitric oxide and prostaglandin E2 release in osteocytes and osteoblasts. *Biochemical and Biophysical Research Communications* **330**, 341–348 (2005).

148. Bakker, A. D., Soejima, K., Klein-Nulend, J. & Burger, E. H. The production of nitric oxide and prostaglandin E2 by primary bone cells is shear stress dependent. *Journal of Biomechanics* **34**, 671–677 (2001).

149. Cherian, P. P. *et al.* Mechanical strain opens connexin 43 hemichannels in osteocytes: a novel mechanism for the release of prostaglandin. *Molecular biology of the cell* **16**, 3100–3106 (2005).

150. Kitase, Y. *et al.* Mechanical induction of PGE2 in osteocytes blocks glucocorticoid-induced apoptosis through both the β-catenin and PKA pathways. *Journal of Bone and Mineral Research* **25**, 2657–2668 (2010).

151. Zhang, J.-N. *et al.* The role of the sphingosine-1-phosphate signaling pathway in osteocyte mechanotransduction. *Bone* **79**, 71–78 (2015).

152. Aziz, A. H., Wilmoth, R. L., Ferguson, V. L. & Bryant, S. J. IDG-SW3 Osteocyte Differentiation and Bone Extracellular Matrix Deposition Are Enhanced in a 3D Matrix Metalloproteinase-Sensitive Hydrogel. *ACS Appl. Bio Mater.* **3**, 1666–1680 (2020).

153. Aziz, A. H., Eckstein, K., Ferguson, V. L. & Bryant, S. J. The effects of dynamic compressive loading on human mesenchymal stem cell osteogenesis in the stiff layer of a bilayer hydrogel. *Journal of Tissue Engineering and Regenerative Medicine* **13**, 946–959 (2019).

154. Galperin, A. *et al.* Integrated Bi-Layered Scaffold for Osteochondral Tissue Engineering. *Advanced Healthcare Materials* **2**, 872–883 (2013).

155. Gan, D. *et al.* Mussel-Inspired Tough Hydrogel with In Situ Nanohydroxyapatite Mineralization for Osteochondral Defect Repair. *Advanced Healthcare Materials* **8**, 1901103 (2019).

156. Kim, B. J. *et al.* Restoration of articular osteochondral defects in rat by a bi-layered hyaluronic acid hydrogel plug with TUDCA-PLGA microsphere. *Journal of Industrial and Engineering Chemistry* **61**, 295–303 (2018).

157. Lin, D. *et al.* A viscoelastic PEGylated poly(glycerol sebacate)-based bilayer scaffold for cartilage regeneration in full-thickness osteochondral defect. *Biomaterials* **253**, 120095 (2020).

158. Liu, K., Liu, Y., Duan, Z., Ma, X. & Fan, D. A biomimetic bi-layered tissue engineering scaffolds for osteochondral defects repair. *Sci. China Technol. Sci.* (2020) doi:10.1007/s11431-020-1597-4.

159. Liu, X. *et al.* A Biomimetic Biphasic Osteochondral Scaffold with Layer-Specific Release of Stem Cell Differentiation Inducers for the Reconstruction of Osteochondral Defects. *Advanced Healthcare Materials* **n/a**, 2000076.

160. Steinmetz, N. J., Aisenbrey, E. A., Westbrook, K. K., Qi, H. J. & Bryant, S. J. Mechanical loading regulates human MSC differentiation in a multi-layer hydrogel for osteochondral tissue engineering. *Acta Biomaterialia* **21**, 142–153 (2015).

161. Zhu, X. *et al.* Biomimetic Bacterial Cellulose-Enhanced Double-Network Hydrogel with Excellent Mechanical Properties Applied for the Osteochondral Defect Repair. *ACS Biomater. Sci. Eng.* **4**, 3534–3544 (2018).

7.2 Chapter 2 References

1. Bellido, T. Osteocyte-Driven Bone Remodeling. *Calcified Tissue International* **94**, 25–34 (2014).
2. Bonewald, L. F. The Role of the Osteocyte in Bone and Nonbone Disease. *Endocrinol Metab Clin North Am* **46**, 1–18 (2017).
3. Burger, E. H. & Klein-Nulend, J. Mechanotransduction in bone - role of the lacuno-canalicular network. *Faseb Journal* **13**, S101–S112 (1999).
4. Bonewald, L. F. Osteocytes as dynamic multifunctional cells. *Annals of the New York Academy of Sciences* **1116**, 281–90 (2007).
5. Dallas, S. L. & Bonewald, L. F. Dynamics of the Transition from Osteoblast to Osteocyte. *Annals of the New York Academy of Sciences* **1192**, 437–443 (2010).
6. Bonewald, L. F. The amazing osteocyte. *Journal of Bone and Mineral Research* **26**, 229–238 (2011).
7. Palumbo, C., Palazzini, S. & Marotti, G. Morphological study of intercellular junctions during osteocyte differentiation. *Bone* **11**, 401–406 (1990).
8. Knothe Tate, M. L., Adamson, J. R., Tami, A. E. & Bauer, T. W. The osteocyte. *Int J Biochem Cell Biol* **36**, 1–8 (2004).
9. Fowler, T. W. *et al.* Glucocorticoid suppression of osteocyte perilacunar remodeling is associated with subchondral bone degeneration in osteonecrosis. *Scientific Reports* **7**, 44618 (2017).
10. Lara-Castillo, N. *et al.* In vivo mechanical loading rapidly activates β-catenin signaling in osteocytes through a prostaglandin mediated mechanism. *Bone* **76**, 58–66 (2015).
11. Robling, A. G. *et al.* Mechanical Stimulation of Bone in Vivo Reduces Osteocyte Expression of Sost/Sclerostin. *Journal of Biological Chemistry* **283**, 5866–5875 (2008).
12. Lewis, K. J. *et al.* Osteocyte calcium signals encode strain magnitude and loading frequency in vivo. *Proceedings of the National Academy of Sciences* **114**, 11775–11780 (2017).
13. Tanaka, T. *et al.* Analysis of Ca2+ response of osteocyte network by three-dimensional time-lapse imaging in living bone. *Journal of Bone and Mineral Metabolism; Tokyo* **36**, 519–528 (2018).
14. Kalajzic, I. *et al.* In vitro and in vivo approaches to study osteocyte biology. *Bone* **54**, 296–306 (2013).
15. Stern, A. R. *et al.* Isolation and culture of primary osteocytes from the long bones of skeletally mature and aged mice. *BioTechniques* **52**, 361–73 (2012).
16. Barragan-Adjemian, C. *et al.* Mechanism by which MLO-A5 Late Osteoblasts/Early Osteocytes Mineralize in Culture: Similarities with Mineralization of Lamellar Bone. *Calcif Tissue Int* **79**, 340–353 (2006).

17. Rath, A. L. *et al.* Correlation of cell strain in single osteocytes with intracellular calcium, but not intracellular nitric oxide, in response to fluid flow. *Journal of Biomechanics* **43**, 1560–1564 (2010).

18. Kato, Y., Windle, J. J., Koop, B. A., Mundy, G. R. & Bonewald, L. F. Establishment of an osteocyte-like cell line, MLO-Y4. *Journal of bone and mineral research : the official journal of the American Society for Bone and Mineral Research* **12**, 2014–23 (1997).

19. Paic, F. *et al.* Identification of differentially expressed genes between osteoblasts and osteocytes. *Bone* **45**, 682–692 (2009).

20. Woo, S. M., Rosser, J., Dusevich, V., Kalajzic, I. & Bonewald, L. F. Cell line IDG-SW3 replicates osteoblast-to-late-osteocyte differentiation in vitro and accelerates bone formation in vivo. *Journal of bone and mineral research : the official journal of the American Society for Bone and Mineral Research* **26**, 2634–46 (2011).

21. Lindberg, I. *et al.* FGF23 is endogenously phosphorylated in bone cells. *Journal of bone and mineral research : the official journal of the American Society for Bone and Mineral Research* **30**, 449–54 (2015).

22. Ito, N., Findlay, D. M., Anderson, P. H., Bonewald, L. F. & Atkins, G. J. Extracellular phosphate modulates the effect of 1α,25-dihydroxy vitamin D3 (1,25D) on osteocyte like cells. *The Journal of steroid biochemistry and molecular biology* **136**, 183–6 (2013).

23. Fujita, K., Xing, Q., Khosla, S. & Monroe, D. G. Mutual enhancement of differentiation of osteoblasts and osteocytes occurs through direct cell-cell contact. *Journal of cellular biochemistry* **115**, 2039–44 (2014).

24. St John, H. C. *et al.* The osteoblast to osteocyte transition: epigenetic changes and response to the vitamin D3 hormone. *Molecular endocrinology (Baltimore, Md.)* **28**, 1150–65 (2014).

25. Xu, H. *et al.* Impact of flow shear stress on morphology of osteoblast-like IDG-SW3 cells. *Journal of Bone and Mineral Metabolism* **36**, 529–536 (2018).

26. Baker, B. M. & Chen, C. S. Deconstructing the third dimension - how 3D culture microenvironments alter cellular cues. *Journal of Cell Science* **125**, 3015–3024 (2012).

27. Bao, M., Xie, J. & Huck, W. T. S. Recent Advances in Engineering the Stem Cell Microniche in 3D. *Advanced Science* **5**, 1800448 (2018).

28. Boukhechba, F. *et al.* Human Primary Osteocyte Differentiation in a 3D Culture System. *Journal of Bone and Mineral Research* **24**, 1927–1935 (2009).

29. Zujur, D. *et al.* Three-dimensional system enabling the maintenance and directed differentiation of pluripotent stem cells under defined conditions. *Science Advances* **3**, e1602875 (2017).

30. Mc Garrigle, M. J., Mullen, C. A., Haugh, M. G., Voisin, M. C. & McNamara, L. M. Osteocyte differentiation and the formation of an interconnected cellular network in vitro. *European Cells & Materials* **31**, 323–340 (2016).

31. Uchihashi, K., Aoki, S., Matsunobu, A. & Toda, S. Osteoblast migration into type I collagen gel and differentiation to osteocyte-like cells within a self-produced mineralized matrix: A novel system for analyzing differentiation from osteoblast to osteocyte. *Bone* **52**, 102–110 (2013).

32. Kurata, K., Heino, T. J., Higaki, H. & Väänänen, H. K. Bone Marrow Cell Differentiation Induced by Mechanically Damaged Osteocytes in 3D Gel-Embedded Culture. *Journal of Bone and Mineral Research* **21**, 616–625 (2006).

33. Sun, Q. *et al.* Ex vivo replication of phenotypic functions of osteocytes through biomimetic 3D bone tissue construction. *Bone* **106**, 148–155 (2018).

34. Lee, K. Y., Alsberg, E. & Mooney, D. J. Degradable and injectable poly(aldehyde guluronate) hydrogels for bone tissue engineering. *Journal of Biomedical Materials Research* **56**, 228–233 (2001).

35. Fairbanks, B. D. *et al.* A Versatile Synthetic Extracellular Matrix Mimic via Thiol-Norbornene Photopolymerization. *Advanced Materials* **21**, 5005–5010 (2009).

36. McKinnon, D. D., Kloxin, A. M. & Anseth, K. S. Synthetic hydrogel platform for three-dimensional culture of embryonic stem cell-derived motor neurons. *Biomaterials Science* **1**, 460 (2013).

37. Sridhar, B. V. *et al.* Development of a Cellularly Degradable PEG Hydrogel to Promote Articular Cartilage Extracellular Matrix Deposition. *Advanced Healthcare Materials* **4**, 702–713 (2015).

38. Amer, L. D. & Bryant, S. J. The In Vitro and In Vivo Response to MMP-Sensitive Poly(Ethylene Glycol) Hydrogels. *Annals of Biomedical Engineering* **44**, 1959–1969 (2016).

39. Silva Paiva, K. B. & Granjeiro, J. M. Bone tissue remodeling and development: Focus on matrix metalloproteinase functions. *Archives of Biochemistry and Biophysics* **561**, 74–87 (2014).

40. Mullen, C. A., Haugh, M. G., Schaffler, M. B., Majeska, R. J. & McNamara, L. M. Osteocyte differentiation is regulated by extracellular matrix stiffness and intercellular separation. *Journal of the Mechanical Behavior of Biomedical Materials* **28**, 183–194 (2013).

41. Kim, K., Dean, D., Mikos, A. G. & Fisher, J. P. Effect of Initial Cell Seeding Density on Early Osteogenic Signal Expression of Rat Bone Marrow Stromal Cells Cultured on Cross-Linked Poly(propylene fumarate) Disks. *Biomacromolecules* **10**, 1810–1817 (2009).

42. Deng, S. J. *et al.* Substrate specificity of human collagenase 3 assessed using a phage-displayed peptide library. *The Journal of biological chemistry* **275**, 31422–7 (2000).

43. Burr, D. B. & Akkus, O. Bone Morphology and Organization. in *Basic and Applied Bone Biology* 3–25 (Elsevier, 2014). doi:10.1016/B978-0-12-416015-6.00001-0.

44. Holmbeck, K. *et al.* MT1-MMP-deficient mice develop dwarfism, osteopenia, arthritis, and connective tissue disease due to inadequate collagen turnover. *Cell* **99**, 81–92 (1999).

45. Mosig, R. A. *et al.* Loss of MMP-2 disrupts skeletal and craniofacial development and results in decreased bone mineralization, joint erosion and defects in osteoblast and osteoclast growth. *Human Molecular Genetics* **16**, 1113–1123 (2007).

46. Vandooren, J., Van den Steen, P. E. & Opdenakker, G. Biochemistry and molecular biology of gelatinase B or matrix metalloproteinase-9 (MMP-9): The next decade. *Critical Reviews in Biochemistry and Molecular Biology* **48**, 222–272 (2013).

47. Vu, T. H. *et al.* MMP-9/Gelatinase B Is a Key Regulator of Growth Plate Angiogenesis and Apoptosis of Hypertrophic Chondrocytes. *Cell* **93**, 411–422 (1998).

48. Tang, S. Y., Herber, R.-P., Ho, S. P. & Alliston, T. Matrix metalloproteinase-13 is required for osteocytic perilacunar remodeling and maintains bone fracture resistance. *Journal of bone and mineral research : the official journal of the American Society for Bone and Mineral Research* **27**, 1936–50 (2012).

49. Robin, M. *et al.* Involvement of 3D osteoblast migration and bone apatite during in vitro early osteocytogenesis. *Bone* **88**, 146–156 (2016).

50. Prideaux, M. *et al.* MMP and TIMP temporal gene expression during osteocytogenesis. *Gene Expression Patterns* **18**, 29–36 (2015).

51. Kaur, K., Das, S. & Ghosh, S. Regulation of Human Osteoblast-to-Osteocyte Differentiation by Direct-Write 3D Microperiodic Hydroxyapatite Scaffolds. *ACS Omega* **4**, 1504–1515 (2019).

52. Golub, E. E. & Boesze-Battaglia, K. The role of alkaline phosphatase in mineralization. *Current opinion in Orthopaedics* **18**, 444–448 (2007).

53. Lu, Y. *et al.* The biological function of DMP-1 in osteocyte maturation is mediated by its. *J Bone Miner Res* **26**, 331–340 (2011).

54. Qin, C., D'Souza, R. & Feng, J. Q. Dentin Matrix Protein 1 (DMP1): New and Important Roles for Biomineralization and Phosphate Homeostasis. *J Dent Res* **86**, 1134–1141 (2007).

55. Rowe, P. S. N. The chicken or the egg: PHEX, FGF23 and SIBLINGs unscrambled. *Cell Biochemistry and Function* **30**, 355–375 (2012).

56. Langhorst, H. *et al.* The IgCAM CLMP regulates expression of Connexin43 and Connexin45 in intestinal and ureteral smooth muscle contraction in mice. *Disease Models & Mechanisms* **11**, dmm032128 (2018).

57. Balla, P. *et al.* Prognostic Impact of Reduced Connexin43 Expression and Gap Junction Coupling of Neoplastic Stromal Cells in Giant Cell Tumor of Bone. *PLOS ONE* **10**, e0125316 (2015).

58. Plotkin, L. I. Connexin 43 and Bone: Not Just a Gap Junction Protein. *Actual osteol* **7**, 79–90 (2011).

59. Zhang, W., Huang, Z.-L., Liao, S.-S. & Cui, F.-Z. Nucleation Sites of Calcium Phosphate Crystals during Collagen Mineralization. *Journal of the American Ceramic Society* **86**, 1052–1054 (2003).

60. Bellido, T., Plotkin, L. I. & Bruzzaniti, A. Bone Cells. in *Basic and Applied Bone Biology* 27–45 (Elsevier, 2014). doi:10.1016/B978-0-12-416015-6.00002-2.

61. Qing, H. *et al.* Demonstration of osteocytic perilacunar/canalicular remodeling in mice during lactation. *J Bone Miner Res* **27**, 1018–1029 (2012).

62. Qing, H. & Bonewald, L. F. Osteocyte remodeling of the perilacunar and pericanalicular matrix. *International journal of oral science* **1**, 59 (2009).

63. Yee, C. S., Schurman, C. A., White, C. R. & Alliston, T. Investigating Osteocytic Perilacunar/Canalicular Remodeling. *Curr Osteoporos Rep* **17**, 157–168 (2019).

64. Bryant, S. J. & Vernerey, F. J. Programmable Hydrogels for Cell Encapsulation and Neo-Tissue Growth to Enable Personalized Tissue Engineering. *Adv Healthc Mater* **7**, 1–13 (2018).

65. Uchihashi, K., Aoki, S., Matsunobu, A. & Toda, S. Osteoblast migration into type I collagen gel and differentiation to osteocyte-like cells within a self-produced mineralized matrix: A novel system for analyzing differentiation from osteoblast to osteocyte. *Bone* **52**, 102–110 (2013).

7.3 Chapter 3 References

1. You, L.-D., Weinbaum, S., Cowin, S. C. & Schaffler, M. B. Ultrastructure of the osteocyte process and its pericellular matrix. *Anat. Rec.* **278A**, 505–513 (2004).

2. Bellido, T., Plotkin, L. I. & Bruzzaniti, A. Bone Cells. in *Basic and Applied Bone Biology* 27–45 (Elsevier, 2014). doi:10.1016/B978-0-12-416015-6.00002-2.

3. Hemmatian, H., Bakker, A. D., Klein-Nulend, J. & van Lenthe, G. H. Aging, Osteocytes, and Mechanotransduction. *Curr Osteoporos Rep* **15**, 401–411 (2017).

4. Ribeiro-Rodrigues, T. M., Martins-Marques, T., Morel, S., Kwak, B. R. & Girão, H. Role of connexin 43 in different forms of intercellular communication – gap junctions, extracellular vesicles and tunnelling nanotubes. *J Cell Sci* **130**, 3619–3630 (2017).

5. Price, C., Zhou, X., Li, W. & Wang, L. Real-Time Measurement of Solute Transport Within the Lacunar-Canalicular System of Mechanically Loaded Bone: Direct Evidence for Load-Induced Fluid Flow. *J Bone Miner Res* **26**, 277–285 (2011).

6. Wu, D., Ganatos, P., Spray, D. C. & Weinbaum, S. On the electrophysiological response of bone cells using a Stokesian fluid stimulus probe for delivery of quantifiable localized picoNewton level forces. *J Biomech* **44**, 1702–1708 (2011).

7. Wu, D., Schaffler, M. B., Weinbaum, S. & Spray, D. C. Matrix-dependent adhesion mediates network responses to physiological stimulation of the osteocyte cell process. *PNAS* **110**, 12096–12101 (2013).

8. Burra, S. *et al.* Dendritic processes of osteocytes are mechanotransducers that induce the opening of hemichannels. *PNAS* **107**, 13648–13653 (2010).

9. Fritton, S. P. & Weinbaum, S. Fluid and Solute Transport in Bone: Flow-Induced Mechanotransduction. *Annual Review of Fluid Mechanics* **41**, 347–374 (2009).

10. Qin, L., Liu, W., Cao, H. & Xiao, G. Molecular mechanosensors in osteocytes. *Bone Res* **8**, 23 (2020).

11. Cabahug-Zuckerman, P. *et al.* Potential role for a specialized β3 integrin-based structure on osteocyte processes in bone mechanosensation. *J Orthop Res* **36**, 642–652 (2018).

12. Litzenberger, J. B., Tang, W. J., Castillo, A. B. & Jacobs, C. R. Deletion of β1 Integrins from Cortical Osteocytes Reduces Load-Induced Bone Formation. *Cel. Mol. Bioeng.* **2**, 416–424 (2009).

13. Haugh, M. G., Vaughan, T. J. & McNamara, L. M. The role of integrin α(V)β(3) in osteocyte mechanotransduction. *J Mech Behav Biomed Mater* **42**, 67–75 (2015).

14. Thi, M. M., Suadicani, S. O., Schaffler, M. B., Weinbaum, S. & Spray, D. C. Mechanosensory responses of osteocytes to physiological forces occur along processes and not cell body and require αVβ3 integrin. *PNAS* **110**, 21012–21017 (2013).

15. Gupta, A. *et al.* Communication of cAMP by connexin43 gap junctions regulates osteoblast signaling and gene expression. *Cellular Signalling* **28**, 1048–1057 (2016).

16. Zhang, C., Bakker, A. D., Klein-Nulend, J. & Bravenboer, N. Studies on Osteocytes in Their 3D Native Matrix Versus 2D In Vitro Models. *Current Osteoporosis Reports* **17**, 207–216 (2019).

17. Bernhardt, A., Weiser, E., Wolf, S., Vater, C. & Gelinsky, M. Primary Human Osteocyte Networks in Pure and Modified Collagen Gels. *Tissue Engineering Part A* **25**, 1347–1355 (2019).

18. Bernhardt, A., Österreich, V. & Gelinsky, M. Three-Dimensional Co-culture of Primary Human Osteocytes and Mature Human Osteoclasts in Collagen Gels. *Tissue Engineering Part A* ten.tea.2019.0085 (2019) doi:10.1089/ten.tea.2019.0085.

19. Skottke, Gelinsky, & Bernhardt. In Vitro Co-culture Model of Primary Human Osteoblasts and Osteocytes in Collagen Gels. *IJMS* **20**, 1998 (2019).

20. Anseth, K. S., Bowman, C. N. & Brannon-Peppas, L. Mechanical properties of hydrogels and their experimental determination. *Biomaterials* **17**, 1647–1657 (1996).

21. Huebsch, N. *et al.* Harnessing traction-mediated manipulation of the cell/matrix interface to control stem-cell fate. *Nature Materials* **9**, 518–526 (2010).

22. Mullen, C. A., Vaughan, T. J., Billiar, K. L. & McNamara, L. M. The Effect of Substrate Stiffness, Thickness, and Cross-Linking Density on Osteogenic Cell Behavior. *Biophysical Journal* **108**, 1604–1612 (2015).

23. Mullen, C. A., Haugh, M. G., Schaffler, M. B., Majeska, R. J. & McNamara, L. M. Osteocyte differentiation is regulated by extracellular matrix stiffness and intercellular separation. *Journal of the Mechanical Behavior of Biomedical Materials* **28**, 183–194 (2013).

24. Mc Garrigle, M., Haugh, M., Voisin, M. & McNamara, L. Osteocyte differentiation and the formation of an interconnected cellular network in vitro. *European Cells and Materials* **31**, 323–340 (2016).

25. McKinnon, D. D., Kloxin, A. M. & Anseth, K. S. Synthetic hydrogel platform for three-dimensional culture of embryonic stem cell-derived motor neurons. *Biomaterials Science* **1**, 460 (2013).

26. Nicodemus, G. D., Skaalure, S. C. & Bryant, S. J. Gel structure has an impact on pericellular and extracellular matrix deposition, which subsequently alters metabolic activities in chondrocyte-laden PEG hydrogels. *Acta Biomaterialia* **7**, 492–504 (2011).

27. Liao, H. *et al.* Influence of hydrogel mechanical properties and mesh size on vocal fold fibroblast extracellular matrix production and phenotype. *Acta Biomaterialia* **4**, 1161–1171 (2008).

28. Schneider, M. C. *et al.* Local Heterogeneities Improve Matrix Connectivity in Degradable and Photoclickable Poly(ethylene glycol) Hydrogels for Applications in Tissue Engineering. *ACS Biomater. Sci. Eng.* **3**, 2480–2492 (2017).

29. Sridhar, B. V. *et al.* Development of a Cellularly Degradable PEG Hydrogel to Promote Articular Cartilage Extracellular Matrix Deposition. *Advanced Healthcare Materials* **4**, 702–713 (2015).

30. Amer, L. D. & Bryant, S. J. The In Vitro and In Vivo Response to MMP-Sensitive Poly(Ethylene Glycol) Hydrogels. *Annals of Biomedical Engineering* **44**, 1959–1969 (2016).

31. Aziz, A. H., Wilmoth, R. L., Ferguson, V. L. & Bryant, S. J. IDG-SW3 Osteocyte Differentiation and Bone Extracellular Matrix Deposition Are Enhanced in a 3D Matrix Metalloproteinase-Sensitive Hydrogel. *ACS Appl. Bio Mater.* **3**, 1666–1680 (2020).

32. Hersel, U., Dahmen, C. & Kessler, H. RGD modified polymers: biomaterials for stimulated cell adhesion and beyond. *Biomaterials* **24**, 4385–4415 (2003).

33. Liu, W. *et al.* TGF-β1 facilitates cell–cell communication in osteocytes via connexin43- and pannexin1-dependent gap junctions. *Cell Death Discov.* **5**, 141 (2019).

34. Schneider, M. C., Chu, S., Randolph, M. A. & Bryant, S. J. An in vitro and in vivo comparison of cartilage growth in chondrocyte-laden matrix metalloproteinase-sensitive poly(ethylene

glycol) hydrogels with localized transforming growth factor β3. *Acta Biomaterialia* **93**, 97–110 (2019).

35. Park, J. S., Woo, D. G., Yang, H. N., Na, K. & Park, K.-H. Transforming growth factor β-3 bound with sulfate polysaccharide in synthetic extracellular matrix enhanced the biological activities for neocartilage formation in vivo. *Journal of Biomedical Materials Research Part A* **91A**, 408–415 (2009).

36. Zhang, K. *et al.* E11/gp38 Selective Expression in Osteocytes: Regulation by Mechanical Strain and Role in Dendrite Elongation. *Mol. Cell. Biol.* **26**, 4539–4552 (2006).

37. Fairbanks, B. D. *et al.* A Versatile Synthetic Extracellular Matrix Mimic via Thiol-Norbornene Photopolymerization. *Advanced Materials* **21**, 5005–5010 (2009).

38. Kitase, Y. *et al.* Mechanical induction of PGE2 in osteocytes blocks glucocorticoid-induced apoptosis through both the β-catenin and PKA pathways. *Journal of Bone and Mineral Research* **25**, 2657–2668 (2010).

39. Holmes, R. *et al.* Thiol-Ene Photo-Click Collagen-PEG Hydrogels: Impact of Water-Soluble Photoinitiators on Cell Viability, Gelation Kinetics and Rheological Properties. *Polymers* **9**, 226 (2017).

40. M. Schultz, K. & S. Anseth, K. Monitoring degradation of matrix metalloproteinases-cleavable PEG hydrogels via multiple particle tracking microrheology. *Soft Matter* **9**, 1570–1579 (2013).

41. Michael Pfaffl. A new mathematical model for relative quantification in real-time RT-PCR. *Nucleic Acids Research* **29**, 2002–2007 (2001).

42. Cao Xian *et al.* Angiotensin II–Dependent Hypertension Requires Cyclooxygenase 1–Derived Prostaglandin E2 and EP1 Receptor Signaling in the Subfornical Organ of the Brain. *Hypertension* **59**, 869–876 (2012).

43. Swartzlander, M. D. *et al.* Immunomodulation by mesenchymal stem cells combats the foreign body response to cell-laden synthetic hydrogels. *Biomaterials* **41**, 79–88 (2015).

44. Yoshida, K. *et al.* Stimulation of bone formation and prevention of bone loss by prostaglandin E EP4 receptor activation. *Proc Natl Acad Sci U S A* **99**, 4580–4585 (2002).

45. Paralkar, V. M. *et al.* An EP2 receptor-selective prostaglandin E2 agonist induces bone healing. *Proceedings of the National Academy of Sciences* **100**, 6736–6740 (2003).

46. Li, M. *et al.* A Novel, Non-Prostanoid EP2 Receptor-Selective Prostaglandin E2 Agonist Stimulates Local Bone Formation and Enhances Fracture Healing. *Journal of Bone and Mineral Research* **18**, 2033–2042 (2003).

47. Aziz, A. H. & Bryant, S. J. A comparison of human mesenchymal stem cell osteogenesis in poly(ethylene glycol) hydrogels as a function of MMP-sensitive crosslinker and crosslink

density in chemically defined medium. *Biotechnology and Bioengineering* **116**, 1523–1536 (2019).

48. Carles-Carner, M., Saleh, L. S. & Bryant, S. J. The effects of hydroxyapatite nanoparticles embedded in a MMP-sensitive photoclickable PEG hydrogel on encapsulated MC3T3-E1 pre-osteoblasts. *Biomed. Mater.* **13**, 045009 (2018).

49. McNamara, L. M., Majeska, R. J., Weinbaum, S., Friedrich, V. & Schaffler, M. B. Attachment of Osteocyte Cell Processes to the Bone Matrix. *The Anatomical Record* **292**, 355–363 (2009).

50. Kamel, M. A., Picconi, J. L., Lara-Castillo, N. & Johnson, M. L. Activation of B-catenin signaling in MLO-Y4 osteocytic cells versus 2T3 osteoblastic cells by fluid flow shear stress and PGE2: Implications for the study of mechanosensation in bone. *Bone* **47**, 872–881 (2010).

51. Cheng, B. *et al.* PGE2 is essential for gap junction-mediated intercellular communication between osteocyte-like MLO-Y4 cells in response to mechanical strain. *Endocrinology* **142**, 3464–3473 (2001).

52. Jee, W. S. S. & Ma, Y. F. The in vivo anabolic actions of prostaglandins in bone. *Bone* **21**, 297–304 (1997).

53. Ke, H. Z. *et al.* Prostaglandin E2 increases bone strength in intact rats and in ovariectomized rats with established osteopenia. *Bone* **23**, 249–255 (1998).

54. Collins, D. A. & Chambers, T. J. Effect of prostaglandins E1, E2, and F2α on osteoclast formation in mouse bone marrow cultures. *Journal of Bone and Mineral Research* **6**, 157–164 (1991).

55. Liu, X.-H., Kirschenbaum, A., Yao, S. & Levine, A. C. Interactive Effect of Interleukin-6 and Prostaglandin E2 on Osteoclastogenesis via the OPG/RANKL/RANK System. *Annals of the New York Academy of Sciences* **1068**, 225–233 (2006).

56. Suzuki, H. *et al.* The role of autonomously secreted PGE2 and its autocrine/paracrine effect on bone matrix mineralization at the different stages of differentiating MC3T3-E1 cells. *Biochemical and Biophysical Research Communications* **524**, 929–935 (2020).

57. Galea, G. L. *et al.* Sost down-regulation by mechanical strain in human osteoblastic cells involves PGE2 signaling via EP4. *FEBS Letters* **585**, 2450–2454 (2011).

58. Genetos, D. C., Yellowley, C. E. & Loots, G. G. Prostaglandin E2 Signals Through PTGER2 to Regulate Sclerostin Expression. *PLoS ONE* **6**, e17772 (2011).

7.4 Chapter 4 References

1. Schaffler, M. B., Cheung, W.-Y., Majeska, R. & Kennedy, O. Osteocytes: Master Orchestrators of Bone. *Calcified Tissue International* **94**, 5–24 (2014).

2. Kamel, M. A., Picconi, J. L., Lara-Castillo, N. & Johnson, M. L. Activation of B-catenin signaling in MLO-Y4 osteocytic cells versus 2T3 osteoblastic cells by fluid flow shear stress and PGE2: Implications for the study of mechanosensation in bone. *Bone* **47**, 872–881 (2010).

3. Cheng, B. *et al.* PGE2 is essential for gap junction-mediated intercellular communication between osteocyte-like MLO-Y4 cells in response to mechanical strain. *Endocrinology* **142**, 3464–3473 (2001).

4. Jee, W. S. S. & Ma, Y. F. The in vivo anabolic actions of prostaglandins in bone. *Bone* **21**, 297–304 (1997).

5. Ke, H. Z. *et al.* Prostaglandin E2 increases bone strength in intact rats and in ovariectomized rats with established osteopenia. *Bone* **23**, 249–255 (1998).

6. Dekel, S., Lenthall, G. & Francis, M. J. O. Release of Prostaglandins from Bone and Muscle After Tibial Fracture. *British Editorial Society of Bone and Joint Surgery* **63-B**, 185–189 (1981).

7. Suzuki, H. *et al.* The role of autonomously secreted PGE2 and its autocrine/paracrine effect on bone matrix mineralization at the different stages of differentiating MC3T3-E1 cells. *Biochemical and Biophysical Research Communications* **524**, 929–935 (2020).

8. Collins, D. A. & Chambers, T. J. Effect of prostaglandins E1, E2, and F2α on osteoclast formation in mouse bone marrow cultures. *Journal of Bone and Mineral Research* **6**, 157–164 (1991).

9. Liu, X.-H., Kirschenbaum, A., Yao, S. & Levine, A. C. Interactive Effect of Interleukin-6 and Prostaglandin E2 on Osteoclastogenesis via the OPG/RANKL/RANK System. *Annals of the New York Academy of Sciences* **1068**, 225–233 (2006).

10. Galea, G. L. *et al.* Sost down-regulation by mechanical strain in human osteoblastic cells involves PGE2 signaling via EP4. *FEBS Letters* **585**, 2450–2454 (2011).

11. Genetos, D. C., Yellowley, C. E. & Loots, G. G. Prostaglandin E2 Signals Through PTGER2 to Regulate Sclerostin Expression. *PLoS ONE* **6**, e17772 (2011).

12. Kumei, Y. *et al. Microgravity induces prostaglandin E2 and interleukin-6 production in normal rat osteoblasts: role in bone demineralization*. (Elsevier, 1996).

13. Lee, C. M., Genetos, D. C., You, Z. & Yellowley, C. E. Hypoxia regulates PGE2 release and EP1 receptor expression in osteoblastic cells. *Journal of Cellular Physiology* **212**, 182–188 (2007).

14. Liu, X.-H. *et al.* Prostaglandin E2 modulates components of the Wnt signaling system in bone and prostate cancer cells. *Biochemical and Biophysical Research Communications* **394**, 715–720 (2010).

15. McGarry, J. G., Klein-Nulend, J. & Prendergast, P. J. The effect of cytoskeletal disruption on pulsatile fluid flow-induced nitric oxide and prostaglandin E2 release in osteocytes and osteoblasts. *Biochemical and Biophysical Research Communications* **330**, 341–348 (2005).

16. Bakker, A. D., Soejima, K., Klein-Nulend, J. & Burger, E. H. The production of nitric oxide and prostaglandin E2 by primary bone cells is shear stress dependent. *Journal of Biomechanics* **34**, 671–677 (2001).

17. Smalt, R., Mitchell, F. T., Howard, R. L. & Chambers, T. J. Induction of NO and prostaglandin E2 in osteoblasts by wall-shear stress but not mechanical strain. *American Journal of Physiology-Endocrinology And Metabolism* **273**, E751–E758 (1997).

18. Cherian, P. P. *et al.* Mechanical strain opens connexin 43 hemichannels in osteocytes: a novel mechanism for the release of prostaglandin. *Molecular biology of the cell* **16**, 3100–3106 (2005).

19. Kitase, Y. *et al.* Mechanical induction of PGE2 in osteocytes blocks glucocorticoid-induced apoptosis through both the β-catenin and PKA pathways. *Journal of Bone and Mineral Research* **25**, 2657–2668 (2010).

20. Zhang, J.-N. *et al.* The role of the sphingosine-1-phosphate signaling pathway in osteocyte mechanotransduction. *Bone* **79**, 71–78 (2015).

21. Westbroek, I. *et al.* Differential Stimulation of Prostaglandin G/H Synthase-2 in Osteocytes and Other Osteogenic Cells by Pulsating Fluid Flow. *Biochemical and Biophysical Research Communications* **268**, 414–419 (2000).

22. Woo, S. M., Rosser, J., Dusevich, V., Kalajzic, I. & Bonewald, L. F. Cell line IDG-SW3 replicates osteoblast-to-late-osteocyte differentiation in vitro and accelerates bone formation in vivo. *J Bone Miner Res* **26**, 2634–2646 (2011).

23. Aziz, A. H., Wilmoth, R. L., Ferguson, V. L. & Bryant, S. J. IDG-SW3 Osteocyte Differentiation and Bone Extracellular Matrix Deposition Are Enhanced in a 3D Matrix Metalloproteinase-Sensitive Hydrogel. *ACS Appl. Bio Mater.* **3**, 1666–1680 (2020).

24. Sun, Q. *et al.* Ex vivo replication of phenotypic functions of osteocytes through biomimetic 3D bone tissue construction. *Bone* **106**, 148–155 (2018).

25. Boukhechba, F. *et al.* Human Primary Osteocyte Differentiation in a 3D Culture System. *Journal of Bone and Mineral Research* **24**, 1927–1935 (2009).

26. Robling, A. G. *et al.* Mechanical Stimulation of Bone in Vivo Reduces Osteocyte Expression of Sost/Sclerostin. *Journal of Biological Chemistry* **283**, 5866–5875 (2008).

27. Lara-Castillo, N. *et al.* In vivo mechanical loading rapidly activates β-catenin signaling in osteocytes through a prostaglandin mediated mechanism. *Bone* **76**, 58–66 (2015).

28. Cherian, P. P. *et al.* Effects of Mechanical Strain on the Function of Gap Junctions in Osteocytes Are Mediated through the Prostaglandin EP2 Receptor. *Journal of Biological Chemistry* **278**, 43146–43156 (2003).

29. Miyaura, C. *et al.* Impaired Bone Resorption to Prostaglandin E2 in Prostaglandin E Receptor EP4-knockout Mice. *Journal of Biological Chemistry* **275**, 19819–19823 (2000).

30. Machwate, M. *et al.* Prostaglandin Receptor EP4 Mediates the Bone Anabolic Effects of PGE2. *Mol Pharmacol* **60**, 36–41 (2001).

31. Yoshida, K. *et al.* Stimulation of bone formation and prevention of bone loss by prostaglandin E EP4 receptor activation. *Proc Natl Acad Sci U S A* **99**, 4580–4585 (2002).

32. Tanaka, M. *et al.* Prostaglandin E2 receptor (EP4) selective agonist (ONO-4819.CD) accelerates bone repair of femoral cortex after drill-hole injury associated with local upregulation of bone turnover in mature rats. *Bone* **34**, 940–948 (2004).

33. Ma, X., Kundu, N., Rifat, S., Walser, T. & Fulton, A. M. Prostaglandin E Receptor EP4 Antagonism Inhibits Breast Cancer Metastasis. *Cancer Res* **66**, 2923–2927 (2006).

34. Patel, D., Sharma, S., Screen, H. R. C. & Bryant, S. J. Effects of cell adhesion motif, fiber stiffness, and cyclic strain on tenocyte gene expression in a tendon mimetic fiber composite hydrogel. *Biochemical and Biophysical Research Communications* **499**, 642–647 (2018).

35. Swartzlander, M. D. *et al.* Immunomodulation by mesenchymal stem cells combats the foreign body response to cell-laden synthetic hydrogels. *Biomaterials* **41**, 79–88 (2015).

36. Wei, X. *et al.* Fibroblasts Express RANKL and Support Osteoclastogenesis in a COX-2-Dependent Manner After Stimulation With Titanium Particles. *Journal of Bone and Mineral Research* **20**, 1136–1148 (2005).

37. Forwood, M. R. Inducible cyclo-oxygenase (COX-2) mediates the induction of bone formation by mechanical loading in vivo. *Journal of Bone and Mineral Research* **11**, 1688–1693 (1996).

38. Sugimoto, Y. & Narumiya, S. Prostaglandin E Receptors. *Journal of Biological Chemistry* **282**, 11613–11617 (2007).

39. Zhang, M. *et al.* EP1−/− mice have enhanced osteoblast differentiation and accelerated fracture repair. *Journal of Bone and Mineral Research* **26**, 792–802 (2011).

40. Paralkar, V. M. *et al.* An EP2 receptor-selective prostaglandin E2 agonist induces bone healing. *Proceedings of the National Academy of Sciences* **100**, 6736–6740 (2003).

41. Wu, Q., Zhou, X., Huang, D., Ji, Y. & Kang, F. IL-6 Enhances Osteocyte-Mediated Osteoclastogenesis by Promoting JAK2 and RANKL Activity ***In Vitro***. *Cellular Physiology and Biochemistry* **41**, 1360–1369 (2017).

42. Zhou, M., Li, S. & Pathak, J. L. Pro-inflammatory Cytokines and Osteocytes. *Curr Osteoporos Rep* **17**, 97–104 (2019).

43. Cao, J., Venton, L., Sakata, T. & Halloran, B. P. Expression of RANKL and OPG correlates with age-related bone loss in male C57BL/6 mice. *J. Bone Miner. Res.* **18**, 270–277 (2003).

44. Cabahug-Zuckerman, P. *et al.* Osteocyte Apoptosis Caused by Hindlimb Unloading is Required to Trigger Osteocyte RANKL Production and Subsequent Resorption of Cortical and Trabecular Bone in Mice Femurs. *Journal of Bone and Mineral Research* **31**, 1356–1365 (2016).

45. Nakashima, T. *et al.* Evidence for osteocyte regulation of bone homeostasis through RANKL expression. *Nature Medicine* **17**, 1231–1234 (2011).

46. Xiong, J. *et al.* Osteocytes, not Osteoblasts or Lining Cells, are the Main Source of the RANKL Required for Osteoclast Formation in Remodeling Bone. *PLoS One* **10**, (2015).

47. Xiong, J. & O'Brien, C. A. Osteocyte RANKL: New insights into the control of bone remodeling. *J Bone Miner Res* **27**, 499–505 (2012).

48. Ducy, P., Desbois, C., Boyce, B. & Pinero, G. Increased bone formation in osteocalcin-deficient mice. *Nature (London)* **382**, 448–452 (1996).

49. Zoch, M. L., Clemens, T. L. & Riddle, R. C. New insights into the biology of osteocalcin. *Bone* **82**, 42–49 (2016).

50. Winkler, D. G. *et al.* Osteocyte control of bone formation via sclerostin,a novel BMP antagonist. *EMBO J* **22**, 6267–6276 (2003).

51. Wijenayaka, A. R. *et al.* Sclerostin Stimulates Osteocyte Support of Osteoclast Activity by a RANKL-Dependent Pathway. *PLoS One* **6**, (2011).

52. Michael Pfaffl. A new mathematical model for relative quantification in real-time RT-PCR. *Nucleic Acids Research* **29**, 2002–2007 (2001).

53. Cao Xian *et al.* Angiotensin II–Dependent Hypertension Requires Cyclooxygenase 1–Derived Prostaglandin E2 and EP1 Receptor Signaling in the Subfornical Organ of the Brain. *Hypertension* **59**, 869–876 (2012).

54. Masters, J. R. & Stacey, G. N. Changing medium and passaging cell lines. *Nat Protoc* **2**, 2276–2284 (2007).

55. Kaur, K., Das, S. & Ghosh, S. Regulation of Human Osteoblast-to-Osteocyte Differentiation by Direct-Write 3D Microperiodic Hydroxyapatite Scaffolds. *ACS Omega* **4**, 1504–1515 (2019).

56. Prideaux, M., Findlay, D. M. & Atkins, G. J. Osteocytes: The master cells in bone remodelling. *Current Opinion in Pharmacology* **28**, 24–30 (2016).

57. Gupta, A. *et al.* Communication of cAMP by connexin43 gap junctions regulates osteoblast signaling and gene expression. *Cellular Signalling* **28**, 1048–1057 (2016).

58. Poole, K. E. S. *et al.* Sclerostin is a delayed secreted product of osteocytes that inhibits bone formation. *The FASEB Journal* **19**, 1842–1844 (2005).

59. Ajubi, N. E. *et al.* Pulsating Fluid Flow Increases Prostaglandin Production by Cultured Chicken Osteocytes—A Cytoskeleton-Dependent Process. *Biochemical and Biophysical Research Communications* **225**, 62–68 (1996).

60. Klein-Nulend, J. *et al.* Sensitivity of osteocytes to biomechanical stress in vitro. *The FASEB Journal* **9**, 441–445 (1995).

61. Bernhardt, A., Weiser, E., Wolf, S., Vater, C. & Gelinsky, M. Primary Human Osteocyte Networks in Pure and Modified Collagen Gels. *Tissue Engineering Part A* **25**, 1347–1355 (2019).

62. Zhang, C., Bakker, A. D., Klein-Nulend, J. & Bravenboer, N. Studies on Osteocytes in Their 3D Native Matrix Versus 2D In Vitro Models. *Current Osteoporosis Reports* **17**, 207–216 (2019).

63. Regan, J. W. EP2 and EP4 prostanoid receptor signaling. *Life Sciences* **74**, 143–153 (2003).

64. Fujino, H., Xu, W. & Regan, J. W. Prostaglandin E2 Induced Functional Expression of Early Growth Response Factor-1 by EP4, but Not EP2, Prostanoid Receptors via the Phosphatidylinositol 3-Kinase and Extracellular Signal-regulated Kinases. *Journal of Biological Chemistry* **278**, 12151–12156 (2003).

65. Suzuki, A. *et al.* PTH/cAMP/PKA signaling facilitates canonical Wnt signaling via inactivation of glycogen synthase kinase-3β in osteoblastic Saos-2 cells. *Journal of Cellular Biochemistry* **104**, 304–317 (2008).

66. Li, M. *et al.* A Novel, Non-Prostanoid EP2 Receptor-Selective Prostaglandin E2 Agonist Stimulates Local Bone Formation and Enhances Fracture Healing. *Journal of Bone and Mineral Research* **18**, 2033–2042 (2003).

7.5 Chapter 5 References

1. Findlay, D. M. & Kuliwaba, J. S. Bone–cartilage crosstalk: a conversation for understanding osteoarthritis. *Bone Research* **4**, 16028 (2016).

2. Funck-Brentano, T. & Cohen-Solal, M. Crosstalk between cartilage and bone: When bone cytokines matter. *Cytokine & Growth Factor Reviews* **22**, 91–97 (2011).

3. Schaffler, M. B., Cheung, W.-Y., Majeska, R. & Kennedy, O. Osteocytes: Master Orchestrators of Bone. *Calcified Tissue International* **94**, 5–24 (2014).

4. Bonewald, L. F. The amazing osteocyte. *Journal of Bone and Mineral Research* **26**, 229–238 (2011).

5. Klein-Nulend, J., Bakker, A. D., Bacabac, R. G., Vatsa, A. & Weinbaum, S. Mechanosensation and transduction in osteocytes. *Bone* **54**, 182–190 (2013).

6. Alliston, T. Biological Regulation of Bone Quality. *Current Osteoporosis Reports* **12**, 366–375 (2014).

7. Hwang, J. *et al.* Increased hydraulic conductance of human articular cartilage and subchondral bone plate with progression of osteoarthritis. *Arthritis & Rheumatism* **58**, 3831–3842 (2008).

8. Stender, M. E., Regueiro, R. A. & Ferguson, V. L. A poroelastic finite element model of the bone–cartilage unit to determine the effects of changes in permeability with osteoarthritis. *Computer Methods in Biomechanics and Biomedical Engineering* 1–13 (2016) doi:10.1080/10255842.2016.1233326.

9. Stender, M. E., Carpenter, R. D., Regueiro, R. A. & Ferguson, V. L. An evolutionary model of osteoarthritis including articular cartilage damage, and bone remodeling in a computational study. *Journal of Biomechanics* (2016) doi:10.1016/j.jbiomech.2016.09.024.

10. Burr, D. B. The importance of subchondral bone in osteoarthrosis: *Current Opinion in Rheumatology* **10**, 256–262 (1998).

11. Fritton, S. P. & Weinbaum, S. Fluid and Solute Transport in Bone: Flow-Induced Mechanotransduction. *Annual Review of Fluid Mechanics* **41**, 347–374 (2009).

12. Hemmatian, H., Bakker, A. D., Klein-Nulend, J. & van Lenthe, G. H. Aging, Osteocytes, and Mechanotransduction. *Curr Osteoporos Rep* **15**, 401–411 (2017).

13. Mazur, C. M. *et al.* Osteocyte dysfunction promotes osteoarthritis through MMP13-dependent suppression of subchondral bone homeostasis. *Bone Res* **7**, 34 (2019).

14. Fritton, S. P., McLeod, K. J. & Rubin, C. T. Quantifying the strain history of bone: spatial uniformity and self-similarity of low-magnitude strains. *Journal of biomechanics* **33**, 317–325 (2000).

15. Tanaka, T. *et al.* Analysis of Ca2+ response of osteocyte network by three-dimensional time-lapse imaging in living bone. *Journal of Bone and Mineral Metabolism; Tokyo* **36**, 519–528 (2018).

16. Lynch, M. E. *et al.* In vivo tibial compression decreases osteolysis and tumor formation in a human metastatic breast cancer model. *Journal of Bone and Mineral Research* **28**, 2357–2367 (2013).

17. Lara-Castillo, N. *et al.* In vivo mechanical loading rapidly activates β-catenin signaling in osteocytes through a prostaglandin mediated mechanism. *Bone* **76**, 58–66 (2015).

18. Lewis, K. J. *et al.* Osteocyte calcium signals encode strain magnitude and loading frequency in vivo. *Proceedings of the National Academy of Sciences* **114**, 11775–11780 (2017).

19. Robling, A. G. *et al.* Mechanical Stimulation of Bone in Vivo Reduces Osteocyte Expression of Sost/Sclerostin. *Journal of Biological Chemistry* **283**, 5866–5875 (2008).

20. Holguin, N., Brodt, M. D. & Silva, M. J. Activation of Wnt Signaling by Mechanical Loading Is Impaired in the Bone of Old Mice. *Journal of Bone and Mineral Research* **31**, 2215–2226 (2016).

21. Metzger, C. E. *et al.* Differential responses of mechanosensitive osteocyte proteins in fore- and hindlimbs of hindlimb-unloaded rats. *Bone* **105**, 26–34 (2017).

22. Rath, A. L. *et al.* Correlation of cell strain in single osteocytes with intracellular calcium, but not intracellular nitric oxide, in response to fluid flow. *Journal of Biomechanics* **43**, 1560–1564 (2010).

23. Liu, C. *et al.* Effects of cyclic hydraulic pressure on osteocytes. *Bone* **46**, 1449–1456 (2010).

24. Galea, G. L. *et al.* Sost down-regulation by mechanical strain in human osteoblastic cells involves PGE2 signaling via EP4. *FEBS Letters* **585**, 2450–2454 (2011).

25. Atkins, G. J. *et al.* Sclerostin is a locally acting regulator of late-osteoblast/preosteocyte differentiation and regulates mineralization through a MEPE-ASARM-dependent mechanism. *Journal of Bone and Mineral Research* **26**, 1425–1436 (2011).

26. Zhang, C., Bakker, A. D., Klein-Nulend, J. & Bravenboer, N. Studies on Osteocytes in Their 3D Native Matrix Versus 2D In Vitro Models. *Current Osteoporosis Reports* **17**, 207–216 (2019).

27. Vazquez, M. *et al.* A New Method to Investigate How Mechanical Loading of Osteocytes Controls Osteoblasts. *Front Endocrinol (Lausanne)* **5**, (2014).

28. Sun, Q. *et al.* Ex vivo replication of phenotypic functions of osteocytes through biomimetic 3D bone tissue construction. *Bone* **106**, 148–155 (2018).

29. Takemura, Y. *et al.* Mechanical loading induced osteocyte apoptosis and connexin 43 expression in three-dimensional cell culture and dental implant model. *Journal of Biomedical Materials Research Part A* **107**, 815–827 (2019).

30. Choudhary, S. *et al.* Hypoxic Three-Dimensional Cellular Network Construction Replicates Ex Vivo the Phenotype of Primary Human Osteocytes. *Tissue Engineering Part A* **24**, 458–468 (2018).

31. Kurata, K., Heino, T. J., Higaki, H. & Väänänen, H. K. Bone Marrow Cell Differentiation Induced by Mechanically Damaged Osteocytes in 3D Gel-Embedded Culture. *Journal of Bone and Mineral Research* **21**, 616–625 (2006).

32. Spatz, J. M. *et al.* The Wnt Inhibitor Sclerostin Is Up-regulated by Mechanical Unloading in Osteocytes in Vitro. *Journal of Biological Chemistry* **290**, 16744–16758 (2015).

33. Mc Garrigle, M., Haugh, M., Voisin, M. & McNamara, L. Osteocyte differentiation and the formation of an interconnected cellular network in vitro. *European Cells and Materials* **31**, 323–340 (2016).

34. Bernhardt, A., Weiser, E., Wolf, S., Vater, C. & Gelinsky, M. Primary Human Osteocyte Networks in Pure and Modified Collagen Gels. *Tissue Engineering Part A* **25**, 1347–1355 (2019).

35. Lynch, M. E. *et al.* Three-Dimensional Mechanical Loading Modulates the Osteogenic Response of Mesenchymal Stem Cells to Tumor-Derived Soluble Signals. *Tissue Engineering Part A* **22**, 1006–1015 (2016).

36. Wang, W., Sarazin, B. A., Kornilowicz, G. & Lynch, M. E. Mechanically-Loaded Breast Cancer Cells Modify Osteocyte Mechanosensitivity by Secreting Factors That Increase Osteocyte Dendrite Formation and Downstream Resorption. *Frontiers in Endocrinology* **9**, (2018).

37. You, L., Temiyasathit, S., Tao, E., Prinz, F. & Jacobs, C. R. 3D Microfluidic Approach to Mechanical Stimulation of Osteocyte Processes. *Cellular and Molecular Bioengineering* **1**, 103–107 (2008).

38. Aziz, A. H., Eckstein, K., Ferguson, V. L. & Bryant, S. J. The effects of dynamic compressive loading on human mesenchymal stem cell osteogenesis in the stiff layer of a bilayer hydrogel. *Journal of Tissue Engineering and Regenerative Medicine* **13**, 946–959 (2019).

39. Galperin, A. *et al.* Integrated Bi-Layered Scaffold for Osteochondral Tissue Engineering. *Advanced Healthcare Materials* **2**, 872–883 (2013).

40. Gan, D. *et al.* Mussel-Inspired Tough Hydrogel with In Situ Nanohydroxyapatite Mineralization for Osteochondral Defect Repair. *Advanced Healthcare Materials* **8**, 1901103 (2019).

41. Kim, B. J. *et al.* Restoration of articular osteochondral defects in rat by a bi-layered hyaluronic acid hydrogel plug with TUDCA-PLGA microsphere. *Journal of Industrial and Engineering Chemistry* **61**, 295–303 (2018).

42. Lin, D. *et al.* A viscoelastic PEGylated poly(glycerol sebacate)-based bilayer scaffold for cartilage regeneration in full-thickness osteochondral defect. *Biomaterials* **253**, 120095 (2020).

43. Liu, K., Liu, Y., Duan, Z., Ma, X. & Fan, D. A biomimetic bi-layered tissue engineering scaffolds for osteochondral defects repair. *Sci. China Technol. Sci.* (2020) doi:10.1007/s11431-020-1597-4.

44. Liu, X. *et al.* A Biomimetic Biphasic Osteochondral Scaffold with Layer-Specific Release of Stem Cell Differentiation Inducers for the Reconstruction of Osteochondral Defects. *Advanced Healthcare Materials* **n/a**, 2000076.

45. Steinmetz, N. J., Aisenbrey, E. A., Westbrook, K. K., Qi, H. J. & Bryant, S. J. Mechanical loading regulates human MSC differentiation in a multi-layer hydrogel for osteochondral tissue engineering. *Acta Biomaterialia* **21**, 142–153 (2015).

46. Zhu, X. *et al.* Biomimetic Bacterial Cellulose-Enhanced Double-Network Hydrogel with Excellent Mechanical Properties Applied for the Osteochondral Defect Repair. *ACS Biomater. Sci. Eng.* **4**, 3534–3544 (2018).

47. Burr, D. B. & Akkus, O. Bone Morphology and Organization. in *Basic and Applied Bone Biology* 3–25 (Elsevier, 2014). doi:10.1016/B978-0-12-416015-6.00001-0.

48. Lories, R. J. & Luyten, F. P. The bone–cartilage unit in osteoarthritis. *Nature Reviews Rheumatology* **7**, 43–49 (2011).

49. Chan, D. D. *et al.* In vivo articular cartilage deformation: noninvasive quantification of intratissue strain during joint contact in the human knee. *Scientific Reports* **6**, 19220 (2016).

50. Wahlquist, J. A. *et al.* Indentation mapping revealed poroelastic, but not viscoelastic, properties spanning native zonal articular cartilage. *Acta Biomaterialia* **64**, 41–49 (2017).

51. Choi, K., Kuhn, J. L., Ciarelli, M. J. & Goldstein, S. A. The elastic moduli of human subchondral, trabecular, and cortical bone tissue and the size-dependency of cortical bone modulus. *Journal of biomechanics* **23**, 1103–1113 (1990).

52. Hargrave-Thomas, E., van Sloun, F., Dickinson, M., Broom, N. & Thambyah, A. Multi-scalar mechanical testing of the calcified cartilage and subchondral bone comparing healthy vs early degenerative states. *Osteoarthritis and Cartilage* **23**, 1755–1762 (2015).

53. Aziz, A. H. & Bryant, S. J. A comparison of human mesenchymal stem cell osteogenesis in poly(ethylene glycol) hydrogels as a function of MMP-sensitive crosslinker and crosslink density in chemically defined medium. *Biotechnology and Bioengineering* **116**, 1523–1536 (2019).

54. Uzcategui, A. C., Muralidharan, A., Ferguson, V. L., Bryant, S. J. & McLeod, R. R. Understanding and Improving Mechanical Properties in 3D printed Parts Using a Dual-Cure Acrylate-Based Resin for Stereolithography. *Adv. Eng. Mater.* **20**, 1800876 (2018).

55. Aisenbrey, E. A. *et al.* A Stereolithography-Based 3D Printed Hybrid Scaffold for In Situ Cartilage Defect Repair. *Macromolecular Bioscience* **18**, 1700267 (2018).

56. Aziz, A. H., Wilmoth, R. L., Ferguson, V. L. & Bryant, S. J. IDG-SW3 Osteocyte Differentiation and Bone Extracellular Matrix Deposition Are Enhanced in a 3D Matrix Metalloproteinase-Sensitive Hydrogel. *ACS Appl. Bio Mater.* **3**, 1666–1680 (2020).

57. Schneider, M. C. *et al.* Local Heterogeneities Improve Matrix Connectivity in Degradable and Photoclickable Poly(ethylene glycol) Hydrogels for Applications in Tissue Engineering. *ACS Biomater. Sci. Eng.* **3**, 2480–2492 (2017).

58. Chu, S., Maples, M. M. & Bryant, S. J. Cell encapsulation spatially alters crosslink density of poly(ethylene glycol) hydrogels formed from free-radical polymerizations. *Acta Biomaterialia* **109**, 37–50 (2020).

59. Aisenbrey, E. A. & Bryant, S. J. A MMP7-sensitive photoclickable biomimetic hydrogel for MSC encapsulation towards engineering human cartilage. *Journal of Biomedical Materials Research Part A* **106**, 2344–2355 (2018).

60. Woo, S. M., Rosser, J., Dusevich, V., Kalajzic, I. & Bonewald, L. F. Cell Line IDG-SW3 Replicates Osteoblast-to-Late-Osteocyte Differentiation in vitro and Accelerates Bone Formation in vivo. *J Bone Miner Res* **26**, 2634–2646 (2011).

61. Langhorst, H. *et al.* The IgCAM CLMP regulates expression of Connexin43 and Connexin45 in intestinal and ureteral smooth muscle contraction in mice. *Disease Models & Mechanisms* **11**, dmm032128 (2018).

62. Balla, P. *et al.* Prognostic Impact of Reduced Connexin43 Expression and Gap Junction Coupling of Neoplastic Stromal Cells in Giant Cell Tumor of Bone. *PLOS ONE* **10**, e0125316 (2015).

63. Plotkin, L. I. Connexin 43 and Bone: Not Just a Gap Junction Protein. *Actual osteol* **7**, 79–90 (2011).

64. Gramsch, B. *et al.* Enhancement of Connexin 43 Expression Increases Proliferation and Differentiation of an Osteoblast-like Cell Line. *Experimental Cell Research* **264**, 397–407 (2001).

65. Buo, A. M. & Stains, J. P. Gap junctional regulation of signal transduction in bone cells. *FEBS Letters* **588**, 1315–1321 (2014).

66. Paic, F. *et al.* Identification of differentially expressed genes between osteoblasts and osteocytes. *Bone* **45**, 682–692 (2009).

67. Uchihashi, K., Aoki, S., Matsunobu, A. & Toda, S. Osteoblast migration into type I collagen gel and differentiation to osteocyte-like cells within a self-produced mineralized matrix: A novel system for analyzing differentiation from osteoblast to osteocyte. *Bone* **52**, 102–110 (2013).

68. Kalajzic, I. *et al.* Dentin matrix protein 1 expression during osteoblastic differentiation, generation of an osteocyte GFP-transgene. *Bone* **35**, 74–82 (2004).

69. Galea, G. L., Lanyon, L. E. & Price, J. S. Sclerostin's role in bone's adaptive response to mechanical loading. *Bone* **96**, 38–44 (2017).

70. Zhang, W., Huang, Z.-L., Liao, S.-S. & Cui, F.-Z. Nucleation sites of calcium phosphate crystals during collagen mineralization. *Journal of the American Ceramic Society* **86**, 1052–1054 (2003).

71. Magne, D., Weiss, P., Bouler, J.-M., Laboux, O. & Daculsi, G. Study of the Maturation of the Organic (Type I Collagen) and Mineral (Nonstoichiometric Apatite) Constituents of a Calcified Tissue (Dentin) as a Function of Location: A Fourier Transform Infrared Microspectroscopic Investigation. *Journal of Bone and Mineral Research* **16**, 750–757 (2001).

72. Jiao, K. *et al.* Complementarity and Uncertainty in Intrafibrillar Mineralization of Collagen. *Advanced Functional Materials* **26**, 6858–6875 (2016).

73. Niu, L.-N. *et al.* Collagen intrafibrillar mineralization as a result of the balance between osmotic equilibrium and electroneutrality. *Nat Mater* **16**, 370–378 (2017).

74. Kamel, M. A., Picconi, J. L., Lara-Castillo, N. & Johnson, M. L. Activation of B-catenin signaling in MLO-Y4 osteocytic cells versus 2T3 osteoblastic cells by fluid flow shear stress and PGE2: Implications for the study of mechanosensation in bone. *Bone* **47**, 872–881 (2010).

75. Cheng, B. *et al.* PGE2 is essential for gap junction-mediated intercellular communication between osteocyte-like MLO-Y4 cells in response to mechanical strain. *Endocrinology* **142**, 3464–3473 (2001).

76. Westbroek, I. *et al.* Differential Stimulation of Prostaglandin G/H Synthase-2 in Osteocytes and Other Osteogenic Cells by Pulsating Fluid Flow. *Biochemical and Biophysical Research Communications* **268**, 414–419 (2000).

77. Klein-Nulend, J. *et al.* Sensitivity of osteocytes to biomechanical stress in vitro. *The FASEB Journal* **9**, 441–445 (1995).

78. Swartzlander, M. D. *et al.* Immunomodulation by mesenchymal stem cells combats the foreign body response to cell-laden synthetic hydrogels. *Biomaterials* **41**, 79–88 (2015).

79. You, J. *et al.* Substrate deformation levels associated with routine physical activity are less stimulatory to bone cells relative to loading-induced oscillatory fluid flow. *J. Biomech. Eng.* **122**, 387–393 (2000).

80. Rath Bonivtch, A., Bonewald, L. F. & Nicolella, D. P. Tissue strain amplification at the osteocyte lacuna: A microstructural finite element analysis. *Journal of Biomechanics* **40**, 2199–2206 (2007).

81. You, L., Cowin, S. C., Schaffler, M. B. & Weinbaum, S. A model for strain amplification in the actin cytoskeleton of osteocytes due to fluid drag on pericellular matrix. *Journal of biomechanics* **34**, 1375–1386 (2001).

82. Han, Y., Cowin, S. C., Schaffler, M. B. & Weinbaum, S. Mechanotransduction and strain amplification in osteocyte cell processes. *Proceedings of the national academy of sciences* **101**, 16689–16694 (2004).

83. Smalt, R., Mitchell, F. T., Howard, R. L. & Chambers, T. J. Induction of NO and prostaglandin E2 in osteoblasts by wall-shear stress but not mechanical strain. *American Journal of Physiology-Endocrinology And Metabolism* **273**, E751–E758 (1997).

84. Kim, Y.-J., Bonassar, L. J. & Grodzinsky, A. J. The role of cartilage streaming potential, fluid flow and pressure in the stimulation of chondrocyte biosynthesis during dynamic compression. *Journal of Biomechanics* **28**, 1055–1066 (1995).

85. Chan, E. P., Deeyaa, B., Johnson, P. M. & Stafford, C. M. Poroelastic relaxation of polymer-loaded hydrogels. *Soft Matter* **8**, 8234 (2012).

86. Rakovsky, A., Marbach, D., Lotan, N. & Lanir, Y. Poly(ethylene glycol)-based hydrogels as cartilage substitutes: Synthesis and mechanical characteristics. *J. Appl. Polym. Sci.* **112**, 390–401 (2009).

87. Bush, B. G., Shapiro, J. M., DelRio, F. W., Cook, R. F. & Oyen, M. L. Mechanical measurements of heterogeneity and length scale effects in PEG-based hydrogels. *Soft Matter* **11**, 7191–7200 (2015).

88. Goulet, G. C., Cooper, D. M. L., Coombe, D. & Zernicke, R. F. Influence of cortical canal architecture on lacunocanalicular pore pressure and fluid flow. *Computer Methods in Biomechanics and Biomedical Engineering* **11**, 379–387 (2008).

89. Ishihara, Y. *et al.* Hormonal, pH, and Calcium Regulation of Connexin 43–Mediated Dye Transfer in Osteocytes in Chick Calvaria. *Journal of Bone and Mineral Research* **23**, 350–360 (2008).

90. Lee, C. M., Genetos, D. C., You, Z. & Yellowley, C. E. Hypoxia regulates PGE2 release and EP1 receptor expression in osteoblastic cells. *Journal of Cellular Physiology* **212**, 182–188 (2007).

91. Tamplen, M. *et al.* Treatment with anti-Sclerostin antibody to stimulate mandibular bone formation. *Head & Neck* **40**, 1453–1460 (2018).

92. Fowler, T. W. *et al.* Glucocorticoid suppression of osteocyte perilacunar remodeling is associated with subchondral bone degeneration in osteonecrosis. *Scientific Reports* **7**, 44618 (2017).

93. Sharma, D. *et al.* Alterations in the osteocyte lacunar–canalicular microenvironment due to estrogen deficiency. *Bone* **51**, 488–497 (2012).

94. Pathak, J. L. *et al.* Systemic Inflammation Affects Human Osteocyte-Specific Protein and Cytokine Expression. *Calcif Tissue Int* **98**, 596–608 (2016).

95. Aziz, A. H. *et al.* Mechanical characterization of sequentially layered photo-clickable thiol-ene hydrogels. *Journal of the Mechanical Behavior of Biomedical Materials* **65**, 454–465 (2017).

96. Aziz, A. H. & Bryant, S. J. A comparison of human mesenchymal stem cell osteogenesis in poly(ethylene glycol) hydrogels as a function of MMP-sensitive crosslinker and crosslink density in chemically defined medium. *Biotechnology and Bioengineering* **0**,.

97. Nicodemus, G. D. & Bryant, S. J. The role of hydrogel structure and dynamic loading on chondrocyte gene expression and matrix formation. *Journal of Biomechanics* **41**, 1528–1536 (2008).

98. Nicodemus, G. D. & Bryant, S. J. Mechanical loading regimes affect the anabolic and catabolic activities by chondrocytes encapsulated in PEG hydrogels. *Osteoarthritis and Cartilage* **18**, 126–137 (2010).

99. Villanueva, I., Hauschulz, D. S., Mejic, D. & Bryant, S. J. Static and dynamic compressive strains influence nitric oxide production and chondrocyte bioactivity when encapsulated in PEG hydrogels of different crosslinking densities. *Osteoarthritis and Cartilage* **16**, 909–918 (2008).

100. Steinmetz, N. J. & Bryant, S. J. The effects of intermittent dynamic loading on chondrogenic and osteogenic differentiation of human marrow stromal cells encapsulated in RGD-modified poly(ethylene glycol) hydrogels. *Acta Biomaterialia* **7**, 3829–3840 (2011).

Chapter 5 Supplementary References

1. Aziz, A. H. *et al.* Mechanical characterization of sequentially layered photo-clickable thiol-ene hydrogels. *Journal of the Mechanical Behavior of Biomedical Materials* **65**, 454–465 (2017).

2. Aziz, A. H., Eckstein, K., Ferguson, V. L. & Bryant, S. J. The effects of dynamic compressive loading on human mesenchymal stem cell osteogenesis in the stiff layer of a bilayer hydrogel. *Journal of Tissue Engineering and Regenerative Medicine* **0**,.

3. Aziz, A. H. & Bryant, S. J. A comparison of human mesenchymal stem cell osteogenesis in poly(ethylene glycol) hydrogels as a function of MMP-sensitive crosslinker and crosslink density in chemically defined medium. *Biotechnology and Bioengineering* **0**,.

4. Michael Pfaffl. A new mathematical model for relative quantification in real-time RT-PCR. *Nucleic Acids Research* **29**, 2002–2007 (2001).

5. Nicodemus, G. D. & Bryant, S. J. The role of hydrogel structure and dynamic loading on chondrocyte gene expression and matrix formation. *Journal of Biomechanics* **41**, 1528–1536 (2008).

6. Nicodemus, G. D. & Bryant, S. J. Mechanical loading regimes affect the anabolic and catabolic activities by chondrocytes encapsulated in PEG hydrogels. *Osteoarthritis and Cartilage* **18**, 126–137 (2010).

7. Villanueva, I., Hauschulz, D. S., Mejic, D. & Bryant, S. J. Static and dynamic compressive strains influence nitric oxide production and chondrocyte bioactivity when encapsulated in PEG hydrogels of different crosslinking densities. *Osteoarthritis and Cartilage* **16**, 909–918 (2008).

8. Steinmetz, N. J. & Bryant, S. J. The effects of intermittent dynamic loading on chondrogenic and osteogenic differentiation of human marrow stromal cells encapsulated in RGD-modified poly(ethylene glycol) hydrogels. *Acta Biomaterialia* **7**, 3829–3840 (2011).

7.6 Chapter 6 References

1. Robling, A. G. & Bonewald, L. F. The Osteocyte: New Insights. *Annual Review of Physiology* **82**, 485–506 (2020).

2. Maurel, D. B. *et al.* Characterization of a novel murine Sost ER T2 Cre model targeting osteocytes. *Bone Research* **7**, 1–13 (2019).

3. Sawa, N., Fujimoto, H., Sawa, Y., Yamashita, J. Alternating Differentiation and Dedifferentiation between Mature Osteoblasts and Osteocytes. *Scientific Reports (Nature Publisher Group); London* **9**, 1–9 (2019).

4. Woo, S. M., Rosser, J., Dusevich, V., Kalajzic, I. & Bonewald, L. F. Cell line IDG-SW3 replicates osteoblast-to-late-osteocyte differentiation in vitro and accelerates bone formation in vivo. *J Bone Miner Res* **26**, 2634–2646 (2011).

5. Kamel, M. A., Picconi, J. L., Lara-Castillo, N. & Johnson, M. L. Activation of B-catenin signaling in MLO-Y4 osteocytic cells versus 2T3 osteoblastic cells by fluid flow shear stress and PGE2: Implications for the study of mechanosensation in bone. *Bone* **47**, 872–881 (2010).

6. Suzuki, H. *et al.* The role of autonomously secreted PGE2 and its autocrine/paracrine effect on bone matrix mineralization at the different stages of differentiating MC3T3-E1 cells. *Biochemical and Biophysical Research Communications* **524**, 929–935 (2020).

7. Liu, X.-H., Kirschenbaum, A., Yao, S. & Levine, A. C. Interactive Effect of Interleukin-6 and Prostaglandin E2 on Osteoclastogenesis via the OPG/RANKL/RANK System. *Annals of the New York Academy of Sciences* **1068**, 225–233 (2006).

8. Galea, G. L. *et al.* Sost down-regulation by mechanical strain in human osteoblastic cells involves PGE2 signaling via EP4. *FEBS Letters* **585**, 2450–2454 (2011).

9. Genetos, D. C., Yellowley, C. E. & Loots, G. G. Prostaglandin E2 Signals Through PTGER2 to Regulate Sclerostin Expression. *PLoS ONE* **6**, e17772 (2011).

10. Kumei, Y. *et al. Microgravity induces prostaglandin E2 and interleukin-6 production in normal rat osteoblasts: role in bone demineralization*. (Elsevier, 1996).

11. Lee, C. M., Genetos, D. C., You, Z. & Yellowley, C. E. Hypoxia regulates PGE2 release and EP1 receptor expression in osteoblastic cells. *Journal of Cellular Physiology* **212**, 182–188 (2007).

12. Liu, X.-H. *et al.* Prostaglandin E2 modulates components of the Wnt signaling system in bone and prostate cancer cells. *Biochemical and Biophysical Research Communications* **394**, 715–720 (2010).

13. McGarry, J. G., Klein-Nulend, J. & Prendergast, P. J. The effect of cytoskeletal disruption on pulsatile fluid flow-induced nitric oxide and prostaglandin E2 release in osteocytes and osteoblasts. *Biochemical and Biophysical Research Communications* **330**, 341–348 (2005).

14. Bakker, A. D., Soejima, K., Klein-Nulend, J. & Burger, E. H. The production of nitric oxide and prostaglandin E2 by primary bone cells is shear stress dependent. *Journal of Biomechanics* **34**, 671–677 (2001).

15. Smalt, R., Mitchell, F. T., Howard, R. L. & Chambers, T. J. Induction of NO and prostaglandin E2 in osteoblasts by wall-shear stress but not mechanical strain. *American Journal of Physiology-Endocrinology And Metabolism* **273**, E751–E758 (1997).

16. Cheng, B. *et al.* PGE2 is essential for gap junction-mediated intercellular communication between osteocyte-like MLO-Y4 cells in response to mechanical strain. *Endocrinology* **142**, 3464–3473 (2001).

17. Cherian, P. P. *et al.* Mechanical strain opens connexin 43 hemichannels in osteocytes: a novel mechanism for the release of prostaglandin. *Molecular biology of the cell* **16**, 3100–3106 (2005).

18. Kitase, Y. *et al.* Mechanical induction of PGE2 in osteocytes blocks glucocorticoid-induced apoptosis through both the β-catenin and PKA pathways. *Journal of Bone and Mineral Research* **25**, 2657–2668 (2010).

19. Zhang, J.-N. *et al.* The role of the sphingosine-1-phosphate signaling pathway in osteocyte mechanotransduction. *Bone* **79**, 71–78 (2015).

20. Jee, W. S. S. & Ma, Y. F. The in vivo anabolic actions of prostaglandins in bone. *Bone* **21**, 297–304 (1997).

21. Ke, H. Z. *et al.* Prostaglandin E2 increases bone strength in intact rats and in ovariectomized rats with established osteopenia. *Bone* **23**, 249–255 (1998).

22. Cherian, P. P. *et al.* Effects of Mechanical Strain on the Function of Gap Junctions in Osteocytes Are Mediated through the Prostaglandin EP2 Receptor. *Journal of Biological Chemistry* **278**, 43146–43156 (2003).

23. Vazquez, M. *et al.* A New Method to Investigate How Mechanical Loading of Osteocytes Controls Osteoblasts. *Front Endocrinol (Lausanne)* **5**, (2014).

24. Sun, Q. *et al.* Ex vivo replication of phenotypic functions of osteocytes through biomimetic 3D bone tissue construction. *Bone* **106**, 148–155 (2018).

25. Takemura, Y. *et al.* Mechanical loading induced osteocyte apoptosis and connexin 43 expression in three-dimensional cell culture and dental implant model. *Journal of Biomedical Materials Research Part A* **107**, 815–827 (2019).

26. Choudhary, S. *et al.* Hypoxic Three-Dimensional Cellular Network Construction Replicates Ex Vivo the Phenotype of Primary Human Osteocytes. *Tissue Engineering Part A* **24**, 458–468 (2018).

27. Kurata, K., Heino, T. J., Higaki, H. & Väänänen, H. K. Bone Marrow Cell Differentiation Induced by Mechanically Damaged Osteocytes in 3D Gel-Embedded Culture. *Journal of Bone and Mineral Research* **21**, 616–625 (2006).

28. Spatz, J. M. *et al.* The Wnt Inhibitor Sclerostin Is Up-regulated by Mechanical Unloading in Osteocytes in Vitro. *Journal of Biological Chemistry* **290**, 16744–16758 (2015).

29. Mc Garrigle, M., Haugh, M., Voisin, M. & McNamara, L. Osteocyte differentiation and the formation of an interconnected cellular network in vitro. *European Cells and Materials* **31**, 323–340 (2016).

30. Fritton, S. P., McLeod, K. J. & Rubin, C. T. Quantifying the strain history of bone: spatial uniformity and self-similarity of low-magnitude strains. *Journal of biomechanics* **33**, 317–325 (2000).

31. Schaffler, M. B., Cheung, W.-Y., Majeska, R. & Kennedy, O. Osteocytes: Master Orchestrators of Bone. *Calcified Tissue International* **94**, 5–24 (2014).

32. You, J. *et al.* Substrate deformation levels associated with routine physical activity are less stimulatory to bone cells relative to loading-induced oscillatory fluid flow. *J. Biomech. Eng.* **122**, 387–393 (2000).

33. Kim, Y.-J., Bonassar, L. J. & Grodzinsky, A. J. The role of cartilage streaming potential, fluid flow and pressure in the stimulation of chondrocyte biosynthesis during dynamic compression. *Journal of Biomechanics* **28**, 1055–1066 (1995).

34. Chan, E. P., Deeyaa, B., Johnson, P. M. & Stafford, C. M. Poroelastic relaxation of polymer-loaded hydrogels. *Soft Matter* **8**, 8234 (2012).

35. Rakovsky, A., Marbach, D., Lotan, N. & Lanir, Y. Poly(ethylene glycol)-based hydrogels as cartilage substitutes: Synthesis and mechanical characteristics. *J. Appl. Polym. Sci.* **112**, 390–401 (2009).

36. Bush, B. G., Shapiro, J. M., DelRio, F. W., Cook, R. F. & Oyen, M. L. Mechanical measurements of heterogeneity and length scale effects in PEG-based hydrogels. *Soft Matter* **11**, 7191–7200 (2015).

37. Aziz, A. H., Eckstein, K., Ferguson, V. L. & Bryant, S. J. The effects of dynamic compressive loading on human mesenchymal stem cell osteogenesis in the stiff layer of a bilayer hydrogel. *Journal of Tissue Engineering and Regenerative Medicine* **13**, 946–959 (2019).

38. Stender, M. E., Regueiro, R. A. & Ferguson, V. L. A poroelastic finite element model of the bone–cartilage unit to determine the effects of changes in permeability with osteoarthritis. *Computer Methods in Biomechanics and Biomedical Engineering* 1–13 (2016) doi:10.1080/10255842.2016.1233326.

39. Goulet, G. C., Cooper, D. M. L., Coombe, D. & Zernicke, R. F. Influence of cortical canal architecture on lacunocanalicular pore pressure and fluid flow. *Computer Methods in Biomechanics and Biomedical Engineering* **11**, 379–387 (2008).

40. Carles-Carner, M., Saleh, L. S. & Bryant, S. J. The effects of hydroxyapatite nanoparticles embedded in a MMP-sensitive photoclickable PEG hydrogel on encapsulated MC3T3-E1 pre-osteoblasts. *Biomed. Mater.* **13**, 045009 (2018).

41. Wang, B. *et al.* Perlecan-Containing Pericellular Matrix Regulates Solute Transport and Mechanosensing Within the Osteocyte Lacunar-Canalicular System. *Journal of Bone and Mineral Research* **29**, 878–891 (2014).

42. Huebsch, N. *et al.* Harnessing traction-mediated manipulation of the cell/matrix interface to control stem-cell fate. *Nature Materials* **9**, 518–526 (2010).

43. Tiede-Lewis, L. M. & Dallas, S. L. Changes in the osteocyte lacunocanalicular network with aging. *Bone* **122**, 101–113 (2019).

44. Wang, K. *et al.* A Novel Osteogenic Cell Line That Differentiates Into GFP-Tagged Osteocytes and Forms Mineral With a Bone-Like Lacunocanalicular Structure. *Journal of Bone and Mineral Research* **34**, 979–995 (2019).

8. Appendix

8.1 Supplementary Tables

Table 7.1: Mean and standard deviation (S.D.) elastic modulus values for each hydrogel condition after 1 and 21 days of culture. The elastic modulus was calculated from the true-stress, true-strain curve.

	Day 1 Elastic Modulus (kPa)		**Day 21 Elastic Modulus (kPa)**	
Condition	Mean	S.D.	Mean	S.D.
ND	2.5	0.1	4.1	0.7
P1-11-RGD	6.6	0.2	17.3	9.3
P1-14-RGD	10.0	0.8	8.1	1.3
P1-11-COL	7.8	0.4	7.3	1.6
P1-14-COL	5.3	0.4	3.5	0.8
P2-11-RGD	9.7	0.9	8.2	3.0
P2-14-RGD	13.2	0.8	10.9	3.1
P2-11-COL	7.7	1.7	5.1	0.3
P2-11-HA	9.9	2.3	7.0	2.2

Table 7.2: Mean strain in the cartilage and bone layers as a function of applied strain used in this study. All values are listed at two significant figures.

Applied Strain [%]	**Cartilage Layer Strain [%]**	**Bone Layer Strain [%]**
5	10	0.016
10	20	0.033
20	40	0.066

Table 7.3: List of materials and suppliers used in this study

Chemical or Material	Supplier
1920 x 1152 Analog SLM	Meadowlark Optics
2-(1H-7-azabenzotriazol-1-yl)-1,1,3,3-tetramethyl uranium hexafluorophosphate methanaminium	Chem-Impex International, Inc.
8-arm PEG (10,000g/mol)	JenKem
8-arm PEG (20,000g/mol)	JenKem
AIBN	Sigma-Aldrich
Ascorbic Acid	Sigma-Aldrich
Calcein AM	Corning
CRGDS	GenScript
Custom Primers	Invitrogen
DAPI	Life Technologies
Dichloromethane	Sigma-Aldrich
Diethyl Ether	Cole-Parmer
Dimethylformamide	Sigma-Aldrich
Ethidium Homodimer	Corning
Fetal Bovine Serum	Atlanta Biologicals
Goat Anti-Rabbit Secondary Antibody Alexa Fluor 568	ThermoFisher
High Capacity cDNA Reverse Transcription Kit	Applied Biosystems
I2959	BASF Company
IDG-SW3 Cell Line	Kerafast
miRNeasy Mini Kit	Qiagen
MMP-sensitive crosslinker	GenScript
Modified Essential Medium (MEM) α	Gibco
N,N-diisopropylethylamine	Chem-Impex International, Inc.
Paraformaldehyde	Sigma-Aldrich
PEGDA 700	Sigma-Aldrich
PEG-dithiol crosslinker	Sigma-Aldrich

penicillin/streptomycin	Invitrogen
PETMP	Sigma-Aldrich
PGE2 ELISA kit	Cayman Chemical
Phosphate Buffered Saline	Corning
QIA Shredder Columns	Qiagen
Rabbit Anti-Collagen I Antibody	Abcam
Rabbit Anti-Connexin 43 Antibody	Abcam
Rat-Tail Collagen Type I	Sigma-Aldrich
Recombinant Mouse Interferon-Gamma (INF-γ)	Peprotech
Silver Nitrate	Sigma-Aldrich
SOLIS-405C	Thorlabs
SYBR Green Master Mix	Applied Biosystems
Sylgard 184 PDMS	DOW CORNING
Technovit 7100 kit	Electron Microscopy Sciences
Tinuvin CarboProtect	BASF Company
TPO	Sigma-Aldrich
β-glycerophosphate	Sigma-Aldrich

Table 7.4: Forward primer, reverse primer, accession number, and calculated efficiency for each gene.

Gene	Forward Primer	Reverse Primer	Accession #	Efficiency
L32	CCATCTGTTTTA CGGCATCATG	TGAACTTCTTGG TCCTCTTTTTGA	NM_172086	1.91
Sost	GGTGGCAAGCC TTCAGGAAT	GGACACATCTTT GGCGTCAT	NM_024449.6	1.92
Dmp1	GCTTCTCTGAGA TCCCTCTTCG	GCGATTCCTCTA CCCTCTCT	NM_016779.2	1.98

8.2 Supplementary Figures

8.2.1 Chapter 2 Supplementary Figures

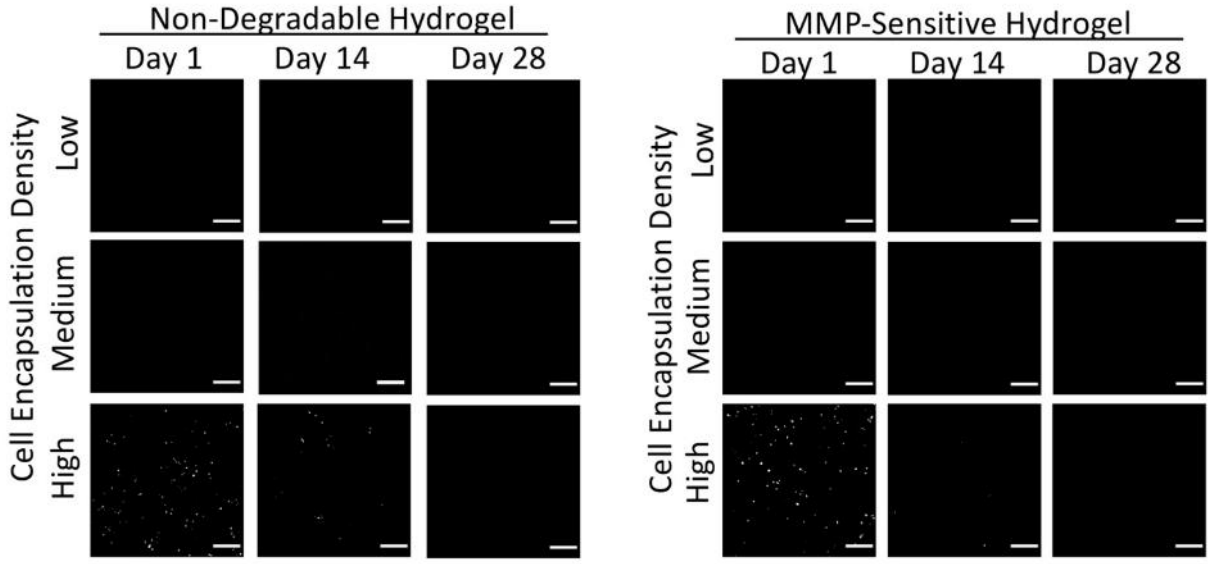

Figure 7.1: Confocal images depicting dead cells stained by ethidium homodimer for IDG-SW3 cells at days 1, 14 and 28 in osteogenic differentiation media encapsulated at low, medium, and high cell seeding densities in MMP-sensitive and non-degradable PEG hydrogels. The fluorescent red stain was converted to white color to enable visualization of the dead cells. Scale bar is 150 μm.

8.2.2 Chapter 3 Supplementary Figures

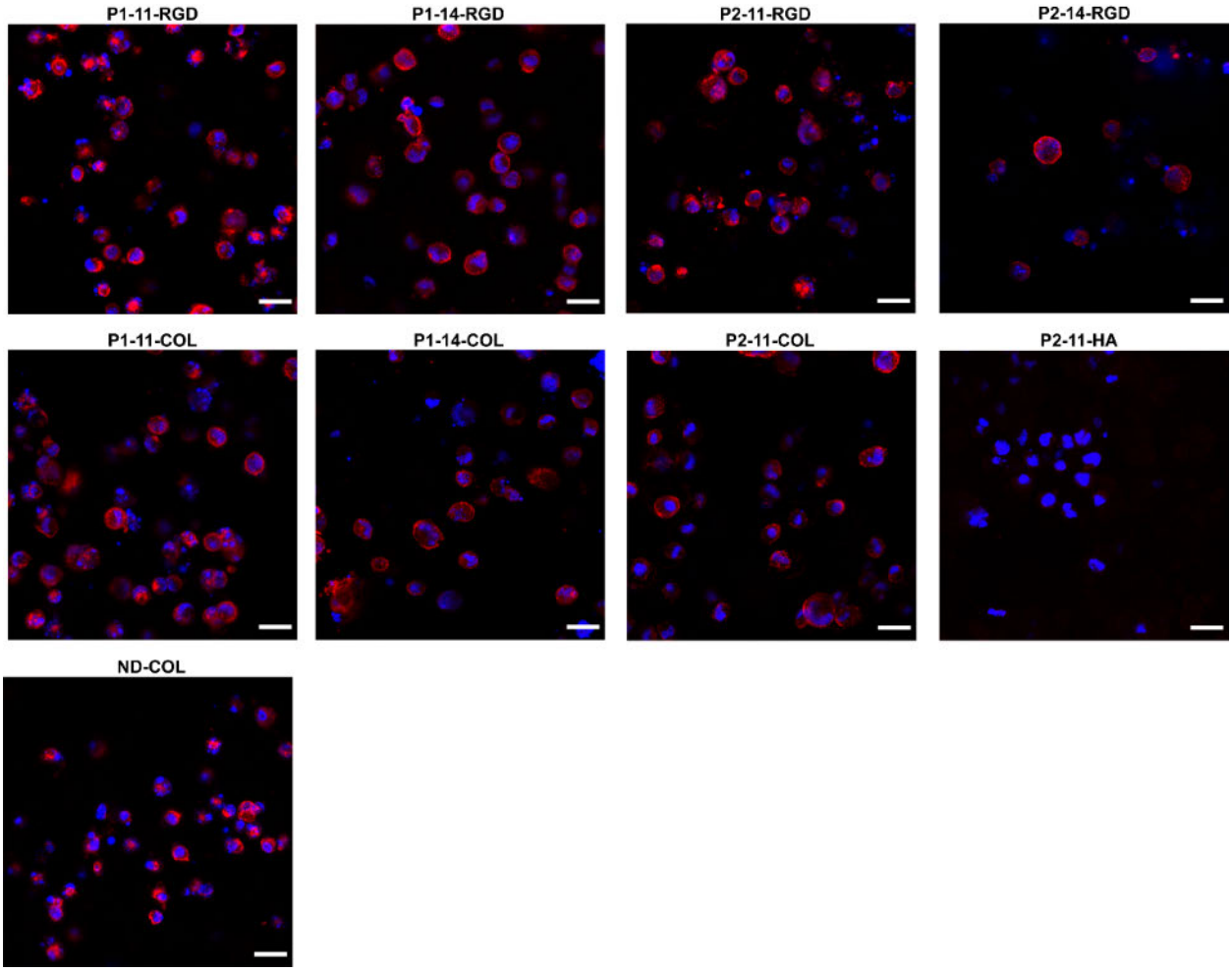

Figure 7.2: Representative images of regions showing only spherical cells in each hydrogel condition. F-actin was stained with Phalloidin (red) and nuclei were stained with DAPI (blue). Images were taken with a 63X objective and are maximum intensity projections of 12 μm depth, with 0.6 μm spacing in between slices. Scale bar is 20 μm.

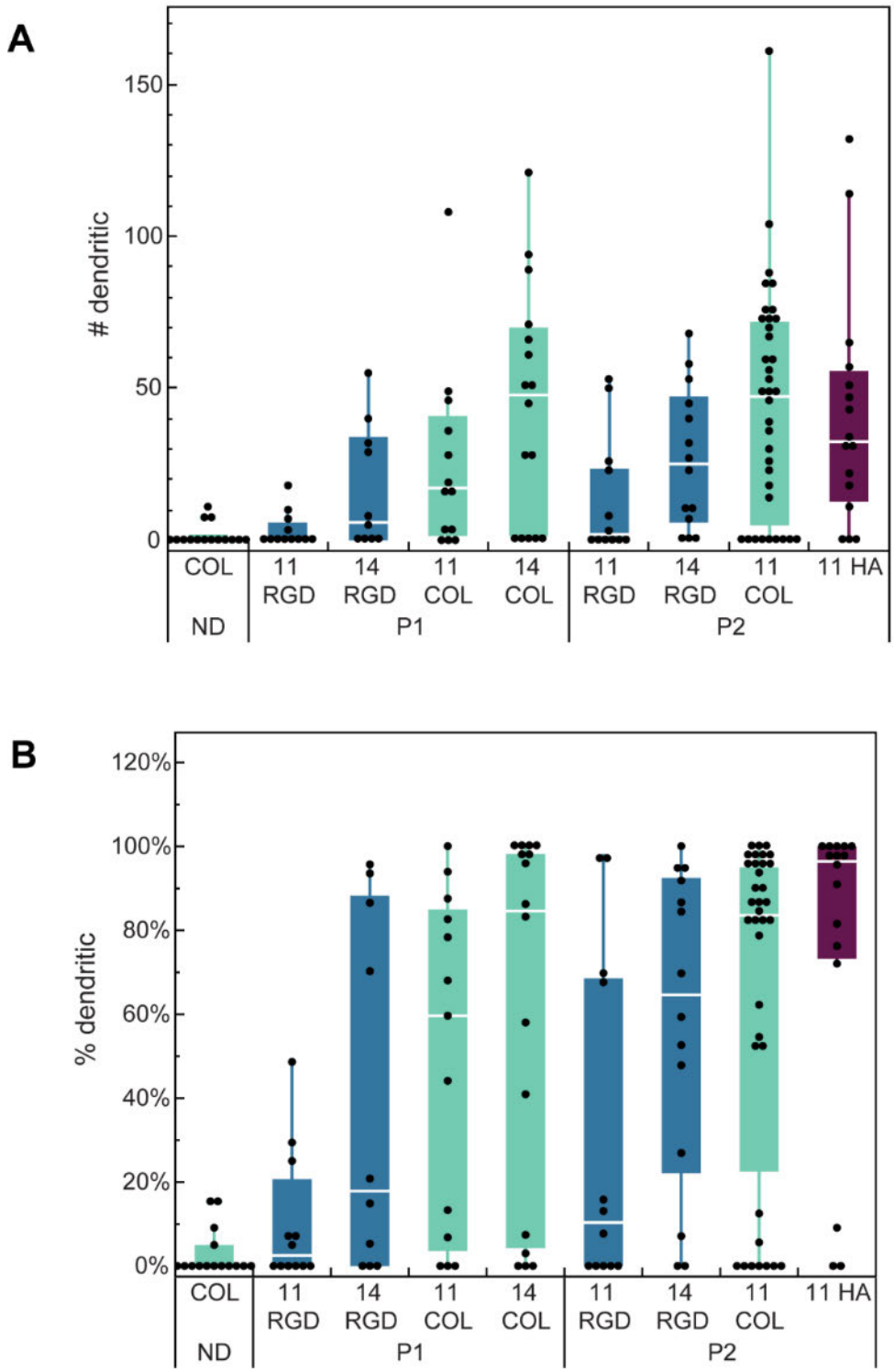

Figure 7.3: Number (B) and percentage (C) of dendritic cells per image for each sample (n=5 images per sample) and condition (n=3 samples per condition). In each image, the number of dendritic nuclei was counted (A) and then divided by the total number of nuclei in that image (C).

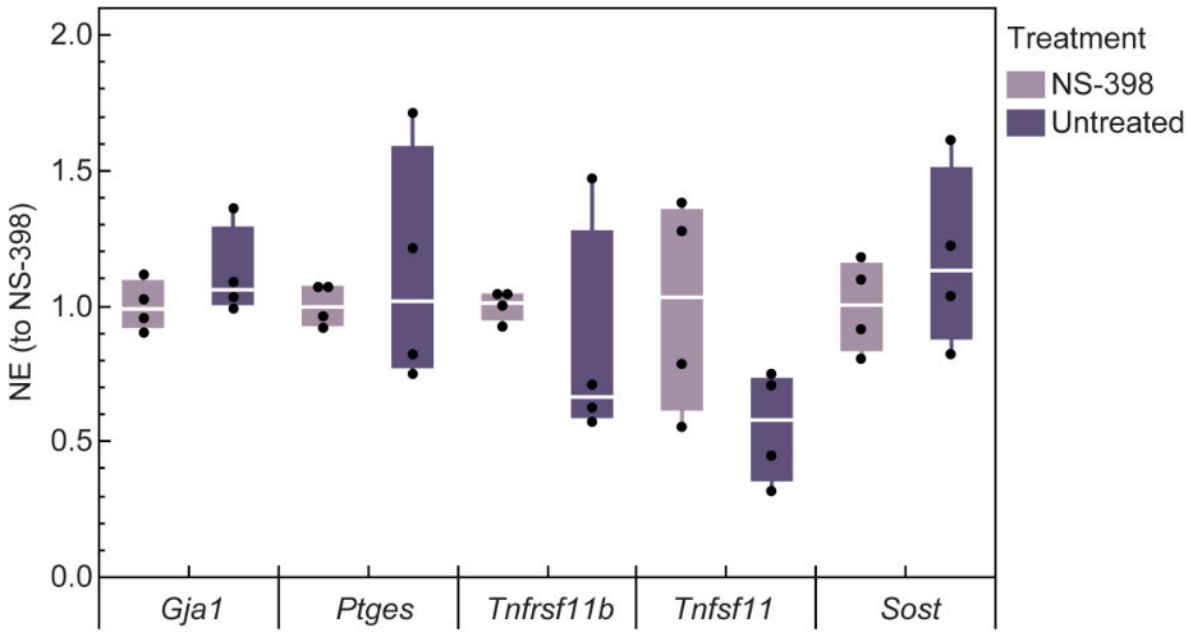

Figure 7.4: Gene expression of *Gja1, Ptges, Tnfrsf11b, Tnsfsf11,* and *Sost* was measured in ND-COL hydrogels after 24-hours of incubation in 1 μM NS-398 or in media alone (untreated). RE was normalized to the NS-398 treated samples to obtain the normalized expression (NE).

8.2.3 Chapter 4 Supplementary Figures

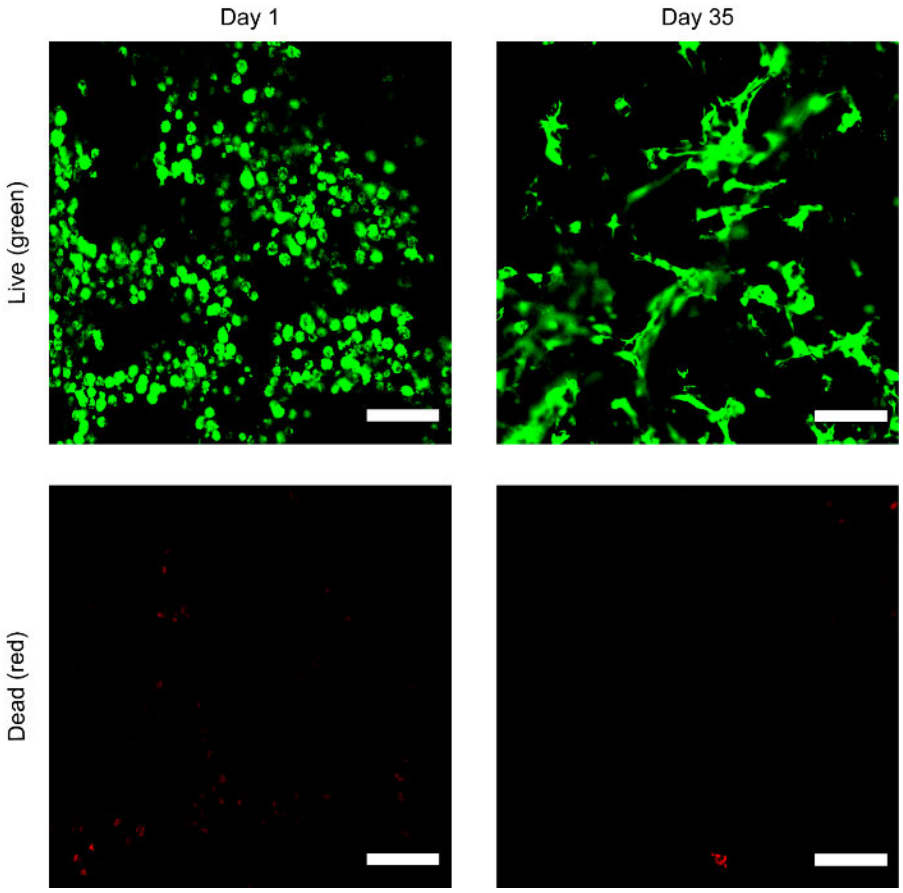

Figure 7.5: Representative images of samples stained with Calcein AM (live, green) and ethidium homodimer (dead, red) on day 1 and 35 of study. Scale bar is 100 μm.

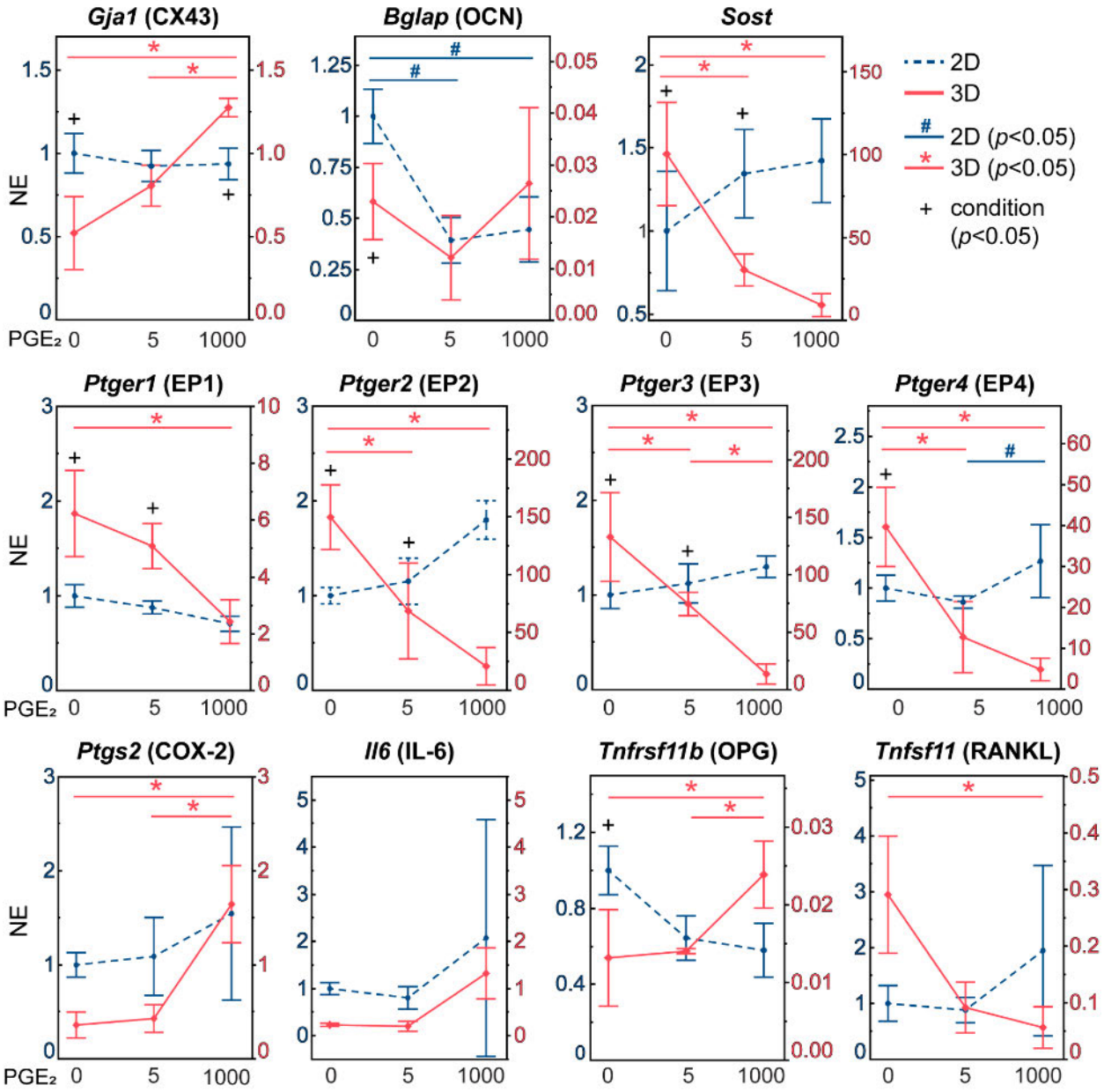

Figure 7.6: Gene expression in 2D and 3D after 24 hours of PGE_2 treatment with different y-axes for 2D and 3D. After 35 days of differentiation, IDG-SW3 cells in 2D (blue) and 3D (red) were treated with 0, 5, or 1000 nM of PGE_2 for 24 hours. Relative expression levels were normalized to the 0nM, 2D condition to obtain the normalized expression (NE). Statistical significance was determined by a two-way ANOVA with PGE_2 concentration and environment (2D vs. 3D) as main effects followed by Tukey's post hoc. Symbols denote significance ($p < 0.05$) from post hoc Tukey's test and are color-coded by condition (# for 2D, * for 3D). + symbols denote significance from post hoc for condition.

8.2.4 Chapter 5 Supplementary Figures

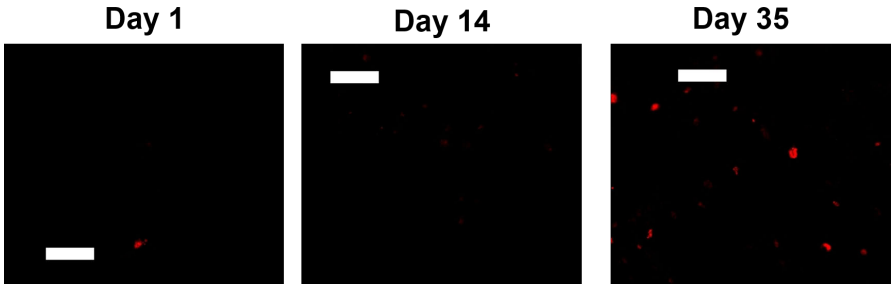

Figure 7.7: Representative images of ethidium homodimer stained samples showing dead cells. Scale bar is 50 μm.

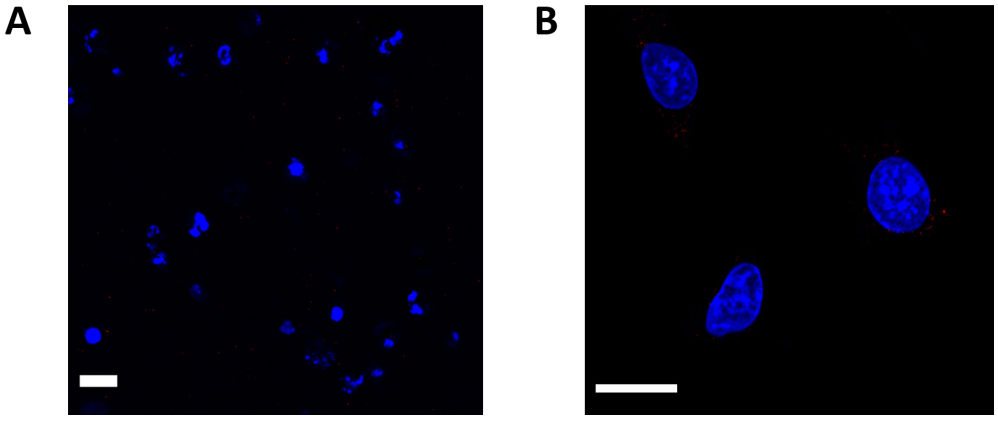

Figure 7.8: Representative immunohistochemistry images of negative control (did not receive primary antibody) Connexin 43 (red) counterstained with DAPI for nuclei (blue) on (A) day 35 within hydrogel and (B) day 3 on collagen type I coated glass dish, scale bar = 20 μm.

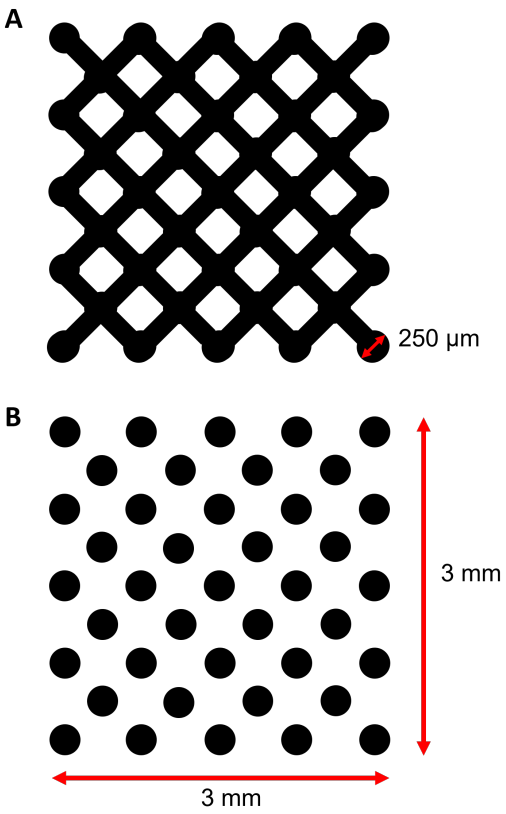

Figure 7.9: The 2D images of the (A) lattice and (B) pillars that were used to print the 3D structure using stereolithography.

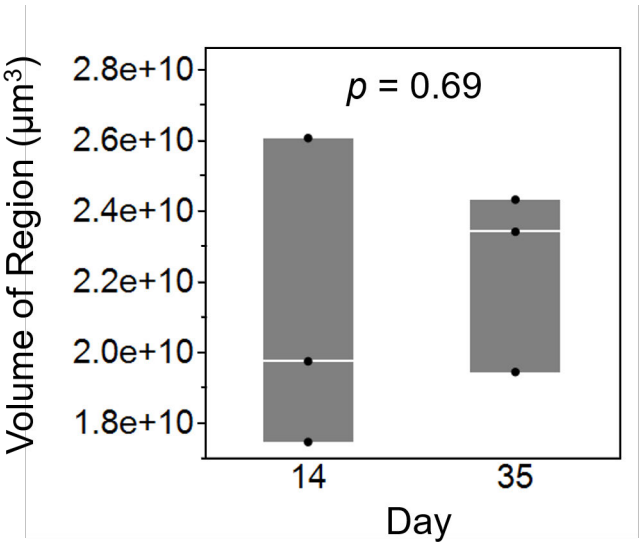

Figure 7.10: Volume of region-of-interest that was analyzed for mineral content from XRM images. There was no significant effect of day.

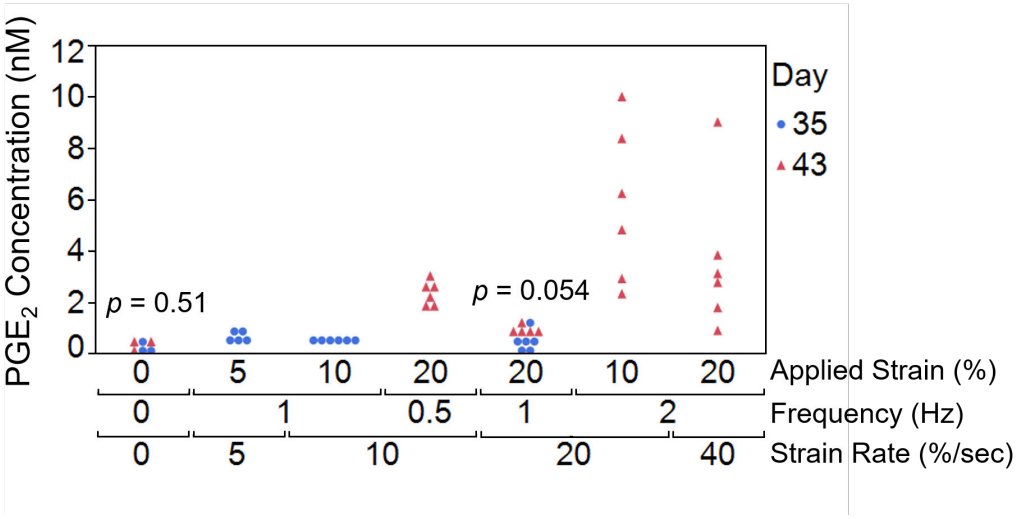

Figure 7.11: PGE_2 concentration in the media directly after loading, colored by day of loading. Data are presented as points colored by day (n = 6 for loaded, n=3 for unloaded). *P*-values comparing the effect of day for the same loading condition are shown.